THE UNIVERSITY *of* EDINBURGH

This thesis has been submitted in fulfilment of the requirements for a postgraduate degree (e.g. PhD, MPhil, DClinPsychol) at the University of Edinburgh. Please note the following terms and conditions of use:

- This work is protected by copyright and other intellectual property rights, which are retained by the thesis author, unless otherwise stated.
- A copy can be downloaded for personal non-commercial research or study, without prior permission or charge.
- This thesis cannot be reproduced or quoted extensively from without first obtaining permission in writing from the author.
- The content must not be changed in any way or sold commercially in any format or medium without the formal permission of the author.
- When referring to this work, full bibliographic details including the author, title, awarding institution and date of the thesis must be given.

Colloidal rods and spheres in partially miscible binary liquids

Niek Hijnen

Doctor of Philosophy
The University of Edinburgh
2013

Abstract

Different scenarios for assembling rod-like and spherical colloidal particles using binary mixtures of partially miscible liquids were investigated experimentally. Suitable rod-like colloids were developed first. The subsequent studies of colloids in binary liquids consisted, on one hand, of systems where particles were partially wetted by both phases and, on the other hand, of systems where particles were completely wetted by the minority phase.

A simple method to prepare large quantities of micrometer-sized akaganéite-silica core-shell rods was developed. These were proven to be very versatile, with the possibility of modifying their properties on different levels. The aspect ratio is simply controlled by a gradual growth of the silica shells. From them, hollow silica rods and rods with an increased responsiveness to a magnetic field could be obtained in straightforward ways.

Bijels were prepared by trapping rod-like particles on a percolating liquid-liquid interface. The familiar bicontinuous organization of liquid domains was observed after structural arrest. At a fixed volume per particle it is demonstrated that for rod-like particles the domain size decreases faster with increasing quantity of particles than in the case of spherical particles. Additionally, the packing of the rods at the interface was elucidated, revealing several characteristic features.

In particle-stabilized droplet emulsions rapid evaporation of the continuous phase and eventual full mixing of the liquid phases can leave a cellular network of particles. The formation and eventual stability of these networks were investigated in detail with confocal microscopy.

When colloids are completely wetted by the minority component of an asymmetric binary mixture there can be substantial temperature and composition regimes outside the binodal where shear-induced aggregation can take place. This happens as adsorbed layers present at the particle surfaces coalesce and bind particles through a liquid bridge. Depending on particle concentration, percolating networks can form of rods wetted by the minority phase after temperature quenching such a system just across the binodal.

Declaration

I declare that this thesis was composed by myself, that the work contained herein is my own except where explicitly stated otherwise in the text, and that this work has not been submitted for any other degree or professional qualification except as specified.

Parts of this work have been published in [1].

(*Niek Hijnen, 2013*)

Acknowledgements

Foremost, I thank my supervisor Paul Clegg for his encouragement and guidance during the entire project, and also for giving me a lot of freedom to pursue my own ideas.

I am also especially grateful to a few people who worked in and around the chemistry lab. Andy Schofield, of course, was always there for assistance, whether it was particles I needed or advice on any colloid (synthesis) related topic. In the first period of the project I had a great time working with Joe Tavacoli, who introduced me to experimenting with colloids in partially miscible liquids. With Job Thijssen I have enjoyed discussing about our silica particles and their surface chemistry, and he always offered useful advice on my experiments.

Steve Mitchell I want to thank for his always kind and pleasant assistance with the TEM, and thanks to Mathias Reufer and Vincent Martinez for doing some DDM with me.

It was good to usually have a small Dutch crew around the lab, so as not to neglect my native language too much: Rut, Gijs, Michiel, Danielle, and of course Job, bedankt! Overall, I spent a lot of time in the chemistry lab, and I'm grateful to many who contributed to making it a nice place to work.

My time spent in Edinburgh to work on this project has been very valuable, and for a great part this is due to many friends. I am extremely grateful for the time we shared playing squash, on trips, in pubs, etc. Especially I want to mention Andy, Iris, Danielle and Joe whose close friendship means a lot to me. Also in the Netherlands are some friends I want to thank: it was good fun every time you came over to visit, or when I saw you back home.

Hens, thanks a lot for your support and interest in my work, and also for sharing more general interests and such.

Finally I thank my family, Mum, Dad, Koen and Floor, for being there for me. Our time spent together and your support I have always found extremely important.

Contents

Results III: Complete wetting of colloids

List of Figures

List of Tables

Chapter 1

Introduction

In soft matter research a very large variety of materials is investigated. This thesis specifically concerns colloidal particles and their properties; these particles are then used as building blocks in directed assembly. Here the main topics are surveyed.

1.1 Colloids

Colloids are systems where one phase of matter is finely dispersed within a continuous medium in the form of small particles. The size of these particles typically ranges from several nm to several μm. In other words, they are intermediate between the bulk of a pure substance and systems where chemical species are homogeneously mixed on a molecular scale. [2]

Such materials can vary hugely in composition, and the phases of matter of which the respective dispersion medium and colloidal particles consist, can assume nearly all thinkable combinations. Only colloidal systems where both components are gaseous do not exist, since they cannot. Otherwise, one can think of any other pair, for example, liquid particles in a gas (e.g. fog) and solid particles within another solid (e.g. pearl) [2]. Consequently, it is not surprising that an immense variety exists, offering a huge range of material properties. For a long time mankind has been making use of colloidal suspensions, and these days the innumerable applications include many everyday products.

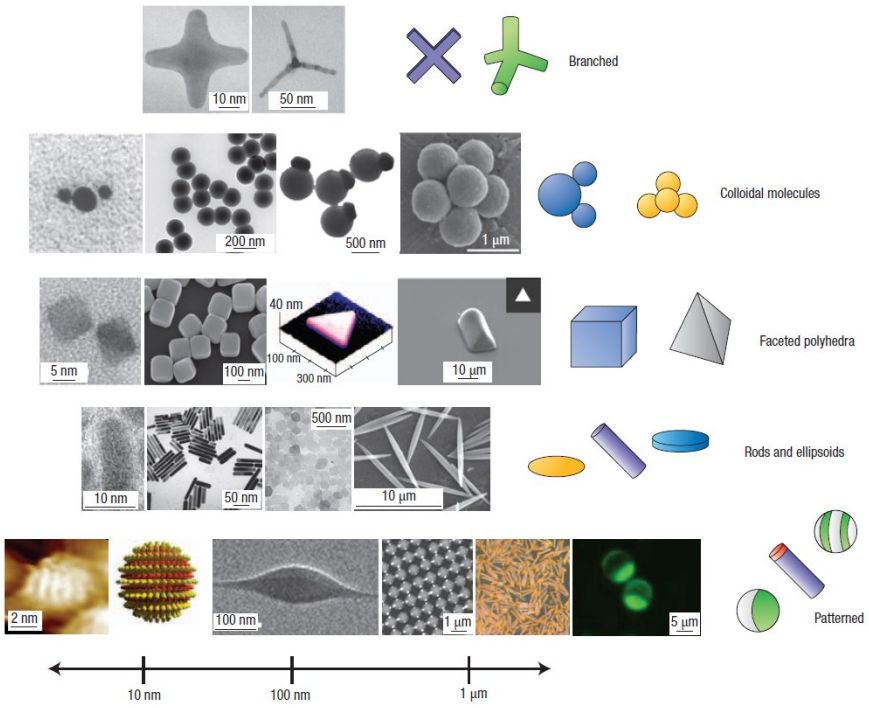

Figure 1.1 *A selection of anisotropic colloidal particles, demonstrating a range of sizes, shapes and materials. Taken from [3].*

As their applications are widespread, so is the need to understand colloidal systems, resulting in colloid science being a very rich and active field of research with a long history. Here, one of the main questions addresses the stability of a colloidal suspension. These systems involve a huge area of interface between the dispersed phase and its host medium, so why do the colloids not combine into a single mass? It appears that the balance of various interactions between individual particles is crucial to preventing this scenario from playing out.

This thesis deals with solid colloidal particles suspended in a liquid medium, mostly within the context of self-assembly. Colloidal self-assembly is a relatively new branch of the research area where, instead of keeping the colloidal particles stably suspended, the aim is to assemble particles into complex structures. In this way, colloids function as building blocks for new materials.

1.2 Directing colloidal assembly

A great deal of control over colloids is required for their assembly into a desired structure. As their purpose now goes far beyond just being colloidally stable, this will involve more complexity in colloidal systems.

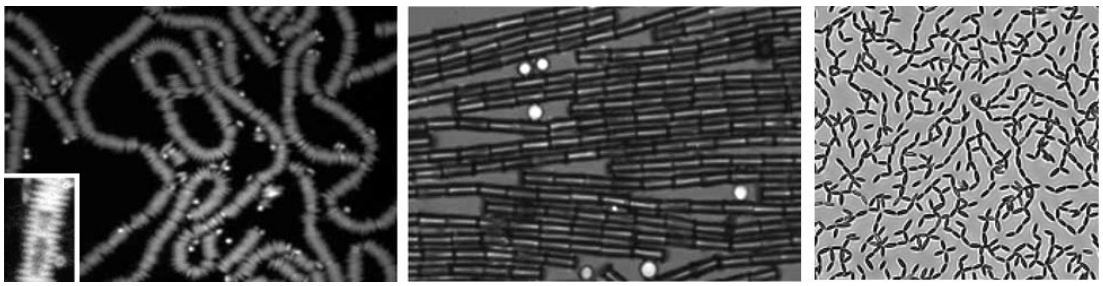

Figure 1.2 *Structures resulting from the self-assembly of rod-like colloidal particles at a flat liquid interface. Taken from [10, 11].*

One level on which control can be achieved are the properties of the colloidal particles (Figure 1.1). Anisotropy in both colloidal shape and interactions are of great current interest, and have already proven to be powerful tools to control properties of self-assembled structures [3–5]. Advances in designing and synthesizing increasingly complex building blocks have aided this [6, 7]. In some of the studies presented in this thesis there is a focus on particle shape, which specifically concerns rods. Interest in colloidal rods is not just recent. Probably a striking example is the seminal work of Onsager from the 1940's [8], predicting them to form liquid crystalline phases on purely entropic grounds, as dictated by the particle shape. As later confirmed and extensively studied in experiments and simulations, their shape can thus lead to the formation of very specific ordered structures. In contrast, disordered structures of rods have also been found to have unique and useful properties [9].

Although colloidal rods by themselves are clearly nothing new, when subjected to new situations their behaviour keeps providing the research field with new possibilities. Recent experiments nicely demonstrate this for rods trapped at liquid interfaces, where the organization of the particles is highly shape-specific and tunable [11–13] (Figure 1.2). Additionally, it was suggested that compared to spherical particles rods could more effectively stabilize the interfaces, making them potentially useful as emulsifiers [14]. These observations partly inspired the current work on rods. In fact, the first presented results will describe the synthesis of versatile rod-like particles, designed with the intention of studying them in the presence of liquid-liquid interfaces.

Another route to controlling colloidal assembly is offered by external stimuli. To this end colloids are introduced to a more complex situation where, under influence of directing agents, external fields or templates, they are driven to assemble. Termed "directed self-assembly" [15], this gives rise to many possibilities.

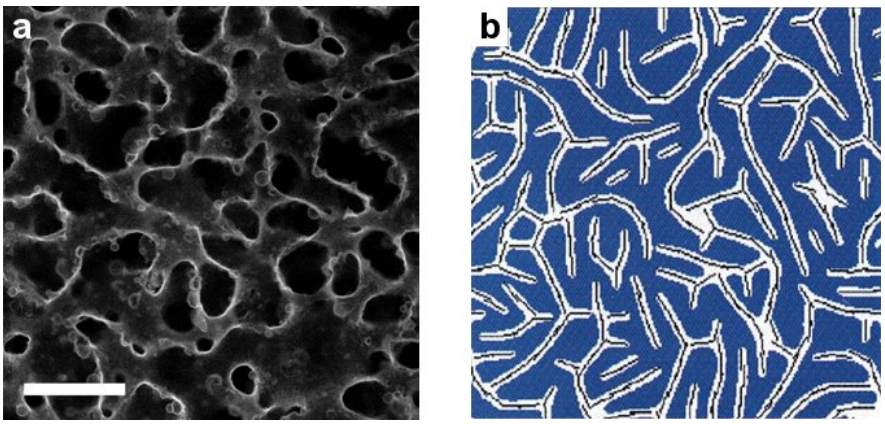

Figure 1.3 *Colloidal assembly directed by a liquid-liquid phase separation. (a) Spherical particles assembled on a percolating interface via liquid-liquid phase separation (the scale bar is 100 μm, taken from [16]). (b) Simulations predict a percolating network to form when rods are trapped inside the minority phase after liquid-liquid phase separation (taken from [17]).*

In one particular approach, a pair of partially miscible liquids is employed to guide particle assembly. Mixing and phase-separation of the host solvent can be controlled by choosing its composition, as well as by externally controlled parameters, like temperature or pressure. During these dynamic processes particles can be guided, through their interaction with the liquids, to assemble into structures. Wetting of the colloidal particles is crucial in this scenario, as it will determine their behaviour. Good control over assembly can be achieved by adjusting this through modification of the colloid surface chemistry.

This thesis, while being motivated by much of the above, builds largely on various studies that have looked into assembling colloids with partially miscible liquids. An important example is the formation of bijels [18], where spherical colloids are trapped on percolating interfaces to stabilize bicontinuous liquid domains (Figure 1.3a). Using the specifically designed colloidal rods, the effect of particle shape on these materials will be investigated. Furthermore, profoundly different routes to directed colloidal assembly in this type of system (e.g. Figure 1.3b) are explored with experiments.

1.3 Thesis outline

Chapter 2 will provide a detailed theoretical background to the topics of the thesis. Based on existing literature, theory and information relevant to the interpretation of results presented in later chapters will be reviewed. This provides a good basis for presenting and discussing the results, which is done in 3 parts, consisting of 2 chapters each. In the **first results part**, the synthesis, properties and modification of colloidal core-shell rods that are used to obtain some of the following results, are described. Where **Chapter 3** details the synthesis, **Chapter 4** focuses on particle properties and modification. The **second results part** studies colloids in partially miscible liquids, where the former are trapped at the interface after liquid-liquid phase separation. More specifically, **Chapter 5** is about rod-stabilized bijels, and **Chapter 6** demonstrates the formation of cellular networks. Colloids in the **third results part**, are completely wetted by the minority phase of a binary liquid mixture. **Chapter 7** is about shear-induced aggregation outside the binodal, and in **Chapter 8** quenches reaching inside the binodal are used to form percolating networks of rods. Finally, **Chapter 9** closes the thesis by summarizing the conclusions and providing a general outlook.

Chapter 2

Theoretical background

This chapter provides the theoretical background for the results presented and interpreted later on in the thesis. First, relevant theory on colloids and partially miscible liquids is discussed. Aspects concerning the situation where these two elements are combined, which will form the main topic of the thesis, are reviewed last.

2.1 Colloidal interactions and phase behaviour

To answer the question, posed in the introduction, of why colloids are stable, the interactions between the colloidal particles must be considered. When they approach, there will be both attractive and repulsive forces acting between suspended particles. Interparticle repulsions are key to keep colloids dispersed, and there are 2 types that are responsible for this. Steric repulsions result from the presence of a polymer layer at the surface of colloidal particles. At short distances, these must overlap, and the corresponding osmotic pressure gives rise to a strong repulsive force between particles. Longer ranged repulsions can be present between like-charged particles, resulting in charge-stabilization. Only this latter case is relevant here, and will now be discussed in some more detail.

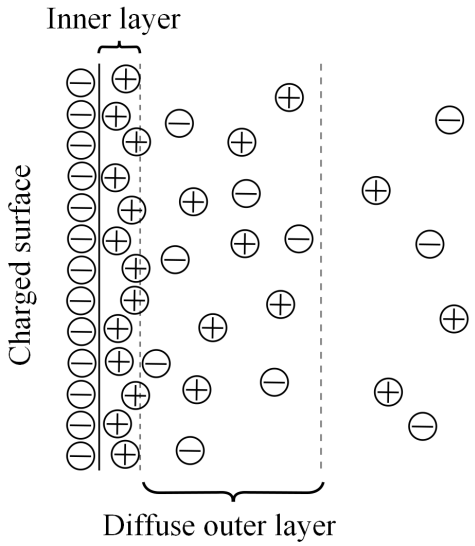

Figure 2.1 *Schematic representation of the electrochemical double layer. Encircled + and − represent solvated ions with, respectively, a positive and negative charge.*

2.1.1 Charge-stabilized colloids

Charges will be present on surfaces of colloidal particles in many, if not most, systems. More than one mechanism exists that can generate surface charge [2, 19]. In this work the relevant mechanism is the ionization of chemical moieties on the colloid surfaces under influence of the dispersing medium.

Charged surfaces will first of all interact with the chemical species in the dispersing solvent, resulting in an electrochemical double layer. Ionic species in the solvent will associate with the charged surface groups resulting in an ion cloud around the particles, which is referred to as the electrochemical double layer. The distribution of ions within it can be described with the Stern-Gouy-Chapman model. It distinguishes an inner layer of ions strongly associated with the surface, and a diffuse outer layer that stretches out towards the bulk (Figure 2.1). In the inner layer ionic species are not significantly affected by thermal fluctuations, and some are only partially solvated due to the proximity of the surface. Away from the inner and into the diffuse layer, the electrostatic potential decays exponentially with distance. The Debye screening length (κ^{-1}) is the distance over which it drops by an exponential factor, and this is usually taken to characterize the thickness of the double layer. [2, 19]

The DLVO potential

For the effective pair potential between charge-stabilized colloidal particles, attractive and repulsive interactions need to be taken into account. DLVO theory presents a model that does just this. Here, by first considering individual contributions, its main outcome will be demonstrated.

Van der Waals interactions. For any molecule or atom, fluctuations in its electron distribution induce a fluctuating dipole, resulting in attractive van der Waals interactions between them. This interaction specifically is known as the London− or dispersion interaction, and even occurs for neutral species. Because colloidal particles consist of many atoms, this interaction introduces an interparticle attraction.

Calculating it for two adjacent colloids involves summing over the interactions between individual pairs of atoms present in the particles. For spherical particles this leads to the following pair potential:

$$V_{VdW} = -\frac{A}{12}\left(\frac{4R^2}{r^2-4R^2} + \frac{4R^2}{r^2} + 2\ln\left(1-\frac{4R^2}{r^2}\right)\right) \tag{2.1}$$

where A is the Hamaker constant, R the particle radius, and r the distance between the particle centers. Since A depends on the polarisability and density of the material, the interaction potential is strongly dependent on the composition of the system. In the case of identical particles within a solvent, the effective Hamaker constant for the particles through the solvent must be used. This can be estimated from the Hamaker constants of the individual materials through a vacuum:

$$A \approx \left(\sqrt{A_{particle}} - \sqrt{A_{medium}}\right)^2. \tag{2.2}$$

Clearly the Van der Waals interactions will be stronger when the mismatch between Hamaker constants is larger. While typically strongly attractive for small separations between particles, the attraction falls off relatively quickly compared to the particle radius. The interaction is therefore usually considered to be short-range. [20, 21]

Double layer overlap. As two charged colloids approach, at some point their electrochemical double layers will start to overlap. Where this happens, the local ion concentration is the sum of the individual ion clouds, meaning that at the mid-point it simply doubles. An increase in osmotic pressure results from the difference between this increased local concentration and the bulk concentration, pushing the particles apart. Thus, ultimately the electrostatic nature of the repulsion is only indirect.

A combination of the Poisson equation and the Boltzmann equation can be used to find the effective pair potential due to double layer overlap. First, in the Debye-Hückel approximation, the Poisson-Boltzmann equation is linearized. When solved the osmotic pressure difference can be integrated with respect to the distance between the surfaces, to arrive at the repulsive energy. For spherical particles, ultimately an approximate potential of a screened Coulomb form was derived by Verwey and Overbeek:

$$V_{dlo} = \pi\varepsilon\varepsilon_0 a^2 \psi_0^2 \frac{\exp(-\kappa(r-2R))}{r} \tag{2.3}$$

where ε_0 is the dielectric permittivity of vacuum, ε is the relative permittivity of the medium, $a = 2R$ is the diameter of the particles, and ψ_0 is the surface potential. In more detail, here the inverse Debye screening length

$$\kappa = \left(\frac{e^2 \sum z_i^2 n_i}{\varepsilon\varepsilon_0 k_B T} \right)^{\frac{1}{2}} \tag{2.4}$$

with z_i and n_i being, respectively, the valency and number density of ions in the solution, Boltmann constant k_B, and temperature T. Naturally, the range and strength of this repulsive pair potential depends heavily on the surface potential and the Debye screening length. [2, 20, 21]

The total potential. Summing individual contributions, a total potential can be obtained:

$$V_{DLVO} = V_{VdW} + V_{dlo} + V_{Pauli}. \tag{2.5}$$

Here, V_{Pauli} originates from the Pauli exclusion principle, and results in a hard-sphere repulsion at contact of the surfaces. [21] This simply entails a strong and

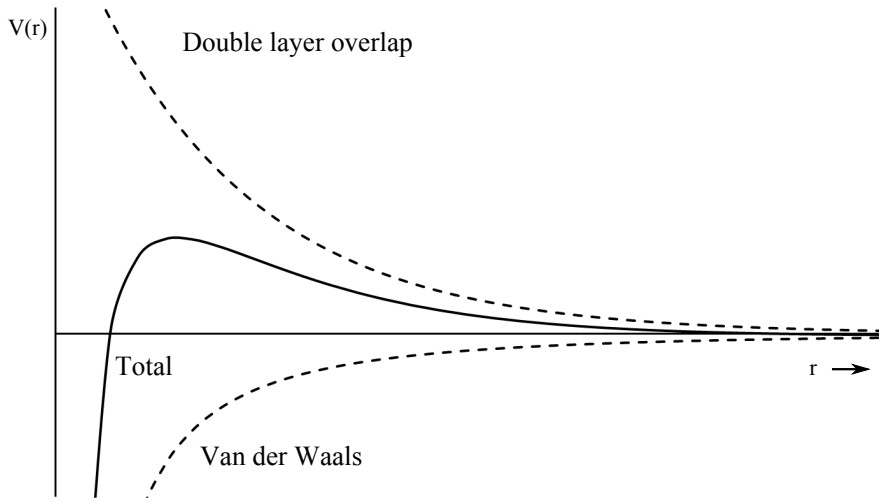

Figure 2.2 *Sketch of the total interaction potential and the individual contributions of Van der Waals interactions and double layer overlap.*

extremely steep repulsive interaction, with as its only consequence that the solid particles remain separate entities. It has no practical significance for colloidal stability.

From combining the Van der Waals and double layer interactions, an effective pair potential follows (Figure 2.2). The most important outcome of doing this is that, depending on the individual contributions, the steeper decay of the Van der Waals term can result in a maximum.

Suspension stability

Now, with the framework offered by DLVO theory, stability in charge-stabilized colloidal suspensions can be discussed. [20, 22]

First, it is noted that in a liquid medium particles are subject to thermal fluctuations in the host material. Solvent molecules, due to their thermal motion, constantly and randomly collide with a dispersed particle. As a result a fluctuating net force acts on it, giving the particle a diffusive ("Brownian") motion. This is characterized by a diffusion coefficient, which for spherical particles is given by the Stokes-Einstein equation:

$$D = \frac{k_B T}{6\pi\eta R} \tag{2.6}$$

where η is the viscosity of the solvent, which determines the time it takes for a particle to travel a certain distance. [23]

Thus, eventually two suspended particles will meet, and interact according to their pair potential. Examining Figure 2.2 in more detail, a primary minimum and an energy barrier can be distinguished. Kinetic stability is therefore achieved when the barrier protects against aggregation due to the Van der Waals forces. Through Brownian motion spherical particles will collide with an energy of $\sim \frac{3}{2}k_BT$, indicating that for a stable suspension the barrier should be significantly higher than this.

Both terms included in the pair potential are proportional to particle size, overall resulting in a higher energy barrier for larger particles. The balance between the attractive and repulsive contributions can also give a secondary minimum at distances further away from the surface than the energy barrier, especially for large particles, when at longer range the attraction dominates again. Only weak flocculation happens here and suspensions are easily re-dispersed by shear.

For the repulsive interaction from the double layer overlap the surface potential ψ_0 and the Debye length κ^{-1} are the main parameters. In the electrochemical double layer a thin layer that is only slightly thicker than the inner layer can be considered stuck to the surface and therefore unaffected by shear. The outer boundary of this layer defines a shear plane, the potential at which is called the ζ-potential. Often it can be measured with electrokinetic methods, and since it can also be expected to be close to ψ_0, it is often used in the calculation of V_{dlo}. Also since it provides a measure for surface charge density, it is important in characterizing colloidal stability.

Now assuming there is a fixed surface potential, it is the Debye screening length (κ^{-1}) that remains as the main parameter. Recalling that this is a measure of the thickness of the double layer, it becomes clear that its alteration will affect the range of repulsive interaction. Equation 2.4 demonstrates the dependence of κ on the ionic strength, revealing that adding salt to the system will decrease the double layer thickness. With the decreasing range of the repulsive interaction, the energy barrier reduces, threatening colloidal stability. When the barrier disappears aggregation can proceed unhindered as particles meet. The critical salt concentration at which this occurs is called the critical coagulation concentration (c.c.c.).

At high ionic strength or a low surface charge density conditions are often such

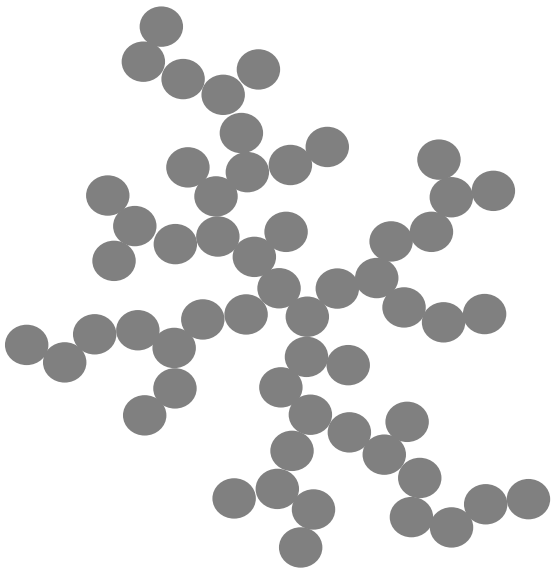

Figure 2.3 *Sketch of a fractal-like aggregate.*

that colloids aggregate. The rate at which this process proceeds depends on whether or not there is still an energy barrier to cross for particles to actually become stuck together. If not, as mentioned above, particles aggregate as soon as they come into contact. This fast aggregation is only limited by diffusion and also happens between for clusters, hence it is often called diffusion-limited cluster aggregation (DLCA). Particles joining a cluster attach at the outside, resulting in a very open aggregate structure with a fractal character (Figure 2.3). The size R and mass M of a fractal-like aggregate are related as $R \sim M^{1/d_f}$, where for DLCA fractal dimension $d_f \approx 1.8$. For comparison, the extreme cases are a needle-like linear aggregate for which $d_f = 1$, and a compact 3-dimensional aggregate for which $d_f = 3$.

Now take the case where there is an energy barrier (V_{max}) preventing aggregation. As the energy of a collision must exceed the barrier to successfully stick them together, there is now a finite probability that this will happen. Also termed reaction-limited cluster aggregation (RLCA), the rate constant associated with aggregation will decrease from the fastest possible rate k_D corresponding to DLCA, to a lower rate k_R. Stability ratio W is defined as k_D/k_R, for which a reasonable approximation can be found relating it to the energy barrier:

$$W = \frac{k_D}{k_R} = \frac{1}{2\kappa R} \exp\left(\frac{V_{max}}{k_B T}\right). \tag{2.7}$$

2.1.2 Phase behaviour of colloids

Returning to stably suspended colloids again, these will in most cases be dilute and due to gravity simply sediment with a velocity v. The force of gravity acting on a single spherical particle having a density difference $\Delta\rho$ with the solvent ($F_g = \frac{4}{3}\pi R^3 \Delta\rho g$) is balanced by a frictional force from viscous drag in the solvent ($F_S = 6\pi\eta R v$). A terminal sedimentation velocity will be reached:

$$v_t = \frac{2R^2\Delta\rho g}{9\eta}. \tag{2.8}$$

The colloidal particles will over time thus effectively be concentrated near the bottom of their container, depending on the gravitational length l_g (for a particle of buoyant mass m, $l_g = \frac{k_B T}{mg}$).

At high colloid concentration sometimes it becomes clear that, while constantly performing Brownian motion, spontaneously ordering can arise among the particles. The initially disordered, purely repulsive particles end up in a crystalline packing. By analogy to atomic systems this is regarded as freezing: a fluid-crystal phase transition. Without the presence of any effective attractions between particles, instead of energy driven, the phase transition must be driven by entropy. Ordering actually appears to be related to an increase in free-volume entropy, as compared to a disordered organization, as particles acquire more freedom to move around in a crystalline packing.

In experiments this has been extensively studied. Most famous are samples prepared by Pusey and Van Megen, demonstrating the freezing of sterically-stabilized colloids with a hard-sphere repulsion [24]. The overall phase diagram for hard spheres is well known, and also displays the formation of an amorphous phase, a colloidal glass, when starting from an overcrowded suspension (Figure 2.4a). If the range of the repulsion is increased by using charge-stabilized colloids crystallization occurs at lower volume fraction. It is important to realize that this phase depends largely on the size uniformity of particles. Polydispersity, defined as the ratio of the standard deviation in the size distribution to the mean particle size, is used to characterize size uniformity. In experimental systems it is often too high for particles to be able to crystallize (although fractionation under gravity can help).

To complete the analogy with atomic systems, introducing weak attractive inter-

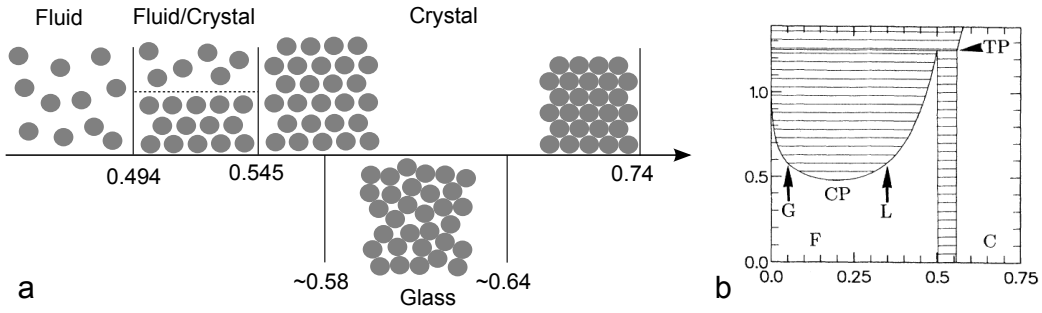

Figure 2.4 *(a) Hard-sphere phase diagram with volume fraction (numbers) increasing from left to right. (b) Phase diagram when adding attraction, where the horizontal axis plots the particle volume fraction, and increasing attraction is plotted upwards along the vertical axis (G = gas, L = liquid, C = crystal) [25].*

actions can result in a colloidal condensation, or gas-liquid phase transition. [23] Colloids form a disordered, condensed phase under the influence of interparticle attractions, most clearly observed when leading to a coexistence between two phases at different density. The phase of high colloid concentration will sink to the bottom and form a macroscopic colloidal liquid with, on top of it, a colloidal gas at low density. Experimentally this can easily be observed by adding a non-adsorbing polymer, to introduce attractive depletion interactions between colloids. In this situation polymer coils are unable to enter the space between two nearby colloids, the osmotic pressure difference between the solvent separating the particles and the bulk pushes particles together. Varying colloid and polymer concentrations a full phase diagram is obtained exhibiting gas-liquid coexistence upon increasing attraction, with a crystalline phase at higher particle volume fraction [25] (Figure 2.4b).

When strong attractions are present non-equilibrium structures will form. As above, following DLCA particles could now become irreversibly stuck and form open structures (e.g. Figure 2.3). It is not hard to imagine that space spanning networks, usually called gels [26], can in this case easily form at relatively low volume fraction.

In addition to the interactions also the shape of the particles can change, where a well-known example is that of rod-like particles. Interestingly, these can exhibit equilibrium phases with a degree of ordering intermediate between that of a disordered liquid and a crystal with long-range positional order, which are therefore called liquid-crystalline. This is due to the possibility of orientational order. At low concentration the rods freely diffuse around without significantly

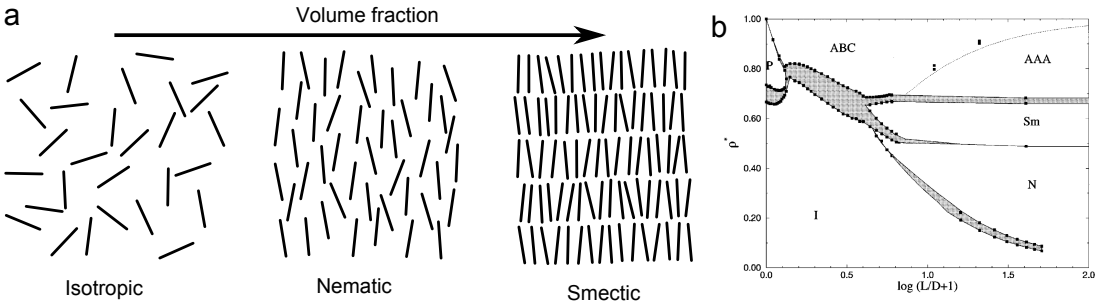

Figure 2.5 *(a) Liquid crystalline phases of rods. (b) Phase diagram from simulations [27].*

affecting each others motion, and without any positional or orientational order this is called the isotropic phase (Figure 2.5a). The nematic phase (Figure 2.5a) is found at higher concentration where the rods show long range orientational order, characterized by a headless vector **n** referred to as the director.

The isotropic-nematic transition is again one of purely entropic nature [8]. Rods will interact through the volume they effectively exclude from being occupied by a nearby particle. This excluded volume will be small as they align, which is at the cost of orientational entropy, but benefits the free volume entropy. Thus, the isotropic-nematic transition happens when the loss in orientational entropy is outweighed by the increase in free volume entropy. With increasing particle aspect ratio, defined as the ratio L/D of the length L to the width D of the rods, this will already be the case at lower particle concentration.

Quite a few other liquid crystalline phases with varying degrees of order exist at higher rod concentration. The smectic phase is a noteworthy example which demonstrates the introduction of some positional ordering (Figure 2.5a). Here the rods form liquid-like layers containing only orientational ordering. The phase diagram for hard rods of varying aspect ratio has been mapped out using computer simulations [27] (Figure 2.5b).

Colloidal rods have been used in many experimental studies so various types are available [9, 28]. They range from inorganic and polymer based rods to rod-like viruses (TMV, fd), and in many cases it has been observed that their suspensions can indeed form various liquid-crystalline phases. To study them the birefringence of the liquid crystalline phases is often used. Birefringence implies that there is a difference between the refractive index parallel and perpendicular to the director **n**, thus the polarization of linearly polarized light passing through the material will change. Positioning the sample between 2 crossed polarizers in

polarizing microscopy, only light that changes polarization due to birefringence will be observed. [29] This provides a direct way to observe and study structure in these suspensions.

2.2 Partially miscible liquids

As put forward in Chapter 1, an important part of the studies presented later is on directing colloidal assembly with binary mixtures of partially miscible liquids. Dynamical processes that can occur in them, as well as their underlying cause, are reviewed in this section. [23, 30, 31]

2.2.1 The equilibrium state

Adding together two liquids, each of a single molecular species, can lead to a homogeneous mixture or two separate volumes of homogeneous liquid, each with a different composition. In other words, a binary liquid mixture can be fully mixed and consist of a single phase, or it can be phase-separated and exhibit two distinct phases. For certain liquid pairs, which of these states is in thermodynamic equilibrium depends on system composition (x) and the pressure (P) and temperature (T). These systems are called partially miscible liquids.

In experiments one typically deals with a fixed composition and pressure, leaving temperature as a control parameter. Adjusting it can change the state of the system, and since here the formation of at least one new phase is involved, the process is referred to as a phase transition. In pairs of partially miscible liquids a simple distinction between mixing and phase-separation can be made.

It will thus be of interest to know the equilibrium state of the mixture at a particular composition and temperature. Thermodynamics dictates that, at a fixed pressure, equilibrium is attained by minimizing the Gibbs free energy of mixing

$$G_{mix} = H_{mix} - TS_{mix}, \tag{2.9}$$

which is the change in the total Gibbs free energy associated with going from the unmixed components to the mixed state. The system will therefore adjust its enthalpy H_{mix} and entropy S_{mix} to achieve this.

Hence the equilibrium state comes down to the balance between entropy and enthalpy. Entropy is the degree of disorder in the system, equivalent to the number of possible configurations, which will be maximal when molecules are fully mixed. Enthalpy represents the total thermodynamic energy of the system, consisting of the sum of internal energy (U) and the work (PV) done on the environment by volume (V) changes. With only slight changes in sample volume, U dominates so that H_{mix} will basically depend on the interaction energies between molecules. These arise from van der Waals forces between molecules. For like molecules these are usually more attractive, corresponding to lower interaction energies, compared to van der Waals forces between different molecules.

At high temperature the second term of equation 2.9 is dominant, and maximizing it will therefore minimize the free energy. A homogeneous mixture will then generally be the equilibrium state, as it maximizes S_{mix}.

At lower temperature the contribution of the interaction energies between molecules become more important. Therefore the dependence of H_{mix} on temperature needs to be evaluated. What will be of significance here are the interaction energies between different molecules relative to those between like molecules. Within the regular solution model this is characterized by interaction parameter χ, which expressed in units of k_BT is inversely proportional to temperature. This reflects that at low temperature (high χ) there are high interaction energies between different molecules compared to like molecules, which would lead to the 2-phase state being equilibrium.

Investigating G_{mix} as a function of composition for various temperatures (i.e. χ) calculated according to the regular solution model, provides the complete picture (Figure 2.6a). Starting at high temperature, for $\chi < 0$ mixing will be energetically favorable, leading to a single minimum in the free energy curve, corresponding to full mixing. At $0 < \chi < 2$ mixing will no longer be energetically favorable, but as this is being offset by entropy, full mixing is still the equilibrium state, as evidenced by a single minimum in the free energy curve. A drastic change occurs when $\chi > 2$, in which case 2 minima are found. As a consequence, a system with a composition in between these minima can lower its free energy by forming two coexisting phases each with a different composition (in Figure 2.6 indicated by x_a and x_d for $\chi = 3$). This is then the equilibrium state.

The instability against mixing at a certain χ can be classified more specifically

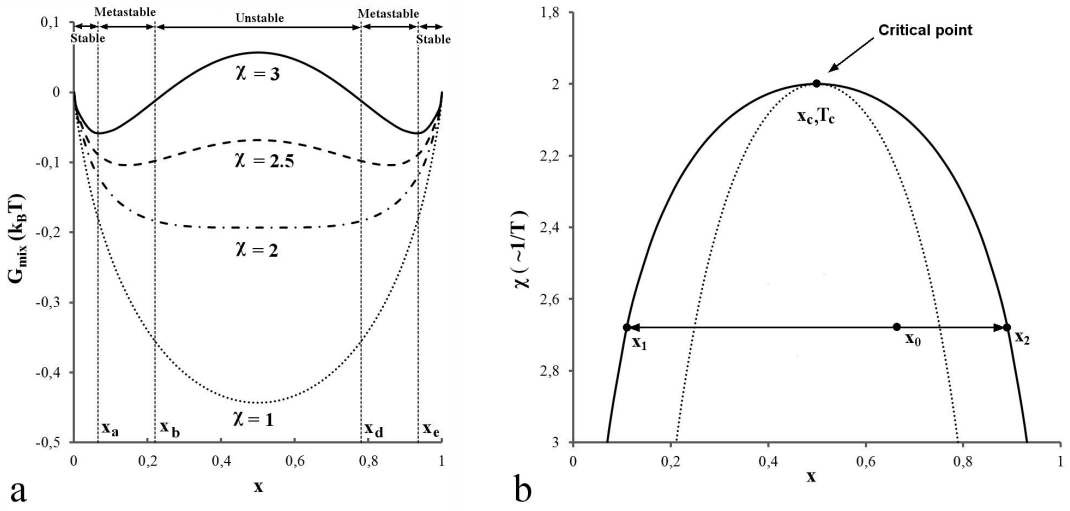

Figure 2.6 *(a) Free energy of mixing plotted as a function of composition (x, the fraction of one of the molecular species) for various interaction parameters χ. (b) Spinodal (dotted) and binodal (solid) lines separating conditions of temperature and composition for which mixtures are stable, metastable and unstable against phase separation.*

by considering the shape of the corresponding free energy curve. For this its local curvature d^2G_{mix}/dx^2 is taken into account. Where a negative curvature is found ($x_b < x < x_d$) any fluctuation in composition will lead to a lowering of the free energy and the system will therefore immediately phase separate. The mixture is unstable against mixing. For a positive curvature at $x_a < x < x_b$ and $x_d < x < x_e$ small compositional fluctuations lead to an increase of the free energy: a larger fluctuation in composition is necessary to give a lowering of the free energy. There is an energy barrier between the mixed and the (equilibrium) phase-separated state, meaning that the system is metastable against mixing.

This allows the full binary liquid phase diagram plotting T against x to be constructed. At a specific χ, $dG_{mix}/dx = 0$ indicates the boundary between stable and metastable compositions of the system, while $d^2G_{mix}/dx^2 = 0$ indicates the boundary between metastable and unstable compositions. These points for varying temperatures are collected into single curves called binodal and spinodal, respectively (Figure 2.6b). Where these meet ($d^3G_{mix}/dx^3 = 0$) is the critical point (x_c, T_c, indicated in Figure 2.6b). This defines the only composition where there can be a direct temperature-induced transition from a stable to an unstable mixture.

The so obtained phase diagram demonstrates miscibility at high temperature and

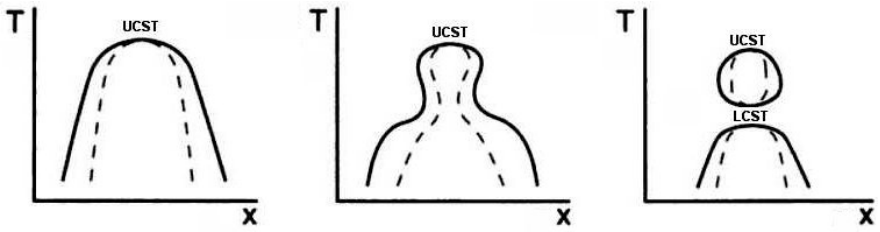

Figure 2.7 *Illustration demonstrating the appearance of a LCST by increasing the contribution of hydrogen bond interactions (left to right). [30]*

coexistence of 2 phases at lower temperature. In the phase coexistence region the spinodal line merely separates metastable mixtures from unstable ones. The binodal line is also called the coexistence curve, and using the lever rule it can be used to extract more quantitative information on the volumes of the respective phases. It considers a mixture of overall composition x_o at temperature T' in the coexistence region, separating into phases with compositions of x_1 and x_2 (Figure 2.6b). Letting the full length of the line between x_1 and x_2 represent the total volume, the length of the line connecting x_1 (x_2) and x_o represents the volume of the phase with composition x_2 (x_1).

With full miscibility at high temperature and phase coexistence at low temperature, the critical point is usually called the Upper Critical Solution Temperature (UCST). This situation is the outcome of the regular solution model, where only purely energetic interactions are included in the interaction parameter χ. Attractive hydrogen bonds between molecules actually also involve an entropic contribution. They are directional by nature, so forming hydrogen bonds to lower the system's internal energy will mean a lowering of the orientational entropy. The balance between energy and entropy now becomes more complicated, and in some cases this leads to a reappearing miscibility at temperatures below the UCST. A Lower Critical Solution Temperature (LCST) exists here. This occurs upon increasing strength of the hydrogen bonds, as at lower temperatures their overall effect in terms of lowering the internal energy is greater compared to their unfavorable effect on entropy (Figure 2.7).

This section is concluded by noting that an intrinsic property of the 2-phase state is the presence of an interface between the 2 liquid phases. As it is never molecularly sharp, the interface is characterized by a concentration gradient. Molecules present in this region will not only interact with like molecules, and consequently experience different forces from those in the bulk liquids resulting in higher interaction energies. The excess free energy per unit area associated with

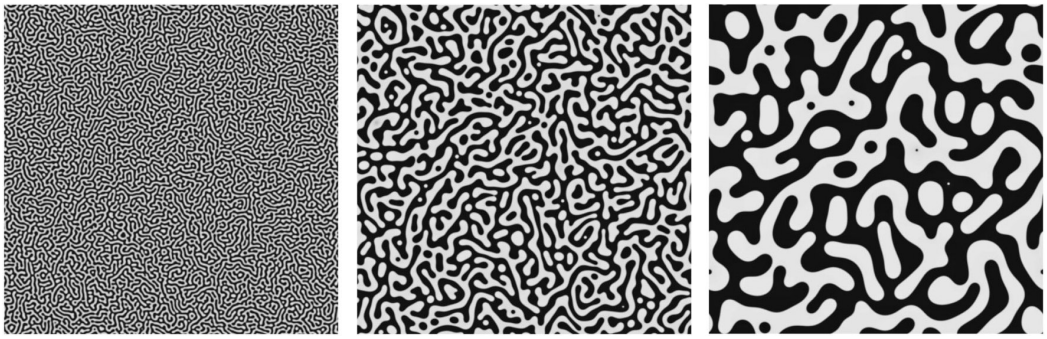

Figure 2.8 *Spinodal morphology from (left to right) early to later stages computed with numerical simulations [33].*

the interface must be included in the internal energy of the system, and therefore also its free energy. [32] It is referred to as the interfacial tension γ, and the reversible work required to create new interfacial area ($d\sigma$) is then $đw_{rev} = \gamma d\sigma$. Thus, interfacial tension is a 2D analog of pressure and can be regarded as a surface pressure, so γ is expressed in units of N/m. Overall, now it is clear that the system will always strive for a minimization of the interfacial area to minimize its free energy. This will be important when discussing phase separation in the following sections.

2.2.2 The mechanisms of phase separation

What remains to be explained is how coexisting phases come about by the process of phase separation. The kinetics of phase separation are different depending on whether it happens when the mixture is unstable or metastable. The corresponding mechanisms are, spinodal decomposition and nucleation & growth. [23]

Spinodal decomposition. In an unstable mixture compositional fluctuations continuously grow to eventually lead to the formation of 2 coexisting phases in equilibrium. Spinodal decomposition, as the process is called, happens spontaneously since it is induced by small and ever-present thermal fluctuations in concentration. Fluctuations grow through diffusion of molecules under the influence of the associated concentration gradients. As mentioned in the previous section, interactions between like molecules will be favorable, i.e. a high chemical potential is associated with a low concentration. Diffusion will therefore occur uphill in the direction of high concentration to amplify the fluctuations.

The rate with which fluctuations grow depends on their wavelength, resulting in a characteristic domain size. Small wavelengths will create large amounts of energy-costly interface, while molecules will need to diffuse long distances if wavelengths are large. An optimum exhibiting the fastest growth exists somewhere in between. This sets a characteristic length scale that is initially fixed, but later grows to give a self-similar evolution of a random pattern of bicontinuous domains which is typical for spinodal decomposition (Figure 2.8).

Nucleation & growth. As indicated in the previous section, if a mixture is metastable only sufficiently large concentration fluctuations are sustainable and lead to phase separation. Constant thermal fluctuations essentially create small regions, or droplets, rich in one of the components. If a droplet tends to grow or dissipate again depends on their free energy to which there are two contributions. [34] The internal energy due to the composition of the droplets will be lower compared to that of the original metastable mixture, thus favoring droplet growth. Opposing growth, however, is the interfacial energy associated with the droplets. Overall the change in free energy when a spherical droplet is formed

$$\Delta G_{droplet}(R) = -\frac{4}{3}\pi R^3 \Delta G_v + 4\pi R^2 \gamma \tag{2.10}$$

where ΔG_v is the amount by which the free energy is lowered per unit volume due to the different composition of the droplet compared to the metastable mixture. A maximum of $\Delta G_{droplet}$ is now found for the critical droplet radius $R_c = \frac{2\gamma}{\Delta G_v}$. This means an energy of

$$\Delta G_c = \frac{16\pi\gamma^3}{3\Delta G_v^2} \tag{2.11}$$

is required to form droplets of the critical size (critical nuclei) from which their growth is favoured.

For metastable mixtures phase separation thus proceeds by the nucleation of sufficiently large droplets that subsequently grow. This process is therefore simply called nucleation & growth. While in principle nucleation would occur homogeneously, in practice conditions typically result in heterogeneous nucleation. Namely, at surfaces in contact with the mixture the energy barrier for nucleation is often lower, so dust particles, container walls, and colloidal particles will all have a pronounced effect.

Finally, a clear comparison between nucleation & growth and spinodal decomposition can be made by considering the concentration profiles over time. This points

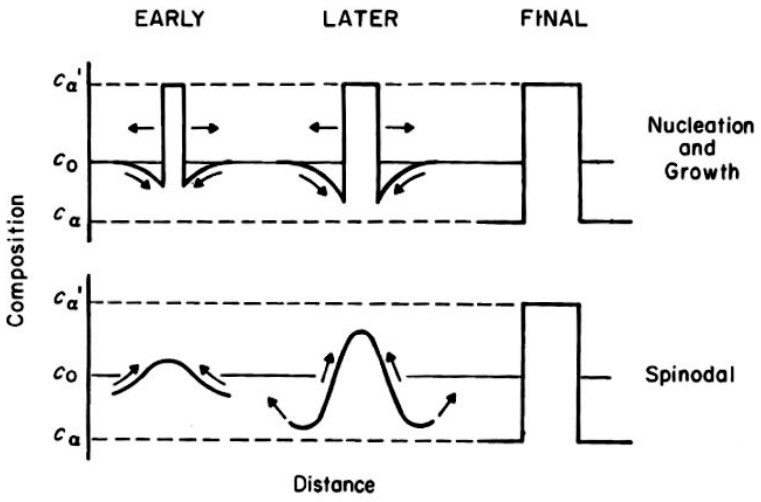

Figure 2.9 *Schematic illustration of the development of concentration profiles in (top) nucleation & growth and (bottom) spinodal decomposition. Original drawings from [35].*

out that immediately nucleation & growth is characterized by abrupt and sharp composition differences, while in spinodal decomposition these develop gradually and are initially separated by smooth gradients (Figure 2.9).

2.2.3 The late stages of phase separation

In the late stages of phase separation liquid domains will grow in size in a process called coarsening [23], until ultimately there is macroscopic separation of the coexisting phases. This is driven by interfacial tension acting to minimize the interfacial area.

What is immediately obvious is that an interface initially created by phase separation possesses curvature. For spherical droplets formed by nucleation & growth the mean curvature is constant. A quick look at the morphology resulting from spinodal decomposition (Figure 2.8) reveals that this is absolutely not the case here. To describe the curvature, the minimum and maximum radii of curvature of the surface, R_1 and R_2 respectively, are used (left panel of Figure 2.10). Their reciprocals are called the principal curvatures, κ_1 and κ_2, and define the Gaussian curvature $K = \kappa_1\kappa_2$ and the mean curvature $H = \frac{1}{2}(\kappa_1 + \kappa_2)$.

Gradients of interfacial curvature play a role in the coarsening of liquid domains. Underlying is the pressure difference ΔP between the 2 phases separated by a

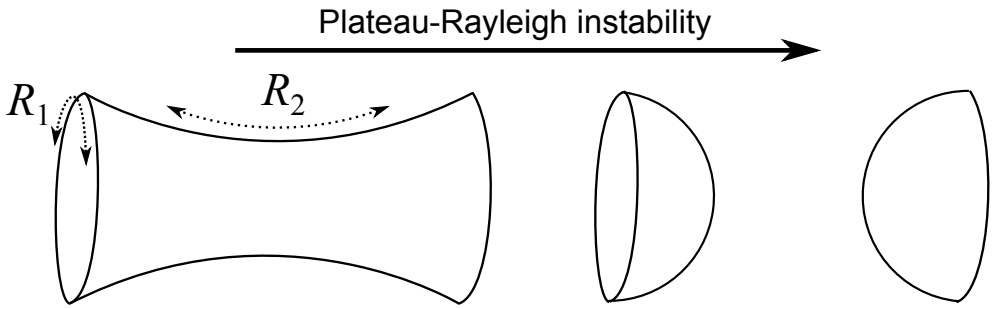

Figure 2.10 *Schematic illustration of a section of (left) a fluid neck, where the principal curvatures are indicated, that eventually undergoes a Plateau-Rayleigh instability to snap into (right) 2 hemispherical parts.*

curved interface. Given by the Young-Laplace equation

$$\Delta P = 2\gamma H = \gamma \left(\frac{1}{R_1} + \frac{1}{R_2} \right) \tag{2.12}$$

it is called the Laplace pressure [36]. With radii of curvature varying all over the place in the spinodal morphology, differences in Laplace pressure will drive fluid flow and deform the interface towards a situation with (more) uniform Laplace pressure. This way coarsening of the spinodal morphology is driven. For droplets $R_1 = R_2 = R$ and simply $\Delta P = \frac{2\gamma}{R}$.

A more specific example of what this can result to is the Plateau-Rayleigh instability. It occurs for fluid necks formed in spinodal decomposition. If the ratio of the length to diameter of the neck increases, at some point it will be energetically favorable to form individual droplets (right panel of Figure 2.10). In the spinodal morphology, instead of forming droplets, often the two parts of a neck which snaps simply retract into the domain they are attached to.

In late stages of phase separation diffusion becomes less important for the growth of liquid domains, which will then mainly proceed by coalescence. This is the merging of liquid domains through their interfaces as they meet, and is therefore mainly relevant to droplets. Furthermore, with increasing domain size, the density difference $\Delta\rho$ between the coexisting phases becomes more important as gravity starts to affect the system. Creaming then takes place, collecting all of the less dense phase at the top, and vice versa, as the gravitational force acts on the liquid domains. The length scale of the deformation of the interfaces due to gravity acting against the interfacial tension is the capillary length $l = \sqrt{\frac{\gamma}{\Delta\rho g}}$.[37]

As a final remark, the mixing of immiscible liquids is briefly noted. Here, contrary

to the phase separation of partially miscible liquids, creation of droplets (*i.e.* interface) needs a high energy input, as suggested by the above description. It can be achieved by mechanical agitation, where the ratio of viscous forces in the sheared liquid to the Laplace pressure (the capillary number) determines the extent to which the interface deforms. As a result droplets are created and these can subsequently also be deformed and broken up due to the Plateau-Rayleigh instability. The capillary number $Ca \approx \frac{\eta_c \dot{\gamma}}{(\gamma/R)}$, where $\dot{\gamma}$ is the shear rate and η_c the viscosity of the liquid outside the droplet, is thus important in setting the final droplet size.

Liquid-liquid interfaces can be stabilized using colloidal particles, and this will be the focus of the rest of the Chapter.

2.3 Wetting of solid surfaces

To the pair of partially miscible liquids a third component, freely dispersed colloidal particles, is added in experiments. When the liquid mixture phase separates, 2 liquid phases and a solid phase will meet, creating an entirely new situation. Before reviewing the specific case of colloids in the next section, here first the wetting of solid surfaces is discussed more generally [32].

2.3.1 Immiscible liquids and a flat solid surface

When 2 immiscible liquids and a flat solid surface coexist, the 3 types of interfaces involved are essential to determine the equilibrium state of the system. Namely, the 3-phase equilibrium relies on a balancing of the corresponding interfacial energies to minimize the free energy. If this results in the solid being in direct contact with both liquids, the situation is referred to as partially wetting (left panel in Figure 2.11). Where the 3 phases meet is a single contact line. There is also a contact angle $0 < \theta < \pi$, which is defined by the individual interfacial tensions through Young's equation

$$\gamma_{S\beta} = \gamma_{S\alpha} + \gamma_{\alpha\beta} \cos\theta. \tag{2.13}$$

Thus, partial wetting takes place when $\gamma_{S\beta} < \gamma_{S\alpha} + \gamma_{\alpha\beta}$. In practice the precise contact angle often varies with position on the surface due to chemical

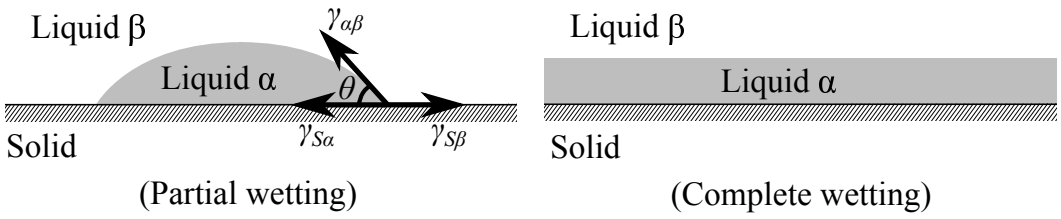

Figure 2.11 *Partial and complete wetting of a solid surface.*

inhomogeneities or varying roughness.

If the solid surface ends up in contact only with a single liquid the situation is referred to as complete wetting (right panel in Figure 2.11). A film is formed on top of the surface, and depending on the film being of liquid α or liquid β, the contact angle is, respectively, 0 or π. Taking liquid α to wet the surface, this would happen according to Young's equation, which relies on equilibrium considerations, when $\gamma_{S\beta} = \gamma_{S\alpha} + \gamma_{\alpha\beta}$. Not following the equilibrium considerations of Young's equation, the energetic cost per unit area of the solid-liquid β interface should be greater than that of the other 2 interfaces combined, and thus the condition becomes $\gamma_{S\beta} > \gamma_{S\alpha} + \gamma_{\alpha\beta}$.

2.3.2 Wetting transitions in partially miscible liquids

Having seen the dependence of wetting on the interfacial tensions involved, it is important to realize that these can change significantly with temperature when dealing with partially miscible liquids. It is clear from the phase diagram (Figure 2.6b) that when 2 liquid phases coexist, their compositions will depend on the temperature. In fact, the difference in composition of the coexisting phases will decrease as the critical point is approached. Associated with this is a decrease in the interfacial tension between the liquid phases, and a change in the surface energies of the solid-liquid interfaces.

Young's equation shows that whether complete or partial wetting takes place depends on the difference between $\gamma_{\alpha\beta}$ and $\gamma_{S\beta} - \gamma_{S\alpha}$. In partially miscible liquids it should now be taken into account how these vary with temperature. Approaching the critical temperature T_c, the interfacial tension of the liquid-liquid interface decreases as $\gamma_{\alpha\beta} \propto |T - T_c|^{\mu}$. For the difference in interfacial tensions of the liquids with the solid surface $\gamma_{S\beta} - \gamma_{S\alpha} \propto |T - T_c|^{\beta}$. Since $\mu > \beta$, there will be a transition from partial to complete wetting when approaching the critical point. According to the above, this happens when $\gamma_{\alpha\beta} = \gamma_{S\beta} - \gamma_{S\alpha}$, and

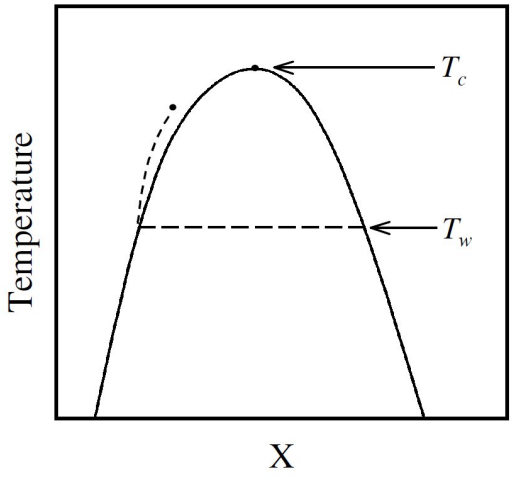

Figure 2.12 *Schematic phase diagram illustrating the wetting temperature T_w and prewetting line. [39]*

is marked by a critical wetting temperature T_w (Figure 2.12). This is known as the Cahn argument for the existence of a wetting transition. [32, 38, 39]

Above T_w, already slightly outside the phase coexistence region there can be a macroscopic film or adsorbed layer rich in molecules of one of the liquid components, the bulk phase of which will ultimately wet the surface. To understand this it is important to first realize that, as a consequence of entropy, there are always some molecules of this phase present at the solid surface. Even in the partially wetting state, outside the droplets of the preferentially wetting phase. These molecules are regarded as forming a microscopic film. The wetting transition coincides with a transition of this microscopic film to a macroscopic wetting film. At this point there is an abrupt change in composition at the region near the liquid-solid interface, which can be regarded as a transition from low to high adsorption. Since such a macroscopic wetting film, or high adsorption layer, also forms from the fully mixed liquids by approaching T_w from T_c, a prewetting line can be defined in the binary liquid phase diagram (Figure 2.12). Thus, a wetting layer exists between the binodal and the prewetting line, and at a surface critical point the distinction between a microscopic film and a macroscopic film disappears. [39]

2.4 Colloids in liquid mixtures

When colloidal particles find themselves in a mixture of 2 liquids, the wetting of their outer surfaces will generally be just like that discussed for a macroscopic flat surface. Only the geometry of the situation is different. There now is a curved surface with a microscopically small area enclosing a similarly small volume, and a comparatively much larger area of liquid-liquid interface.

2.4.1 Colloids trapped at a liquid-liquid interface

If the surface of a colloidal particle is partially wetted by 2 liquids, it can become trapped at the liquid-liquid interface [37, 40]. Analogous to partial wetting of a flat surface (Figure 2.11), this situation can be depicted schematically for a spherical particle at a flat liquid-liquid interface (Figure 2.13a). Again Young's equation governs the contact angle θ that sets the equilibrium condition for the system. Here one can regard the colloidal particle as an additive to the pair of liquids between which an energetically costly interface exists. By being partially wetted it will remove part of the liquid-liquid interface, leading to a reduction in energy of

$$\Delta G_{sphere} = \pi R^2 \gamma_{\alpha\beta}(1 - |\cos\theta|)^2. \tag{2.14}$$

This represents the minimum energy required to remove the particle from the interface into a bulk liquid phase, and can be called the detachment or trapping energy.

Now taking into account the actual energy scales in the system the full extent of the situation can be clarified. A simple colloidal particle passively diffusing in a bulk fluid possesses a thermal energy of $\sim k_B T$. The energy associated with the interface between 2 immiscible liquids is many orders of magnitude larger. Equation 2.14 reveals that for a typical colloidal sphere ($R = 0.25$ μm) with contact angle $\theta = 90°$ and a typical interfacial tension between an immiscible combination of an oil and water ($\gamma = 0.036$ N/m for water-toluene), $\Delta G_{sphere} \sim 10^6 k_B T$. Thus, compared to the colloidal energy scale, often there is a large trapping energy associated with a particle being partially wetted by 2 liquids.

Nonetheless, to achieve this situation is often not as easy as it seems. This is due to energy barriers preventing a 3-phase contact line being established, leading

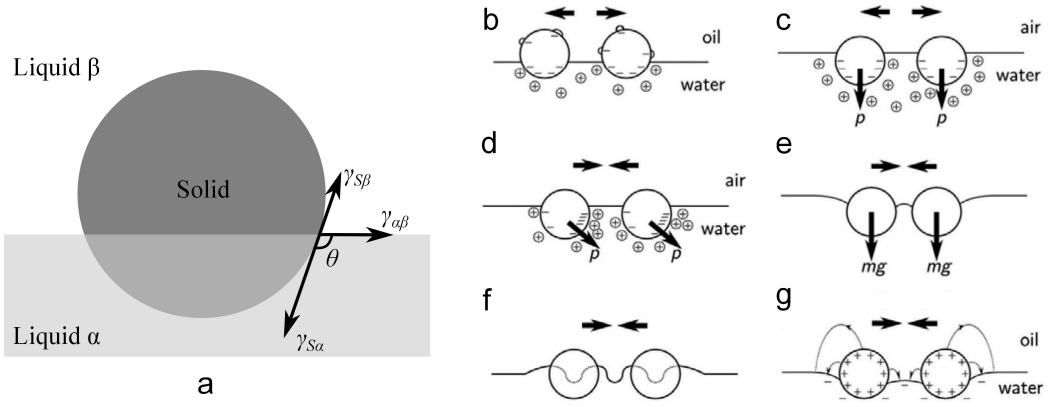

Figure 2.13 *(a) Schematic illustration of a spherical colloid trapped at the interface between 2 immiscible liquids. (b - g) Schematic illustrations of various possible interparticle interactions at a fluid interface (b to g: original drawings from [41]).*

to a subsequent relaxation to the equilibrium situation defined by the contact angle. One simply comes from the fact that with the contact line there is a corresponding line tension representing the energy cost of the 3-phase line. When charged colloids are involved there often is also an electrostatic repulsion between interface and particle. This long-range interaction can arise from ions adsorbed at the interface (*e.g.* hydroxyl ions adsorb at some oil-water interfaces) or an image charge effect when there is a large dielectric constant difference between the liquids [41]. Finally, it is worth mentioning that kinetics often play a role in interfacial trapping, since in situations that allow the barriers to be crossed, the interface and particles will not be static. Think for instance of interfacial trapping of particles during phase separation of a partially miscible liquid, or when mechanically agitating immiscible liquids.

Interparticle interactions. Being exposed to 2 different liquids, attached at the interface the effective interactions between particles will be very different from the bulk case [41]. Electrostatics play an important part in this. At a water-oil interface, particle surface charges on the oil side result in a strong electrostatic repulsion due the absence of ionic species (and thus charge-screening) and a low dielectric constant (Figure 2.13b). Surface charges can also give particles at a water-air interface an electric dipole moment, since the particle surface exposed to air is uncharged, resulting in dipolar interactions. While usually repulsive, they can be attractive when the coverage of charged groups is patchy (Figures 2.13c,d).

An interaction purely mediated by the interface itself result from capillary forces.

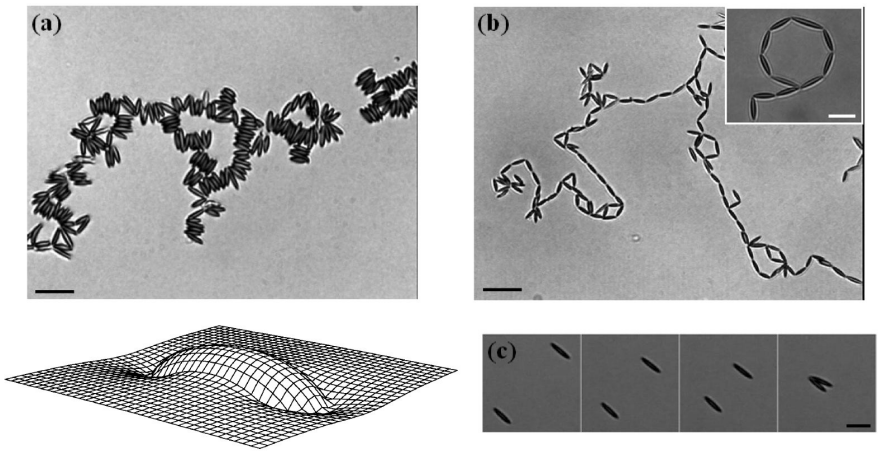

Figure 2.14 *Ellipsoids trapped at a fluid interface, with (lower left corner) an illustration of the interfacial deformation. (a,b) Depending on the contact angle their attractive interaction cause them to arrange in different structures. (c) A time sequence of images (time progresses from left to right) demonstrates the attractive interaction. Taken from [12].*

These arise from interfacial deformations caused by particles. For very small spherical particles interfacial deformations are usually negligible (as appears from Figure 2.13a), but can in certain cases be present due to gravity acting on very large particles, surface roughness resulting in an undulated contact line or an electric field from charged particles (respectively, Figures 2.13e,f,g). For shape anisotropic particles they are often induced by the particle shape alone, since to satisfy Young's law for a fixed contact angle an overall flat interface has to be deformed around the particle [10, 42, 43] (Figure 2.14). Overlap of the deformations generates a capillary interaction between the particles. Most commonly the sign of the curvature of the deformations around particles is the same, resulting in attractive interactions [12, 44].

Even for rod-like particles alone the exact shape is important in determining the interfacial deformations, and therefore the nature of the capillary interactions. To maximize ΔG_{rod} (analog to ΔG_{sphere}), rod-like particles have to orient their long axis parallel to the interface. Then, when taking a cylinder with spherical end caps no interfacial deformation at all is to be expected. In contrast, the case of a prolate ellipsoid or a normal cylinder does induce strong deformations of the interface. These particular examples have been studied in some detail both experimentally and theoretically.

For ellipsoids, experiments have characterized the interfacial deformations. The interface is found to be pulled down near the tips of the particles and elevated

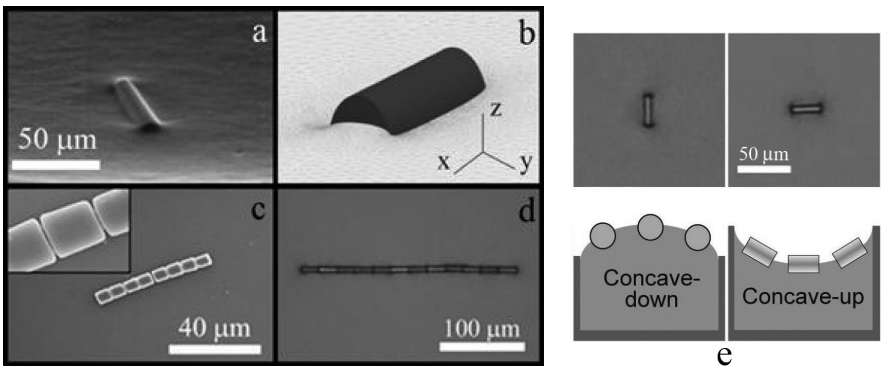

Figure 2.15 *Cylinders trapped at a fluid interface. In the left panel (a,b) the interfacial deformations are demonstrated, as well as (c,d) the particle assemblies these lead to. (e) The orientation of rods on differently curved interfaces. Taken from [44, 45].*

near the middle of the particles (Figure 2.14). Theory demonstrated that the deformations change with contact angle and aspect ratio [42]. Larger differences in height of the interface are present when particle aspect ratio is increased. On the other hand the interface around ellipsoids can be completely flat again when $\theta = 90°$. Since corresponding to quadrupolar symmetry, the interfacial deformations result in an anisotropic capillary interaction between particles. Attractions can be oriented side-side, tip-tip, or an intermediate of these 2 extremes, depending on the specific interfacial deformations (Figure 2.14). They are weak at long distances, but there is a steep minimum at short distance, with a contact energy of $\sim 10^4 k_B T$, making them dominant in determining the particle structuring at the interface. [11, 12]

Cylinder shaped particles have also been investigated [13, 44–46]. For this shape the interface strongly curves upwards at the straight end faces and is slightly pressed down along the long edges (Figure 2.15a,b). The transition between the two is very abrupt. At large distances the behaviour will be similar to that of ellipsoids, while at short distances the particles strongly favor an end-to-end arrangement (Figure 2.15c,d). A strong concave-up background curvature aligns the particles parallel to the interface gradient, while for concave-down a perpendicular orientation is adopted (right panel of Figure 2.15). The former suppresses the deformations at the end faces, and therefore end-to-end arrangements, allowing side-to-side pairing.

Colloids as emulsifiers. When many particles are present in most cases they form dense, jammed layers at the interface, which can stabilize the interfaces of many microscopic liquid domains. Thus, particles can act as emulsifiers [40].

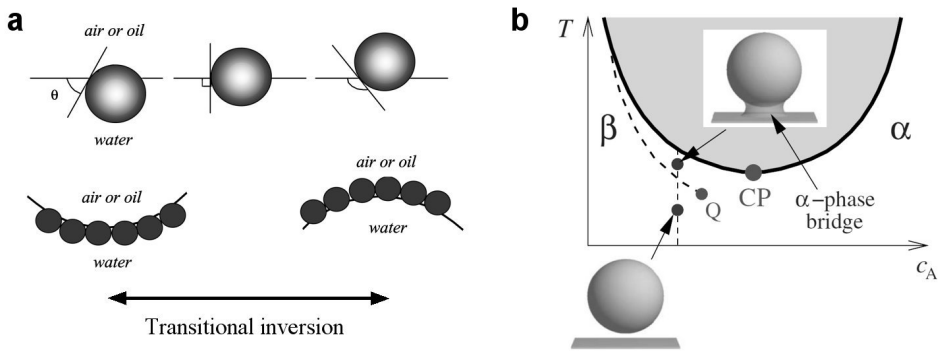

Figure 2.16 *(a) Preferred curvature of dense colloidal monolayers at a liquid interface. (b) The temperature-dependent formation of a liquid bridge between a particle and a flat substrate, shown situated in the binary liquid phase diagram. (Panel a taken from [49] and Panel b taken from [50])*

Droplet emulsions formed in such way are commonly referred to as Pickering emulsions after an early paper of Pickering [47], although it was Ramsden [48] who first noticed this potential of small solid particles.

Also here the contact angle is a very important parameter. First of all, the trapping energy (equation 2.14) depends on it, being maximum at $\theta = 90°$. Secondly, usually the particles are preferentially wetted by one of the liquids, into which they therefore extend to a larger degree (Figure 2.13a). For a densely packed layer of colloids this will make the interface curve towards the other liquid (Figure 2.16a), hence making it the more likely phase to be included in the droplet phase of a resulting emulsion. By changing the ratio of the liquids, however, the preferentially wetting phase can sometimes be the droplet phase when its volume is made sufficiently smaller than that of the other liquid. This is called catastrophic inversion, and will only occur for a moderate preference of the particles towards one of the liquids. Alternatively, transitional inversion takes place by changing the particle wetting, and thus the contact angle, so that the other liquid will preferably wet the colloids. There is no preferred curvature when $\theta = 90°$.

Pickering emulsions are kinetically stabilized against coalescence, relying on the particles at the interfaces. These colloidal monolayers at the interface are solid-like, as is evidenced by their ability to support very angular interfaces with extreme curvatures. Owing to this the emulsions often show long-term stability.

2.4.2 Colloidal interactions in partially miscible liquids

In partially miscible liquids, approaching liquid-liquid coexistence, 2 new types of interactions between colloidal particles are introduced even before they become trapped on any interfaces. A distinction can be made between an interaction induced by wetting, and an interaction induced by compositional fluctuations. Varying with temperature, they happen at different compositions, however, the crossover between them is indistinct.

Critical Casimir forces between particles arise from compositional fluctuations. It is the thermodynamic analog of the quantum-electrodynamical Casimir force first predicted theoretically in 1948. Compositional fluctuations are present when the temperature and composition of a stable liquid mixture is close to the critical point (Figure 2.6b). This becomes clear when looking at the free energy curve for $\chi = 2$ (Figure 2.6a), where instead of a well defined minimum, there is a flat plateau extending over a large range of compositions. As the fluctuations are confined between two colloidal particles, there will be a pressure caused by the fluctuations of the compositional field from outside pushing the particles together. The force can also be repulsive, which is the case when the 2 particles prefer different components at their surface. Recently, the critical Casimir force between a colloidal particle and a flat surface was directly measured, and also theoretically it has been studied in detail [50, 51].

A different effect comes into play when the composition deviates significantly from the critical composition. Here the prewetting line of Section 2.3.2 is encountered again (Figure 2.12). Namely, crossing the prewetting line, wetting films form at the colloid surfaces, which form a liquid bridge between particles when they coalesce. In experiments this was directly observed for a particle near a flat surface (schematically in Figure 2.16b). It must be noted that this effect only occurs when the colloid surfaces (strongly) prefer the minority component of the liquid mixture. Essentially, capillary condensation in narrow spaces between solid surfaces [52, 53] is analogous to this.

Of course, it is relevant to take the DLVO potential into account here. With the liquid composition near the colloid surface changing drastically, both electrostatic repulsions and Van der Waals attractions may change. Using DLVO theory, for a particular system the wetting layer was found to screen the long-range electrostatic repulsions [54]. The wetting films can then coalesce, upon which

electrostatic repulsion through the wetting phase itself might prevent the primary minimum from being reached. Temperature reversibility was indeed observed for this kind of colloidal aggregation, and was already regarded as an important feature in the early observations [55].

As a final remark, it is still unclear where the transition from critical Casimir to wetting-induced interactions occurs. One thing that most definitely is clear, is that colloidal aggregation can be mediated by partially miscible liquid mixtures close to liquid-liquid coexistence.

2.4.3 Colloidal silica

As is now clear, the wetting of colloidal particles is a crucial property when experimenting with colloids in partially miscible liquids. Having it as an easily adjustable parameter would therefore be extremely valuable; this is one of the attractive features of colloidal silica (SiO_2).

Synthesis. First, it is necessary to take a look at the preparation of colloidal silica, with a special interest in obtaining particles quite uniform in size and shape. The required control over the formation of particles is offered by a condensation (also often called precipitation) method. Its starting point is a molecular solution of which the solutes are forced to precipitate or polymerize, making them come out of solution in the form of colloidal particles. For silica particles several precursors exist, but the focus here will be solely on alkoxysilanes.

The Stöber method [56] is a well-k nown route to preparing monodisperse silica spheres. Here tetraethyl orthosilicate[1] (TEOS, or also known as TES, tetraethoxysilane) is used as a precursor in a mixture of aqueous ammonia and ethanol. TEOS hydrolyzes as [57]

$$\mathrm{Si(OC_2H_5)_4 + nH_2O \longrightarrow Si(OC_2H_5)_{4-n}(OH)_n + nC_2H_6O},$$

after which polymerization of partially hydrolyzed TEOS molecules takes place through condensation reactions like

$$\mathrm{(OR)_3Si{-}OH + HO{-}Si(OR)_3 \longrightarrow (OR)_3Si{-}O{-}Si(OR)_3 + H_2O},$$

$$\mathrm{(OR)_3Si(OR) + HO{-}Si(OR)_3 \longrightarrow (OR)_3Si{-}O{-}Si(OR)_3 + C_2H_6O},$$

[1] TEOS is most common. Other alkoxysilanes have been investigated as well [56].

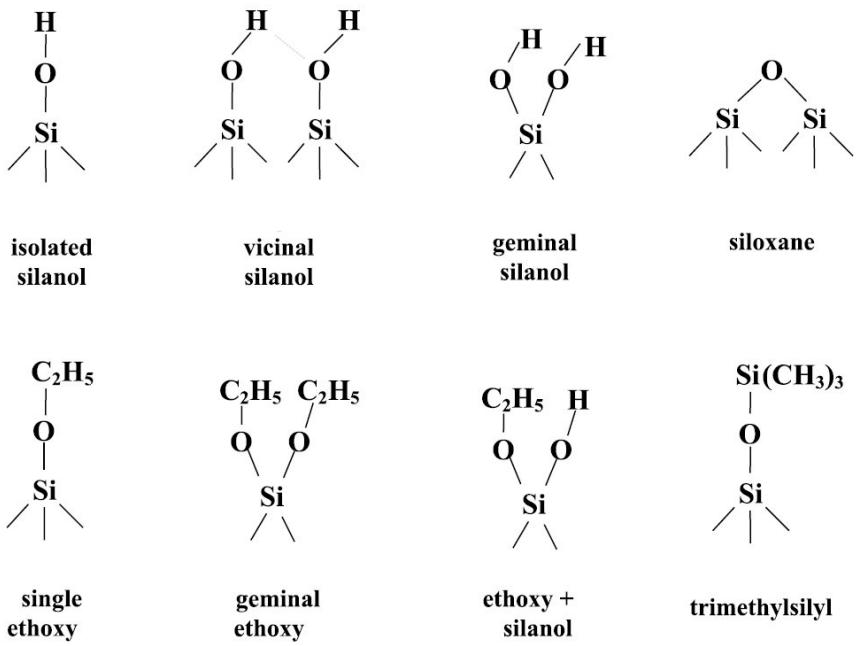

Figure 2.17 *Various chemical groups that can be present on the surface of a silica particle. All except the TMS group are possible directly after synthesis. TMS groups can result from a reaction of HMDS with silanol groups. Taken from [60].*

where R = C_2H_5. Ammonia simply acts as a catalyst in this process. The method gives good control over particle size, and there is extensive literature documenting the effect of various conditions on the resulting particles. For example, gradual further growth can easily be achieved by the addition of TEOS to already formed particles in ethanol/ammonia.

Fluorescent labeling of Stöber silica particles for experimental purposes is straightforward. A linker molecule, (3-aminopropyl)triethoxysilane (APTES), is used for this. Compared to TEOS, APTES simply has one of the ethoxy groups substituted by a short alkyl chain terminated with an amine group. An addition reaction of the amine group with an thioisocyanate group of some specific fluorophores results in a covalent bond between the linker and dye. The reaction product will be incorporated in the particles when present during formation of silica particles by the Stöber method, fluorescently labeling them. [58, 59] Samples prepared with these can be conveniently studied with fluorescence (confocal) microscopy to specifically observe the labeled particles.

Surface chemistry. A crucial property of the silica particles is their surface chemistry. It sets the surface energy of the interface between particle surface and a liquid, and therefore determines particle wetting. Additionally, the presence of

charged, and therefore ionizable, chemical groups at the surface is required for colloidal stability.

After synthesis in ethanol/ammonia the chemical composition of the surface already consists of a large variety of functional groups. Especially important are several types of hydrophilic silanol groups (top row of Figure 2.17), which dissociate at higher pH (already at pH $> \sim$2 in water) to give a negatively charged surface. In too basic environment, however, silica is known to dissolve [61]. More hydrophobic ethoxy groups can be present as well after synthesis (bottom row of Figure 2.17). [60]

Subsequent dispersing solvents can significantly change the surface chemistry. Aqueous dispersions show aging effects like an increasing pH. [57] Under these conditions it is likely, for instance, that ethoxy groups are removed from the surface, resulting in new silanol groups. Additionally, particles are often stored in one solvent (usually ethanol) only to be used later in other solvents when performing experiments. In the transfer from one to another solvent particles are sometimes dried and subsequently re-dispersed. As silica is notoriously hygroscopic, there will exist a layer of physically adsorbed water at the particle surface. The drying is therefore another determining step, and can, depending on temperature, even combine silanol groups into siloxane groups. [62]

The reactive nature of silanol groups also allows easy modification of the surface chemistry. Many silane coupling agents, like the previously encountered APTES, exist that can on one side be hydrolyzed to form reactive silanols, while also carrying another functional group that is to be attached to the silica surface. As a result, the chemical and physical properties of silica surfaces can be varied to a huge extent. A particular way of adjusting particle wetting is by replacing silanol groups by trimethylsilyl (TMS) groups (Figure 2.17) to a controlled extent. In apolar solvents, where silica particles aggregate due to a lack of charge-stabilization, this can be done using dichlorodimethyl silane (DCDMS) [63]. Using hexamethyl disilazane (HMDS), however, it can be done in the ethanol/ammonia mixtures familiar from the Stöber method, where particles are stably dispersed [60]. This has been successfully applied to precisely tune particle wetting in partially miscible liquids [64].

Results I

Versatile core-shell colloidal rods

Chapter 3

Synthesis of akaganéite-silica core-shell rods

A method to synthesize of akaganéite-silica core-shell rods is described in this chapter. The first step consists of the preparation of needle-like akaganéite particles that act as the core, which was investigated in some details to optimize the product for this purpose. Secondly, a silica shell is grown around them. The effect on the particle dimensions and aspect ratio are discussed, as well as fluorescent labeling.

3.1 Introduction

Colloidal particles are often seen as building blocks of materials, so their properties are crucial. One of the key properties that underly their particular behaviour, is the particle shape. Most commonly encountered colloids are spherical, but currently a whole wealth of differently shaped particles can be synthesized. [3, 6, 7]

Possibly the most obvious anisotropic shape is a rod, with its anisotropy being described by the aspect ratio of length-to-diameter (L/D). Rod-like colloids, and suspensions thereof, have already been the subject of extensive investigations due to the great variety of extremely shape-specific behaviour. Stable suspensions of rods show a rich phase behaviour. Namely, lyotropic liquid-crystalline phases, like nematic and smectic, can be formed by orientational ordering of the rods on

entropic grounds. For hard rods this was predicted theoretically by Onsager [8] and phase diagrams have nowadays been computed [27]. Experimentally these phases have been observed as well, even including cholesteric phases [65–69].

Also for disordered structures consisting of rods, formed by attractive interactions or jamming, the particle shape has significant consequences [9]. Both random packing volume fraction and the percolation threshold decrease with increasing aspect ratio [70–72]. Rods can therefore allow the formation of structures with relatively low densities. As building blocks, overall, rod-like particles contribute to a solid-like mechanical response. This feature is often exploited in materials encountered in nature and industry.

Furthermore, when confined to liquid-liquid interfaces, rod-like particles behave distinctly different from spherical particles [12, 43]. This originates from strong capillary interactions and frustration in dense 2D packings [14, 73]. Possibly related to this, rods were reported to act as more effective emulsifiers than their spherical counterparts [11]. Alternatively, it was suggested that their shape might facilitate the initial attachment to the interface.

Clearly, in a composite material, replacing constituent spherical particles by rods will open up a route to tuning properties. An interesting option would be a bijel [18, 74], where colloids are trapped on a percolating liquid-liquid interface. These materials require the wetting characteristics of the particles to be finely tuned. Investigating the effect of particle aspect ratio on bijel properties, also demands large quantities of particles with adjustable aspect ratio. While these are the main concerns, micron sized particles would be convenient to allow direct visualization of the rods jammed together on the interface.

A first step is to find a way for preparing colloidal rods that fulfills all of these demands. For the purpose of controlling the wetting characteristics of particles, experiments so far have employed silica particles, whose surface chemistry can easily be modified. Previously, silica rods and ellipsoids have been prepared by adding a silica coating onto anisotropic inorganic particles [75, 76], and recently methods for directly preparing silica ellipsoids [77, 78] and rods [79] have been reported.

After initially considering some of these existing methods, a method for the preparation of the required colloidal rods, that better suited the situation, was developed. The latter provides an easy route to prepare μm-sized core-shell rods on a large scale, by taking a specific type of iron oxide particles as the template

for growing rod-shaped silica.

For the iron oxide cores, akaganéite (β-FeOOH) particles are prepared via the forced hydrolysis of a ferric chloride solution, which is a simple method known to produce elongated particles [80]. In general, suspensions of small akaganéite particles with relatively low aspect ratios (<10) have been investigated, mainly in the context of (liquid crystalline) ordered structures [81–83]. In studies of this forced hydrolysis method, they are often reported as an intermediate or precursor for hematite colloids, with the transformation taking place via a dissolution-reprecipitation mechanism [84]. In this process, akaganéite precipitates first due to its lower energy of nucleation, but ultimately dissolves in favor of the formation of hematite. However, at higher Fe(III) and Cl^- concentrations, akaganéite nucleation is favored, effectively suppressing the formation of hematite [85], and, under these conditions, particles with much larger aspect ratios are obtained [80]. The latter is also shown in more-recent studies for increasing ferric chloride [86] and hydrochloric acid concentration [87, 88] and is linked to the concentration of Cl^- ions which adsorb selectively on the crystal faces, directing anisotropic growth. At high ionic strength the high-aspect-ratio needles are generally found aggregated in rafts that act as templates to form cube-like hematite particles [84, 89]. This aggregation can be fatal for the formation of well-dispersed needles required for preparing core-shell rods. Therefore, the forced hydrolysis method is then investigated in some detail to find optimal conditions for obtaining a high yield of well-dispersed high-aspect-ratio needles to prepare suitable template particles.

An existing method [90] is used for seeded growth of a silica shell around the template particles. This reduces the aspect ratio with increasing shell thickness, introducing a way of adjusting the aspect ratio, as done previously for ellipsoids [75]. In this case, the high aspect ratio (20-30) of the akaganéite needles aids in keeping a fairly high aspect ratio of the final core-shell rods. Apart from the silica shell allowing wetting characteristics to be controlled, it can also be labeled with a fluorescent dye for use with CLSM.

Below, after detailing the experimental methods, first the initially considered methods are briefly discussed. This is followed by a detailed investigation and discussion of the preparation of core-shell rods. Finally, conclusions and outlook close this chapter.

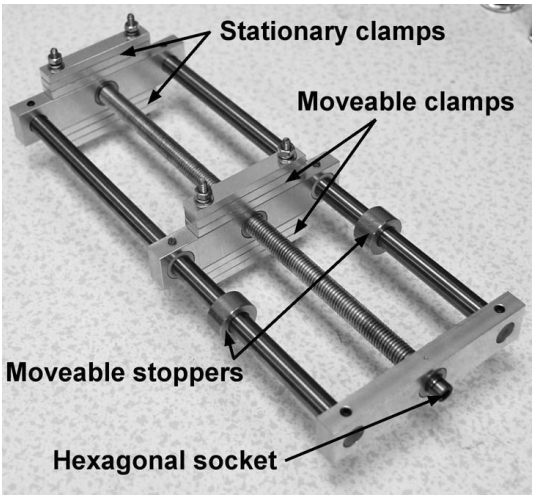

Figure 3.1 *Device for mechanical stretching of polystyrene particles embedded in a PVA film.*

3.2 Experimental section

Materials

Iron (III) chloride ($FeCl_3$, reagent grade 97%), tetraethyl orthosilicate (TEOS, reagent grade 98%), poly(vinylpyrrolidone) (PVP, average M_w = 40 kg/mol), (3-aminopropyl) triethoxysilane (APTES), Poly(vinyl alcohol) (PVA, Mowiol 40-88, average M_w = 205 kg/mol), and fluorescein-isothiocyanate (FITC, Isomer I, 90%) were obtained from Sigma Aldrich and used as recieved. Hydrochloric acid (fuming, 37%), ammonium hydroxide solution (35%) of reagent grade were obtained from Fisher and ethanol (absolute) and isopropyl alcohol (analytical reagent) from VWR. Distilled water was used for synthesis.

Polystyrene ellipsoids

A suspension of spherical, uncrosslinked polystyrene particles (0.55 wt%, lab code: ASEAP10), charge-stabilized by sulfonate groups, in an aqueous PVA solution (4.5 wt%) was prepared first. This suspension (∼260 mL) was spread onto a flat surface (∼800 cm^2), and left to dry overnight to result in a solid film with a thickness of about 0.1-0.15 mm. The film was cut into strips of 4 by 6 cm, which were mounted in a stretching device[1] (Figure 3.1), 6 at a time. On one end the

[1]Constructed by Derek Low

films were fixed in a stationary clamp, and on the other end in a moveable clamp (each clamp taking up 0.5 cm of the length of the film, over its full width). This setup was then immersed in an oil bath at 150-160 °C, and, to stretch the polymer films, the moveable clamps were driven through turning a screw thread with an electric screwdriver. For the latter, one end of the screw thread had a hexagonal socket to fit a hex key. The end position of the moveable clamps was fixed by stoppers, which could be moved around to set the stretching ratio (initial-to-final distance between the stationary and moveable clamps). After stretching the films, the setup was removed from the oil bath, and allowed to cool down. As much excess oil as possible was then removed from the polymer film with paper tissues.

Of the stretched polymer films, parts fixed to, and near the clamps were discarded. Only the straight, middle parts of the stretched films were used to recover particles from. These were cut into little pieces, and washed with IPA to remove residual oil. The polymer matrix in which the particles were embedded was dissolved in a stirred solvent of 30% IPA in water, heated to 80 °C, for 30 minutes. This was repeated 3 times to ensure sufficient removal of the PVA. Then particles were washed several times with water.

Akaganéite template particles

Concentration series

Solutions of varying [$FeCl_3$] and [HCl] were prepared by dissolving $FeCl_3$ in appropriate amounts of a 0.5 M HCl solution and topping up the solution to 25 mL with distilled water. The solutions were filtered (Whatman, qualitative) to remove impurities and stored in tightly sealed vials. The vials were then placed in a preheated oven (Binder, set to 121 °C) at 98±1 °C. After 24 hours the vials were removed from the oven, quenched to room temperature under a running tap and the particles were washed several times with distilled water.

Upscaled synthesis

A 500 mL solution of 0.6 M $FeCl_3$ and 0.07 M HCl was made up in a 500 mL pyrex bottle. First, $FeCl_3$ was dissolved in 100 mL water after which hydrochloric acid (fuming, 37%) was added, followed by water to top up to a total volume of 500 mL. The solution was passed through a filter (Whatman, qualitative) to remove

impurities. This was aged in an oven at 98±1 °C, or in an oil bath (100±2 °C) whilst gently being stirred (300 rpm) using a magnetic stirrer bar. Afterwards, the mixture was cooled down under a running tap and the particles washed several times with distilled water. After aging in the oven a layer of solid material is present on top of the hot solution; in later syntheses this is poured off together with as much of the hot supernatant as possible.

Silica coating

Typical silica coating. Akaganéite particles were dispersed (2.5 mg/mL) in a 100 mL aqueous PVP solution (55 mg/mL). This was sonicated for a few hours (VWR sonic bath) and left to stir over night. The particles were subsequently spun down at 2000 rpm for 1 hour and redispersed in 180 g ethanol by sonication. 14.6 g of ammonium hydroxide solution (35%) was then added, followed by a 1:1 (v/v) TEOS/ethanol mixture via 0.75 mL additions (dropwise and under stirring) with intervals of 20-30 minutes to ensure the growth of a smooth silica layer and avoid secondary nucleation. The amount of added TEOS was used to vary shell thickness and, typically, 8 additions resulted in a shell thickness of about 90-100 nm for seed particles prepared using heating in an oven and about 50 nm for the smaller particles prepared using heating in an oil bath. After all TEOS additions the mixture was left overnight under stirring. The particles were washed multiple times with ethanol and distilled water. For a fluorescent silica shell the procedure was essentially the same as described above. The pure ethanol in the mixture used to add TEOS was now replaced by a solution of FITC (0.66 mM) and APTES (0.17 M) in ethanol which had been stirred overnight in the dark to covalently attach the FITC to APTES. Another difference was the addition of extra PVP through a 25 mL addition of a solution of PVP in ethanol (100 g/L) after 4 TEOS additions.

Fluorescent cores. Core-shell particles with a fluorescent inner layer in the shell were prepared via a 2-step silica coating. Akaganéite particles were stabilized with PVP and subsequently transferred into ethanol (160 g) as described above. Then, 14.6 g ammonium hydroxide solution (35%) was added, followed by 2 additions (with a 30 minute interval) of a 0.75 mL ethanol/APTES/FITC/TEOS mixture (concentrations as described above), dropwise and under stirring. For the first 2.5 hours the mixture was sonicated (while preventing it from heating by regularly replacing the water in the ultrasonic bath), and a PVP solution (0.1 g/mL in

ethanol) was added 2 hours after the first TEOS/dye addition. The mixture was then left under stirring overnight. The next day the particles were washed, typically first once with ethanol and then several times with water until a neutral pH was obtained (and no dye appeared present in the supernatant anymore). For the following coating with plain silica the particles were transferred into PVP/ethanol (160 g, 0.65 wt% PVP) and left under stirring overnight. The rest of the silica coating proceeded similar to described above, adding 13.6 g ammonium hydroxide solution (35%), and 8 additions (30 minute intervals) of 0.75 mL TEOS/ethanol (1:1 v/v), with after the 4th addition a mixture of 1.5 g PVP, 1 g ammonia (35%), and 12 g ethanol. This was left overnight, and the particles were then washed several times with ethanol. To ensure no PVP was at the particle surface, a thin silica layer was coated onto the particles (0.74 g rods, 140 g ethanol, 11.5 g ammonia (35%), 0.3 mL TEOS). Particles were washed several times with ethanol, in which they were finally stored.

Characterization

To determine approximate yields cleaned suspensions were dried in weighed vials (50 °C under vacuum overnight), after which the mass difference was used to determine the mass of the particles. X-ray diffraction (XRD) measurements of products were performed using a Bruker D2 Phaser powder diffractometer (Cu Kα radiation (λ = 1.5406 Å), 2θ range 5-70°, 0.33°/s) on particles deposited on a glass slip by drying of a concentrated suspension, and a Bruker D8 advance powder diffractometer (Cu Kα radiation (λ = 1.5406 Å), 2θ range 5-90°, 0.1°/min) on a ground down powder transferred into a glass capillary. The results were compared to diffraction patterns from the powder diffraction file to find the best match. For inspecting particle morphology and determining size distributions TEM micrographs (Philips/FEI CM120, typically operating at 80 kV) were taken. A drop of dilute suspension (in water for akaganeite particles and ethanol for core-shell and hollow particles) was dried on a 200 mesh copper grid coated with a formvar/carbon support film. For the particle size and aspect ratio (A) distributions of a sample the length L and diameter D of 250-300 particles were measured by hand using ImageJ [91]. Polydispersities were defined as the ratio of the standard deviation (σ) to the average: $s_L = \sigma/L$, $s_D = \sigma/D$ and $s_A = \sigma/A$.

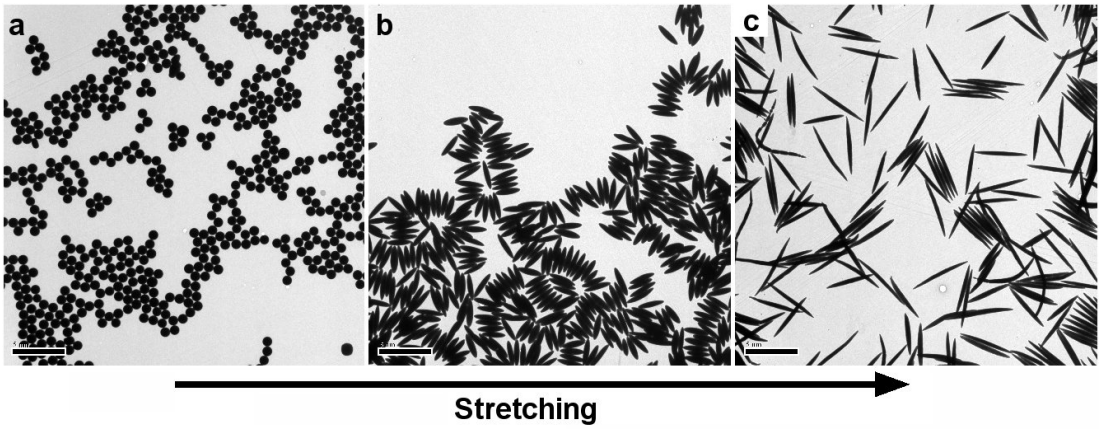

Figure 3.2 *(a) Polystyrene spheres which were elongated by stretching the polymer films in which they were embedded at a stretching ratio of (b) 3 and (c) 5. Scale bars are 5 μm.*

3.3 Finding suitable colloidal rods

In the early stages of the project various routes to rod-like colloids were considered, in order to find one that best suited the requirements. One of them was a method [92] where spherical polymer particles (Figure 3.2a), embedded in a solid film of another polymer, were stretched into ellipsoids (Figures 3.2b,c). Here the softening of both polymers above their glass transition temperature (T_G) is used to allow this, so uncrosslinked particles are required. Recovery of the stretched particles to again obtain a suspension, is achieved by dissolving the polymer matrix in which they are embedded.

Conveniently, selecting the spherical particles fixes the particle size, and by setting the stretching ratio the final aspect ratio of particles can be controlled. Using fairly monodisperse spheres, and only the uniformly stretched parts of the polymer film, produced ellipsoids are also quite uniform. Obtained aspect ratios roughly agree with what can be expected from the applied stretching ratios, from having particles with a fixed volume. A stretching ratio of 3 would theoretically result in an aspect ratio of 5.2, and an aspect ratio of 5.0 is found experimentally. Comparing theory and experiment for a stretching ratio of 5 gives aspect ratios of 11.2 and 11.6, respectively. This latter stretching ratio is practically the limit, as is suggested by the presence of some oddly shaped particles, indicating they become structurally unstable.

A considerable disadvantage of this method is that it is very labour intensive and yields fairly small amounts of particles. Upscaling the method, a single

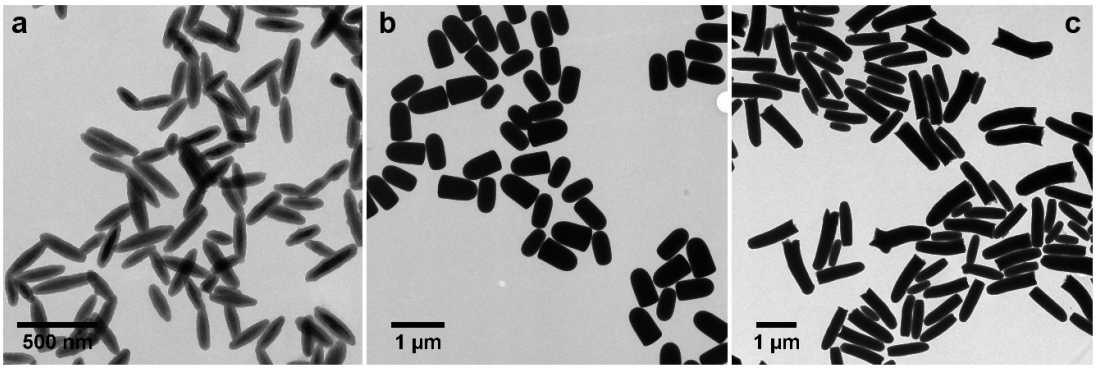

Figure 3.3 *(a) Silica coated hematite ellipsoids, and (b and c) silica bullets.*

batch requires a few stretching runs and, depending on the stretching ratio, yields several hundred milligrams of particles. Additionally, the uncrosslinked polystyrene particles dissolve in some organic solvents, which are often one component of the partially miscible binary liquids they are intended for use with. Also for the required possibility of surface chemistry modification, it would be necessary to coat them with silica. A well-established method for this exists, and initial attempts resulted in very rough coating, instead of an intended smooth layer. Overall, this means adding another step to an already time consuming method. Ultimately, keeping in mind that their intended use requires frequent experiments with large quantities of particles, the yield of this method did not justify the effort of producing them.

An alternative is offered by silica-hematite core-shell ellipsoids[2] [75] (Figure 3.3a). Preparation of the hematite cores is a straightforward chemical procedure, that can easily be scaled to produce large quantities of particles. Their dimensions do limit the range of achievable aspect ratios to <6, after addition of the silica shell by the same method as mentioned above. Overall, these core-shell particles are quite uniform, but smaller, and more dense than the polystyrene ellipsoids.

At the time, a paper appeared on the direct synthesis of bullet-like silica rods [79]. These grow from the interface of aqueous emulsion droplets containing a high concentration of polymer (PVP), which feed the growing silica particle with reactants from one side to result in anisotropic growth. By adjusting parameters the length of the rods can be tuned, while the diameter remains fairly constant, to give control over aspect ratio up to high values. Since the rods end up covered with PVP, they require an additional silica coating, which allows them

[2]Provided by Prof. Jan Vermant

to be fluorescently labeled. Attempts[3] to prepare rods of aspect ratio ∼10 with this method yielded short (aspect ratio <2), and oddly shaped rod-like particles (Figures 3.3b,c).

3.4 Akaganéite-silica core-shell rods

Instead of settling for one of the above colloidal rods, a possibility for developing a new route to suitable rods was found, and subsequently pursued. It, first of all, seemed to have great potential due to the simplicity and versatility in preparing rods at a high yield. Secondly, the resulting particles, consisting of a needle-like akaganéite core buried within a silica shell, could be prepared with relatively high aspect ratios, and had dimensions that allow direct observation by optical microscopy.

Akaganéite cores

The formation of akaganéite needles by forced hydrolysis of a ferric chloride solution was investigated in order to find optimal conditions for preparing a good yield of well dispersed needles to use as templates for micron sized silica rods. A series of aqueous solutions at varying [$FeCl_3$] and [HCl] were aged at a single temperature (100 °C) and for a fixed time (24 hours) to explore the effect of the concentrations on the products. All gave a dense sediment that after washing is easily dispersed in water with the resulting yellow-brown suspensions showing a strong flow birefringence. The IEP of these particles is pH ∼7.4, with the particles being optimally charged at pH < 4 (positive) and pH > 10 (negative) [80, 93], but no difference was noticed in particle stability between dispersions in distilled water (pH 6) or at high/low pH. High concentrations of Fe(III) and Cl^- ions in the aged solutions promotes the formation of akaganéite over hematite [85], and X-ray diffraction patterns[4] (Figure 3.4, bottom) indeed closely match that of synthetic akaganéite from the powder diffraction file (JCPDS 34-1266). Particles orient themselves parallel to the surface of a flat substrate when they are deposited by evaporating the liquid of a dense suspension. This is demonstrated by measurements in reflection mode on such samples (Figure 3.4, top), which now miss diffractions of the planes containing the 001 direction (the growth direction

[3]By Dr. Andy Schofield
[4]Performed by Dr. Gary Nichol

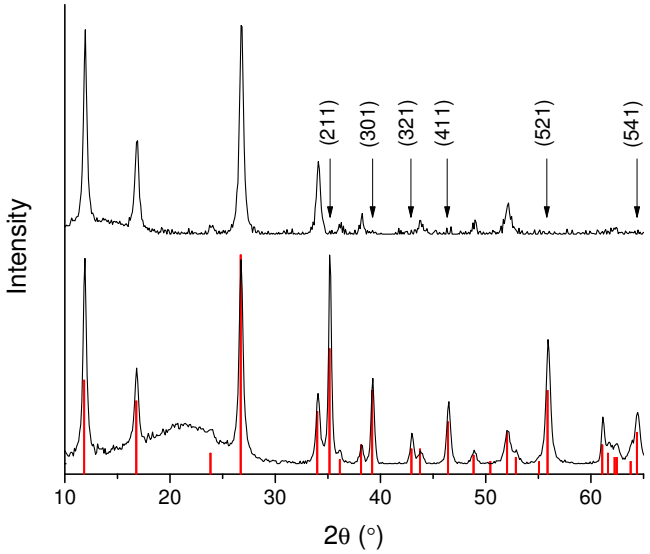

Figure 3.4 *Powder X-ray diffraction patterns of S5 (see Table 3.1) dried, ground down and well packed in a capillary (bottom) and of particles deposited onto a glass slip by drying a concentrated suspension (top). Arrows indicate missing diffractions due to the preferred orientation of the needles parallel to the substrate in the latter case. The reference data from the powder diffraction file are shown in red.*

of the long axis [84]) due to particles being oriented perpendicular to the wave vector transfer.

Particle yield strongly depends on the two concentrations used (Figure 3.5a). It rapidly decreases with increasing [HCl] and [$FeCl_3$], suggesting that this is related to the decreasing pH, typically with only very few particles forming at [HCl] > 0.1 M and [$FeCl_3$] > 1 M. Saturation concentrations of Fe(III) ions are much higher at low pH [84], so the concentration quickly drops below the saturation value stopping further precipitation. Another factor possibly involved in the observed trends may be dissolution of the needles (evidence for this is reported later), which could be related to the non-monotonic decrease in yield with [$FeCl_3$]. Recovery of the yield at higher [HCl] for 0.6 M [$FeCl_3$] appears a genuine observation and could be due to the balance between dissolution and (re-)precipitation of akaganéite.

A second effect observed in initial samples, is the strong, or even irreversible, aggregation into dense bundles of more or less aligned needles. This needed to be minimized to obtain suitable template particles for preparing well-defined core-shell rods. Bundling becomes evident after silica coating (discussed later in this section), when not individual needles, but instead mainly bundles of needles are coated (Figure 3.5b). More thorough attempts to disperse and stabilize particles

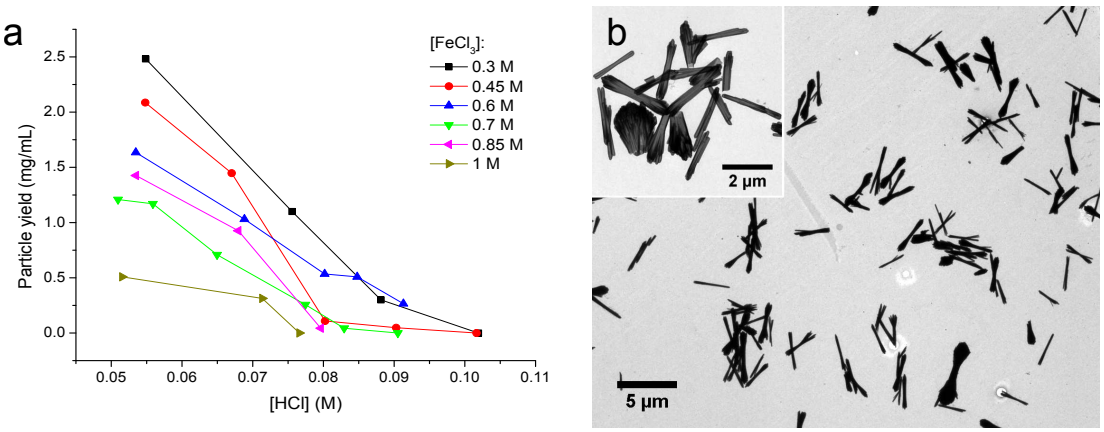

Figure 3.5 *(a) The dependence of the particle yield as a function of [HCl] for various $FeCl_3$ concentrations, and (b) core-shell particles made using template particles prepared at 0.45 M $FeCl_3$ and 0.03 M HCl, with hollowed out silica shells as inset, showing bundling of the rods.*

prior to, and during, coating by sonication or changing the pH of the aqueous PVP solution appeared futile. This bundling is likely to be similar to parallel aggregation of akaganéite rods into rafts, encountered in similar experiments, which act as templates for the formation of hematite cubes [84, 89]. At any point during the formation of the particles the ionic strength is very high, so there will be no barrier preventing the otherwise charge-stabilized particles from aggregating. Like most iron oxide particles the akaganéite needles are expected to have a high Hamaker constant in water (α-Fe_2O_3: $A_h \approx 6{\cdot}10^{-20}$ J [94], γ-FeOOH: $A_h \approx 5.5{\cdot}10^{-20}$ J [95]), resulting in strong van der Waals forces. Particles are most strongly bound when the contact area is large, probably explaining why in the coated aggregates the long axes of the needles are parallel, while the rods being rectangular rather than cylindrical [80] also aids in having a large contact area. The occurrence of aggregation in the formation of the particles is thus far from surprising, and according to this reasoning it is conceivable that some particles may become so strongly bound that they are not re-dispersed by the employed methods.

Alternatively, a more speculative possible origin of the bundling is the floating solid layer formed on top of the heated solutions. Since it was never completely prevented from mixing with particles formed in solution, its effect on the final product is unclear. In the case of agitating the heated solutions, whatever solids result from processes at the liquid-air interface these are automatically mixed-in with the main product. Evaporation will likely be involved, but also quite possibly the growth of particles, which will proceed under conditions different to

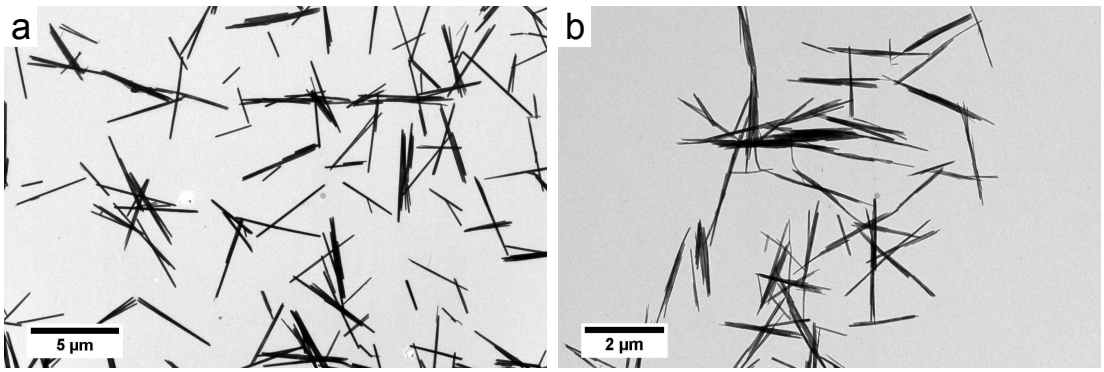

Figure 3.6 *Representative TEM images of akaganéite needles prepared by aging in (a) an oven (sample S1), and (b) in an oil bath (sample S5).*

those in the bulk solution.

Bundling is found to be minimized by increasing both ferric chloride and hydrochloric acid concentrations (Figure 3.6a) of the aged solutions. Here, the high Fe(III) concentration is probably responsible for the increased particle size. A decrease in the presence of aggregates with increasing ionic strength is somewhat counterintuitive. However, in all samples the ionic strength is very high, so a further increase of the concentrations will not affect the possibility of aggregation. We expect the decreasing bundling to be related to the increased Cl^- concentration, due to its adsorption onto the particle surface, making it less likely for particles to aggregate irreversibly. There might also be an effect of the lower pH of the solutions, but this was not checked independently. Agitating the solution during aging (discussed in more detail below) increases bundling, probably due to orthokinetic aggregation (Figure 3.6b). This might suggest that the presence of more Cl^- does actually introduce some barrier preventing the irreversible aggregation, which is overcome more easily by providing some kinetic energy (by stirring) to the particles.

Ideally the irreversible bundling of the needles in oven-aged samples, is minimized while still obtaining a good yield. To meet these criteria samples prepared at higher concentrations are of interest: 0.45 M $>$ [$FeCl_3$] $>$ 1 M and 0.05 M $>$ [HCl] $>$ 0.09 M. TEM images (see Figure 3.6a for a representative image) show that products are very similar with no significant differences in terms of bundling. Average particle lengths are around 3 μm and average particle diameter about 100 nm, giving average aspect ratios of $\sim$30. The spread in particle length, and therefore that of the aspect ratio, is large and polydispersities around 40% are found. Surprisingly the aspect ratio distributions in many of the analyzed samples

Table 3.1 *The effect of heating method, volume and time on resulting particle yield, average particle dimensions (with polydispersities s) and aspect ratio for aging a 0.6 M [$FeCl_3$] / 0.07 M [HCl] solution.*

Sample	Heating method	Volume (mL)	Time (h)	Yield (mg/mL)	L (s_L) (μm)	D (s_D) (μm)	A (L/D)
S1	Oven	25	24	1.03	2.71 (0.44)	0.11 (0.31)	24.1
S2	Oven	500	24	1.22	3.53 (0.30)	0.12 (0.34)	29.5
S3	Oven	500	16	0.39	3.22 (0.30)	0.12 (0.39)	26.6
S4	Oil bath	500	24	1.28	1.46 (0.46)	0.06 (0.46)	23.4
S5	Oil bath	500	16	1.51	1.48 (0.37)	0.06 (0.38)	26.0
S6	Oil bath	500	8	0.95	1.92 (0.31)	0.08 (0.28)	22.7

are found to be bimodal (Figure 3.8, "bare"). This bimodality (discussed in more detail later) is more pronounced in some samples than others and originates from the length distribution which shows the same feature.

Scaling up and modifying the aging procedure

To scale up the yield, the synthesis was performed at a larger volume (500 mL), and some aspects of the aging procedure were varied for fixed concentrations and temperature. Concentrations of a sample from our previous experiments which resulted in little bundling and a good yield (0.6 M $FeCl_3$, 0.07 M HCl) were identified and the effect of varying the aging procedure on the product was investigated (Table 3.1).

The samples aged in an oven show significant differences in both particle length and yield (Table 3.1). The primary effect of the increased volume will be the decreased heating rate, resulting in the solution effectively aging for a shorter time at the final temperature. With the previously reported dissolution-reprecipitation mechanism [84] in mind, this would suggest that the higher yield and larger particle length of S2 is related to the dissolution of akaganéite having progressed less far, whereas for S3 most of the nucleation and growth still needs to take place. The effective dissolution at later times, as evidenced by the decreasing yield and particle size, would be a result of the Fe(III) concentration dropping and causing the dissolution rate to overtake the precipitation rate.

A curious feature of the length distributions that underlies the observed changes in average particle length, is the emergence of a bimodality (Figure 3.7a). Increasing the aging time from 16 hours (S3) to 24 hours (S2) results in the distribution

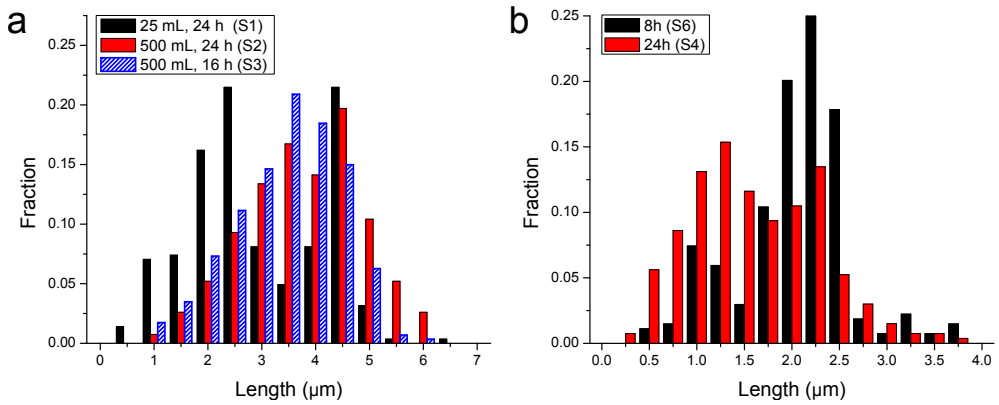

Figure 3.7 *Comparison of particle length distributions of samples in Table 3.1: S1, S2, S3 (a) and S4, S6 (b).*

changing from a monomodal distribution to a distribution that slightly hints at bimodality. The sample with the smallest volume (S1), and effectively the longest aging time, shows a clear bimodal distribution. While the time-evolution of the length distribution is correlated with trends in yield, the relationship between the two is not yet understood.

Since aging solutions in an oven without agitation allows particles to settle into a dense sediment, and will not be a very homogeneous process in terms of temperature and solute concentrations, the effect of agitating the solution while aging was investigated. Solutions were aged in an oil bath to allow homogenization by stirring at low speeds, which in addition increases the heating rate. This results in higher yields at shorter times and smaller particles (Table 3.1). TEM images (Figure 3.6b) reveal a product looking more 'fibrous' and, as discussed earlier, appearing more bundled. Again the yield is found to decrease upon prolonged aging, occurring when extending aging from 16 to 24 hours, indicating the effective dissolution of akaganéite. Particle length distributions are bimodal (Figure 3.7b), confirming that this is not just an effect of the particles ending up in a dense sediment when heating solutions in an oven.

These results clearly show that the aging time has a pronounced effect on the yield and the size distributions of the obtained particles. The change in yield can be understood in terms of the changing balance between dissolution and precipitation. What exactly is the mechanism behind the evolution of the length distribution, which could be slightly different for the 2 heating methods, remains unclear. It is unknown whether the emergence and growth of a peak at smaller lengths, which accompanies the decreasing average length and yield, is exclusively the result of the dissolution of larger particles, while growth maintains part

of the population at larger length, or if nucleation is involved as well. Such mechanisms are most likely to result in a continuous distribution of lengths - in contrast to our observations. Nucleation at a later stage seems unlikely since the Fe(III) concentration can be expected to have dropped sufficiently to suppress it completely. A non-uniform dissolution and growth of particles therefore appears the most sensible explanation at this point, which also fits in with the dissolution-reprecipitation mechanism, but the involvement of nucleation cannot be ruled out.

Silica shells

The main challenge in coating iron oxide particles with a silica shell via the Stöber process [56] is preventing aggregation before or during the shell growth [96]. Similarly, the akaganéite needles appear stable in ethanol, but are destabilized and flocculate rapidly upon addition of ammonia. An adsorbed layer of PVP [90] as steric stabilization was previously found to be an excellent solution to prevent aggregation [75]. This is also found true here and we were able to grow a silica shell of fairly homogeneous thickness around template particles, resulting in core-shell rods (Figures 3.8a&b, contrast with Figure 3.5b). The bundling was not completely removed and still occurs to a small extent, but it does not have a strong effect on the rod-like morphology of the final core-shell particles. Adding a shell onto the template particles prepared by aging in an oil bath results in more irregular rods for thinner shells (Figure 3.8d) due to the increased bundling, while increasing shell thickness nicely smooths out irregularities (Figure 3.8e). A striking effect of the added silica coating is that it significantly increases particle stabilization. This is confirmed by bright-field microscopy of particles in dispersion (images not shown), where in aqueous suspensions of uncoated needles small aggregates are observed to be a regular occurrence, while this is not the case for the core-shell rods. It is also evident from TEM images where coated particles are generally better separated compared to bare particles.

Detailed characterization of the particle dimensions from TEM images reveals how these are affected by the silica shell. As expected, most significant is the effect of the silica coating on the aspect ratio (Figures 3.9 and 3.8c). The relative increase of the particle diameter is much larger than that of the particle length, resulting in a rapid decrease of the aspect ratio with shell thickness. Since the shell thickness is fairly homogeneous around the particles, the aspect ratio of

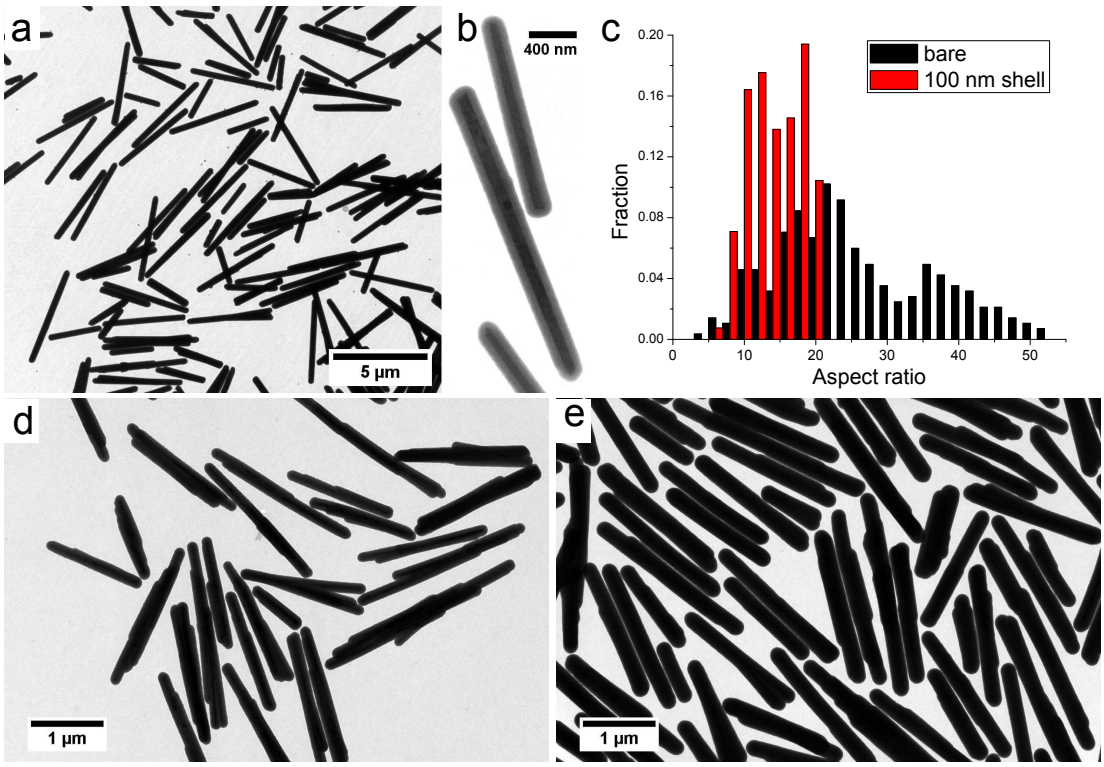

Figure 3.8 *(a) A representative TEM image of akaganéite needles (S1) coated with a 100 nm silica shell. (b) A zoomed-in image reveales the core-shell structure, and (c) the corresponding aspect ratio distributions. The bottom row shows smaller akaganéite needles (S5) prepared by aging in an oil bath coated with a (d) 55 nm, and (e) 90 nm silica shell.*

particles is expected to roughly decrease as

$$A = \frac{L + 2x}{D + 2x} \tag{3.1}$$

where x is the shell thickness. Figure 3.9 shows that the aspect ratio obtained from TEM images agrees quite well with this model. The decrease of the aspect ratio however is consistently slower than expected. The inset graph in Figure 5 show that this is due to the average length increasing ($\sim$13%) more than expected while the particle diameter nicely follows the expected trend. While the thickness of the shells at the tips of the particles is much less consistent compared to that at the sides, the observed increase in average particle length will primarily originate from fractionation. This most likely occurs when spinning down particles from the aqueous PVP solution, where the supernatant is often still turbid indicating that small particles are discarded when transferring the PVP stabilized particles into ethanol.

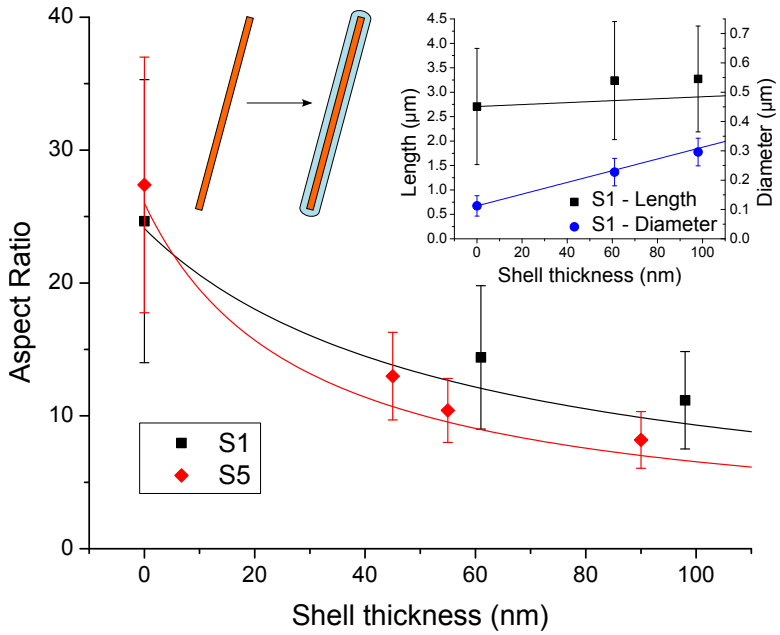

Figure 3.9 *Aspect ratio of S1 and S5 determined from TEM images (symbols, with the standard deviations as error bars) as function of silica thickness, with the evolution of the length and diameter of S1 with shell thickness as inset, where solid lines are expected trends from a homogeneous coating of a rod (equation 3.1) with the same dimensions as the average values found for the bare needles.*

The observed decrease in the standard deviation of the aspect ratio is expected, since as L/D decreases its standard deviation becomes increasingly dominated by that of D which is significantly smaller than that of L. However, the observed decrease will be positively influenced by the fractionation mentioned previously. The slight increase of the standard deviation of D with silica coating is remarkable, but is probably due to a slight increase in measured bundles since individual bundles become easier to identify after silica coating. Trends in the standard deviations and average dimensions combined, result in the polydispersities to decrease by about 10% after the addition of a shell of 90-100 nm resulting in $s_A \approx 30\%$ (S1) and $s_A \approx 24\%$ (S5).

The silica shell can easily be chemically modified, for instance, by incorporating a fluorescent dye into the shell during its growth. Fluorescent labeling of the particles makes them fit for being imaged with fluorescence (confocal) microscopy. With the entire shell being fluorescent, however, observing single particles in dense packings becomes impossible. To solve this problem a 2-step growth of the can be applied, where first a thin shell of fluorescent silica is grown, followed by a thick non-fluorescent silica layer. The latter separates the fluorescent parts of the

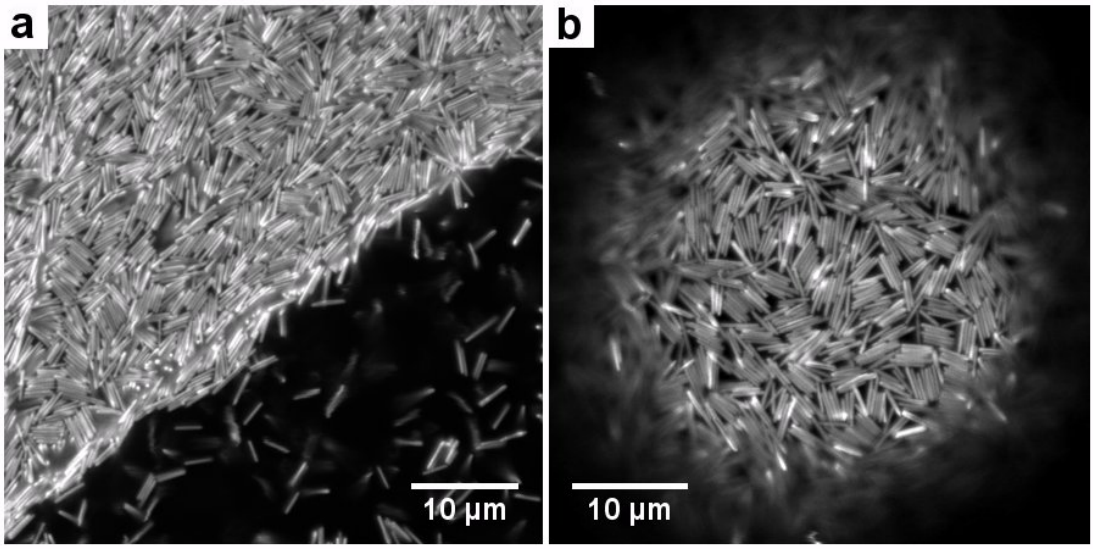

Figure 3.10 *CLSM snapshots of dense packings of rods on a liquid-liquid interface, (a) affected by being pressed onto the glass surface through which the sample was observed, and (b) the bottom of a droplet unaffected by confining glass surfaces.*

shell, so that individual particles can be distinguished when using an objective of sufficiently high NA. This is demonstrated by imaging these particles in a dense packing on the interface of a rod-stabilized emulsion droplet (Figure 3.10). Here clearly side-side stacks of rods can be observed, as well as holes in the packing.

3.5 Conclusions

A simple method for preparing a new type of micron-sized core-shell rods, composed of an akaganéite (β-FeOOH) core and a silica shell, was found and investigated in some detail. These particles fit well the requirements imposed by their intended use in proposed experiments with colloidal rods. There are alternative rod-like colloids that could have done so as well, although most of them to a lesser extent. Mainly the silica bullets would have been a good option, however the reproducibility and aspect ratio control, especially towards higher values, of this method seemed to be lacking.

The synthesis of the akaganéite needles was optimized for their use as templates for silica rods. Exploring it in some detail, trends in yield and particle size distributions with concentrations and time were found. These were discussed in the context of previous reports on the preparation of akaganéite particles.

Irreversible aggregation into compact bundles was found to be the biggest obstacle for the purpose of coating individual needles, and this is almost completely removed by adjusting the concentrations. However, some further improvements could possibly be made by enhancing particle stabilization (e.g. steric) during preparation. Another idea would be to investigate the influence of processes that form solids at the liquid-air interface, as is observed in aging stationary solutions in an oven. This would require preventing these solids from mixing with particles formed in bulk solution.

The subsequent growth of a smooth silica shell around the template particles reduces the aspect ratio in a controlled way (with the final aspect ratio depending on the shell thickness), while it also decreases the polydispersity. The silica coating strongly increases colloidal stability, and offers many routes to varying the particle properties, thereby greatly enhancing the potential uses of the system. Chemical modification of the silica shell is easily achieved, giving control over surface chemistry (this is used in Chapter 6) and functionality. Here it was demonstrated that a 2-step growth of the shell, with the thin inner layer being fluorescent allows visualization of dense packings on a liquid interface.

All in all, these easy to prepare core-shell rods are well-suited for the proposed experiments they are intended for, and in general offer interesting possibilities in many directions, as will be demonstrated in the next Chapter.

Acknowledgments

Various people have contributed to this chapter: Dr. Gary Nichol (XRD measurements), Steve Mitchell (assistance with TEM), Prof. Jan Vermant (hematite-silica ellipsoids), Dr. Andy Schofield (silica bullets, polystyrene spheres), Derek Low for constructing the polymer-film stretcher.

Chapter 4

Properties and modification of akaganéite-silica rods

This chapter further explores the potential of akaganéite-silica core-shell rods. First their response to a magnetic field is investigated to find weak alignment, with the long axes orienting perpendicular to the field direction. This behaviour is altered drastically by modifying the magnetic properties of the cores, leading to very strong alignment parallel to a magnetic field, and particles that interact strongly via dipole-dipole interactions. The method to achieve this is also studied in a more general sense. Finally, the iron oxide cores are removed, to leave hollow silica rods. Their liquid crystalline ordering in sediments, and the route to obtaining fluorescent hollow rods, is discussed.

4.1 Introduction

For the range of possible uses of colloids as building blocks for new self-assembled materials, or as model systems, the ability to tune particle properties is key. Modifying the shape or interactions of particles, or their response to external fields, to provide control over their behaviour, is especially valuable in this respect. [3–7, 15]

The akaganéite-silica core-shell rods, presented in Chapter 3, possess some interesting options for adjusting particle properties. Their fairly straightforward preparation was already shown to offer some flexibility in terms of dimensions,

aspect ratio, and fluorescent labeling. Here, in contrast to the iron oxide cores merely being a precursor for the shape, the focus is on their contribution towards other properties. This brings to light that they can be harnessed even further, to manipulate particles, and change their properties. The latter takes advantage of the porosity of the silica shells, which allows (selective) chemical treatment of the cores.

The iron oxide cores provide magnetic properties, and thereby the prospect of manipulating the rods with a magnetic field. This would be a powerful tool, as it could allow, on demand, structural reorganization, or directed self-assembly. Akaganéite, is an antiferromagnetic material, and some recent reports have shown it to exhibit superparamagnetic behavior when in the form of nanoparticles [97–99]. The magnetic properties of our particles might well be different from that of the previously studied nanoparticles, because of their much larger size and possible effects of the silica coating [100]. However, what is known so far about akaganéite in bulk and colloidal form, suggests that only a weak magnetic response can be expected.

Much more exciting is the possibility of modifying the magnetic properties through the iron oxide cores. The transformation of spindle-like hematite cores inside silica shells into iron, magnetite and maghemite were previously demonstrated [101–103], resulting in a stronger magnetic response [103]. Akaganéite particles have attracted some attention because of the same potential of this polymorph to be transformed to more-stable iron oxides (hematite, magnetite, maghemite) using simple methods [86, 87, 99, 101]. These most often rely on heating the particles to high temperatures (>300°C), and significantly change the particle morphology. In this case, when transforming akaganéite into magnetite, transformation into hematite is always performed as a first step. However, more recently [86, 99] the direct transformation of akaganéite particles into magnetite, was achieved under milder conditions and in solution. This also allowed the particle shape to be retained.

While interesting for their magnetic properties, for microscopy having iron oxide cores is disadvantageous. This has to do with the strong optical absorbance of iron oxides in the visible spectrum. For a similar type of colloid, having hematite cores within a silica shell, the removal of the cores was simply achieved by dissolving them in acid, through the porous silica shells [75]. While this made the particles less optically absorbing, the treatment was destructive to the fluorescent labeling. In any case removal of the akaganéite cores would lead to hollow silica rods, with

a reduced density. There for microscopy purposes, improved optical properties would more easily allow imaging of samples at high particle concentration. This is interesting since rod-like particles are known to be able to exhibit liquid crystalline ordering.

Below the experimental methods will be described first, followed by results on the magnetic field response of the core-shell rods. Subsequently, results related to modifying and removing the cores are are presented. The final section contains conclusions and an outlook.

4.2 Experimental section

Materials

Akaganéite-silica core-shell rods, prepared as described in Chapter 3. Hydrazine monohydrate (64-65%, reagent grade 98%), fluorescein-isothiocyanate (FITC, Isomer I, 90%), Tetraethyl orthosilicate (TEOS, reagent grade 98%), and poly(vinylpyrrolidone) (PVP, average M_w = 40 kg/mol) were obtained from Sigma Aldrich and used as recieved. Hydrochloric acid (fuming, 37%), ammonium hydroxide solution (35%), and dimethyl sulfoxide (DMSO) of reagent grade were obtained from Fisher and ethanol (absolute) from VWR.

Hydrazine treatment and additional silica growth

Aqueous suspension of core-shell rods (5 mL, 0.3 wt% FeR23SiO_2-FITC) at various hydrazine concentrations (90, 140, 180, 270, and 360 mM) were aged in an oven (3 hours, Binder VD23, 97±1 °C) with regular shaking for homogenization. Afterwards particles were washed with water until neutral pH, and stored in ethanol.

For silica growth to 'fix' the shells, the particles were first stored in a 0.1 g/g PVP in ethanol solution for 5 hours. Re-dispersed particles (0.01 g) in ethanol (10 mL), added 0.8 g ammonium hydroxide solution (35%), and 3 additions (30 minute intervals) of 0.05 mL TEOS/ethanol (1:1 v/v). After the first TEOS addition the samples, containing teflon plugs for optimal agitation, were shaken using a mechanical shaker, and left like this overnight. Finally, particles were

washed several times with ethanol, in which they were finally stored.

Removing akaganéite cores

Hollow silica rods were obtained by spinning down an aqueous suspension of core-shell particles, taking off the supernatant and redispersing the sediment in a concentrated hydrochloric acid solution (37%). This was sonicated for about 15 minutes after which the akaganéite cores were completely dissolved. This was followed by several washes with water to remove the iron and chloride ions from the dispersion. Cores of particles with an FITC labeled shell were removed by dispersing particles in a 20% hydrochloric acid solution for 5-6 hours, after which the colour dispersion turned yellow; it was subsequently washed with water. For reviving fluorescent properties the particles were then redispersed in ethanol containing 1 mM FITC, stirred for 2 days and washed multiple times with water and ethanol to remove excess dye molecules.

Microscopy

Original core-shell rods. A very dilute aqueous suspension (10^{-3} wt%) of core-shell rods (FeR12SiO_2) was transferred into a Vaseline-sealed capillary (VitroCom, 0.4×8 mm), and left to sediment before viewing the particles using a Nikon TE300 eclipse microscope with a 20× objective. A magnetic field was applied with an electromagnet (Newport Instruments, type C) mounted on the microscope. The same setup, but with a 4× objective, was used to record data to measure anisotropic dynamics in the suspensions. The applied technique is a generalization of differential dynamic microscopy (DDM), which uses a time series of optical microscopy images with short time intervals to extract information about the dynamics of the sample. The microscope was equipped with a CMOS camera (Mikrotron MC 1362), mounted at a 45° angle with the field (see Figure 4.1), and movies (1000 fps) were acquired at fixed values of the field strength. The capillary was turned over after taking a single movie to prevent sedimentation from affecting the measurements. The analysis of the data to extract the diffusion coefficients parallel and perpendicular to the magnetic field[1], is described in [104].

[1]performed by Mathias Reufer

Modified core-shell rods. First, a dilute suspension was shaken vigorously for proper dispersion. Imaging of the suspended particles was done in a drop of this dispersion placed on a cover slide (Menzel Gläser 22×50mm). Imaging was done with a Nikon TE300 eclipse microscope in combination with a Nikon 100×, NA 1.40 oil immersion objective, and a CMOS camera (Mikrotron MC 1362). A magnetic field was applied by positioning a magnet at some distance from the sample.

Hollow rods. Fluorescent rods in DMSO were observed with a Zeiss LSM confocal and a 63× oil immersion objective.

Hollow silica rods dispersed in millipore grade water at 0.5 wt% were left to sediment in a flame-sealed VitroCom capillary (0.2×4 mm). The sediment was viewed through crossed polarizers using a Nikon Eclipse E800 microscope with 10× and 20× objectives.

Electron microscopy

For inspecting particle morphology and determining size distributions TEM micrographs (Philips/FEI CM120, typically operating at 80 kV) were taken. A drop of dilute suspension in ethanol was dried on a 200 mesh copper grid coated with a formvar/carbon support film.

4.3 Results & discussion

This section first presents experiments looking into the manipulation of the akaganéite-silica core-shell rods with a magnetic field. Subsequently, the transformation of the akaganéite cores into a different iron oxide polymorph, as well as the dissolution of the cores to obtain hollow silica rods, are investigated.

4.3.1 Akaganéite-silica rods in a magnetic field

Instead of studying the magnetic properties of the core-shell particles in detail, their response to a magnetic field was investigated. Due to the particle-size and -density they sediment quickly, to collect at the bottom glass surface of the sample container (a rough calculation using the expression on page 14 gives $l_g < 1$ nm).

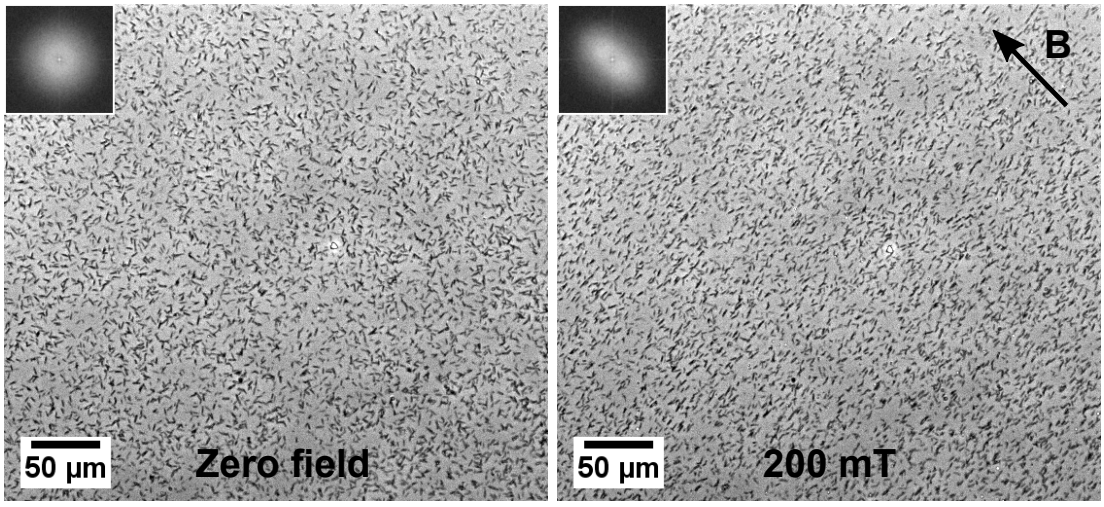

Figure 4.1 *Microscope images showing the effect of a magnetic field on particle orientation. Insets show fourier transforms of the images.*

This somewhat constrains their orientational and translational freedom. A resulting, dilute, quasi-2D suspension is easily observed with optical microscopy (Figure 4.1). The particles are still completely mobile due to electrostatic repulsions between particles and glass, and some are even able to rotate their long axes perpendicular to the glass wall, as observed by occasional 'blinking' in the phase-contrast imaging. Switching on a homogeneous magnetic field affects the orientation of the particles, with the arising anisotropy being highlighted in fourier transforms of the images (Figure 4.1). The short axes align parallel to the magnetic field direction, while the long axes become increasingly restricted to the plane perpendicular to the magnetic field. This is observed clearly due to the latter preferentially being parallel to the glass wall. Similar behaviour is reported for hematite ellipsoids [100, 105], while goethite (α-FeOOH) rods are found to first align with their long axes parallel to the magnetic field before the induced magnetic moments along the short axes take over at higher fields, and the effect becomes more like that observed here [106, 107].

Alignment in response to a magnetic field will give rise to anisotropic dynamics in the suspension. Recently, a technique (DDM) to characterize two dimensional dynamics was reported [104]. Through proper analysis, this allows the effective translational diffusion coefficients parallel ($D^{\parallel}_{eff}$) and perpendicular ($D^{\perp}_{eff}$) to the field direction to be extracted.

Analysis of image sequences for a bulk suspension of the core-shell rods as a function of magnetic field strength, demonstrates the departure from isotropic to anisotropic diffusion of the particles (squares in Figure 4.2). At low field

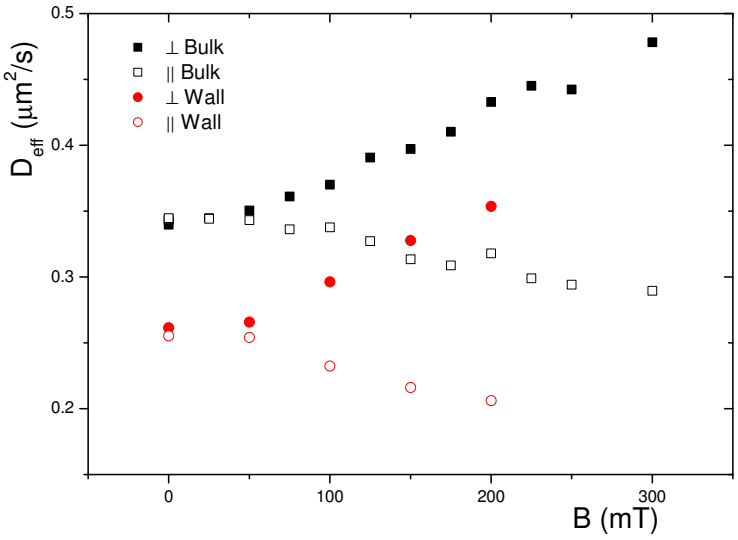

Figure 4.2 *DDM measurements of particles shown in Figure 4.1.*

strength, there is no difference between the diffusion perpendicular and parallel to the field direction, corresponding to isotropic diffusion. For a prolate ellipsoid, which is a reasonable approximation to the current rod-like colloids, the isotropic translational diffusion coefficient is generally defined as the average of the diffusion coefficients along its 3 axes. This is expressed as

$$D_{ISO} = \frac{1}{3}(D_l + 2D_d) \tag{4.1}$$

with D_l and D_d being the diffusion coefficients parallel to the prolate ellipsoid's long and short axes, respectively. Here, always $D_l > D_d$ up to a limit of $D_l/D_d = 2$ for an infinitely long and thin cylindrically symmetric rod.

Increasing the field strength shows a slowing down of the diffusion parallel to the field direction, alongside a speeding up of the diffusion perpendicular to it (squares in Figure 4.2). Thus, the dynamics become anisotropic, with particle diffusion in the 2 directions being different. Qualitatively, the observed trends correspond to the alignment of the short axes parallel to the field direction, as seen with microscopy (Figure 4.1). Namely, approaching the limit of perfect alignment of the short axes parallel to the field direction, $D^{\parallel}_{eff}$ would approach D_d and therefore decrease with respect to D_{ISO}, while $D^{\perp}_{eff}$ would approach $\frac{1}{2}(D_l + D_d)$ and increase.

Returning to the case of the quasi-2D suspension, studied above by direct observation with a microscope (Figure 4.1), demonstrates the effect of the confinement near a glass surface on particle diffusion. Overall, particle movement

is impaired by the glass wall, as evidenced by the slowing down of the dynamics compared to the bulk case (circles in Figure 4.2). The general feature of the emerging anisotropy is still there, and is even more pronounced. While most likely hydrodynamic coupling with the wall plays a role, the orientational freedom of the particles being limited by the wall does so as well. The long axes become confined by the surface, and now lie predominantly in the plane parallel to the glass wall. In the limit of true 2D (where $D_{ISO} = \frac{1}{2}(D_l + D_d)$), and approaching perfect alignment, $D_{eff}^{\parallel}$ would still approach D_d. However, $D_{eff}^{\perp}$ would approach D_l instead of $\frac{1}{2}(D_l + D_d)$, and therefore loses its smallest component. The increased slowing down of $D_{eff}^{\parallel}$ appears even more significant. Intuitively this might be understood by considering that it will probably be affected by the wall more than its counterpart will. These simple arguments partly explain the increased difference between $D_{eff}^{\parallel}$ and $D_{eff}^{\perp}$ at a fixed field strength, when going from a bulk suspension to this quasi-2D suspension.

4.3.2 Modifying the cores of akaganéite-silica rods

The weak alignment of the original core-shell particles at high field strength is interesting, but to be useful a much stronger response is required, preferably already at low field strength. Therefore, the treatment of the core-shell rods with hydrazine solutions, for transforming the akaganéite core material into magnetite/maghemite [86, 99], was explored. Akaganéite (β-FeOOH) is an iron(III) oxide-hydroxide, and hydrazine can reduce Fe(III) to Fe(II) to result in iron(II,III) oxide (Fe_3O_4, magnetite), which involves dehydration:

$$3\,\mathrm{FeOOH} + \mathrm{N_2H_5^+} \longrightarrow \mathrm{Fe_3O_4} + 2\,\mathrm{H_2O} + \mathrm{N_2H_4} \tag{4.2}$$

In the presence of oxygen, magnetite readily oxidizes to maghemite (γ-Fe_2O_3), an iron(III) oxide.

Several samples of core-shell particles were kept for 3 hours at 100°C in hydrazine solutions of increasing concentration. At low concentrations, after this treatment, the suspensions are only slightly darker brown compared to the original suspension. This cannot really be seen from photographs (Figure 4.3, 90 mM sample in Panel 1), however, introducing the suspension to a magnetic field clearly reveals that particles have in fact been affected by the treatment. The field introduces colour gradients from darker brown to light

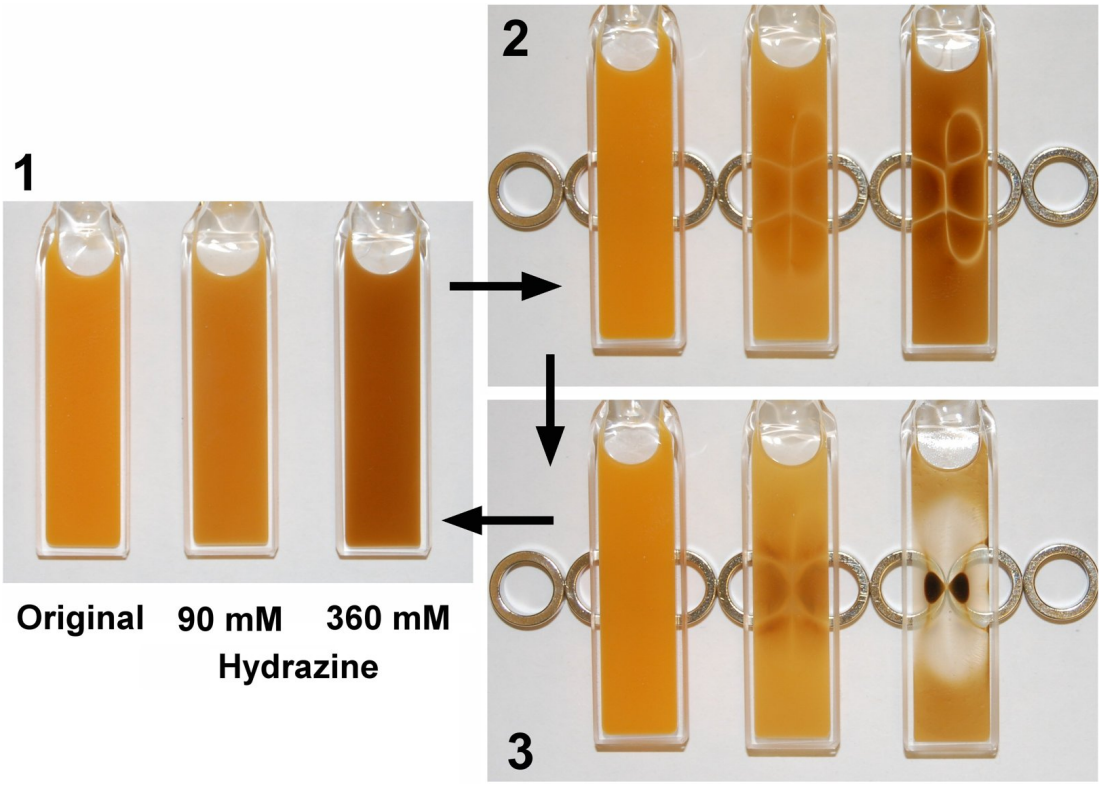

Figure 4.3 *Suspensions of original core-shell rods and hydrazine treated core shell rods, (1) in absence of a magnetic field, and (2) in the presence of a chain of ring-like magnets. (3) The same samples after having left them in the presence of the magnets for about 30 minutes.*

brown, which create a texture according to the field lines, while the appearance of the untreated suspension remains perfectly homogeneous (Figure 4.3, Panel 2). As the hydrazine concentration is increased, the colour of the particle dispersions gradually changes and, starting from orange/brown, a dark brown suspension is obtained at the highest concentration of 360 mM (Figure 4.3, Panel 1). The response to a magnetic field becomes even more dramatic (Figure 4.3, Panel 2), and, depending on the magnetic field it is subjected to, can impose various textures on the suspension. These changes in appearance happen instantly upon introducing or re-orientating a magnetic field, and therefore suggest alignment of the rods by the field. After some time, while the original suspension remains homogeneous, particles in the hydrazine-treated suspensions collect where the field is strongest. This effect is most pronounced for the sample treated with a hydrazine solution of higher concentration.

The stronger magnetic-field response of suspensions with increasing hydrazine concentration, suggests that the magnetic moments of the particles have increased significantly. This corresponds to the transformation of antiferromagnetic

akaganéite into the ferrimagnetic magnetite or maghemite, as does the colour change of the suspension [99]. However, the sample at the highest hydrazine concentration being dark brown rather than black [86, 99], probably suggests that still only partial conversion of akaganéite has taken place.

Particle morphology

Hydrazine is a base, and this has consequences for the silica shells of the treated particles. At the high pH of the aqueous solutions, colloidal stability is retained, since the silica shells are well-charged. However, at the same time the high pH also promotes the dissolution of silica [61], and the high temperatures in this case will only accelerate this process. High-magnification TEM images reveal the effect of treatment on the silica shells (Figures 4.4a,b). The initially smooth and homogeneous looking silica shells (Figure 4.4a) are partially dissolved at the highest hydrazine concentration (360 mM) (Figure 4.4b). The remaining silica, while still homogeneous in thickness, is now extremely porous/heterogeneous.

Something else can be noted from the akaganéite cores buried inside the silica shells. These can typically be better observed by increasing the beam intensity to overexpose the image, since otherwise they are obscured by the thick shells (Figure 4.4a). This, however, is less of an issue for the hydrazine-treated particles due to the partial dissolution of the shells (Figure 4.4b). Compared to the original particles, after (partial) conversion the cores are more heterogeneous. There are lighter areas that contrast strongly against the rest of the very dark cores (Figure 4.4b). This most likely has to do with the conversion process. It namely involves an increase in density (β-FeOOH = 3.64 g/cm^3 [108], Fe_3O_4 = 5.17 g/cm^3), and with the dehydration, the structure collapses to result in heterogeneities. For uncoated particles this is often witnessed by drastic changes in the particle shape [86, 109], or an increased porosity [86, 99]. Additionally, the process of the probably partial conversion may be quite heterogeneous in itself, starting from the outside of the particles.

While the silica shell partially dissolving is obviously disadvantageous, the presence of the shell has something to offer as well. As bare particles were observed to aggregate in a hydrazine solution, the shells give colloidal stability, and will probably help in maintaining shape. The shell also makes it easier to alter the particles after the procedure. By simply 'fixing' the silica shells by growing additional silica, to result in homogeneous smooth shells again (Figure

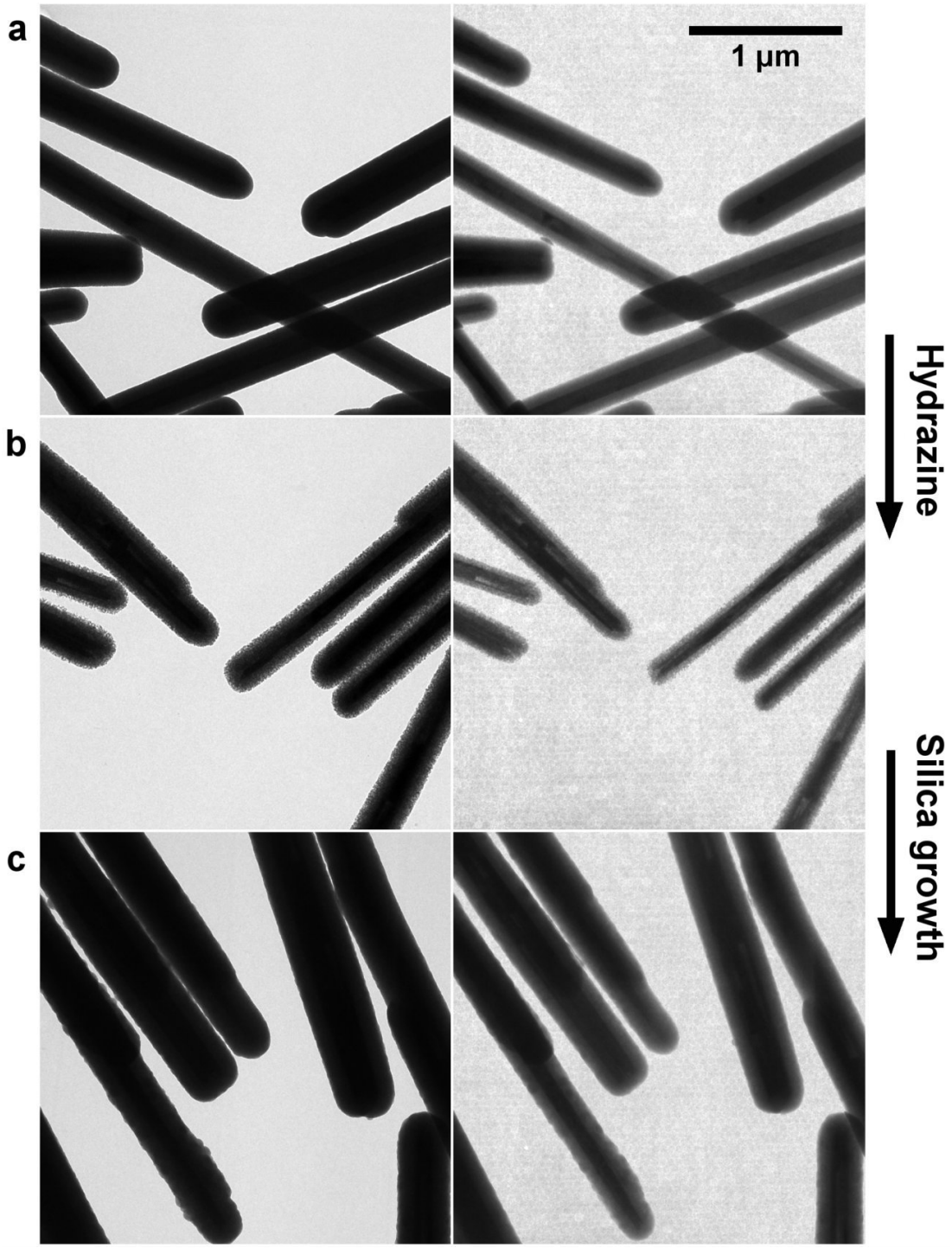

Figure 4.4 *Normally- and over-exposed TEM images (left and right panels, respectively) of (a) original akaganéite core-shell rods, (b) after hydrazine treatment (360 mM), and (c) hydrazine-treated particles with additional silica grown onto the shells.*

4.4c). It seems, however, that a slightly more bumpy surface results, possibly due to the heterogeneities in silica density introduced by the dissolution process. Additionally, it must be noted that additional silica growth on individual rods

is somewhat hindered by the tendency of particles to aggregate due to their magnetic dipole moments (this is demonstrated below). A non-magnetic method of agitation to keep particles separated is required here.

Structure formation in suspension

The transformation of the core material also affects the interparticle interactions, and this can be visualized with optical microscopy. Rods that have been subjected to a hydrazine solution of low concentration remain fairly well suspended, except for some small anisotropic clusters (Figure 4.5a). In contrast, large anisotropic clusters form over time when the rods were treated with a more concentrated hydrazine solution (Figure 4.5b). The chain-like aggregates start out as small anisotropic clusters, which over time are linked together to form larger, more tortuous clusters. The linear bits are relatively thick, and thus, most likely, consist of bundles of more or less parallel rods. Only very few particles are not included in the chain-like clusters.

The observed aggregation is due to dipole-dipole interactions. As demonstrated above by an increased response to a magnetic field, the performed conversion into a ferrimagnetic iron oxide introduces significant magnetic dipole moments in the cores. Another manifestation of this is the formation of the elongated, chain-like aggregates due to the strongly anisotropic dipolar interactions. These structures, involving mainly parallel aggregation of the rods, suggest that the dipole moment is (at least close to being) parallel to the long axes. Namely, if the moment was oriented perpendicular to the long axes, side-side aggregation would be much more favored. This would not result in the relatively slender, elongated chain-like structures observed here. A previous observation of maghemite/magnetite nanorods obtained by hydrazine treatment of akaganeite particles, also appears to agree with the magnetic moment being oriented parallel to the long axes [99], since an easy magnetization axis was found parallel to the growth direction.

Brownian motion and electrostatic repulsions between the rods make an important contribution to the structures. Due to the former, particles remain stabilized against aggregation into the primary van der Waals minimum, and therefore the aggregates are very flexible and loose. This implies that particles are very easily re-dispersed by shear, which breaks up the clusters. Orientational freedom of the rods in 3 dimension is explored through Brownian motion. Since the chains are flexible they can explore space, leading to inter-chain connections in many ways.

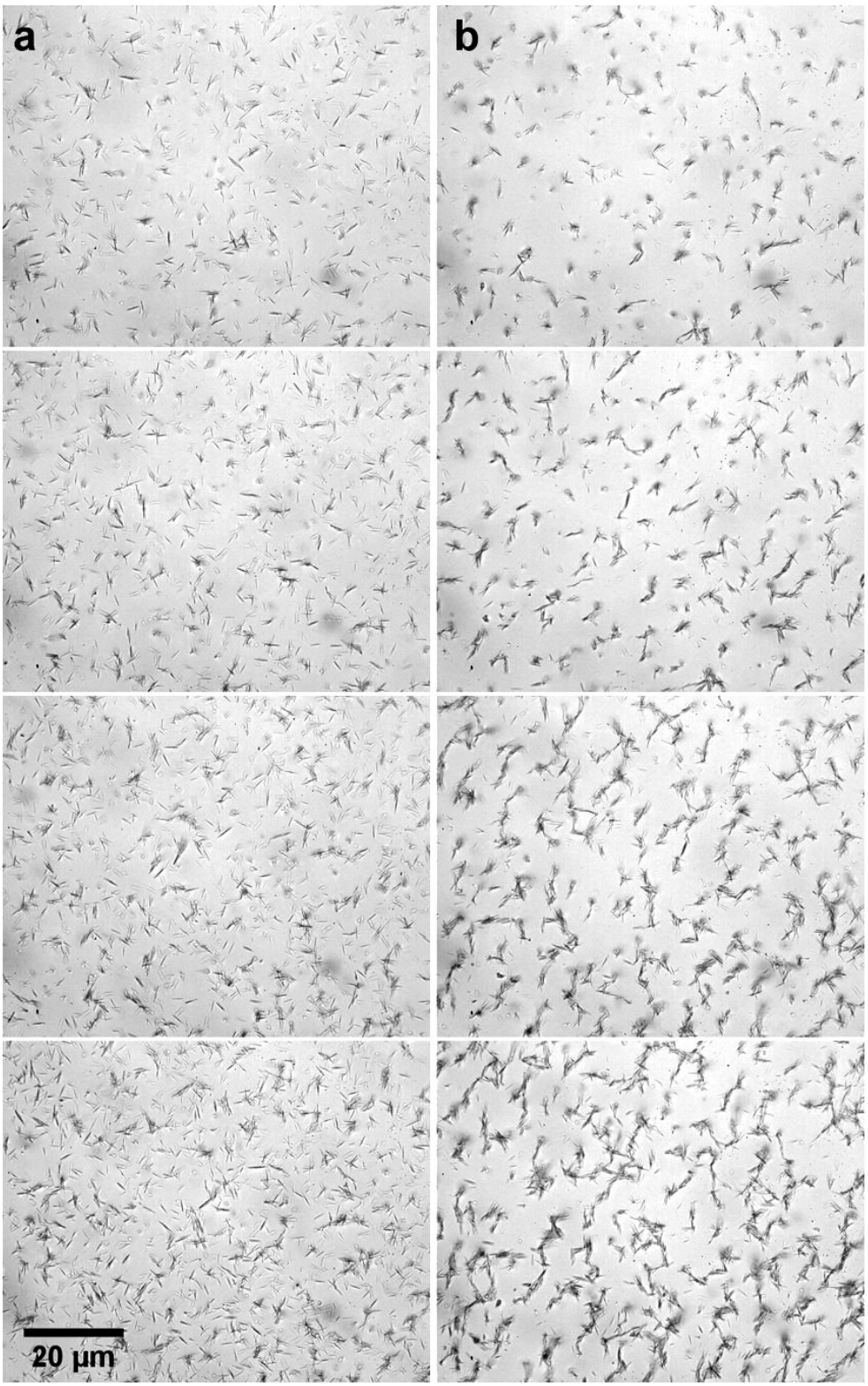

Figure 4.5 *Time series of microscopy images taken at the glass surface onto which hydrazine-treated particles sediment from a dilute aqueous suspension. (a) 90 mM, and (b) 360 mM, where the rows from top to bottom are at approximately 10, 13, 20, and 30 minutes.*

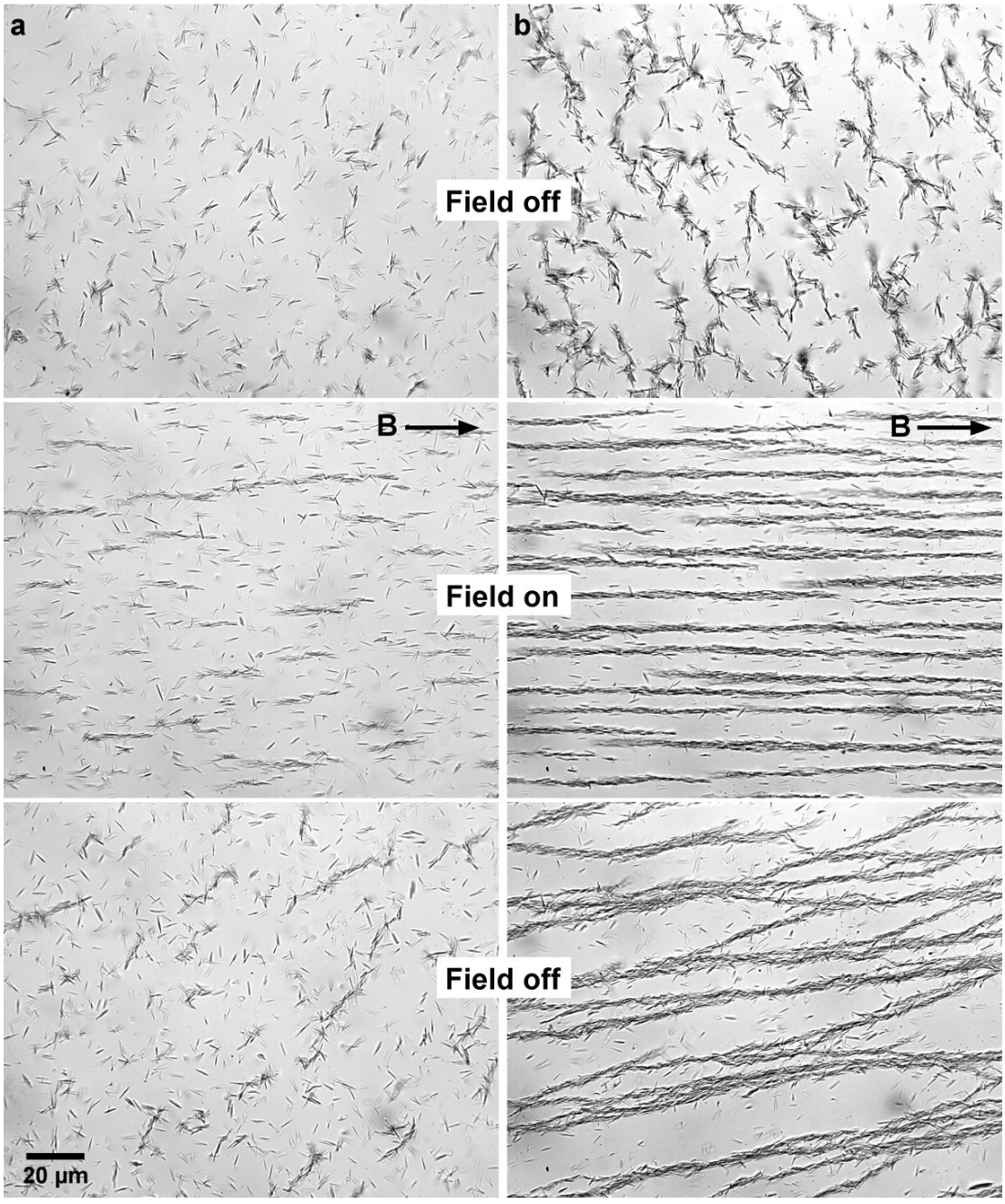

Figure 4.6 *Effect of introducing a field to a quasi-2D suspension of rods aged in hydrazine solutions, at concentrations of (a) 90 mM and (b) 360 mM. Image sequences show the quasi-2D suspension (top) in the absence of applied field, (middle) after applying a field by positioning a magnet next to the sample, and (bottom) after removing the magnet.*

Observing macroscopically the effect of applying a magnetic field on a suspension of hydrazine-treated particles, suggests that it changes structuring in the suspension (Figure 4.3, panel 2). Now, using microscopy, this can directly be visualized. In a suspension of particles treated at low hydrazine concentration,

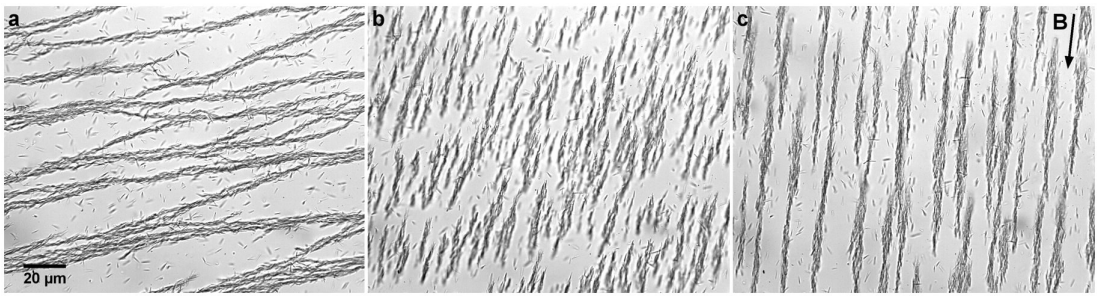

Figure 4.7 *Effect of applying a magnetic field approximately perpendicular to the lanes of the structure created as demonstrated in Figure 4.6. Image sequence shows the quasi-2D system (a) before, and at times (b) ∼2 seconds and (c) 4 minutes after applying a magnetic field.*

chains are seen to form parallel to the field direction (Figure 4.6a, top and middle panels). Within the chains the long axes are aligned in the same direction, confirming that their magnetic dipole moments are oriented along this axis. A large fraction of the particles, however, remain suspended freely. Some of them are observed to align in a similar manner with their long axes parallel to the field direction, while other appear unaffected. Upon removing the field, chains relax, with included particles not being as strongly aligned in the field, and they also partly fall apart (Figure 4.6a, bottom panel).

Rods treated with a hydrazine solution at higher concentration show a much stronger effect. Now almost much all rods strongly interact with the field, and they form large chains parallel to the field direction with the rods tightly packed, and pointing along the same direction (Figure 4.6b, top and middle panels). Since the particles are electrostatically stabilized, after removing the field these structures can relax through Brownian motion. With no restriction of the rods aligning along the external field, the parallel chains can now interconnect (Figure 4.6b, bottom panel). Subsequently applying a magnetic field perpendicular to the chains, these structures are reorganized (Figure 4.7). The chains shatter in smaller fragments (Figure 4.7b) that reorient and then slowly build up longer, thicker chains oriented along the new field direction (Figure 4.7c).

These observations confirm that with hydrazine treatment the magnetic moments of the rods increase, but also reveal that apparently there is some spread in their magnitude. While some particles not being included in aggregates probably already hints at this, it is most obvious after applying a magnetic field. In this case, especially for rods subjected to a low hydrazine concentration, some particles clearly interact more strongly with the field than others (Figure 4.6).

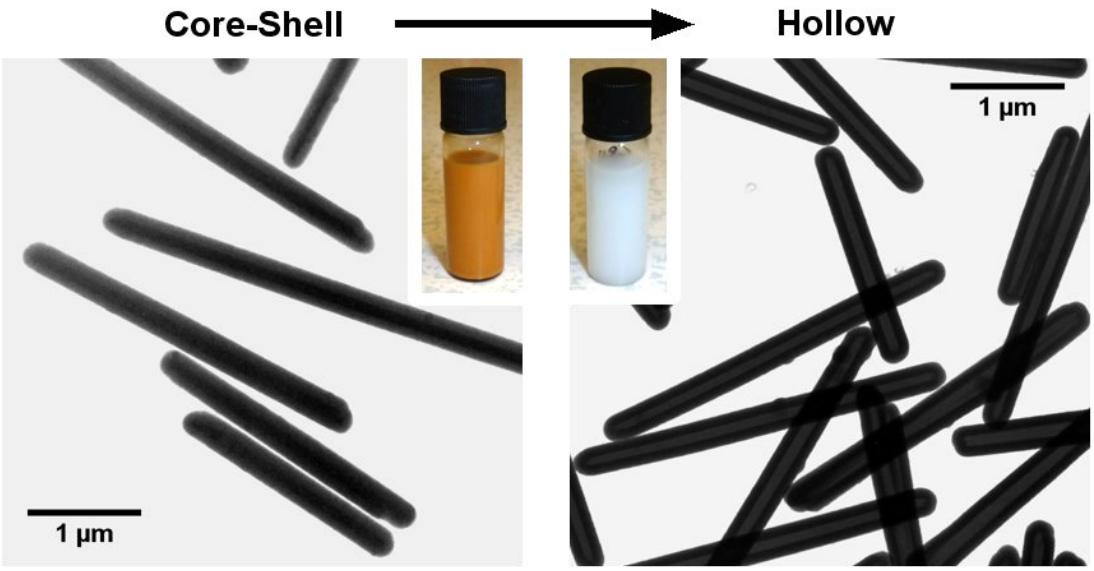

Figure 4.8 *TEM images of (left) original core-shell rods, and (right) hollow silica rods obtained after dissolution of the cores. Insets show photographs demonstrating the colour change of suspensions after the iron oxide cores have been removed.*

It is something that can be expected. The magnetic moment depends on the volume of the material, and the particle size distribution exhibits considerable polydispersity (Chapter 3). Additionally, there is the extent of conversion, which could vary. Magnetic separation, and due to aggregation, rapid sedimentation of magnetic rods, provide easy routes for removing rods with small magnetic moments. In the end, how exactly the treatment affects the dipole moments, and thereby the dipole-dipole interactions, is still unclear at this point. The observed heterogeneities in the cores, for instance, could point to another aspect through which the specific interactions between particles might vary.

4.3.3 Hollow silica rods

While the iron oxide cores provide the possibility of manipulating the rods with a magnetic field, they hinder optical microscopy by absorbing light strongly. Fortunately, they can easily be removed by dissolution in hydrochloric acid. This exploits the porosity of the silica shells, which do not dissolve at low pH, and are left hollow after removal of the cores, so that the colour of the suspension turns from orange/brown into white (Figure 4.8).

The shells are quite thick in the case of larger particles, and as suggested

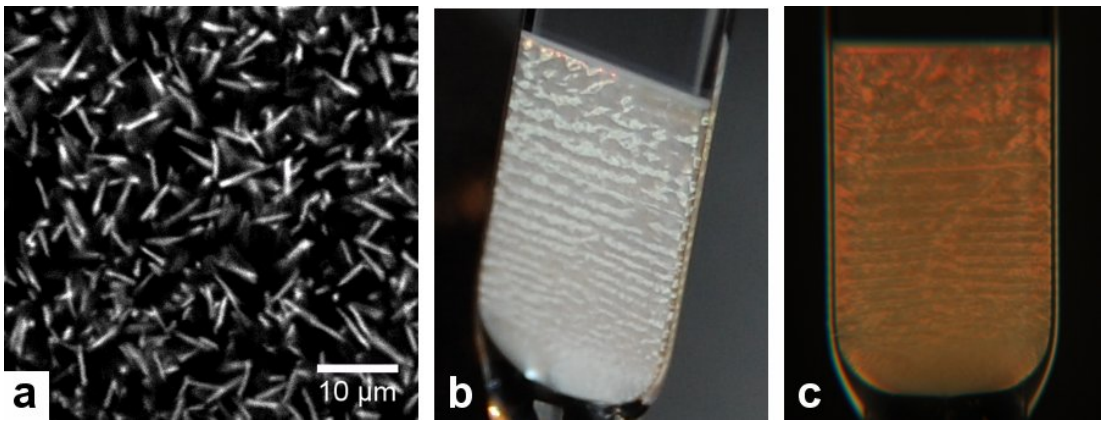

Figure 4.9 *(a) Confocal microscopy snapshot of fluorescent hollow rods, after reviving the fluorescent properties. Photographs showing a sediment of hollow (non-fluorescent) rods (b) directly, and (c) through crossed polarizers.*

previously, the silica becomes less porous as thickness increases [75]. While no additional PVP was added after starting the coating process to increase porosity, it is still possible to rapidly dissolve the iron oxide cores out of thick shells by dispersing them in fuming hydrochloric acid (lower concentrations worked extremely slowly, as no dissolution of the cores was observed within a day). The resulting hollow particles can be somewhat fragile depending on shell thickness, probably due to their large size and aspect ratio, as indicated by the occasional broken rod in TEM images. Breaking of particles most likely occurs in the washing steps where particles are pressed into a dense sediment by centrifugal forces. This is especially significant for particles with thin silica shells (see for instance Figure 3.5b) and therefore usually a shell of 75-100 nm (in the case of rods of $L \approx 3$ μm) is grown before removing the core, limiting somewhat the aspect ratio of hollow particles. Alternatively, dispersions of hollow particles could be cleaned by dialysis to circumvent centrifugation steps to finally obtain intact hollow particles even for thin silica shells.

Starting from rods with FITC labeled silica shells things change slightly. In this case often PVP is added in excess during silica growth, resulting in more porous shells. Hollowing out fluorescently labeled shells is disastrous for their fluorescent properties as is demonstrated by a very noisy and faint fluorescence signal [75]. However, it is found here that afterwards FITC can be linked to the free amine groups (from excess APTES used in the synthesis) on the silica surface throughout the porous shells. This 'revival' of the fluorescent labeling results in nicely fluorescent particles that give clear CLSM images (Figure 4.9a). These

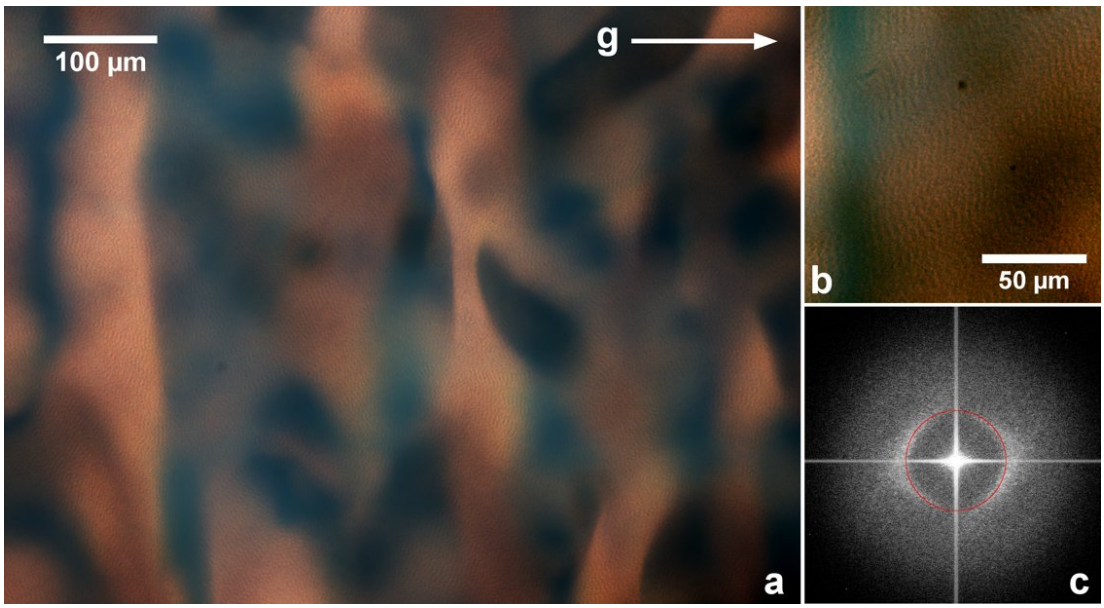

Figure 4.10 *(a,b) Polarizing microscopy of the sediment shown in Figure 4.9b,c. (c) FFT of panel a, with a red ring corresponding to the q-value of the peak found by radial averaging (corresponding to $L = 4.0$ µm).*

particles are well stabilized in ethanol or water and addition of a (thin) non-fluorescent shell around these particles is straightforward and can have various advantages (e.g. distinguishing closely packed particles).

Suspensions sediment quite quickly into a dense region within which the particles exhibit liquid crystalline ordering. To demonstrate this an aqueous suspension of hollow silica rods was left to form a dense sediment over the course of a few days (Figure 4.9b). A photograph of the sediment taken through crossed polarizers reveals the birefringence of the sample (Figure 4.9c). Polarization microscopy offers a closer look at this sediment, and shows the birefringence textures in more detail (Figure 4.10a). While different orientations of the rods could result in dark regions, here a distinct possibility appears to be that the densely stacked rods have their long axes oriented perpendicular to the plane of view. The layering observed macroscopically (Figure 4.10b,c) might then indicate alternating regions where particles stack either parallel or perpendicular to the flat glass walls of the container. What is striking is the presence of striped regions in the coloured domains (Figure 4.10b). A Fourier transform of the main image (Figure 4.10c) reveals bands confirming the existence of some typical length scale. Using radial averaging a peak is found at a q value corresponding to 4.0 μm (red ring in bottom right inset) corresponding well to the average length ($L = 4.1$ μm) of these particles. The image was taken in the top region of the

sample, which might explain the broadening of the peaks towards higher q. Some fractionation will probably have taken place over the long distance the particles had to sediment from the top of the sample, resulting in the top region of the sediment containing mainly smaller particles. This might also have aided the observed smectic ordering, as locally the size distribution is narrower compared to the original dispersion. Further evidence for this effect is that closer to the bottom of the sediment the broadening towards higher q disappears and the q value of the peaks obtained from radial averaging the Fourier transforms of images decreases up to values corresponding to a length scale of about 5 μm. While this clearly indicates the presence of local smectic ordering and fractionation, with the latter probably aiding the former, it can very well be that the bulk ordering (i.e. without fractionation) of the sediment is nematic.

4.4 Conclusions and outlook

Various aspects of the akaganéite-silica core-shell rods were explored. In this, the akaganéite cores, and their accessibility through the porous silica shells, played a central role.

Relatively high magnetic fields needed to be applied to observe a weak alignment of the original core-shell rods with their short axes parallel to field direction. These particles therefore must have a small (possibly field-induced) magnetic moment perpendicular to their long axis. How this alignment affects the diffusion of the particles was measured using DDM, demonstrating increasingly anisotropic dynamics at higher field strengths.

The magnetic-field response of the particles was increased by transforming the antiferromagnetic akaganéite cores (partly) into a ferrimagnetic iron oxide, magnetite/maghemite. The procedure entails the aging of particles in a hydrazine solution at elevated temperature, and is quick and easy. In the future, XRD could be used to determine the extent of conversion and study the composition of the resulting cores. For this silica shell can easily be removed by dissolution in a NaOH solution. The treatment, in fact, already partially dissolves the silica shell, but its repair is straightforward by the growth of additional silica. Since after the treatment FITC-labeled particles do not appear to be fluorescent anymore, this would allow particles to be fluorescently labeled again.

The structuring of the particles was observed with microscopy, more clearly showing an increase of the magnetic moments of particles when using higher hydrazine concentrations. The magnetic moments appeared to be parallel to the long axes of the rods, and in the absence of an applied field, resulted in the formation of flexible, anisotropic clusters of particles. By applying a magnetic field, according to their magnetic moments, rods align and form chains parallel to the field direction. Removing the field relaxes the chain-like structures, and connections between adjacent chains are formed. To study this system in more detail it would be nice to have better control over the strength and orientation of the magnetic field. For instance, being able to apply a field perpendicular to the plane of the quasi-2D suspension would align the dipoles so that they repel, allowing on-demand re-dispersion.

Apart from modifying the cores, they can also be removed, which is advantageous for microscopy. This leaves the porous silica shells intact, resulting in much less dense and less optically absorbing hollow silica rods. Although the procedure destroys the fluorescence, this can be fixed in a simple way to obtain fluorescent rods suitable for fluorescence microscopy. A sediment of hollow rods was studied and was found to be birefringent due to liquid crystalline ordering and, in suspensions of hollow silica rods in water, evidence is found of fractionation and smectic ordering.

Overall, the core-shell nature of the particles was demonstrated to allow selective modification of the two components of which the particles consist. Transformation and removal of the akaganéite cores offer routes to tune, respectively, the magnetic and optical properties. Furthermore, the silica shell can be chemically modified by for instance incorporating a fluorescent dye, or changing its surface chemistry. Thus, aside from their easy preparation (Chapter 3), by allowing properties to be modified on these different levels, the particles are also extremely versatile.

Acknowledgments

Mathias Reufer and Vincent Martinez are thanked for helping with magnetic field work on original core-shell rods.

Results II

Partial wetting of colloids

Chapter 5

Bijels stabilized by rod-like particles

This chapter presents a confocal microscopy study focused on the use of rod-like particles to produce bijels, a composite material consisting of colloids jammed together on percolating liquid-liquid interfaces. Traditionally, ordinary spherical colloids are used for the formation of these structures, so these are taken as comparison. To investigate the influence of only the particle shape on the structure of the bicontinuous fluid domains, the batches of spherical and rod-like colloids had a nearly identical volume per particle. While on large length scales only limited structural changes are observed, there is, however, a difference in the rate at which the domain size decreases with increasing particle volume fraction. Finally, by studying the packing of rods at the interface, more is learned about the jamming of rods on the curved interfaces that separate the coarsening liquid domains, which is the underlying process of bijel formation.

5.1 Introduction

Almost a decade ago now, computer simulations predicted a route to the formation of a new composite material [74]. For this, colloidal particles were included in the process of phase separation via spinodal decomposition of a binary liquid mixture. When equally wetted by the two emerging liquid phases ($\theta \approx 90°$), these particles are trapped on the percolating interface, where they jam into a closely packed monolayer without imposing any preferred interfacial curvature. As a result, coarsening of the spinodal structure is arrested into a rigid state, and

a bicontinuous interfacially jammed emulsion gel, in short 'bijel', is formed.

Initial simulations left some doubt, however, since they do not show a complete end of domain growth in the very limited physical time they can achieve. That permanent structural arrest takes place, can easily be argued by considering the energy required to detach a particle from the interface, which is typically many orders of magnitude larger than the thermal energy, k_bT. Certainty was provided only a couple of years later, when bijels were realized in experiments [18]. This required careful tuning of colloid surface chemistry to achieve close to neutral wetting.

So far, only very few pairs of simple liquids have demonstrated the feasibility of bulk bijel formation in experiments. The first system to succeed in this, consisted of silica particles, which were carefully dried to tune their wetting character, in a mixture of water and 2,6-lutidine [18]. As already suggested by its basic concept, the resulting bijels were confirmed to have a yield stress, owing its solidity to the closely packed layer particles at the percolating interface. Additionally, it appeared to be possible for the particle structure to remain intact after removal of the interfacial scaffold by re-mixing of the liquid phases [110]. This is direct evidence for the presence of attractive interactions between particles. Another system, using silica particles with a fine-tuned surface chemistry in mixtures of nitromethane and ethylene glycol, was found to be possibly even more robust [64]. Notable differences compared to water/lutidine bijels (LCST $\approx 34°$C) are the stability at room temperature (UCST $\approx 40°$C), and the reported absence of monogel formation [111].

With an amorphous structure, fluid bi-continuity, and a yield stress, bijels possess an, until now, unique combination of properties, and are therefore considered a new class of soft materials [16]. This also provides potential towards applications. For instance, application as a cross-flow microreaction medium was proposed, making use of intimate contact of the 2 inter-penetrating continuous fluid domains, through the porous solid membrane formed by the colloids [16]. Current research towards applications focuses on using bijels as templates for porous materials [112, 113]. To this end, one of the fluid domains is selectively polymerized, followed by a removal of all liquids, to obtain a fully solid material. Further processing steps can then be undertaken, for instance, allowing the polymer to be replaced by another (porous) material without losing the original bijel structure. The first step of selectively polymerizing a domain is crucial, and this was recently linked to monogel formation [111]. Namely,

the bicontinuous structure in monogel forming bijels was found to easily survive selective polymerization, in contrast to bijels that do not form monogels. Extra strength provided by interparticle bonds is thus highly advantageous for post-processing.

The process of formation allows easy tuning of some of the final bijel properties. This can already simply be done by selecting colloid size and concentration, leading to control over the domain size [18, 64], and thereby the amount of interfacial area. As a consequence, also the mechanical properties are affected, resulting in stronger bijels at higher particle concentration[111]. Additionally, related to the temperature dependence of the interfacial tension, increased bijel strength is achieved by deeper quenches past the critical point [111].

An unexplored possibility of tuning bijel properties may lie in using rod-shaped particles. This becomes clear when simply considering colloids trapped at liquid interfaces, a basic element in bijels. In this situation, namely, rod-like particles behave very differently from spherical particles. The shape of particles plays a major role here, since it can induce strong deformations of an otherwise flat interface, leading to strong capillary interactions [12, 45]. This has to do with the fixed orientation of the long axes of rods being parallel to the interface, in order to maximize the removed area of liquid-liquid interface. Here, edges and changes in the radius of curvature involved with the shape of the particles, demand the interface to be curved around the rods since, according to Young's law the contact angle is fixed. Resulting capillary interactions have been studied in detail, and strongly depend on contact angle and shape (aspect ratio) [10, 12, 42]. Depending on these parameters, the anisotropic interparticle forces, mediated purely by the interface, guide the assembly of particles into various structures [10–12].

For their role as stabilizers of liquid-liquid interfaces, the effect of rods at high interfacial packing fractions are very relevant. The structures formed by rods, influenced by capillary interactions, more easily span the area compared to spheres. Gradually reducing the interfacial area, starting from a low particle coverage, demonstrates this, as increasing aspect ratios generally show an earlier increase in surface pressure. Upon further compression of the particle packing, but still prior to buckling, some of the rods flip out of plane, and also expulsion of rods from the interface is observed, contrasting with behaviour of spherical particles [73]. Surface rheological measurements show significantly higher surface moduli for rods when compared to spheres. Clearly, the presence of a monolayer of rods makes much stronger, rigid and highly elastic interfaces. As well as the

strong capillary interactions between particles, the structure of the packing could be behind this behaviour [14]. One study even suggests that rods are more efficient emulsifiers than spheres, and links this to the capillary interactions. However, an important, so far unstudied, role of the shape could also be to facilitate attachment to the interface [14].

While these are striking examples, bijels, and their formation, involve quite different factors. The interfaces are extremely tortuous, and particles are quickly jammed into a closely packed layer. Furthermore, interfacial tensions are low and the particles near neutrally wetted, suggesting that any present capillary interactions will be weak. Still, considering the interplay between the shape of the particles and that of the interface, the jamming of rods on curved interfaces is an interesting situation. How this occurs might well have a significant influence on final bijel structure. Recently, some computer simulations started exploring the use of short rods in bijels [114, 115]. Their main outcome was that at constant particle number and volume fraction, increasing particle aspect ratio leads to smaller domains [114]. This is a consequence of the fact that more interfacial area is taken up by the rods, to more quickly give structural arrest.

In order to be able to experimentally investigate bijels stabilized by rod-like instead of spherical colloids, new particles were developed, as outlined in Chapter 3. Due to its previously shown robustness, and offering bijel stability at room temperature, the liquid pair nitromethane / ethylene glycol ('NM/EG') was selected. It was hoped that this would allow easy comparison of bijels, as well as the use of high NA oil immersion objectives, ultimately enabling the packing of rods being resolved.

Below, first the experimental methods are explained. The results are subsequently presented and discussed in detail, before finishing with conclusions and suggesting possible future work.

5.2 Experimental methods

Materials

Colloids. Rods used in NM/EG were akaganéite-silica core-shell particles (Figure 5.1), with average dimensions of L = 3.05 μm (s_L = 17%), D = 0.32

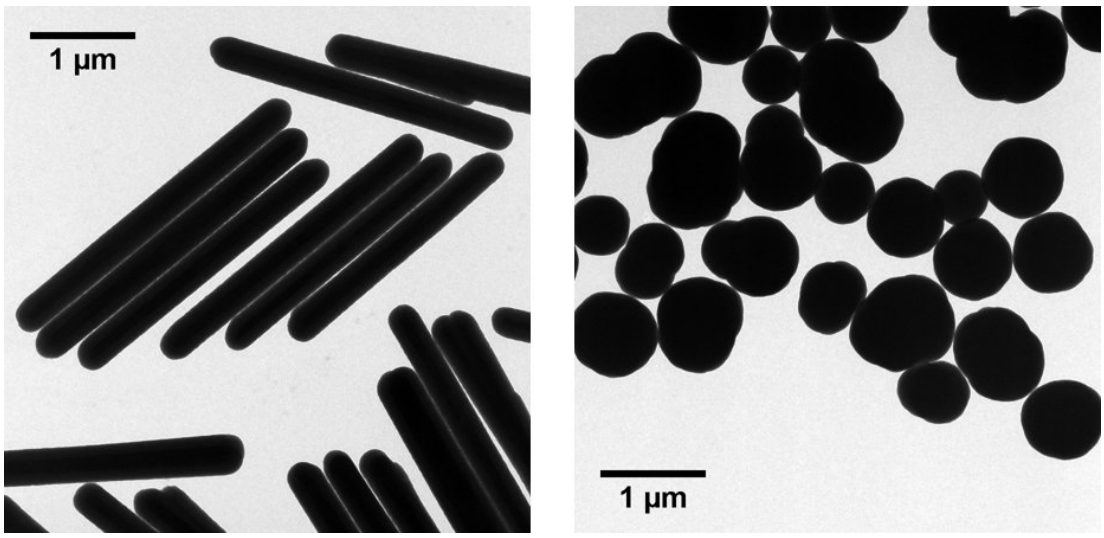

Figure 5.1 *TEM images of the colloidal (left) rods and (right) spheres used to produce NM/EG bijels.*

μm (s_D = 14%), AR = 9.6 (s_A = 19%) determined from TEM images. The shells consisted of a thin Fluorescein isothiocyanate (FITC)-labeled inner layer and a thick unlabeled outer layer. Rods used in water/2,6-lutidine were core-shell akaganéite-silica particles with the shells fully FITC-labeled. Preparation of the rods is described in Chapter 3. The composition of the rods was determined by dissolving the iron oxide cores of a known amount of core-shell particles. Knowing the mass fraction of iron oxide cores (∼0.3) and the densities of silica (ρ_{SiO_2} = 1.8 g/cm^3) and akaganéite ($\rho_{\beta-FeOOH}$ = 3.64 g/cm^3 [108]), an estimate for the overall particle density could be calculated: $\rho_{core-shell} \approx 2.35$ g/cm^3. Near-spherical Rhodamine B isothiocyanate (RITC)-labeled silica particles were also used in *NM/EG* (Figure 5.1), with an average radius R = 0.37 μm (s_R = 18%) determined from TEM images.

Chemicals. Ethylene glycol (anhydrous, 99.8%), hexamethyldisilazane (HMDS, reagent grade, ≥99%), Nile Red (technical grade), Fluorescein, and 2,6-lutidine (purified by redistillation, ≥99%) were used as received from Sigma Aldrich. Rhodamine B (99+%) and nitromethane (99+%, stored under nitrogen) were obtained from Acros Organics. Water was taken from a MilliQ system, ethanol (absolute) was obtained from VWR, and ammonium hydroxide solution (35%, reagent grade) was obtained from Fisher Scientific.

Tuning surface chemistry of colloids

Nitromethane/ethylene glycol system. For each batch of particles (after synthesis only washed with ethanol) a stock dispersion of known concentration (by weight) in ethanol was prepared. HMDS treatment of colloids to modify their wetting properties was done iteratively to find conditions resulting in bijel formation, as described below. This was performed on small samples (in 7 mL vials), by diluting down the stock suspension with ethanol to obtain a suspension of approximately 0.3 g rods (0.1 g spheres) in 4 g ethanol. Then, HMDS was added (typically in the range of 0.3-0.4 g for rod-bijels, and ∼0.7 g for sphere-bijels) followed by 0.1 g ammonium hydroxide solution (35%). The obtained mixture was stirred for 24 hours (6-position magnetic stirrer, 1000 rpm). Subsequently, particles were washed 5 times in the same vial with ethanol, and finally dried. For drying (∼100 °C, Binder VD23 oven set to 121 °C) first bulk solvent was allowed to evaporate in 30 minutes, after which the solid layer of particles was ground into a more fine powder using a spatula (this appears to be important to get the wetting right). Finally, drying was continued for another 60 minutes, but now under full vacuum. Particles were mostly used immediately after drying, but when needed, they were tightly sealed and stored in a desiccator.

Water/2,6-lutidine system. Fluorescent core-shell particles were simply dried from ethanol, under vacuum, at 120 °C for 24 hours (Binder VD23 oven).

Sample preparation and imaging

Nitromethane/ethylene glycol system. All samples, including throughout the iterative process working towards bijel-forming particles, the same procedure was followed. Dry particles were directly dispersed in a NM/EG mix (64 wt% nitromethane) using a hot ultrasonic bath (1.7 mL vials, 50 °C, 15 minutes). Vials containing the samples were then transfered into an aluminium mantle heated (50 °C) by a hotplate. Quickly, VitroCom capillaries, heated on the same hotplate, were filled by dipping them into the hot sample, and then quenched onto an aluminium block (23 °C). Samples were then fixed on a glass slide using silicone sealant on both ends. Finally, they were studied using a Zeiss LSM 700 confocal with an oil immersion objective (40× or 63×), and in some cases also a 20× objective was used. For imaging with the 20× and the 40× oil-immersion objective 0.2×4 mm capillaries were used, and for the 63× oil-immersion objective

0.1×2 mm capillaries were used. FITC (rods) and fluorescein (EG) were excited with a 488 nm laser line, and Nile Red (NM) and RITC (spheres) were excited with a 555 nm laser line. Emitted fluorescence of the 2 dyes present in a sample was sent to separate photomultipliers, split at 530 nm using a variable dichroic mirror. The light going to the PMT receiving $\lambda > 530$ nm (from Nile Red or RITC) was passed through a 560 nm long-pass filter.

Water/2,6-lutidine system. Particles were dispersed directly into water/2,6-lutidine mixtures (20 and 28 wt% (critical composition) 2,6-lutidine) containing 6×10^{-6} mM Rhodamine B dye at 3 wt% (by sonication, while minimizing heating). Samples were transferred into flame-sealed capillaries (VitroCom, 0.2×4 mm), mounted onto an aluminum slide heated to 50 °C (heated with a resistance heater controlled by a Lakeshore 331 PID) and subsequently studied using a Zeiss LSM 700 confocal with oil immersion objectives (40×, 63×), similar as described above.

5.3 Results and discussion

Formation of rod-stabilized NM/EG bijels was done with akaganéite-silica core-shell rods. Akaganéite cores provide the desired shape of the particles, while the silica shells offer the required functionality. The purpose of the latter is twofold, and lies in (1) finely tuning the surface chemistry to allow bijel formation, and (2) labeling particles with a fluorescent dye to be able to directly visualize them using microscopy. First, the emphasis will be on (1), whereas (2) plays a more important role in the later part of this section.

Tuning the wetting of rods for bijels

To fulfill the, for bijel formation, crucial demand of the colloids being (near) neutrally wetted, particle surface chemistry was modified in a systematic manner. The method employed to this end is a treatment of the rods with hexamethyldisilazane ('HMDS'). It introduces trimethylsilyl moieties onto their surfaces, and at the same time removes silanol groups, rendering the colloids more hydrophobic, and reduces the possibility of surface-charge formation. In combination with the NM/EG liquid mixture, this was shown to be a robust method for achieving (near) neutral particle wetting for bijel formation [64].

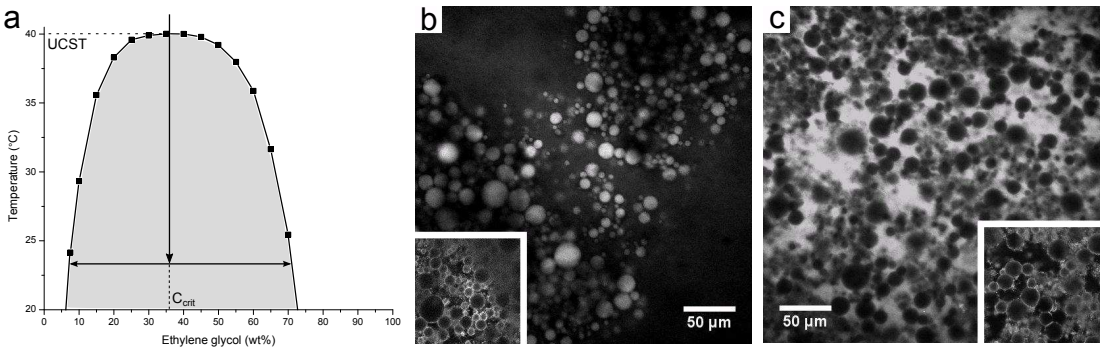

Figure 5.2 *(a) The phase diagram of nitromethane and ethylene glycol, with an arrow roughly indicating the temperature quench applied in experiments. Pickering emulsions resulting from such a quench in the presence of rods modified with HMDS at a (b) low, and (c) high concentration. The main images show Nile Red fluorescence from the NM-rich phase, and insets show FITC fluorescence from the rods.*

Modifying the particle surface chemistry to different extents by varying the amount of HMDS, systematically varies the contact angle. To ensure consistency, it is of great importance that the overall procedure is kept as constant as possible, even in the smallest details, as silica surfaces are known to be strongly affected by many relevant environmental conditions [116, 117]. For the rods, an additional complication is that they are produced on a smaller scale compared to spherical particles. To avoid using too many particles in the process, modifying the surface chemistry was done iteratively on small samples.

To follow the changes in contact angle, bijel formation was attempted with every batch of modified rods. This first involved their dispersion (3 vol.%), in a fully mixed NM/EG mixture at critical composition. Subsequently, the temperature was quickly lowered to room temperature to achieve phase separation through spinodal decomposition of the liquid mixture. Since the phase diagram is symmetric, this leads to approximately equal volumes of NM-rich and EG-rich phase. (Figure 5.2a)

Samples were then studied with fluorescence confocal microscopy. In this way, the NM-rich phase can be visualized due to fluorescent dye (Nile Red) dissolved in the liquid mixture, while the particles contain FITC that allows them to be observed separately. Rods modified at low HMDS concentration, are found to be preferentially wetted by the EG-rich phase. This is indicated by the formation of NM-rich droplets, stabilized by rods trapped at their interface (Figure 5.2b), as a result of the curvature imposed by the particles on the interface. Transitional

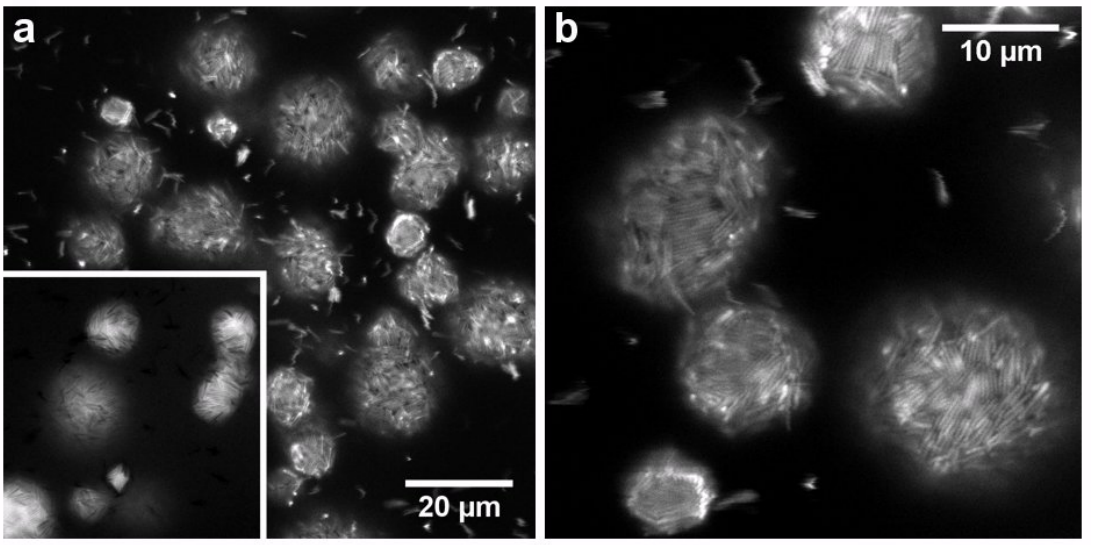

Figure 5.3 *High magnification images (63× objective) of rod-stabilized droplets resulting from a spinodal decomposition of the host solvent. (a) An image showing the FITC fluorescence from the rods for a larger collection of droplets at lower magnification, with the inset showing Nile Red fluorescence from the NM-rich phase. (b) A higher magnification image showing the FITC fluorescence from the rods, giving a closer look at the structuring of the particles.*

inversion of the emulsion occurs when the HMDS concentration is significantly increased. In this case the continuous phase is NM-rich as it now preferentially wets the rods due to the drastically changed surface chemistry (Figure 5.2c).

The rods trapped on the droplets have silica shells that are composed of a thin inner layer labeled with a fluorescent dye, and a thick unlabeled outer layer, allowing their packing to be resolved. Closer to neutral wetting of the particles, more oddly shaped droplets are formed, and at higher magnification details start to be revealed (Figure 5.3a). In general it can be seen that the stabilizing layer of rods are quite rough. While less obvious for larger droplets, small droplets have clearly angular shapes, with facets on the scale of the rod-length. Zooming in on the droplets, the arrangement of the particles can be observed in some detail (Figure 5.3b). Some local ordering is observed in the form of small side-side stacks of rods. The roughness of the stabilizing layer appears to originate from rods sticking out and overlapping each other. This structuring resembles closely that of calcium carbonate rods trapped on air bubbles [118].

As the iterative process towards neutral wetting advances, confocal microscopy observations continue to indicate how the HMDS concentration should be adjusted in subsequent modification. At moderate HMDS concentration, tube-

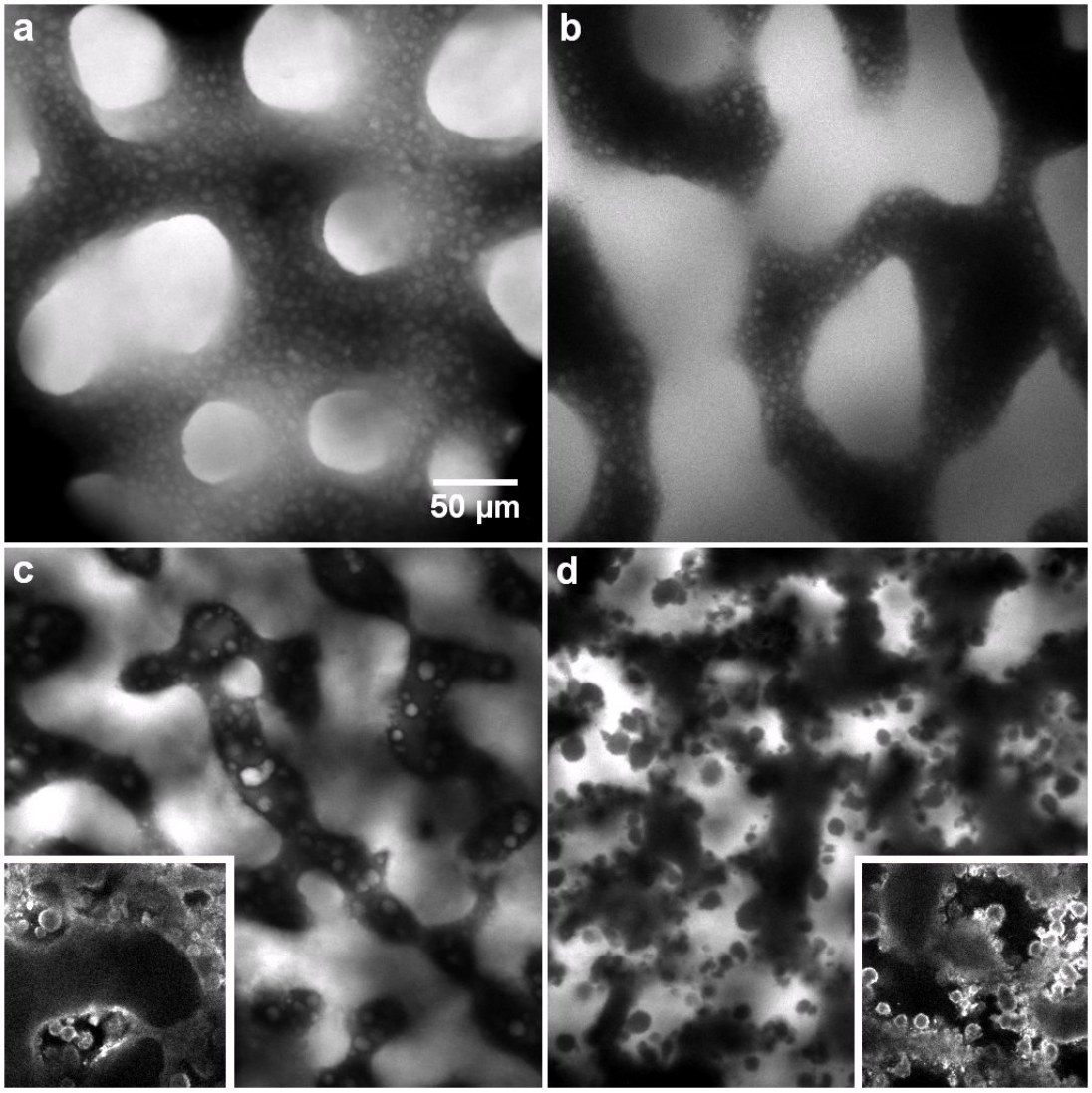

Figure 5.4 *Confocal microscopy images (40× objective) showing the (a - d) fluorescence of Nile Red from the NM-rich phase, with (c,d) insets showing the fluorescence of FITC from the rods. Rods stabilizing the observed liquid domains have, from (a) top left to (d) bottom right, been treated with increasing HMDS concentration.*

like structures can form that hint at fluid bicontinuity (Figure 5.4a). It clearly does not display the morphology of the liquid phases that is characteristic of spinodal decomposition, and probably is merely a remnant of this. Droplets that are tightly packed in the tubes clearly indicate that overall particles are still wetted more by the *EG*-rich phase. Further increasing the HMDS results in large bicontinuous fluid domains that are more reminiscent of spinodal decomposition (Figure 5.4b). Still droplets are abundant in the *EG*-rich domain. Adjusting the HMDS concentration again, liquid domains become smaller while there still is clear presence of *NM*-rich droplets (Figure 5.4c). Ultimately, as modification is

overdone slightly, droplets are formed in the NM-rich domain (Figure 5.4d).

It must be noted that polydispersity in particle wetting possibly plays a role as well. To prevent this as much as possible, the final drying of the rods prior to an experiment is preceded by grinding down the powders after initial evaporation of the bulk solvent. Additionally, the temperature quench is an important factor in bijel formation. For instance, an unwanted secondary phase separation could happen in a slow quench, which can lead to the formation of droplets in one of the domains. Here the temperature quench was fixed for consistency in the experiments.

Bijel structure

Eventually particle modification led to bijel formation. When increasing the particle concentration, rods take up a larger proportion of the interfacial area, leading to smaller liquid domains, due to an earlier structural arrest of the spinodal decomposition. This is demonstrated qualitatively by low magnification images (Figure 5.5a-d). For comparison, bijels were also prepared with spherical particles (Figure 5.5e,f). Here, the EG-rich channel is observed through fluorescence of Fluorescein, as the colloids were labeled with a Rhodamine dye (RITC). One thing that is obvious immediately, is that rod bijels exhibit much smaller domain sizes for similar particle concentration (comparing, in Figure 5.5, images c & d with e & f, respectively).

Using approximations, scaling of the domain size with particle concentration can be discussed in a more detailed and quantitative fashion. For a fixed $\phi_{colloid}$, the final domain size will depend solely on the effective area covered by the jammed layer of colloids trapped at the interface. The situation can be approximated by a spherical droplet being fully covered by colloids, which is contained within a liquid of a volume equal to that of the droplet [119]. This reflects spinodal decomposition, since the volumes of the 2 phases are roughly equal, where the droplet diameter (L) represents the domain size (also referred to as L hereafter). Given this scenario and spherical colloids that are neutrally wetted it is found that

$$L = 2\nu d_{sphere}\frac{1}{\phi_{colloid}} \tag{5.1}$$

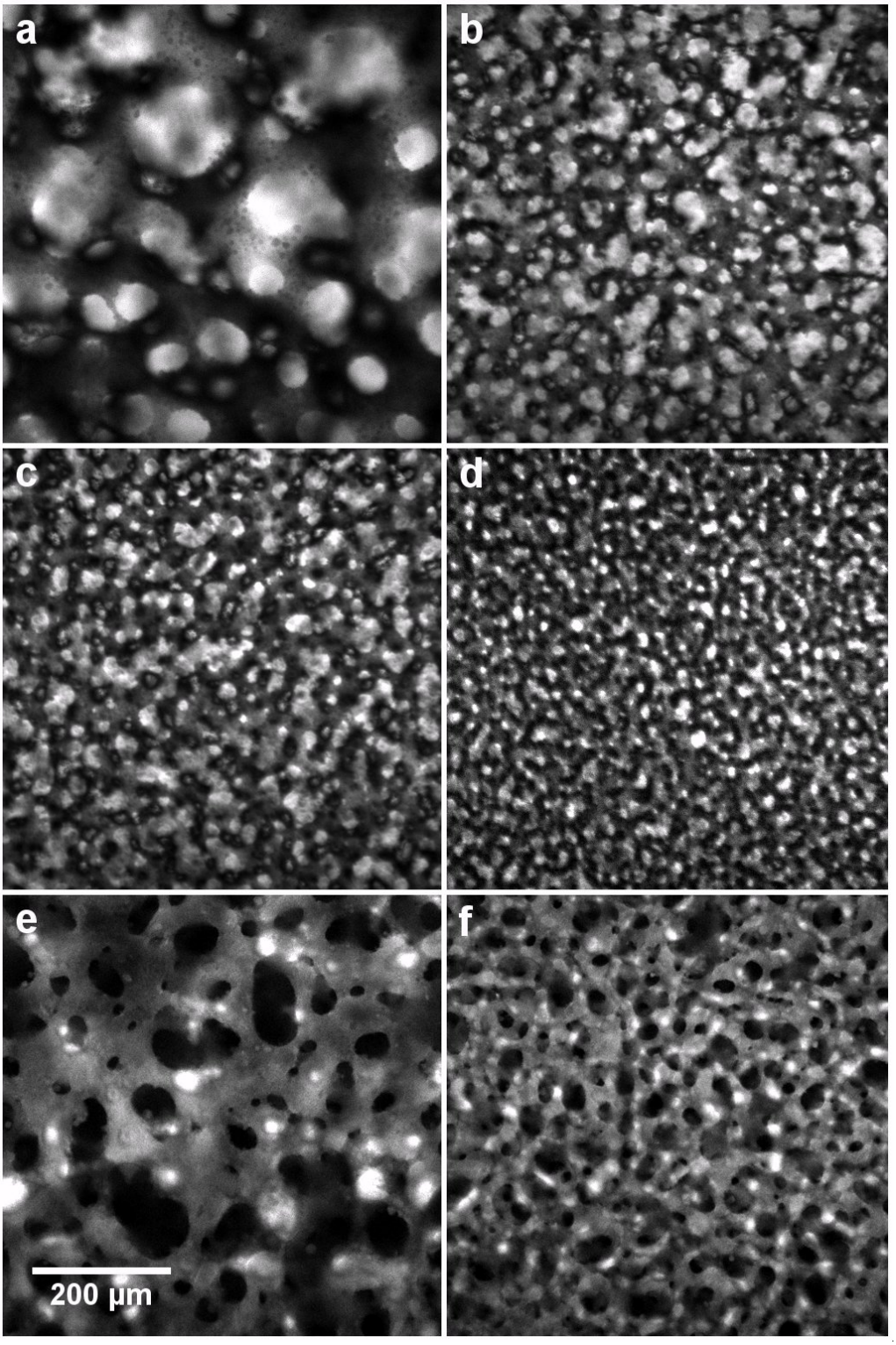

Figure 5.5 *Low magnification confocal microscopy images (20× objective) of bijels stabilized by (a - d) 1, 2, 3, and 5 vol.% rods, and (e & f) 3 and 5 vol.% spheres, respectively. Observed fluorescence is from (a - d) Nile Red in the NM-rich phase, and (e & f) Fluorescein in the EG-rich phase.*

where ν is the packing fraction of the particles at the interface, and $\phi_{colloid} = \frac{V_{colloid}}{V_{liquids}}$. As observed qualitatively in Figure 5.5, this indeed demonstrates that the domain size can be reduced by increasing the particle concentration. Related to the number of particles and the reduction of interfacial area per colloid, decreasing the particle diameter offers an alternate route to smaller domains. That the domain size indeed scales as $L \propto \phi_{colloid}^{-1}$ was demonstrated in experiments [18].

To quantify the domain size of the created bijels, for each sample several images like those shown in Figure 5.5 were used. The images were obtained at different locations in the sample (see Figure 5.6a for a few examples from the same sample). By taking the radial averages of their squared 2D Fourier transforms, the structure factors were calculated. Those belonging to a single set of a particular sample were averaged (for example, the red squares in Figure 5.6b) to improve statistics. The dominant length scale in the sample, the domain size, is represented by a knee in the curve at the corresponding wave vector (q). This is similar to observations in SANS measurements of sponge phases in surfactant solutions [120, 121], the structure of which is a (dynamic) analogue to the bijel structure. To extract q corresponding to the knee, the curves were fitted by the shifted average of 2 slightly adapted cumulative distribution functions:

$$I(q) = c_1 + \frac{1}{2}\left(c_2 \operatorname{erfc}\left(\frac{\ln\left(\frac{q}{c_3} - \mu_1\right)}{\sigma_1\sqrt{2}}\right) + c_4 \operatorname{erfc}\left(\frac{\ln\sqrt{\left(\frac{q}{c_5} - \mu_2\right)^2}}{\sigma_2\sqrt{2}}\right)\right)$$

where all c_x, μ_x and σ_x are fitting parameters. Doing this yields a smooth curve with a well-defined knee, the peak of which was located by numerical differentiation (Figure 5.6b).

The so obtained domain sizes can be plotted against the inverse volume fraction for comparison. As expected from equation 5.1, a linear increase is found (Figure 5.6c). Linear fits through the origin give the slopes, revealing that for rod-stabilized bijels there is a significantly faster decrease of the domain size with increasing $\phi_{colloid}$ (as seen qualitatively in Figure 5.5). Although only 2 sphere bijels were used, this approach is still valid, considering equation 5.1, as well as according to previous experiments [18].

Taking $\frac{\pi}{2\sqrt{(3)}}$, the maximum packing of discs on a plane, for ν and the experimentally determined particle diameter, equation 5.1 can approximate more quantitatively the domain size at a fixed $\phi_{colloid}$. In previous experiments this

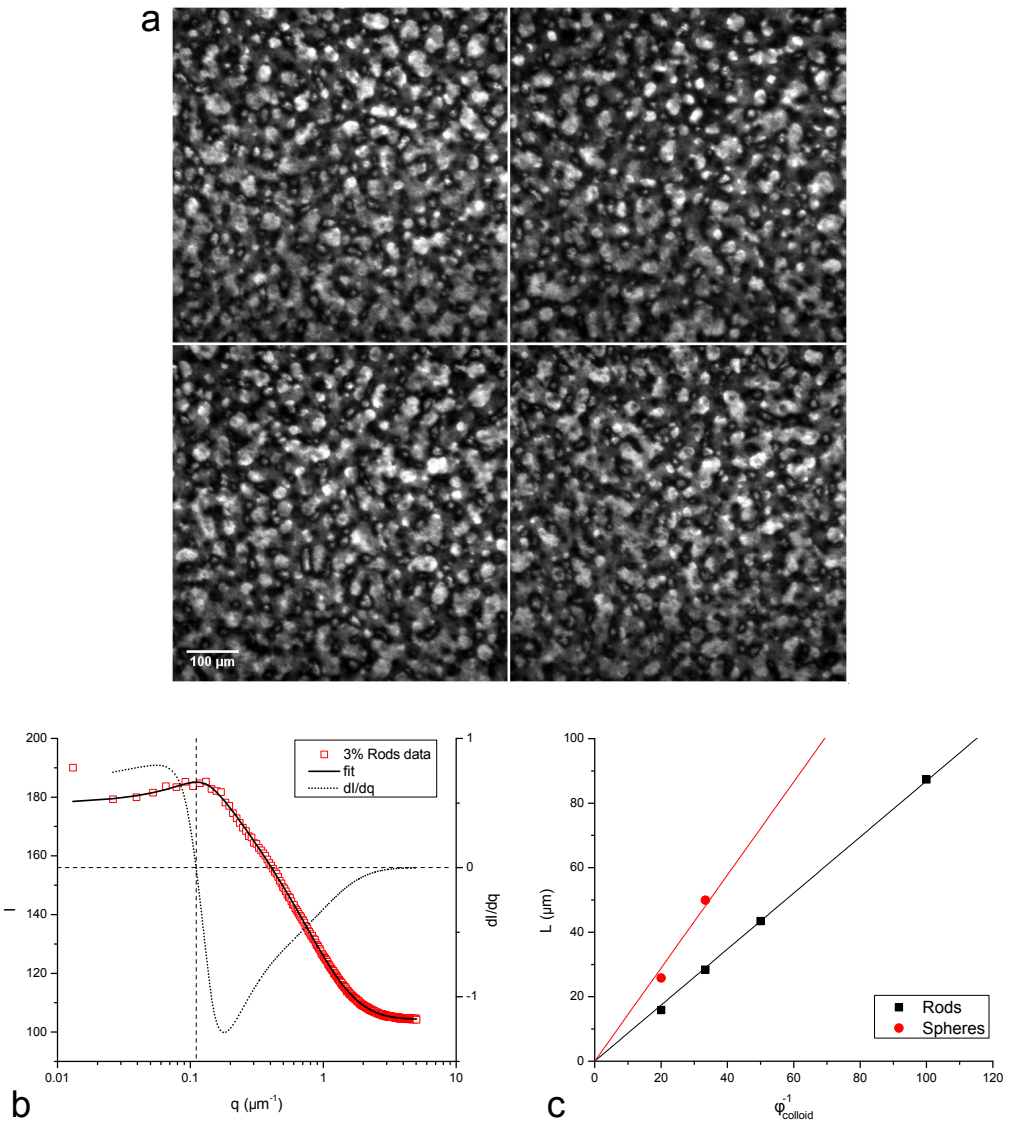

Figure 5.6 *(a) Some more examples of images (3 vol.% rods, the same sample as Figure 5.5c) used to obtain the domain size as described in the main text. (b) An example demonstrating how q_{knee} was obtained from an average of the radially averaged FFTs of several images like those in Panel (a) (red, empty squares). A fit (solid black line) overlaps the data, and a dotted black line plots the local slope (dI/dq) of the curve. (c) The obtained domain sizes plotted as a function of $\phi_{colloid}$, fitted with a linear curve through the origin.*

showed not very quantitative agreement, but at least the right order of magnitude was obtained [18]. Of course, the pre-factor of the relationship between L and $\phi_{colloid}$ depends on the shape of the domains, which was in this case approximated by a sphere. Various experimental also factors introduce uncertainties. These include particle density, the fraction of particles trapped at the interface, and possible inhomogeneities in quench or particle concentration. Here, the slope

found for spheres (1.44 μm) is in relatively good agreement with the value resulting from equation 5.1 (1.36 μm) when using the current particle size.

Changing colloid shape from spheres to rods will change the relationship between L and $\phi_{colloid}$. Namely, both the area taken up by a single particle and the 2D packing fraction change when only the particle shape is changed at constant particle volume. Judging from the densely packed rods on droplets (Figure 5.3), it can be expected that there will not be much of a difference in ν. The effect of a change in the area taken up by single particles is probably much more significant. For instance, a neutrally wetted cylinder takes up twice as much interfacial area when its volume is kept fixed, and its aspect ratio is increased from 1 to 8. The rate at which the domain size changes with $\phi_{colloid}$ can thus be expected to change significantly. Using the same scenario as described above for spheres to approximate the relationship between domain size and colloid concentration, for cylindrical particles

$$L = \frac{3}{4}\pi\nu d_{rod}\frac{1}{\phi_{colloid}} \tag{5.2}$$

is found, where d_{rod} is the full width of a cylinder. Possibly rather counterintuitive is that, in terms of particle dimensions, the domain size at fixed $\phi_{colloid}$ merely depends on the width of the rods. This can simply be understood by considering a change in length at fixed diameter. When the colloid concentration is also fixed, varying only the particle length means that particle volume changes. Thus, to keep $\phi_{colloid}$ constant, this must be balanced by a change in the number of particles, leaving the domain size unaffected. Hence, only d_{rod} appears in equation 5.2, and nothing that links to particle aspect ratio.

As the domain size at a fixed $\phi_{colloid}$ depends on particle size, a similar volume per particle is important for a clear comparison by particle shape alone. Spheres with an equivalent volume per particle to the rods used here, would have a diameter of approximately 776 nm. With $d_{sphere} = 750$ nm, the spheres used here to compare results with rods are nearly perfect. As remarked above, for rods the domain size decreases faster with increasing particle concentration. Intuitively, this is easily understood by considering the argument provided above, that increasing aspect ratio increases the interfacial area taken up by a single particle. Plotting data against $\phi_{colloid}^{-1}$, a slope of 0.87 μm is found, compared to 1.44 μm (Figure 5.6b). Taking $\nu = 1$ and d_{rod} determined with TEM, equation 5.2 comes up with a value of 0.75 μm for the slope. This demonstrates a larger discrepancy with the

experimental result than for the sphere bijels. The difference does probably not predominantly originate from the assumed ν, as it can only be adjusted to lower values, and result in a larger difference. Possibly the most significant observation is the fact that here equation 5.2 predicts an even faster decrease of L with $\phi_{colloid}$ than observed. This could be related to the observation that at the interface of droplets, particles poke out and overlap indicating that they are partly expelled from the interface. Their potential to reduce the interfacial area is thus not fully used, and the gain from changing particle shape smaller than expected from simple geometrical arguments.

At higher magnification the structures can be studied in more detail (Figure 5.7). Now it is clearly seen that channels are clear of droplets, except the odd few tiny ones of both phases, in stark contrast to when particle wetting is not yet properly tuned (Figure 5.4). These images also allow better structural comparison between bijels prepared with spheres and rods, than the low magnification images (Figure 5.5) used for obtaining the domain sizes. At first sight the structures clearly do look different, but it is hard to put a finger on what exactly the difference is. Overall, the liquid domains stabilized by spherical particles may appear more smoothly curved, with possibly more angular and tortuous domains formed by the rods.

Two factors must be taken into account when discussing and comparing these images. While in principle it should not make a difference, for the rod-stabilized bijels the NM-rich phase is visualized, in contrast to the sphere-stabilized bijels where the EG-rich phase is observed. Secondly, the depth into the sample at which these images should be considered. Starting from the glass surface, first a continuous layer of pure EG-rich phase is found, followed by a more bijel-like layer consisting mainly of nitromethane-rich phase (Figure 5.8a). Through the latter, EG-rich necks point upwards, perpendicular to the glass surface. This is reminiscent of simulations where layering was observed in spinodal decomposition close to a preferentially wetted surface (by EG in this case) [122]. Further in, the phase volumes show no clear asymmetry anymore (Figure 5.8b), and at a depth of roughly 25 μm images like those shown in Figure 5.7 could be acquired. Upon increasing imaging depth, the pictures blur very rapidly (Figure 5.8c), mainly showing fluorescence that only passes through the single particle layer at the bottom of the sample. Vertical slices provide a side view of this structuring (Figure 5.8d). The optically absorbing akaganéite cores of the particles probably play a major role in limiting the imaging depth. Bijels prepared with the pure

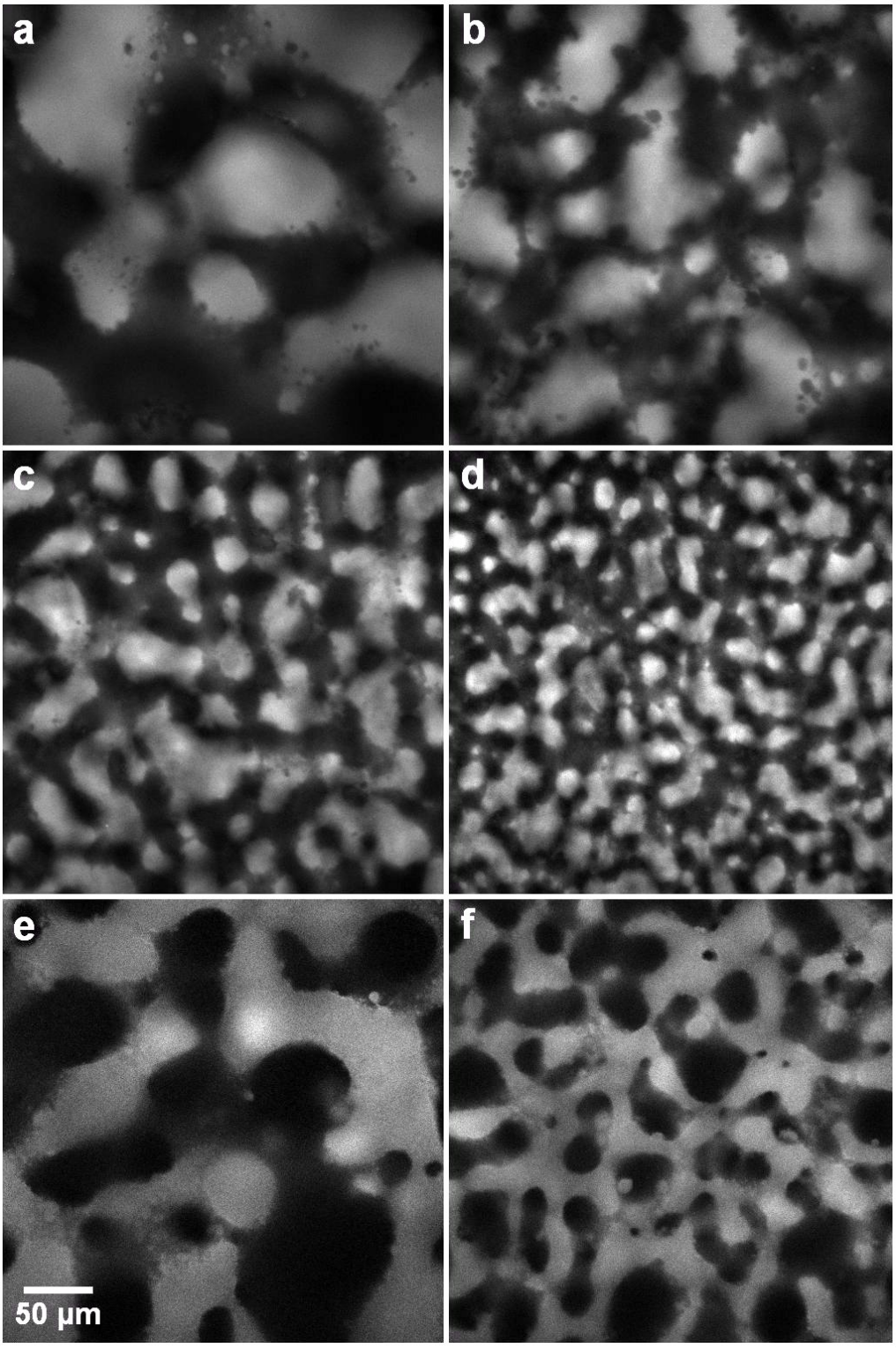

Figure 5.7 *Higher magnification confocal microscopy images of bijels stabilized by (a - d) 1, 2, 3, and 5 vol.% rods, and (e & f) 3 and 5 vol.% spheres, respectively. Observed fluorescence is from (a - d) Nile Red in the NM-rich phase, and (e & f) Fluorescein in the EG-rich phase.*

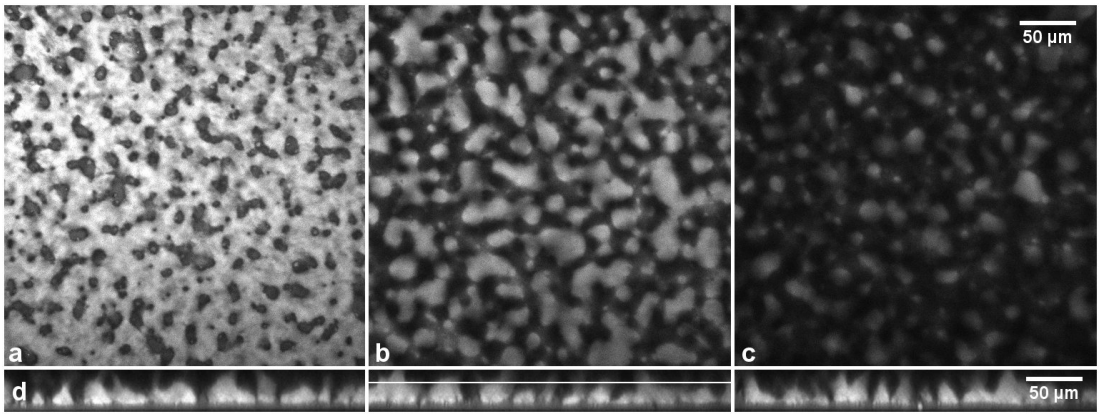

Figure 5.8 *Images taken from a CLSM z-stack of a bijel formed at 5 vol.% rods. Horizontal slices at approximate depths (a) 10 µm, (b) 20 µm, and (c) 30 µm into the sample (thickness = 100 µm) are shown. (d) At the bottom 3 representative vertical slices are presented, where the white line in the middle panel roughly indicates the depth at which images shown in Figure 5.7 were taken.*

silica spheres showed the same EG wetting layer, and the layer of predominantly NM-rich phase, but better imaging was possible at greater depth into the sample. Clearer images like those shown in Figure 5.7 were taken not much deeper into the sample (30-35 μm), compared to the images of rod bijels.

Despite this, images of the type shown in Figure 5.7 give a qualitative 2D comparison of bijel structures. They clearly demonstrate bicontinuous structuring characteristic of bijels. The surface-wetting effects clearly present at smaller depth, are probably only reflected in some enclosed domains of nitromethane-rich phase, which are also present in images of sphere bijels.

To attempt a more quantitative comparison, structure factors were again calculated, as already discussed for the lower magnification images. Plotting the data for the bijels stabilized by rods, a shift to higher wave vector is found, corresponding to the decreasing domain size (Figure 5.9). Due to the higher magnification, here the knee only clearly appears for the smallest domain sizes, and agrees well with dominant length scales found in higher magnification images. All curves decay to a plateau value at high q that is independent of particle concentration, which is related to noise in the images. The shift of the knee relative to this probably results in the observed rate of decay after the peak.

With quite closely matched domain sizes, a side-by-side comparison of the ϕ_{rods} = 3 vol.% and ϕ_{speres} = 5 vol.% samples is most relevant with respect to the shape of the domains. Comparing the obtained data, however, does not show a clear

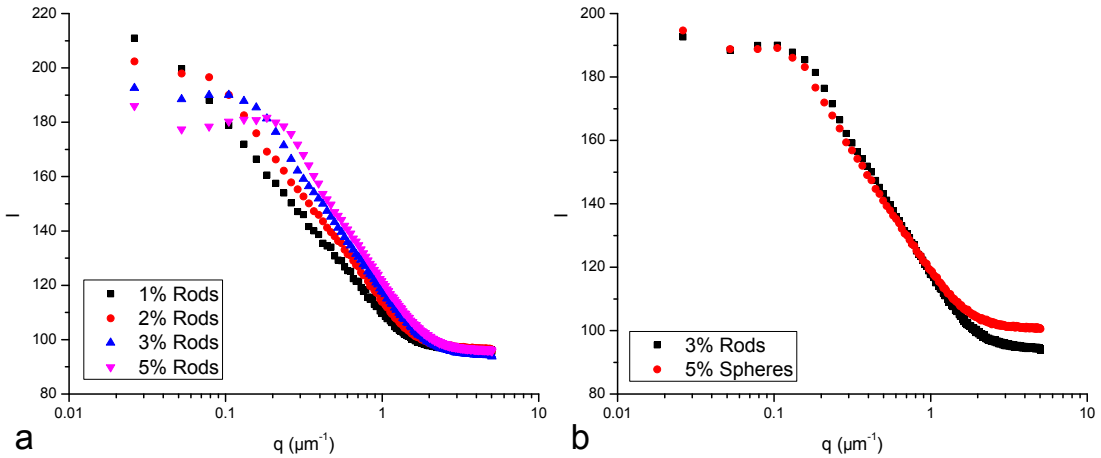

Figure 5.9 *Structure factors for the bijels, calculated by taking the averages of sets of radially averaged FFT's of images like those shown in Figure 5.7). The panels display results for (a) the rod-stabilized bijels, (b) the sphere-stabilized bijels, and (c) a comparison between a rod- and a sphere-stabilized bijel.*

difference. A slower decay after the knee for the rod data is most probably the result of smaller domain sizes. The sphere data demonstrates a higher plateau value at high q, indicating more noise which is observable by eye in the images (Figure 5.7e,f). This makes the direct comparison even more difficult. Thus, at least at first sight, no clear difference domain shape is evident from this data.

Overall, these results show that any changes in the domain shape will only be subtle. This is not surprising, since it is the spinodal decomposition that is the driving force behind structure formation. Additionally, the obtained data is certainly not perfect for detailed structural comparison. Different dyes to visualize the liquid domains, and the presence of akaganéite cores in the rods, will have resulted in the slightly different appearance of the images. Furthermore, the preferred wetting of the glass wall also looks to have a slightly more significant effect on domain structuring in the rod case. All of this makes pinning down subtle changes difficult. At most one could possibly say that domains stabilized by spheres curve more smoothly and gradually than those stabilized by rods. The latter appear to have slightly more wavy and angular domains. Still, the main result here is that there is no significant change in bijel structure, apart from the different rate at which L changes with $\phi_{colloid}$.

In the various stages of studying rod-stabilized NM/EG bijels, some other noticeable observations were made that have not been pursued in any detail. Some more tube-like structures were found to form in some cases, and also NM/EG

monogel formation was found upon prolonged aging. For completeness, these results are presented in the appendix to this chapter, with brief descriptions.

Packing of rods at the interface

The specific design of the rods can now be exploited to study the packing of the rods that stabilize the bicontinuous liquid domains. Selections of images have been presented in Figures 5.10 and 5.11. These are mainly of the bottom part of the bijel, as high resolution imaging deeper into the sample was not possible. Since still a good picture is obtained of how rods are jammed together on a curved interface, including necks and other more extreme shapes, this is not an issue.

Just observing the fluorescence from the rods (Figure 5.10) is the obvious choice for studying the packing of the rods. Fluorescence from the NM-rich phase, however, was also found to contain information, not only about the domain shape, but also about the rod packing. The rods leave their imprint in the form of short, dark stripes in otherwise bright areas, due to the light-absorbing properties of the iron oxide cores. Combining the Nile Red and FITC fluorescence made it possible to create images with a slightly different feel, with in some places a slightly enhanced visualization of the particle packing (Figure 5.11). The only loss in detail is the clear observation of any gaps in the packing. In the end, these images appear to give a more overall representation of the structure, with a better sense of depth.

Looking at these images, it is clear that no great long-range translational or orientational ordering of the rods is present. Mainly on fluid necks one can see a general alignment. This occurs both parallel and perpendicular to the length of the necks, which might well be related to whether a neck was stretched or compressed prior to structural arrest. Especially the ability of rods to align along a thinning neck results in some very thin liquid bridges (*e.g.* Figure 5.10a).

Studying the packing more closely, several characteristic features can be identified. Regularly, several rods are found in small side-by-side stacks. With their usually rather random orientation, these quite well-defined and tightly-packed structural elements end up causing significant, often triangular gaps. The density of the resulting packing is thus somewhat heterogeneous. Another distinctive feature is the presence of rods that are sticking out of the interface, as also appeared to occur on droplets. Occasionally, when observed as tiny bright dots,

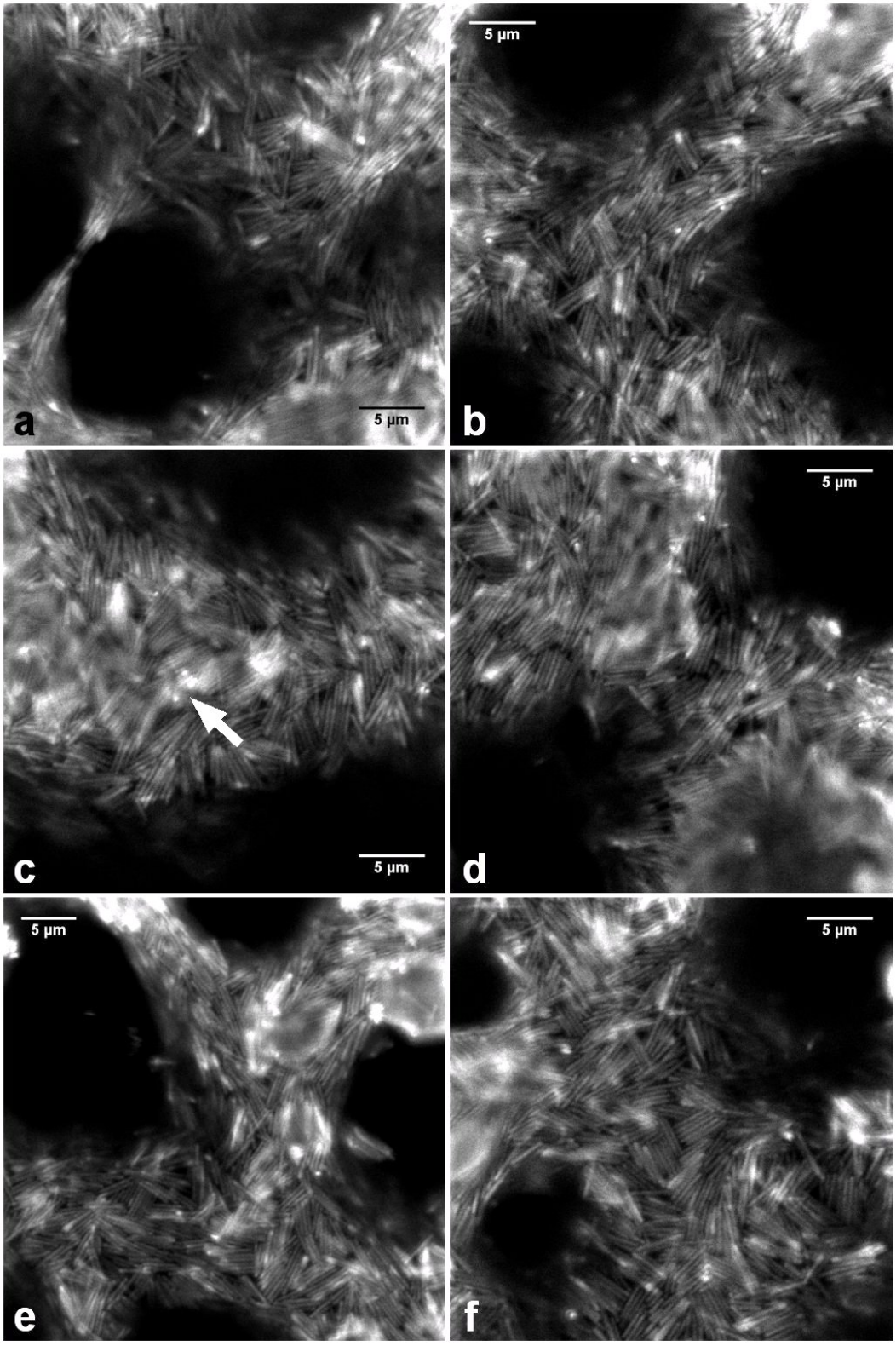

Figure 5.10 *Selection of high magnification images showing FITC fluorescence from the rods, of the (a-d) 2 vol.% sample, and (e,f) the 3 vol.% sample.*

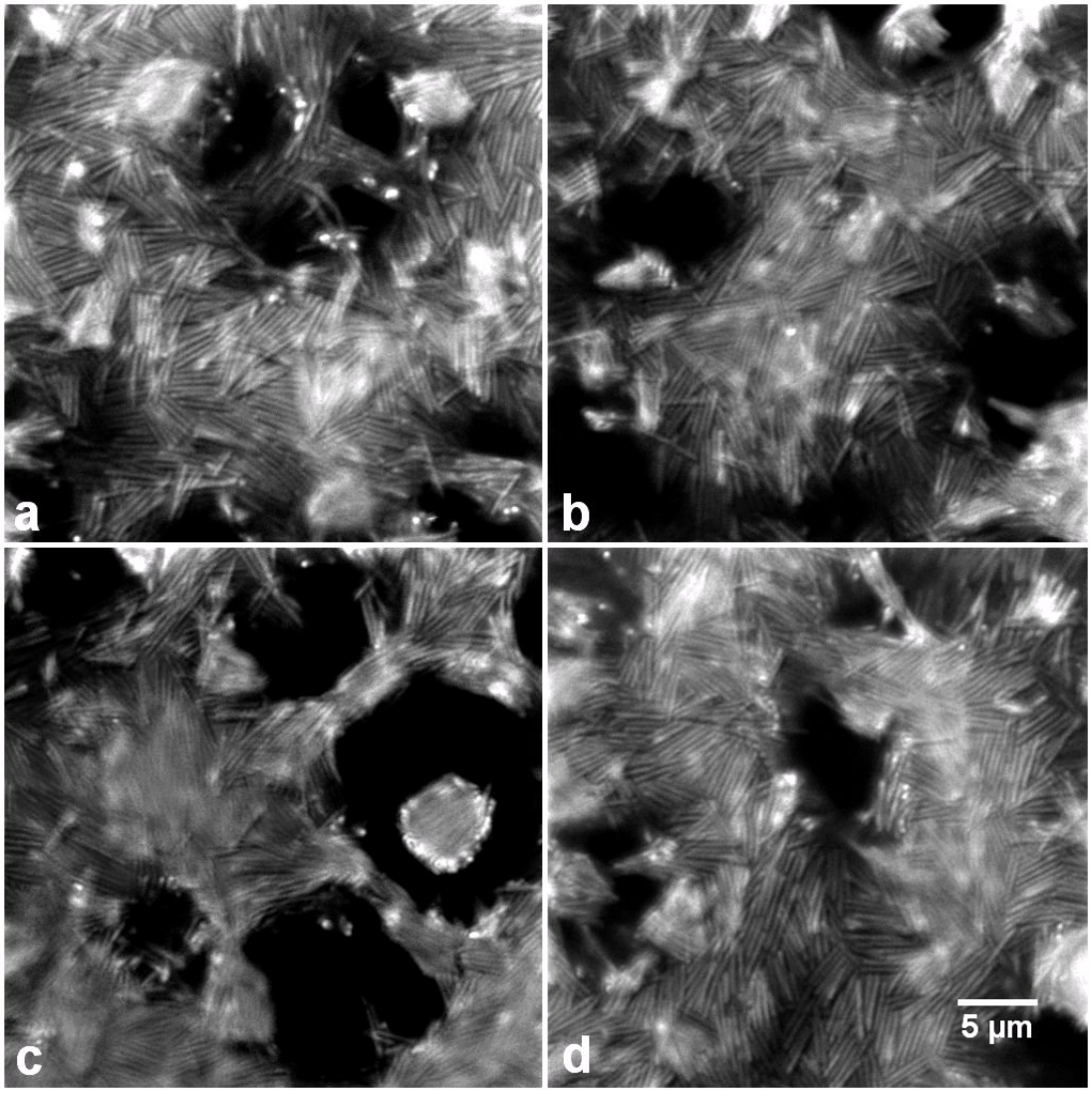

Figure 5.11 *High magnification, composite images showing FITC and Nile Red fluorescence, taken from the 5 vol.% sample.*

they even are perpendicular to the interface ('flippers', a small group of them is pointed out in Figure 5.10c).

While obviously being the result of the jamming of the rods at the interface, capillary interactions might well be involved in determining the final packing. A likely clue that this is indeed the case is the presence of the side-by-side stacks, which have similarly been observed to be caused by capillary interactions for ellipsoids at flat interfaces [11, 12]. Similarly, triangular features have been observed [11], however, the triangular gaps here are probably more packing related. It must be realized that in this case, where the rods are neutrally wetted, the capillary interactions would arise from the interplay between curvature of the interface and the shape of the particles. That is, at a flat interface neutrally

wetted rods would not induce a deformation of the interface [42]. Here, the curvature of the interface might also affect orientation of rods [44].

Rapid jamming is clearly the main driving force behind organization of the rods. As a result the overall structure is mostly isotropic, and the packing contains many cases where particles are forced into energetically unfavorable arrangements. The latter includes flippers, and gives rise to gaps. Flippers have been observed for ellipsoidal colloids at interfaces, just before a compressed monolayer buckles, and on droplets [14, 73]. The situation here effectively involves the compression of a monolayer of rods at a curved interface, as the domains coarsen. It is easy to imagine a scenario where 2 rods collide head-on, but still at an angle due to the curved interface, one of them might well end up on top of the other, and be forced off the interface. Apparently an event somewhat like this probably results in flippers, as well as particles sticking out at other angles to remain trapped on the interface to a larger extent. The rods tilted intermediately with respect to the interface, contrasts the observation of only complete flippers at flat interfaces, and might well be related to the curvature of the interface.

Naturally, the packing of the rods at the interface is related to the global bijel structure. First of all, it links to the relationship between the domain size and the colloid concentration, as it determines how much of the interfacial area the rods effectively take up. Structural features such as the observed flippers, stacks and gaps are of importance here. Gaps would lower ν, while particles sticking out of the interface would increase ν. Returning to the observed difference between the rough approximation from equation 5.2 and the experimental result, the 'flippers' are suggested to be more significant. From these images it is hard to judge how realistic this is. In any case, the effect of the specific interfacial structuring on how the domain size changes with particle concentration will be relatively small compared to the effect of changing the particle shape from spheres to rods.

Secondly, as was found in the results presented above, on a large scale, the rods do not affect structuring imposed by the spinodal decomposition of the liquid mixture. This reflects the overall isotropic structure of the rods at the interface, caused by a rapid jamming on the curved interface. Only on a smaller scale can the shape of the rods make a difference, where thin liquid bridges are a striking example. It appears that their ability to align does allow the stabilization of smaller features. Here, smaller radii of curvature are at play, and then the length of the rods becomes more significant as it can prevent the interface to curve.

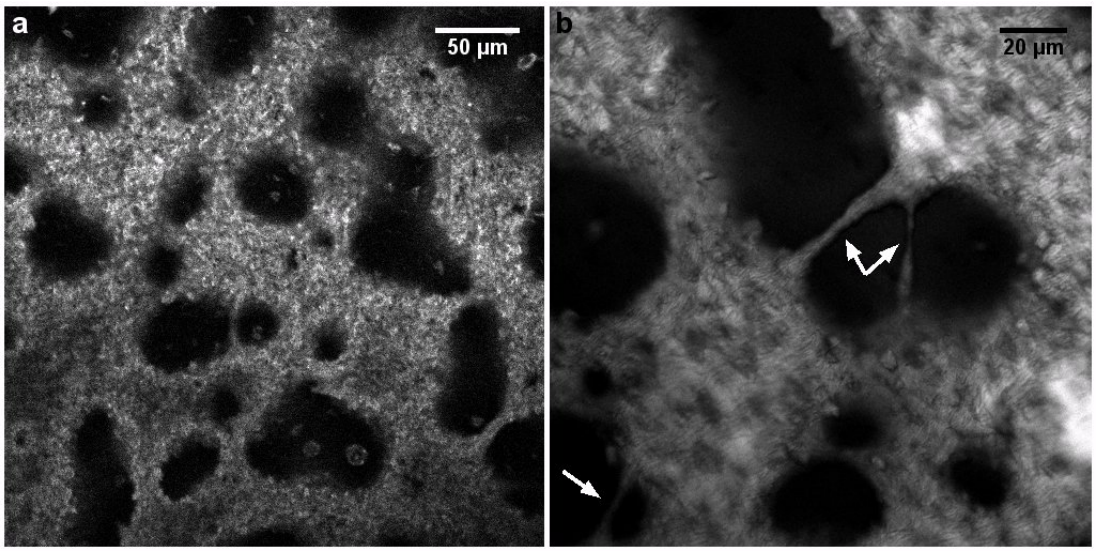

Figure 5.12 *Interfaces of water and 2,6-lutidine, stabilized by hollow fluorescent rods. (a) FITC fluorescence from the rods, and (b) rhodamine B fluorescence from the 2,6-lutidine-rich phase.*

Finally, it is briefly pointed out that some initial tests with water and 2,6-lutidine were done. A bijel-like structure was found stabilized by fluorescent hollow rods that formed a very rough stabilizing layer, as can be seen from its texture (Figure 5.12a). Here also thin liquid bridges are found, confirming this as a more general feature of rod-stabilized bijels (Figure 5.12b).

5.4 Conclusions and outlook

Bijels were created with colloidal rods ($AR \approx 10$) and spheres ($AR \approx 1$) of nearly identical volume per particle. After describing in some detail the route towards the preparation of rod-stabilized bijels, the scaling of the domain size with colloid concentration was presented and discussed. Since, due to their shape, the rods take up a larger area of the interface, jamming occurs more rapidly, resulting in smaller domains compared to the spheres at the same volume fraction. Relationships between the domain size and particle concentration based on simple geometrical arguments showed good qualitative agreement.

Higher magnification images clearly showed the shapes of the liquid domains, allowing a close comparison of rod- and sphere-stabilized bijels with similar domain size. Imaging- and wetting-related effects limited this effectively to a 2-dimensional comparison of the packing. No clear difference in domain shapes

could be pointed out between the two counterparts. This demonstrated that, on a large scale, the type of bijel structure is not significantly altered by changing spherical particles into rods. Thus, here the faster decrease of the domain size L with increasing particle volume fraction $\phi_{colloid}$ is the main structural effect of using rod-like instead of spherical colloids.

After establishing this, the specific design of the used rods was employed to elucidate packing of rods. Several characteristic structural features were identified. The packing contained side-by-side stacks of several particles, the formation of which could well have involved capillary interactions, judging from previous studies. Overall organization is isotropic due to a rapid jamming after phase separation, resulting in significant gaps where packing is frustrated, as well as some particles being partly pushed off the interface. These features have consequences for how fast the domain size changes with particle concentration. The approximate relationship between L and $\phi_{colloid}$ (equation 5.2), assuming a perfect packing of rods, was compared with the experimental result. This appears to suggest particles being pushed off the interface somewhat undermines the gain in area of interface taken up per particle by changing spheres into rods.

More locally, alignment of rods on fluid necks could be observed. Both parallel and perpendicular orientation with respect to the necks was observed, which is likely related to, respectively, stretching out or compression of the necks due to the liquid domains it connects. This way, the ability of rods to align could result in extreme cases of very thin liquid bridges. It appears that the shape and size of the rods becomes significant in stabilizing interfaces when small radii of curvature are involved, as the length of the rods can prevent the interface from curving in one direction, but not the other. In terms of interfacial curvatures, the rods will thus mainly have an effect on a smaller scale.

Based on findings of the current studies suggestions can be made towards future studies. Here, sphere bijels were done with RITC-labeled particles and Fluorescein labeled liquids, a combination aimed at eventually preparing rod/sphere bijels. This was attempted, however, the two types of particles, while individually stable, heavily aggregated when combined. This must be related to surface chemistry differences, with a pure silica surface for the rods, and the presence of amine-groups and covalently attached dye molecules on the surface of the spheres. It could be that the surface charges are of opposite sign, as, for example, in water amine groups typically carry a positive charge while silanol groups are negatively charged.

In this case, structural comparison would actually have benefited from using same dye combination for spheres as for rods. In that respect, hollow rods would also have helped by improving imaging. A final adjustment would be in preventing preferential wetting of the glass walls of the sample container. Making the glass hydrophobic using dichlorodimethylsilane would be a good first attempt.

Changing experimental parameters in future experiments might provide a route to significantly different structures. Some results presented in the Appendix possibly suggest that the quench characteristics could be an important factor. For instance, quenching samples in ice-water leads to a higher and more rapid increase of interfacial tension. Consequently, capillary interactions will be stronger, possibly leading to a more pronounced effect of the rods. Furthermore, it might be worth increasing the aspect ratio of the rods. This can be done by only growing a very thin layer of silica on akaganéite needles. However, it seems that rod length compared to radius of curvature is most important, in which case the length of the current rods is insufficient for significantly affecting overall domain shapes. Additionally, it would mean that small domains and long rods would be required for a significant effect. Rods might then just stick out of the interface more, as observed for long rods on relatively small droplets [118].

A possibly important contribution of rods towards bijel properties would be its mechanical response. This is most certainly suggested by surface-rheology of rods at interfaces, where they show markedly higher moduli compared to spherical particles [14]. Therefore rod-bijels could be considerably stronger compared to sphere-bijels. Currently, no setup to directly measure this was readily available. A simple qualitative comparison could possibly entail low-speed centrifugation of rod- and sphere-bijels of similar domain size.

Overall, the presented results have demonstrated the ability to study rod-stabilized bijels in great detail. While not being perfect, it clearly points out the main characteristics, also in comparison with spheres. Thereby, it paves the way, and indicates the most promising directions for potential future studies of rod-stabilized bijels.

Acknowledgments

Andy Schofield provided the RITC-labeled silica spheres, and Steve Mitchell assisted with TEM.

Appendix

Tube-like structures were observed occasionally, where it appears that it is always the EG-rich phase forming a network of interconnected 'tubes' within the NM-rich phase, which therefore often appears as near-spherical domains (bottom left half of the top Panel of Figure 5.13a). In one sample they were observed to coexist with a more bijel-like structure (Figure 5.13a, top), possibly suggesting that the formation is related to the phase separation kinetics. Namely, different parts of the sample can be subjected to slightly different temperature quenches, or composition if significant evaporation takes place. In other parts of the same sample sharper angles are involved in the structure (Figure 5.13a, bottom).

Another more remarkable structure was formed upon quench made by a quench in ice-water (Figure 5.13b). Here narrow, straight EG-rich (again) channels enclose larger NM-rich domains.

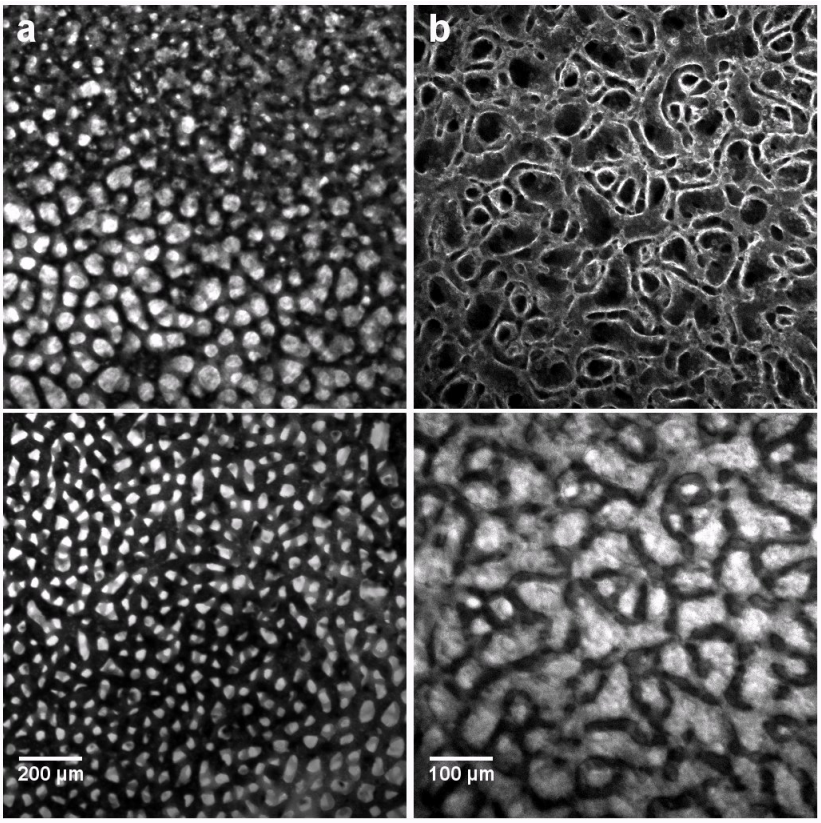

Figure 5.13 *(a) In one sample, prepared as described in Section 5.2, (top) a bijel coexisted with a more tube-like structure, and in other parts (bottom) tube connections appeared very sharply curved. (b) A sample of NM/EG with hollow FITC-labeled rods in a 1 mm path length cuvette (Starna), narrow and straight EG-rich channels formed upon a quench in ice-water.*

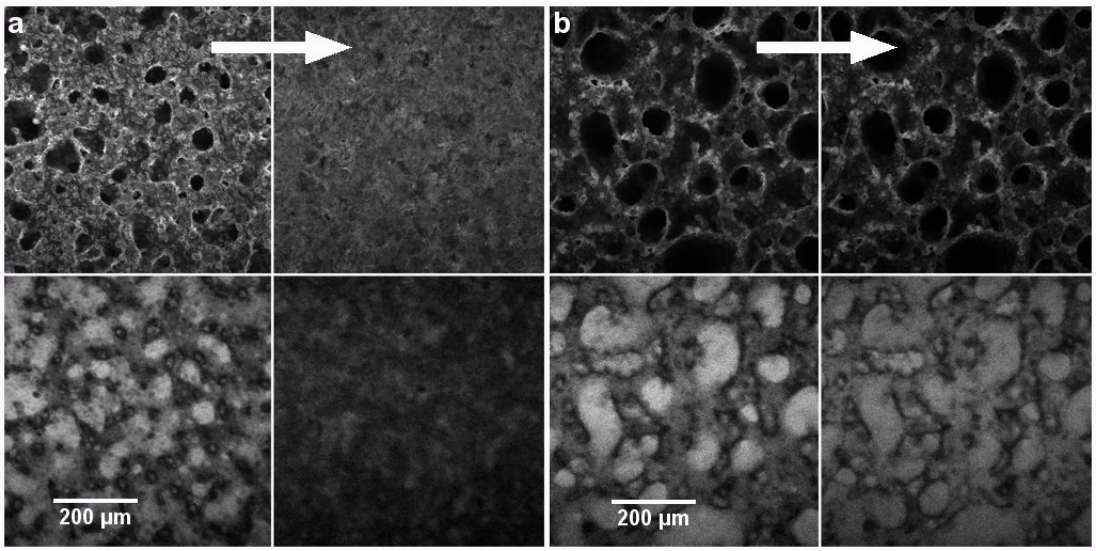

Figure 5.14 *Monogel formation in NM/EG. (a) Structure aged for 13 days, heated to 50 °C. (b) structure aged for 19 days, heated to 50 °C.*

It was previously found in water/2,6-lutidine bijels that the particle structure can remain intact after re-mixing of the liquids [110]. The resulting material was termed 'monogel'. Successful monogel formation in nitromethane / ethylene glycol was here observed upon prolonged aging of samples. For a sample aged 13 days, heating a sample to 50 °C resulted in a collapse of the structure, leaving bigger aggregates of particles (Figure 5.14a). The Nile Red fluorescence drops significantly as mixing occurs, related to the changed solvent composition and the presence of large aggregates. Increasing aging time to 19 days, the particle structure remains intact when the liquid phases re-mix after heating the sample to 50 °C, so a monogel is formed (Figure 5.14b). In contrast, in water/2,6-lutidine only 20 minutes of aging is required for monogel formation [111]. Here, mixing of the liquid phases is observed by Nile Red fluorescence, which decreases as the solvent composition changes, while contrast differences disappear, except for the black 'imprint' caused by the particle structure. It is unclear why in NM/EG such long aging is necessary for monogel formation. Its eventual stability could be due to a slow (surface) chemical changes where particles touch. For instance, covalent bonds between particle surfaces could be introduced at a slow rate, by the condensation of adjacent silanol groups.

Chapter 6

Cellular networks of colloids via emulsions of partially miscible liquids: A compositional route

A new and simple method to assemble colloids into a cellular network is presented in this chapter. It relies on compositional changes in a colloid-stabilized emulsion of partially miscible liquids induced by evaporation of the continuous phase. Since the liquid phases eventually mix, the resulting network is contained within a single fluid phase. After studying in detail the formation of the networks, their structural properties, stability, and post-formation processing are discussed. The results are put into a broader context by considering the use of other constituent materials, and by comparison to a closely related study.

6.1 Introduction

Porosity is essential for a great variety of materials applications although it can be demanding to incorporate. Hence, much effort is put into making and designing porous materials, and they are also common in nature. A class of macroporous materials (pores > 50 nm) are cellular solids which contain a space-filling packing of polyhedral voids (the cells), separated by solid cell walls; these therefore are a type of foam [123]. The main characteristic of a cellular material is that its density, relative to that of the material from which the cell walls are made, is

very low. Additionally, properties like the mechanical response, surface area, and thermal conductivity are very different compared to the non-porous counterpart [123]. A cellular structure could also act as backbone, or underlying scaffold, in a composite material. Here, it would for instance offer mechanical strength or a conducting pathway.

It is clear that these structures have great potential for developing new materials, and one way to create them is through the assembly of colloidal particles. An example is a liquid crystal-colloid composite, where colloids are in a thermotropic nematic liquid crystal [124]. The particles form a network when the suspending liquid is quenched from the isotropic phase into the nematic phase, due to the particles becoming trapped in between growing nematic regions. Freeze-drying an aqueous colloidal suspension is another example [125]. Similar to the liquid crystal case, this involves a transition of the dispersing liquid into a more ordered state, particles become stuck in between growing ice crystals.

A more commonly employed method of making cellular solids from colloids takes colloid-stabilized emulsions of immiscible liquids as templates. High internal phase emulsions (HIPEs) serve this purpose well, as they already have a foam-like structure, with droplets packed densely inside a minority fluid. Cellular solids can be obtained from these emulsions by polymerization of the continuous minority phase, or by drying and sintering of the emulsion [126, 127]. Starting from emulsions with approximately equal volumes of the 2 liquids is also an option. Such an emulsions of water and toluene, stabilized by silica particles, can result in the formation of macroporous silica upon evaporation of both liquids at ambient temperature [49, 128, 129]. Here, an excess of particles are present in the continuous phase as filler for walls separating the pores, and slow evaporation ($>$ 1 week) is required for a stable structure to form. Ultimately, structures resulting from methods relying on Pickering emulsions of immiscible liquids mostly look like a dense packing of droplets, due to spherical, or at least more rounded cells, as opposed to a true foam structure with flat-walled polyhedral cells.

Recently, a way to assemble colloids into a more foam-like cellular network (Figure 6.1a) was reported, starting from colloid-stabilized emulsions (schematically represented in Figure 6.1b-1) of partially miscible liquids [130]. It entails varying the temperature towards re-mixing of the liquid phases. As this happens, buoyancy, phase behaviour, and changes in interfacial tension all play roles in the formation of the network. Locally, creaming of the droplets makes the continuous phase the minority phase, and droplets are observed to grow while

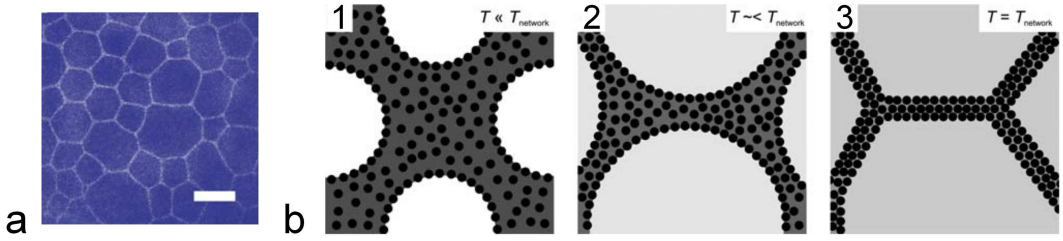

Figure 6.1 *Images taken from [130]: (a) Cellular network of particles (white) formed by taking a solid-stabilized emulsion of partially miscible liquids, and quenching the temperature to near the temperature at where the liquid phases mix. (b) Schematic representation of network formation as the temperature is brought close to where the liquids are fully miscible.*

the 2 liquid phases exchange material and become more alike (Figure 6.1b-2). The associated drop in interfacial tension facilitates droplet coalescence, as the particles more easily detach from the interface and attractive capillary interactions between particles are reduced. Eventually, the overall process also induces droplet deformation since droplets get pushed together and Laplace pressure decreases. Therefore, with the minority phase disappearing, the particles at the interface and in the liquid separating droplets end up in a cellular network (Figure 6.1b-3). The dense packing of particles slows film thinning and rupture. After further mixing of the liquids, particles possibly retain a wetting layer and, through capillary necks, particles can remain aggregated longer. There is only temporary stabilization of the networks, as evidenced by coarsening over time, similar to coarsening through film thinning and rupture in liquid foams. The networks also fall apart upon complete mixing the liquid phases. Still, fragments of cell walls are reported to remain intact, demonstrating a potential to fix the structure upon aging, in a manner similar to monogels (See [110], and the Appendix of Chapter 5).

Here, a new method of assembling colloids into a similar cellular structure is presented, also taking a colloid-stabilized emulsion as template. It combines elements of the methods starting from both Pickering emulsions of partially miscible and those prepared from fully immiscible liquid pairs. However, the final structure and its formation most closely resemble that of the cellular networks observed in partially miscible liquids en route to remixing. Below, details of the experimental methods employed in the study are described first. The experimental system allows studying the formation of these structure in an easy and detailed way, and this will be demonstrated and subsequently discussed. Additionally, their properties, containing one fundamental difference compared

to previously reported structures, and possible post-formation processing are discussed.

6.2 Experimental section

Materials

Ethylene glycol (anhydrous, 98.5%), Tetraethyl orthosilicate (TEOS, reagent grade 98%), 3-[Tris(trimethylsiloxy)silyl]propyl methacrylate (TPM, 98%), hexamethyldisilazane (HMDS, reagent grade, ≥99%), photoinitiator 2-hydroxy-2-methylpropiophenone (97%), Nile Red (technical grade), and propanal (propionaldehyde, FG, Kosher, ≥97%) were used as received from Sigma Aldrich. Nitromethane (99+%, stored under nitrogen) was used as received from Acros Organics. Ammonium hydroxide solution (35%) of reagent grade was obtained from Fisher and ethanol (absolute) from VWR. For the particles FITC-labeled silica spheres (lab code: ASSi25) were used.

Particle modification

FITC labeled particles were coated with an additional layer of silica, since the bare particles preferred too much the ethylene glycol-rich phase (see Chapter 7).

Dried FITC labeled spherical silica particles (4 g) were dispersed in ethanol (180 g) using sonication. Next, 14.8 g ammonium hydroxide solution (35%) was added, followed by 3 additions (dropwise and under stirring, 30 minute intervals) of 0.6 mL TEOS/ethanol mixture (1:1 v/v). After leaving this under stirring overnight, the particles were washed several times with ethanol, and stored in ethanol as a stock suspension. Resulting particle size: $R_{TEM} = 0.35$ μm with $s_R = 12\%$.

Hydrophilic particles: Particles from the stock dispersion were dried at ∼100 °C (Binder VD23 set to 120 °C). First for 30 minutes without vacuum, after which the solid layer of particles was broken up with a spatula, followed by another 60 minutes under vacuum.

Hydrophobic silica particles: The stock suspension was diluted with ethanol/ammonia to obtain a final mixture containing 1.7 wt% particles, and

0.83 wt% ammonium hydroxide solution (35%). Finally, HMDS was added to a final concentration of 0.9 wt%. Particles were kept in this mixture under stirring overnight. Subsequently, after several washes with ethanol, they were dried at ∼100 °C (Binder VD23 set to 120 °C). First for 30 minutes without vacuum, after which the solid layer of particles was broken up with a spatula, followed by another 60 minutes under vacuum.

TPM-silica particles: The same procedure as for the hydrophobic particles was followed, except now the prepared mixture contained 0.9 wt% TPM, instead of 0.9 wt% HMDS. Washing and drying of the particles was also done as described for the hydrophobic particles.

Sample preparation and imaging

Appropriate amounts of particles and nitromethane (in which Nile Red was dissolved when required) were weighed out, followed by sonication to disperse the particles. An appropriate amount of ethylene glycol was then added to obtain the desired sample composition, and subsequently the vial was vortex mixed (30 seconds) for emulsification. With a pipette a fraction of the emulsion was deposited directly onto a coverslide, after which evaporation could proceed and, depending on the sample, lead to network formation. Samples were observed with a Zeiss LSM confocal microscope using 40× and 63× oil-immersion objective, as well as a 20× objective.

When adding the photoinitiator (∼0.01 g for a sample volume of ∼1 mL), this was done after adding ethylene glycol, so that it would be mixed into the sample during emulsification. In one case the emulsion was transfered into a cuvette (Starna, 1 mm path length) and illuminated with a Blak-Ray B-100A longwave UV lamp. This sample was heated in an aluminium block (heated with a resistance heater controlled by a Lakeshore 331 PID) mounted on top of a Zeiss LSM confocal microscope. For networks, the emulsion was transferred into a special holder, consisting of a cut-off top of a vial glued onto a coverslide, from which evaporation was allowed to take place. After network formation (overnight), this sample container was illuminated with a UV lamp for a few minutes. The same setup was used for imaging as described above.

6.3 Cellular networks from EG/NM emulsions

The liquid pair used in these studies consists of nitromethane (*NM*) & ethylene glycol (*EG*). At room temperature these liquids are only partially miscible with a maximum solubility of ∼30 wt% *NM* in *EG*. In the presence of silica colloids with controlled surface chemistry, colloid-stabilized emulsions can be prepared from this liquid pair by mechanical agitation. These are the starting point for all samples of the CLSM (Confocal Laser Scanning Microscopy) investigations presented here. For studying network formation, also a fluorescent dye (Nile Red) is added for directly observing the *NM*-rich phase, as well as the mixing of the liquid phases. This is possible due to a strong Nile Red fluorescence signal detected from the *NM*-rich phase when the liquid mixture is phase-separated.

Formation

Since the vapour pressure for nitromethane (3.7 kPa) is orders of magnitude higher than its counterpart ethylene glycol ($8 \cdot 10^{-3}$ kPa), whenever these liquids are mixed, it is this component that will dominate the composition of the evaporated phase. Fairly hydrophilic silica particles can stabilize an emulsion of *NM*-rich droplets within an *EG*-rich continuous phase, and when leaving such an emulsion exposed to the lab's atmosphere, over time, liquid will evaporate. Nitromethane evaporating from the continuous phase will then be replenished from within the droplets. Visualizing the layer of particles trapped at the interface between the 2 liquid phases, reveals that during this process the droplets crumple and eventually completely collapse, with the particles dispersing into the single liquid phase (Figure 6.2, top row). Fluorescence from Nile Red confirms the complete disappearance of the *NM*-rich phase, indicating that the liquid components are fully mixed again due to the change in composition (Figure 6.2, bottom row).

A different situation is observed when changing the liquid composition to reverse the location of the phases (i.e. effect a catastrophic inversion). The particles exhibit partial wetting, with a slight preference for the *EG*-rich phase as demonstrated by the *NM/EG* emulsions, formed when volumes of the liquid phases are approximately equal (Figure 6.2). Therefore, many free particles, and even some small particle-stabilized NM-rich droplets are observed within the

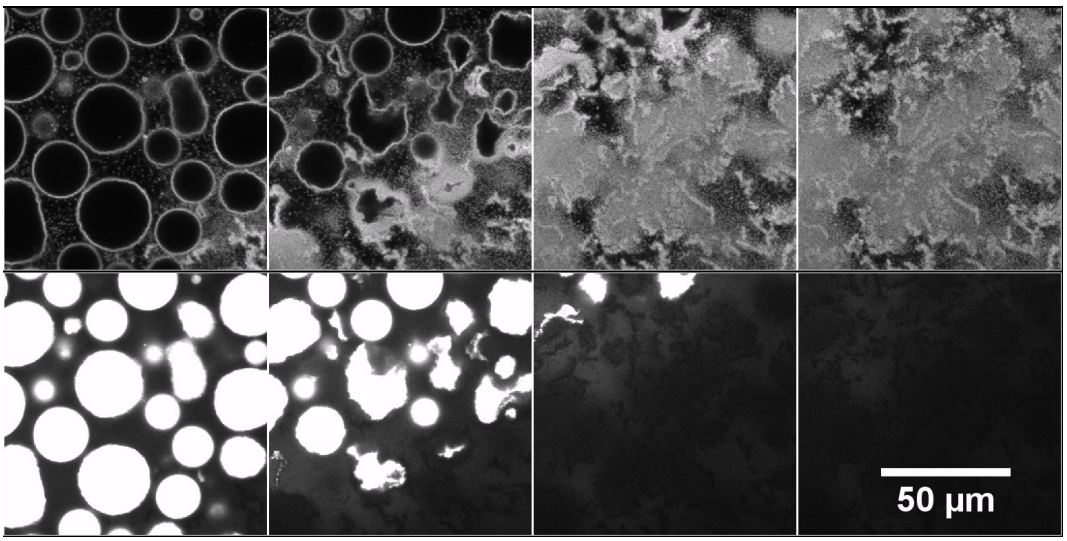

Figure 6.2 *Hydrophilic particles (4 vol.%) stabilizing a NM in EG emulsion, left for liquid to evaporate (time proceeds from left to right). The top row shows fluorescence from the particles and the bottom row shows fluorescence from Nile Red located in the NM-rich phase.*

EG-rich droplets (Figure 6.3a, top row).

In this case it is the continuous phase that evaporates more rapidly. A situation develops, that is visually quite similar to what was observed previously driving a temperature quench towards mixing of the liquid phases (Figure 6.1). The particles trapped at the interface and inside the continuous phase form a cellular structure upon the disappearance of the continuous phase through NM evaporation (Figure 6.3a, rows 2 - 4). Fluorescence of Nile Red shows that NM-rich phase is initially trapped in the walls of the cellular structure (Figure 6.3a, row 3). At a later stage the liquids completely mix, as observed by a disappearance of Nile Red signal from the cell walls, and an increase in Nile Red signal within the cell compartments (Figure 6.3a, row 4). Shortly after the liquid phases fully mix, the structure collapses (Figure 6.3a, rows 5 & 6). This probably corresponds to the previously reported collapse of a cellular network after using a temperature quench to fully mix the liquids. A feature occurring in both cases is that some fragments of wall remain.

Increasing particle hydrophobicity by introducing methyl groups onto their surfaces, resulted in particles that more readily form *EG* in *NM* emulsions (Figure 6.3b, top row). These particles prefer the *NM*-rich phase to an extent that catastrophic inversion of the emulsion could not be achieved. Again allowing NM to evaporate, particles located at the interface and in the continuous phase form a cellular network as discussed before (Figure 6.3b, rows 2-3). A major

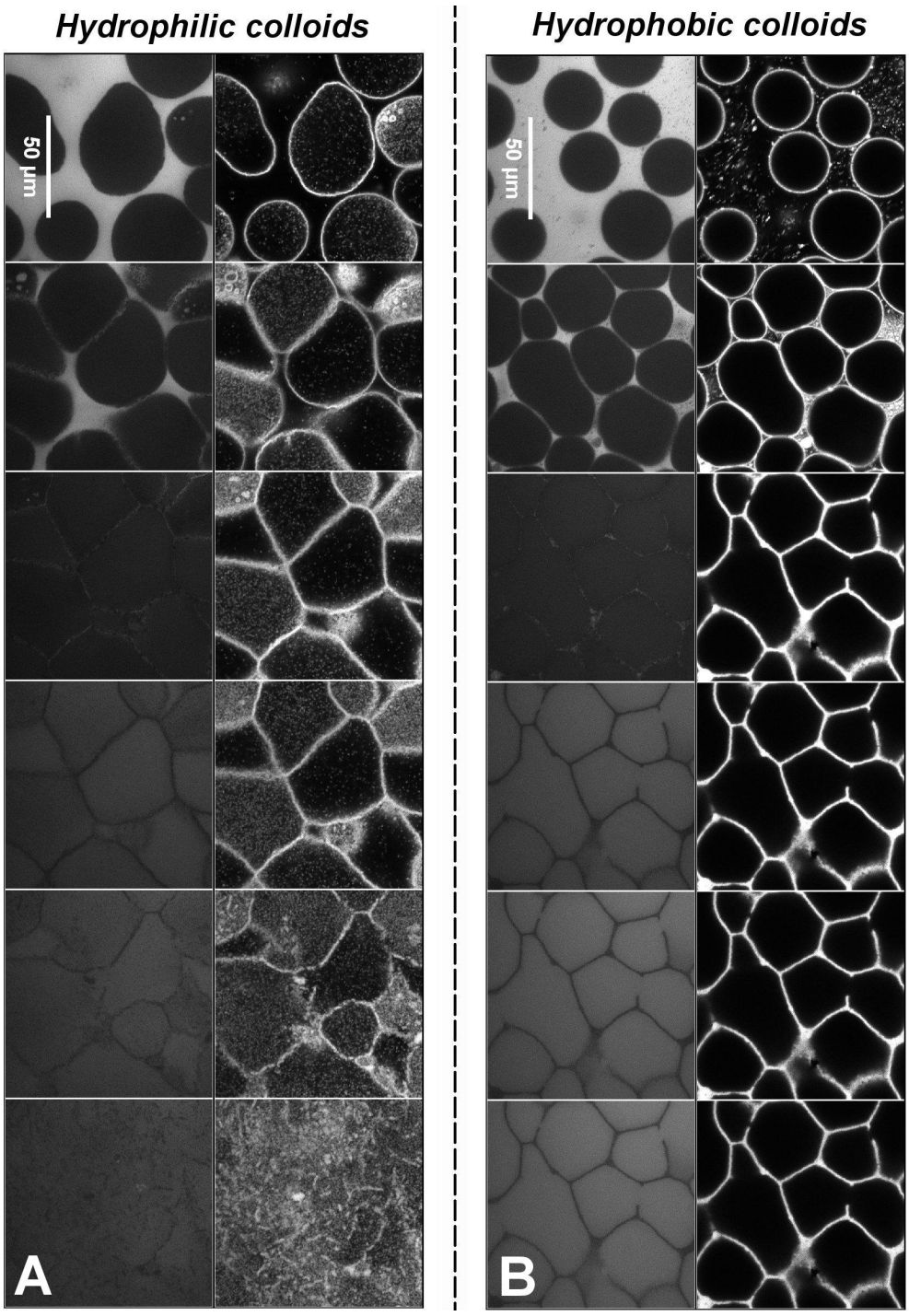

Figure 6.3 *Emulsions for which liquid evaporates as time proceeds (top to bottom): (A) Hydrophilic particles initially stabilizing a EG/NM emulsion, and (B) hydrophobic particles initially stabilizing a EG/NM emulsion.*

difference with the network formed by the more hydrophilic particles is that in this case the structure does not collapse, but remains stable as the liquids mix (Figure 6.3b, rows 4-6).

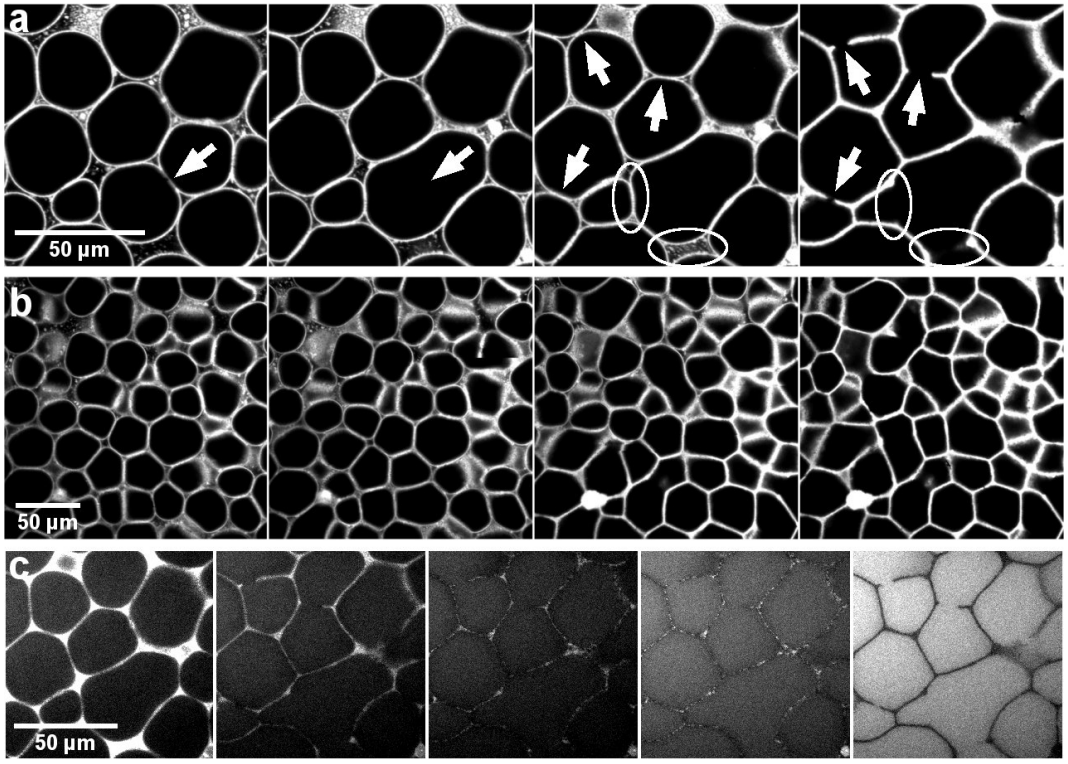

Figure 6.4 *(a) Colloid channel demonstrating in detail coalescence and wall rupture events during network formation. (b) Colloid channel demonstrating the effect of coalescence and wall rupture on a larger scale. (c) Nile red channel demonstrating what happens to the nitromethane-rich phase.*

From the particle channel some events can be identified that play a part in network formation. Coalescence of emulsion droplets that are being pressed together occurs during the final moments prior to lock-in of the final structure (arrows in the first 2 images of Figure 6.4a). Then, quite suddenly a jamming of particles occurs through confinement, guided by the presence of the interfaces and driven by disappearance of the continuous phase (last 2 images in Figure 6.4a). The final structure has locked in. In this event, the walls and nodes of the particle network are formed, and fixed into place. Surplus particles in the continuous phase get pushed into the gaps where 3 or more droplets meet. In this way, they fortify the nodes of the network.

As was mentioned before, network formation is very similar to that in a previous report. There, slow coarsening of the structure led to an analogy with the dynamics of liquid foams. It appears justified to make that analogy here as well, since film thinning and rupture are clearly involved as evidenced by coalescence of 2 droplets being pressed together (Figure 6.4). Unlike in the previous report, here

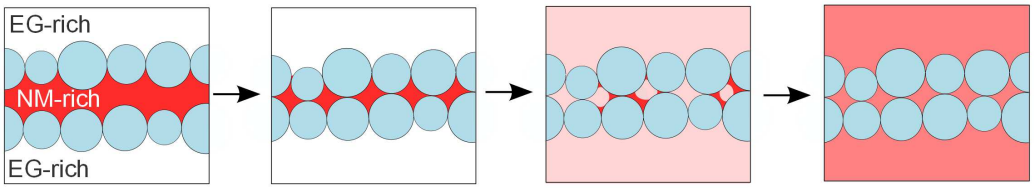

Figure 6.5 *Sketch of what appears to happens to the liquids/dye in the formation of cell walls.*

these processes eventually stop, preventing a slow coarsening of the structure. I.e. due to a quick removal of the continuous phase, the particles suddenly jam into place as they get dragged along by the interface, and the volume of the continuous phase is reduced past some critical value. Film rupture occurring at the very last moments can therefore be arrested by the presence of the particles. In this case the film cannot pull back completely, resulting in holes in the cell walls (arrows in the last 2 images in Figure 6.4a). Also, fortified sections of the wall can result from film rupture just before structure lock-in, when particles are dragged along by the interface of the film (ellipses in the last 2 images in Figure 6.4a). On a larger scale it is revealed that due to coalescence events the cell-size of the final structure is clearly larger than the droplet-size of the parent emulsion (Figure 6.4b). Another feature hinting at a liquid interfaces being involved in formation are some walls separating a small and a large cell, where the curvature is inwards into the large cell. This is a result of a balance of the Laplace pressures prior to jamming of the particles.

Looking at the Nile Red fluorescence in some more detail, we can follow the process that drives structure formation. First, the droplets get pushed together and deform, until only thin films of continuous phase are left (1st image in Figure 6.4c). Confinement through continuous-phase evaporation and gravity drive this process. Additionally, droplet deformation is facilitated by a decreasing interfacial tension as the compositions of the liquid phases become more alike. Just after lock-in of the structure (2nd image in Figure 6.4c), *NM*-rich phase is clearly still abundant inside the cell walls. So, just after formation of the final structure, remaining *NM*-rich phase is being confined within it. It is observed to slowly disappear in a heterogeneous fashion (3rd image in Figure 6.4c), and eventually Nile Red clearly diffuses into the cells (4th image in Figure 6.4c). The latter indicates that the dye stops being confined within the *NM*-rich phase, and mixing of continuous phase with the droplet phase occurs. This must happen through mixing of distinct pockets of continuous phase trapped between the closely packed

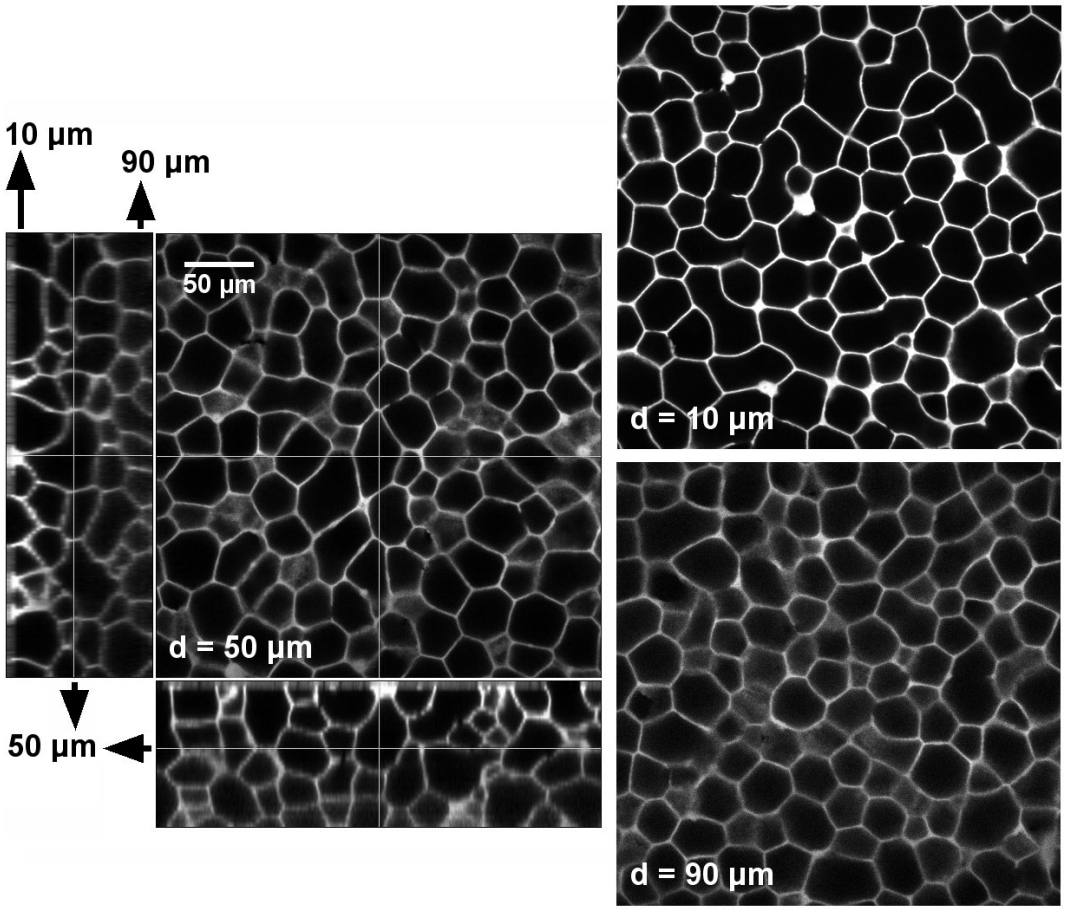

Figure 6.6 *CLSM z-stack: XY slices at 3 different depths(center and 2 on the right), and XZ- and YZ-slice (bottom center and far left, respectively). Scale identical for all images.*

particles with the droplet phase. Eventually, the liquids mix completely and the Nile Red has diffused throughout the cells, leaving the cell walls devoid of any fluorescence signal to be detected, due to the presence of the particles (5th image in Figure 6.4c). The increasing similarity of the 2 liquid phases is of a different origin compared to exchange of the components through diffusion that occurs upon a temperature quench. In this case it is less diffusion (if at all), but more a removal of the main component of the continuous phase by evaporation. What happens to the liquid phases just before and after structure lock-in, can now be summarized by schematic drawings (Figure 6.5).

Structure

So far only 2D data was presented, leaving the reader to guess about how the structure fills 3D space. To supplement the previous results, a CLSM z-stack

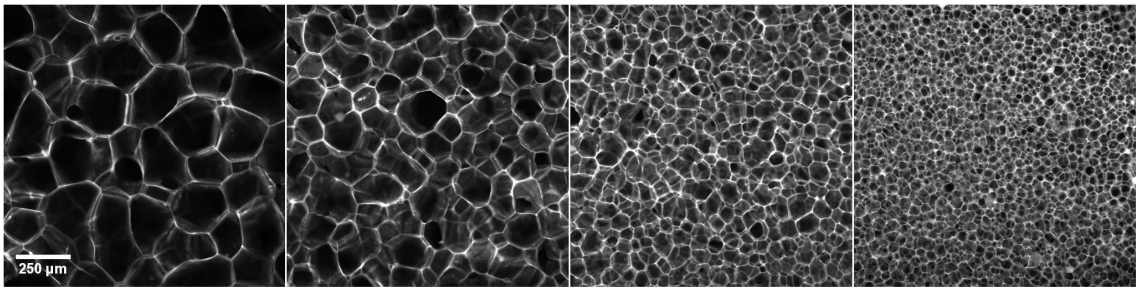

Figure 6.7 *Networks formed from emulsions at particle concentrations of 0.5, 1, 2 and 4 vol.% (going from left to right).*

confirms that this is truly a self-supporting 3D structure (Figure 6.6). Imaging was possible up to a depth of 4-5 cells, beyond which imaging was overly obscured by the structure below. The glass surface at the bottom of the structure, on which the walls of the bottom layer of cells rest, appears to have only a very minor effect. Cells bordering the glass surface are slightly larger than subsequent layers, possibly indicating that more coalescence events occur in the vicinity of the glass surface (top right, Figure 6.6). It could also be that larger droplets are concentrated at the bottom due to sedimentation.

Emulsions with smaller sized droplets can be created by increasing the particle concentration. As the volume of the liquid phases remains the same, a larger area of interface is necessary to accommodate all the particles that become trapped on it. This means smaller droplets result from the emulsification step, leading to a decreasing cell-size (Figure 6.7).

Stability

After demonstrating that these structures are really 3-dimensional self-supporting networks, and with their formation being understood at least qualitatively, the question remains: why can they be stabilized against collapse? The very similar networks observed in a related system were only temporarily stable in a very small temperature range, and would collapse upon complete mixing of the liquids [130]. Temporary stabilization of the particle network depended solely on the cohesive effect of residual continuous phase present within the walls. This corresponds to what was observed in emulsions prepared with hydrophilic particles (Figure 6.3a). After changing particle surface chemistry, however, observations appear to quite convincingly demonstrate that the liquids fully mix (Figures 6.3b and 6.4c) without a collapse of the network. The self-supporting structures remain

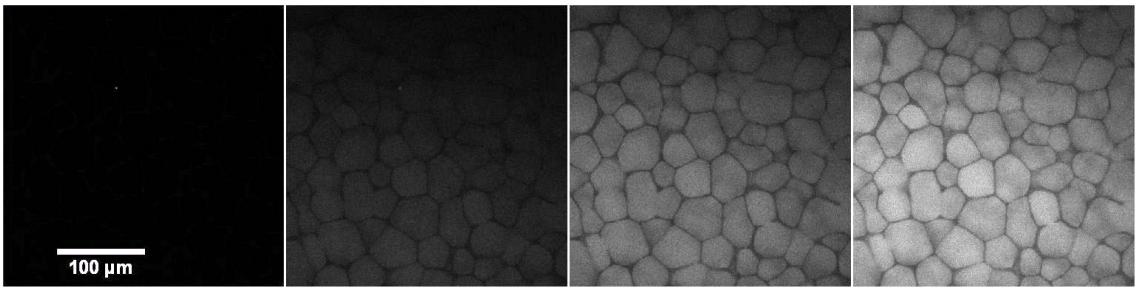

Figure 6.8 *Ethanol is diffusing into the structure, visualized by fluorescence from Nile Red that was dissolved in the ethanol (diffusion progresses from left to right).*

intact while surrounded by a single liquid phase that is kept stationary. They are, however, very sensitive to mechanical disturbances. Flow of the liquid medium under gravity, or evaporation of the liquid, destroys the structure. While the strength of the network might increase upon aging, this will likely not make them fully robust.

To check if, despite the CLSM observations, some residual continuous phase could be responsible for network stability, additional experiments were performed. Heating structures to 60°C, which is far above the UCST (∼40°C, i.e. re-mixing is no longer a relevant issue), did not yield any observable change in the network structure. Mixing of the liquid components can also be induced by the addition of ethanol [64]. Preparing a structure in the absence of Nile Red and putting the sample in contact with a solution of the dye in ethanol, allows imaging of diffusion into the structure (Figure 6.8). The network also appears resistant to this.

Since it is now confirmed beyond doubt that residual continuous phase is not responsible for network stability, it is most likely that attractive interparticle interactions hold the structure together. This may explain why the networks are stable once formed with more hydrophobic particles. Silica particles normally rely on charge stabilization originating from charged groups on their surface. In making them hydrophobic these are largely removed, making it likely that there is no mechanism to properly stabilize them against aggregation by Van der Waals interactions. Hence particles will be bonded together this way during network formation. Firstly, at the interface where particles are jammed into each other to form a dense packing, and secondly, when 2 of these monolayers are pushed into each other (both schematically in Figure 6.5). After the interfaces have pushed all particles into each other to form the network, they disappear as the liquid

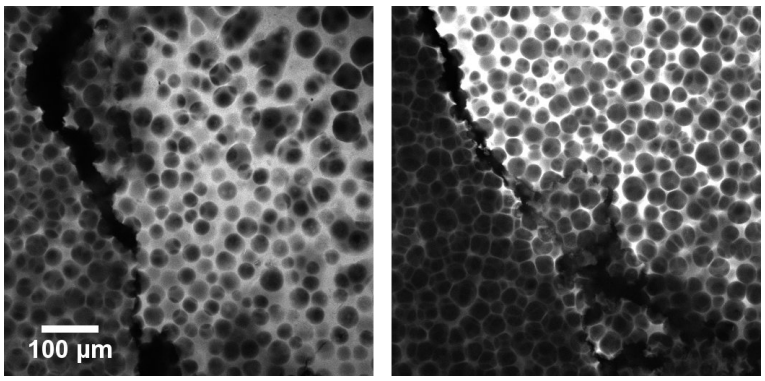

Figure 6.9 *Examples of cracks in the structure, here caused by the structure floating upwards inside a closed container upon addition of ethanol.*

phases mix. Since the hydrophobic particles are only experiencing attractive interparticle interactions, there is only relatively weak thermal energy that could drive them apart into the surrounding liquid. Thus, they remain trapped inside the network. Cracks are occasionally observed in the structure, demonstrating a sort of solidity, in further support of this idea (Figure 6.9).

6.4 Post-formation fortification of networks

For actual applications, further modification or processing of the structure will be required to give permanence. The initially quite fragile materials need to be fortified so they can withstand, for instance, the removal or exchange of the immersing liquid. To this end, a method for cross-linking the particles inside the network has been investigated.

The ease with which surfaces of the silica particles can be modified, is utilized to functionalize them with propyl methacrylate groups. These groups can be reacted together, resulting in the formation of covalent bonds between particles. After network formation this reaction can be triggered by UV illumination in the presence of a photoinitiator. As a proof of principle, photoinitiator was added to an *EG* in *NM* emulsion stabilized by these particles, and the sample illuminated with UV light. Subsequent heating of the emulsion, removing the interface as the liquid phases mix, leaves behind cross-linked capsules of particles instead of dispersed particles (Figure 6.10a). Some of the capsules possess cracks demonstrating their fragility. Allowing an air bubble to pass through the sample underlines this, as all but a few of the capsules are shattered (Figure 6.10b).

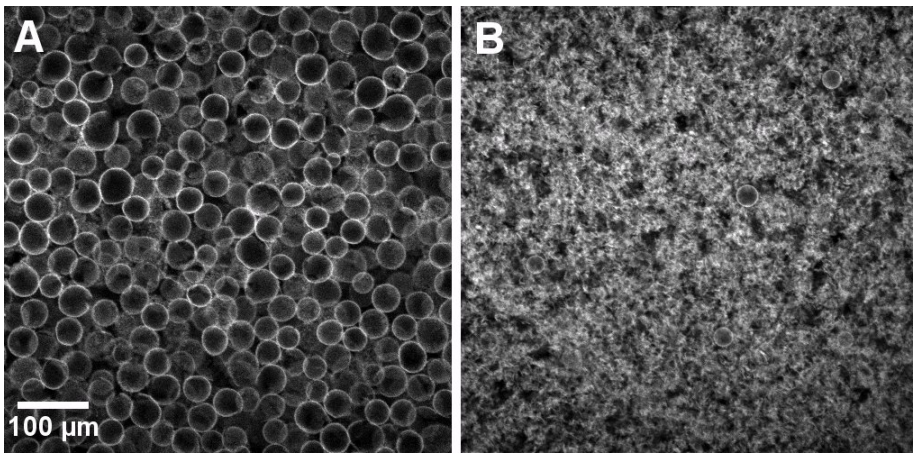

Figure 6.10 *(a) Capsules of covalently bonded particles left upon mixing of the liquids by heating (45 °C). (b) Letting an air bubble pass through the samples shatters the capsules.*

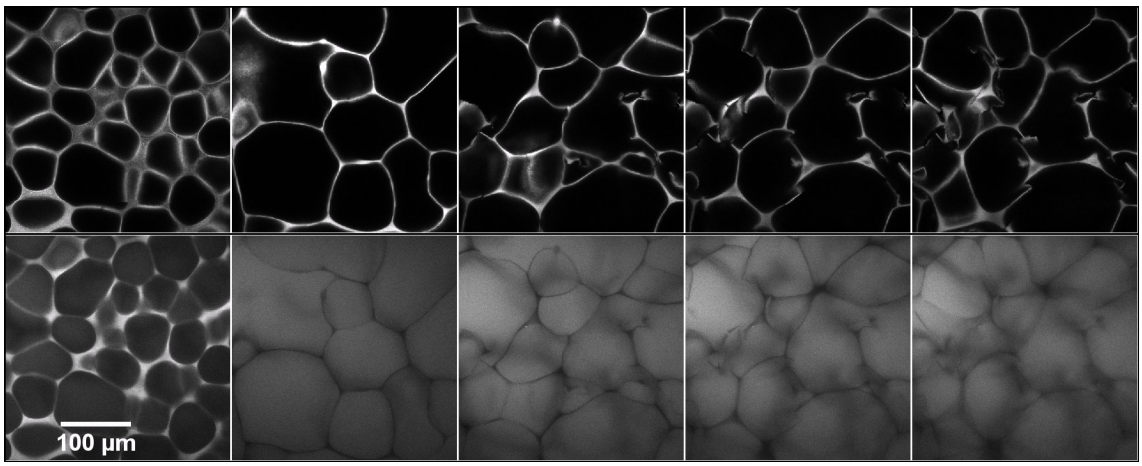

Figure 6.11 *Formation and collapse of a network in an emulsion prepared with 2 vol.% TPM-silica particles using vortex mixing.*

Changing surface chemistry might affect network formation and stability, as was demonstrated before (Figure 6.3). The TPM-silica particles indeed are quite hydrophobic, like the HMDS-silica particles, and easily form stable EG in NM emulsions required for network formation. The transition from HIPE (Figure 6.11, 1st image) to network (Figure 6.11, 2nd image) involves much more coalescence compared to the case of hydrophobic particles (Figure 6.3b). The formed network also does not appear to be stable. It collapses under its own weight as the liquids mix, and parts of the structure come tumbling down (Figure 6.11, images 3 - 5). This was already at 2 vol.% particles whereas the previously stable networks were formed at much lower particle concentrations. Additionally, network collapse is clearly of a different nature than for hydrophilic particles (Figure 6.3b), with it only breaking at weak spots, leaving behind sections consisting of many particles.

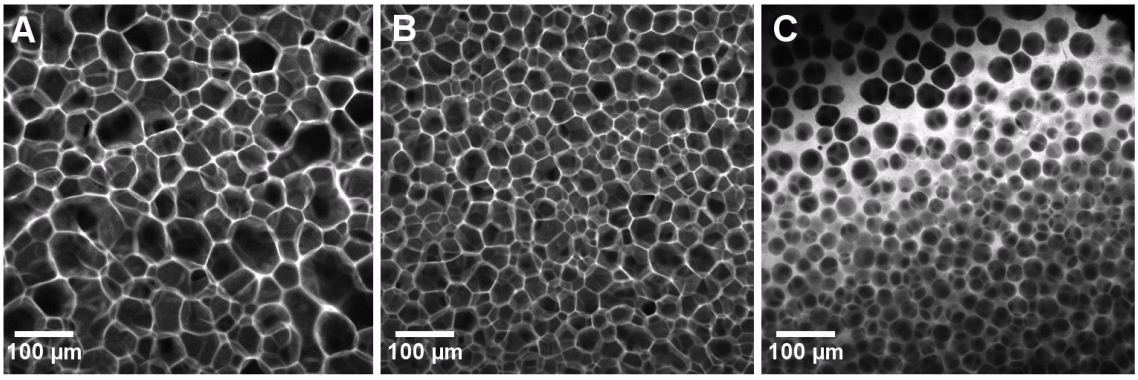

Figure 6.12 *(a) Network formed from an emulsion prepared with 4 vol.% TPM-silica particles using vortex mixing. (b) Network formed from an emulsion prepared with 4 vol.% TPM-silica particles using a rotor stator mixer. (c) Network formed in a larger container over a longer time, here tilted when imaging resulting in observing a depth gradient: top-left close to bottom glass surface, bottom-right deeper into the structure.*

What is left behind confirms that these weak spots are in the cell walls, containing long sections of only a bilayer of particles, and not the nodes. As the liquid mix the particles building up the structure should be held together by attractive interparticle interactions. While these are present, in places they are clearly insufficient to support the network. In any case, these observations do contribute to our understanding of network stability.

Increasing the concentration of the TPM-silica particles, and still in the absence of photoinitiator, structures with smaller cells are prepared that do not collapse (Figure 6.12a). Smaller cells thus result in a structure where the load is better distributed, due to smaller walls and more nodes, allowing self-supporting structures to be again produced. Even smaller cell sizes can be obtained from a parent emulsion with smaller drops prepared with a rotor stator mixer (Figure 6.12b).

Clearly, this new surface chemistry makes networks even more fragile, but the stable networks can still be formed with smaller cell sizes. For cross-linking the networks using the aforementioned method, samples of considerably larger volumes were left for selective evaporation. Structure formation took much longer compared to the drops of emulsion left to dry on coverslips, and was left to proceed overnight. Sedimentation of surplus particles during formation now had a pronounced effect. A gradient of wall thickness developed, with the walls being very thick at the bottom, and getting thinner upwards, away from the bottom

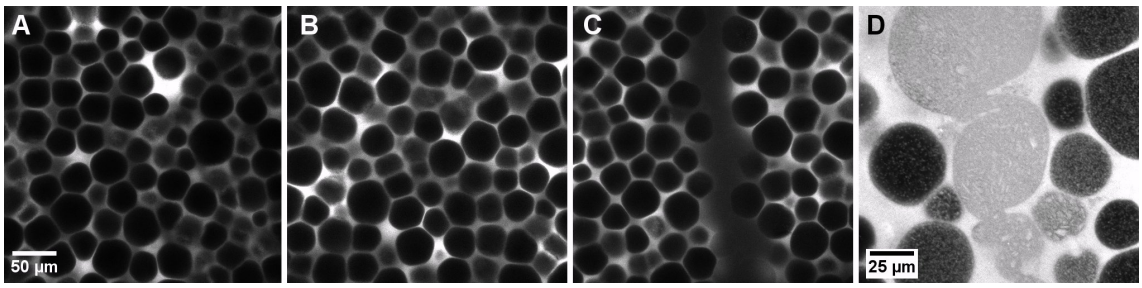

Figure 6.13 *(a) Network of TPM-silica particles formed by 2 vol% emulsion containing photoinitiator in larger volume container, after UV illumination. (b) Same samples as (a) but after immersing liquid has been replaced by ethanol, dried, and immersed again in EG. (c) Portion of a macroscopic crack running through the structure. (d) large magnification image of part of same crack, but at the bottom glass surface. (scale bars same for a - c)*

glass surface, into the network (Figure 6.12c). Overall, cells were more rounded compared to previously made structures, due to the increased size of the nodes.

A network prepared in this manner, was subsequently cross-linked by UV illumination (Figure 6.13a). The immersing liquid (*EG*) was then washed out with, and replaced by ethanol. This allowed quick drying of the structure in an oven. For imaging purposes, to check if it had survived exchange and evaporation of the immersing liquid, it was again immersed in *EG*. The network had indeed survived the treatment (Figure 6.13b) confirming successful reinforcement to allow for further processing.

A macroscopic crack running through the structure, probably a result of the shaking applied during solvent exchange, was clearly visible when dry. The white haze observed within it when viewed under a CLSM (Figure 6.13c), indicates the presence of suspended material originating from the structure. At higher magnification (Figure 6.13d) it is confirmed that close to the bottom glass surface free particles are suspended, both in the crack and also some in surrounding cells. Additionally, there are bigger fragments broken off from the structure. This demonstrates a brittleness of the material, as well as the possibility for individual particles to detach, and be suspended again in an immersing liquid.

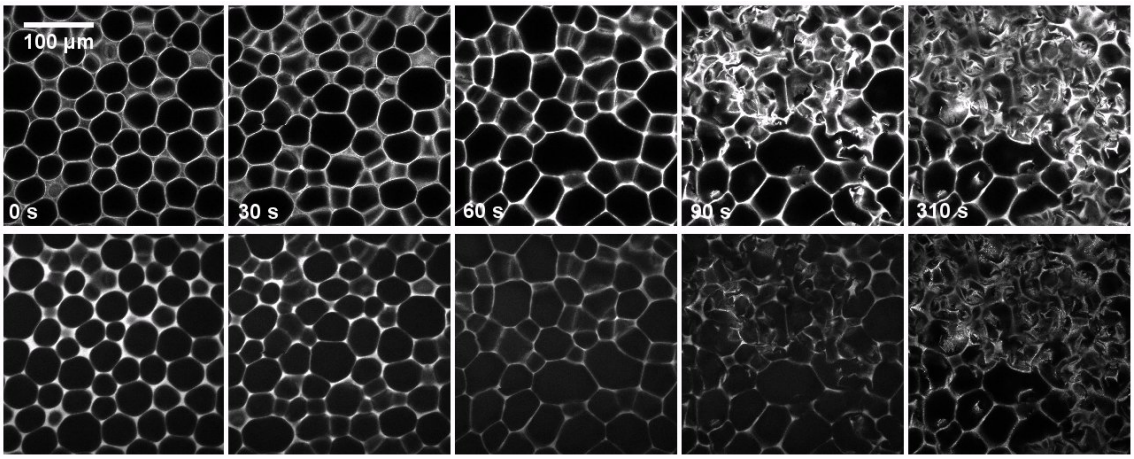

Figure 6.14 *Time sequence demonstrating evaporation in a colloid-stabilized emulsion of water-rich droplets in a propanal-rich continuous phase. CLSM images of colloids are displayed in the top row, and corresponding images of the propanal-rich phase visualized through Nile Red in the bottom row.*

6.5 Generalizing the method

Since all the presented results were obtained with a single liquid pair, it is interesting to consider universality of the method, in particular with respect to the choice of liquids. From the previously presented results it appears that succeeding in the formation of a stable structure at least requires

- a Pickering emulsion with the main component of the continuous phase evaporating at a higher rate than that of the droplet phase (comparing Figures 6.2 and 6.3a),
- the continuous phase and droplet phase to be partially miscible at the temperature at which evaporation takes place (Figure 6.4c), and
- the particles to bind strongly to each other once forced together under influence of the interfaces (comparing Figures 6.3a and 6.3b).

Assembly of a stable cellular network from a water-in-propanal emulsion was attempted. This liquid pair can completely mix at room temperature, and was also selected because of the large difference of their vapour pressures (2.3 kPa (water), 34.4 kPa (propanal)). As propanal evaporates much more quickly than water, the particles indeed get forced from a HIPE into a cellular structure (first 3 pairs of images in Figure 6.14). However, the network is not stabilized and

collapses in a dramatic fashion (last 2 pairs of images in Figure 6.14). Again, the continuous phase was labeled with Nile Red (bottom row of Figure 6.14), however its diffusion throughout the sample at a later stage, is not observed in this case. The mixing of the liquids is observed as a slowly decreasing Nile Red fluorescence intensity within the network, with bright pixels suddenly turning dark. This is still proceeding during and after collapse, and happens much more slowly than liquid mixing in the *NM/EG* mixture. That many structural features stay intact, could be a result of interparticle interactions, or capillary forces exerted by residual propanal-rich phase trapped between particles. Collapse here is more reminiscent of that of the TPM-silica colloids than that of the hydrophilic silica particles in *NM/EG*. Since here hydrophilic particles were used that are normally well-charged in water, one would expect them to disperse upon collapse. This might suggest that residual propanal-rich phase is sticking particles together.

It is clear from results in previous sections that particle networks will have to rely on interparticle forces for structural integrity. The conditions required to achieve a stable structure, in terms of the liquid pair, are not fully understood. Obviously, whether a network remains upon full mixing of the liquids, depends on the balance between the strength of the structure and the forces that exert stresses on the network. The former is determined by structural properties (cell size, wall thickness, number of interparticle contacts) and the actual attractive forces that hold the particles together. The forces that work on the network and could lead it to collapse, result from gravity, flows in the surrounding liquid and interfacial tension. To increase the probability of an intact and stable network forming, these should be minimized, while attractive interactions between particles should be maximized.

The question is whether, at the final stages of the process where continuous phase is disappearing from the particle network, the liquid trapped in between the particles can itself fracture the structure. For instance, due to its decreasing volume it could exert forces as it minimizes its surface to volume ratio. Or, compositional gradients caused by local mixing of the liquids would result in interfacial tension gradients, and therefore Marangoni flows. Therefore, the physical properties of the liquid pair might be important. As was found when comparing results from 2 liquid pairs, there indeed are significant differences in the way the disappearance of the liquid within the network proceeds.

In general, the low interfacial tensions of partially miscible liquids close to the binodal will be beneficial for retaining the structure. Any conditions promoting

particle aggregation are valuable as well. Since the options for choosing liquid mixtures are more limited, varying particle stability will probably be a more flexible tool for achieving stable networks.

6.6 Summary and outlook

This work describes a method to assemble colloids into cellular networks that are contained within a single liquid phase. It takes particle-stabilized emulsions of partially miscible liquids as a template and involves removal of the continuous phase to push the colloids into a network. The method offers a robust and simple route to form this type of structures, and the studied system also conveniently allows detailed imaging of the formation process.

The possibility to construct cellular networks, starting from Pickering emulsions of partially miscible liquids, was already found in a previous study. A severe limitation in this case was that structures were only temporarily stable in a narrow temperature range just before complete mixing of the liquids. In the current work, this is overcome by the choice of starting materials. Whereas the mechanism of assembly is very similar, here a different route is taken. Contrary to the method presented in the previous report, the approach here simply requires a constant temperature, while changes in liquid composition drive the assembly by selective evaporation of the continuous phase. Emulsion droplets are thereby squeezed together, pushing the particles trapped at their interface into a cellular network. This is made possible by taking a liquid pair that has a large difference in vapour pressure of its individual liquid components. Another feature of the liquid pair is partially miscible at room temperature. Leaving evaporation to proceed at room temperature, the continuous phase therefore eventually mixes with the droplet phase, and can leave a stable 3-dimensional self-supporting cellular network.

Formation of the networks could easily be followed with CLSM, tracking both the assembly of the particles and the presence of the continuous phase. This made it possible to elucidate some details of the process, including the disappearance and eventual mixing of the continuous phase.

Previously reported networks were held together solely by the presence of residual continuous phase in the spaces separating the constituent particles. Surprisingly, in these studies the assembled particle networks could remain intact upon full

mixing of the liquid phases. Particle surface chemistry appeared to play a crucial role here. It determines if particles can become stuck together by attractive interparticle interactions, which can prevent structural collapse when the liquid interfaces disappear. Depending on the surface chemistry, the cell size can as well be important for stabilizing the network after the liquid phases mix. As a side note, another recent study of a different system also reveals how particle surface chemistry is essential to the aggregation of particles at the interface, and relates this to the possibility of a structure assembled by the interface to remain stable upon removal of this scaffold by mixing of the liquids (monogel [110]). For the system studied here, it could be nice to get additional information on the stability of particle in individual liquids, for instance, by ζ-potential measurements.

It was demonstrated that there are simple and straightforward possibilities to modify the structures. Cell size depends on droplet size of the parent emulsion, which could be changed by varying particle concentration or emulsification methods. Fortification of the structure was realized by creating covalent bonds between the particles in the assembled network. This allowed exchange and evaporation of the immersing liquid.

Many other potential ways to modify these networks are left to be explored, which could be interesting with possible applications in mind. Changing the constituent materials is an obvious option. General requirements for the method to be able to succeed followed from studying formation and stability in one system. This will facilitate identifying suitable liquid mixtures and particles. Judging from one failed attempt using another liquid pair, the main task at hand appears to be ensuring that the network of colloids survives complete mixing of the liquid components. To this end one can either try to change structural properties or make the interparticle bonds stronger. Increasing network strength by the former could be achieved through smaller cells (higher initial particle concentration) or thicker cell walls (by increasing the particle concentration in the continuous phase). For stronger interparticle bonds the colloidal stability should be reduced. This can be done by changing the colloids intrinsically (surface chemistry, material), or by adding an additional component that reduces the effectiveness of any present stabilization mechanism. An issue here is that it is uncertain how the parent emulsion will be affected by any of these measures.

Something else to investigate is the assembly of networks spanning a larger volume. It will take longer for the structure to form and liquid components to fully mix as the sample volume is increased. In the current study this introduced

a gradient of cell wall thickness due to sedimentation of free particles in the continuous phase. Speeding up evaporation by a continuous air flow over the sample would help preventing this. A possibly more straightforward way to reduce the effect of sedimentation during a prolonged formation time would be to use smaller particles. There might also be structural effects when particle size is decreased, as walls become thinner, while the number of interparticle bonds increases. Additionally, pores within the walls due to spaces separating particles would become smaller.

Ultimately, a variety of network properties might also be changed by introducing additional components (solid particles, polymers, etc.) in the emulsion template. For them to be incorporated in the network these would have to be in the continuous phase.

Overall, this study has brought a significant improvement to the applicability of this route of assembling colloids into cellular networks for the design of new materials. The presented method was studied to get insight into details of the formation and stability of the networks. It was shown to be quite flexible in terms of changing network properties, and there is much potential for further development.

Acknowledgments

Thanks to Andy Schofield for the fluorescent silica particles used for further modification.

Results III

Complete wetting of colloids

Chapter 7

Shear-induced aggregation in partially miscible liquid mixtures

This chapter presents an investigation of a peculiar aggregation behaviour observed for colloids dispersed in a variety of partially miscible liquids. In contrast to being trapped at the interface, the colloids are completely wetted by one of the two liquid phases when the mixture is phase-separated. In this study the miscibility gap is approached by gradually increasing the concentration of this component at a constant temperature, starting from a pure suspending liquid. Adsorption to the colloids can eventually cause aggregation through capillary condensation. Surprisingly, as will be shown here, this can be brought about by shearing an otherwise stable suspension. The study is facilitated by mainly using liquids that are partially miscible at room temperature.

7.1 Introduction

Stable colloidal suspensions rely on repulsive interactions between constituent particles to prevent it from flocculating, which is an essential feature in many cases. In contrast, when some attractive interparticle interaction dominates, colloids can assemble (aggregate) into larger structures to result in a material with potentially useful properties. Being able to tune colloidal interactions in a straightforward way is therefore very attractive.

Interest in using partially miscible liquid mixtures to this end was initiated by

Beysens and Estève, who in 1985 reported on temperature-reversible wetting-induced colloidal aggregation in such a solvent [55]. Just before reaching the miscibility gap of the pure liquid mixture, they found a narrow window where aggregation occurs. It mainly spans a range of compositions on the side of the miscibility gap poor in the component that is preferred by the particles. Bringing the samples into the miscibility gap of the liquid mixture, the preference is demonstrated by the colloids being collected in the phase rich in this component. The overall behaviour can be drawn schematically by including an aggregation region bordering the coexistence curve of a liquid pair (Figure 7.1). Subsequent studies looked into the details of the phenomenon, also studying different colloidal particles and liquid mixtures [131]. The resulting understanding regarding the underlying mechanisms of aggregation, and its dependence on chemical composition is briefly reviewed below.

Two mechanisms are at play here that can cause the temperature− and composition−dependent aggregation in question. The first is due to the existence and growth of adsorbed layers, rich in the component preferred by the colloid surface, which precedes aggregation as has been confirmed by light scattering [132]. Recent experiments have directly shown that these adsorbed layers can coalesce to form a liquid bridge resulting in abrupt aggregation [50, 51, 133]. Another mechanism enters the picture once composition is relatively close to the critical composition, due to the presence of critical fluctuations in the concentration. When confined between identical particles these can result in interparticle attractions. Recently, this so-called critical Casimir effect, after its quantum-electrodynamical analog, was measured directly [50, 51]. In this respect, it is the aggregation where liquid bridges bind the particles that could really be called wetting-induced aggregation. Alternatively, similar systems have also been interpreted as true ternary mixtures [134].

Especially the critical Casimir effect has attracted a lot of attention. It has been applied in studying colloidal aggregation, glasses, phase transitions and surface-chemistry directed assembly [135–138]. The nature of the attractive interactions, however, must be treated with some caution, since the transition between the two mechanisms is not very well distinguishable.

The aggregation in these systems can be temperature-reversible when particles surfaces keep repelling each other through electrostatic interactions, preventing aggregation into the primary minimum. This means particles can be dispersed again upon changing the temperature, removing the critical fluctuations or the

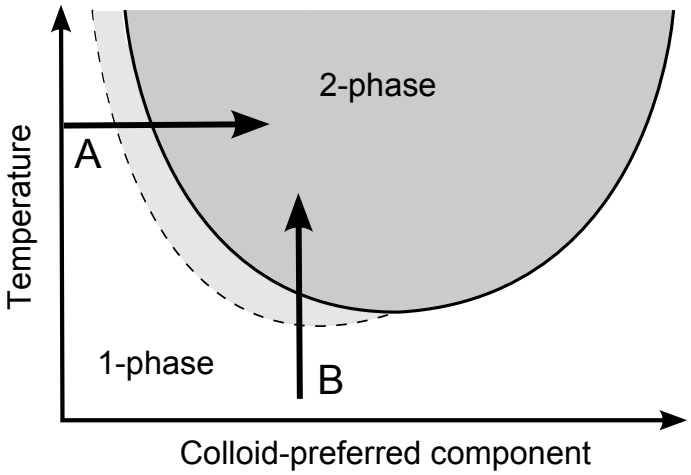

Figure 7.1 *Sketch of the experimental situation with respect to the liquid coexistence curve (black solid curve, bordering the dark grey '2-phase' area), where arrow A indicates the path employed in the current study to approach the binodal and arrow B that of previous studies. The light gray area bordered by the dashed line indicates where aggregation was observed previously.*

liquid bridges by re-mixing. In aggregates, large distances separating particles, and even particles arranging themselves in crystalline structures, have indeed been observed [132, 139]. Also theory has suggested this to be possible for one of the investigated systems in the case where a liquid bridge forms from adsorbed layers [54, 140]. Moreover, the interparticle interactions will not only be affected by adsorption, but also in general depend on liquid composition as appears already from DLVO theory [141, 142].

So far this aggregation behaviour is observed and studied for only a very limited number of liquid mixtures. The 2 types of binary liquid mixtures are water & pyridine-related compounds (2,6-lutidine, 3-methylpiridine) [50, 55, 137, 143] and water & n-alkyl polyglycol ethers (nonionic surfactants) [134, 139, 144], which have similar coexistence curves with a LCST above 25°C. This is convenient for experiments since samples of predefined compositions can be prepared at room temperature, and then heated in a controlled manner to approach the point of liquid phase-separation. In Chapter 8 an additional system of colloids dispersed in water & propylene glycol propyl ether is shown to behave similarly. The experimental situation for these systems as they were approached previously, is indicated by arrow B in Figure 7.1.

Here related experiments are presented for systems of overall similar characteristics, but consisting of alternative binary liquid mixtures. In the samples studied here

- colloids are charge-stabilized in both individual liquids,
- the liquid combinations (with one exception) are only partially miscible at room temperature, and
- particles partition into one of the liquid phases (complete wetting) for compositions where the liquids separate into two phases.

The latter indicates that one of the components strongly prefers the particle surface (the colloid-preferred component, hereafter referred to as "CPC") so that, judging from previous reports, wetting-induced aggregation can be expected near the binodal of the liquid mixture, through capillary condensation. In contrast with aforementioned liquid combinations, the investigated liquid mixtures are only partially miscible at room temperature. This conveniently allows the binodal to be approached by changing liquid composition rather than temperature (arrow A in Figure 7.1). Thus, as indicated in Figure 7.1, the experimental situation in the current studies is slightly different.

Following this approach, aggregation is indeed observed upon increasing the CPC concentration, however the aggregation behaviour shows some remarkable features that have not been reported before. The experimental methods employed to acquire the presented results are detailed below. Subsequently, the characteristics of the observed aggregation are reported, and evidence for a proposed mechanism behind the effect is presented and discussed. The results are summarized at the end, and suggestions are made for possible future efforts.

7.2 Experimental section

Materials

Propanal (propionaldehyde ≥97%, FG, Kosher, Sigma Aldrich), 2-butanol (99%, Fisher Scientific), nitromethane (99+%, stored under nitrogen, Acros Organics), ethylene glycol (anhydrous, 99.8%, Sigma Aldrich), propylene glycol propyl ether

(PGPE, 1-propoxy-2-propanol, 99%, Sigma Aldrich), and Nile Red (Technical grade, Sigma Aldrich) were used as received. Particles used were silica spheres prepared by the Stöber method. Non-fluorescent particles used with the water/propanal and water/2-butanol ($R_{TEM} = 0.38$ μm with $\sigma = 7\%$) and FITC labeled particles used with nitromethane/ethylene glycol. Particles used with water/PGPE were the same FITC labeled particles, but coated with unlabeled Stöber silica ($R_{TEM} = 0.35$ μm with $\sigma = 12\%$).

Preparation & handling of samples

Silica particles were washed several times with water (basic pH) after synthesis, and then stored in ethanol. Particles were dried at 100°C (Binder VD23 oven) for 30 minutes to let bulk solvent evaporate. Then, the resulting cake was ground into a fine powder using a spatula, and subsequently this was dried at 100°C under vacuum for 60 minutes.

The preparation of samples depended slightly on the required liquid composition. Samples with a liquid composition for which the components were completely mixed at room temperature, were prepared by dispersing the colloids directly into the liquid mixture using an ultrasonic bath (VWR). When preparing a sample with a liquid composition for which the liquids were phase-separated at room temperature, the particles were first dispersed into the majority component before adding the minority component that preferably wets the particles.

Samples were photographed in a thermostatted (21±1°C) room using an SLR camera (Canon EOS 40D with a Tamron 70-300 mm Tele-Macro lens), controlled by a computer using the Canon EOS utility software. Time-lapse photography was used to monitor sedimentation. Samples were studied before and after applying shear by 30 seconds of vigorous shaking using a vortex mixer.

For determining the fraction of shear-aggregated colloids samples were left for 10 minutes after vortex mixing, allowing aggregates to settle to the bottom of the vial. A known amount (by weight) was transferred into weighed vials, particles were spun down and clear supernatant removed to subsequently dry the particles (100°C, 15 minutes) and determine the mass fraction of colloids in the supernatant. This was then related to the initial sample composition to obtain the fraction of shear-aggregated colloids.

ζ-potential measurements

Samples of, typically, a few mL were prepared by dispersing the colloids (0.2 vol%) directly into mixtures of various liquid compositions. Measuring the ζ-potential was done using a Malvern Zeta Sizer Nano Z. For the measurements, 2-butanol/water samples were transferred into disposable folded capillary cells, while for propanal/water samples a dip cell was used in combination with a glass square cuvette. Solvent properties of the majority solvent were used to extract the ζ-potential from the electrophoretic mobility.

Fluorencence spectroscopy

In order to be able to measure fluorescence spectra of Nile Red in the bulk propanal/water solvent of dispersions, first stock mixtures at 4, 8 and 12 wt% water ($\sim$25 mL) were prepared containing 1 μM Nile Red. Subsequently, particles were dispersed at varying concentration in the stock mixtures, to obtain samples of $\sim$5 mL. After shearing the samples for 30 seconds using a vortex mixer, particles were spun down and the clear supernatant transfered into a square cuvette (10 mm pathlength, optical glass, from Starna Scientific) for the measurements. The remaining stock mixtures were used as blanks and measured in between supernatant samples of the dispersions. For measuring the spectra a Varian Cary Eclipse Fluorescence Spectrophotometer was used, and for every measurement multiple (typically 5) spectra were recorded. Processing and peak-fitting was done in Origin 8.5 using batch processing, outputting the relevant fit parameters and measures of statistical accuracy.

7.3 Suspensions with the CPC as the minority liquid component

Here, the general behaviour of suspensions with liquid compositions relatively poor in the CPC is presented separately for the various systems studied. Those investigated more extensively are aqueous mixtures and will be presented first. For completeness, they are supplemented by a non-aqueous liquid mixture and an aqueous mixture that is fully miscible at room temperature, similar to that used in previous studies.

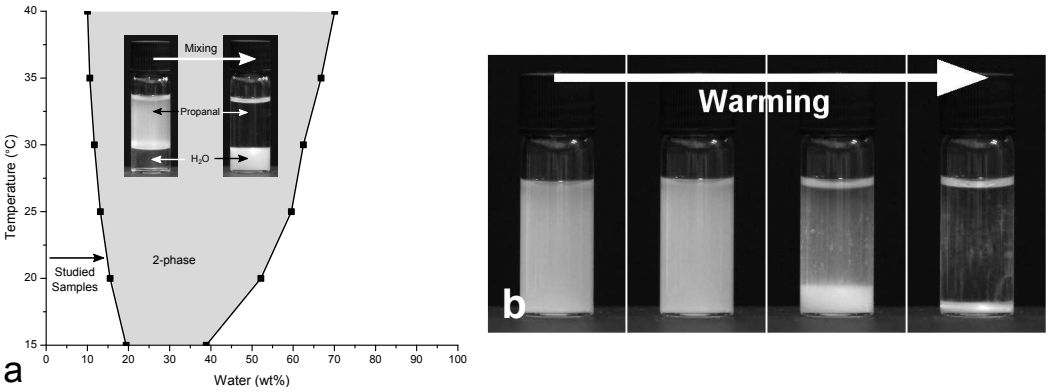

Figure 7.2 *(a) Phase diagram of water & propanal [145] with inset demonstrating partitioning of particles into the water-rich phase. (b) Warming a sample of 1 vol% silica in a water/propanal mixture consisting of 25 wt% water to room temperature (21 °C) after it being cooled in ice-water. Frames 2, 3 and 4 are taken respectively 10, 15 and 35 minutes after the first image.*

Propanal & water

Mixtures of water and propanal are partially miscible at room temperature (Figure 7.2a). In the left hand vial of the inset in Figure 7.2a a dispersion of silica particles in propanal is added on top (lower density) of some water, which makes up 30 wt% of the total liquid in the vial. At this composition the liquids phase-separate at room temperature, and after vigorously shaking the sample all the particles transfer into the bottom (since higher density), water-rich phase, indicating that water in this case is the CPC. Alternatively, this is confirmed by observing the colloids locating themselves into the water-rich phase after a temperature quench leading to phase-separation of the liquids (Figure 7.2b).

A series of suspensions with increasing water concentration was prepared, using sonication to disperse the particles into the liquid mixtures (Figure 7.3a). Stable suspensions were obtained up to 16 wt% water, with the subsequent sample at 18 wt% water being phase-separated. The particles are charge-stabilized and carry a negative surface charge (Figure 7.3c). As expected from their size and density mismatch with the solvent, they were observed to sediment slowly to the bottom of the vial, where eventually all particles are collected within a concentrated layer.

While this behaviour is consistent over the entire range of samples, the response of the formed sediments to gravity is not. In the absence of water and at very low water concentrations, the dense sedimented layer of charge-stabilized particles flows in response to gravity when tilting the vial backwards (Figure

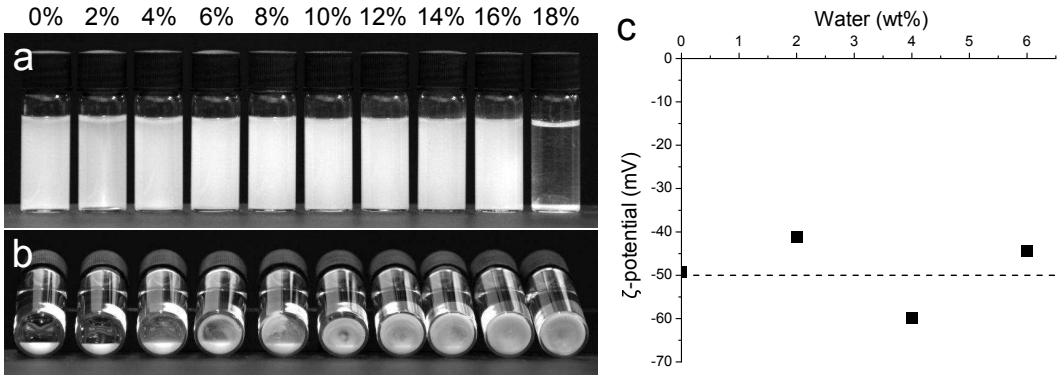

Figure 7.3 *(a) Vials containing suspensions of silica particles (1 vol.%) in propanal/water mixtures at various liquid compositions. The water content of the solvent is indicated in percentage by weight. (b) A photograph of the same samples tilted backwards after the particles have sedimented under gravity into compact layers. (c) ζ-potential of the silica particles in propanal/water mixtures as a function of the water concentration in the solvent.*

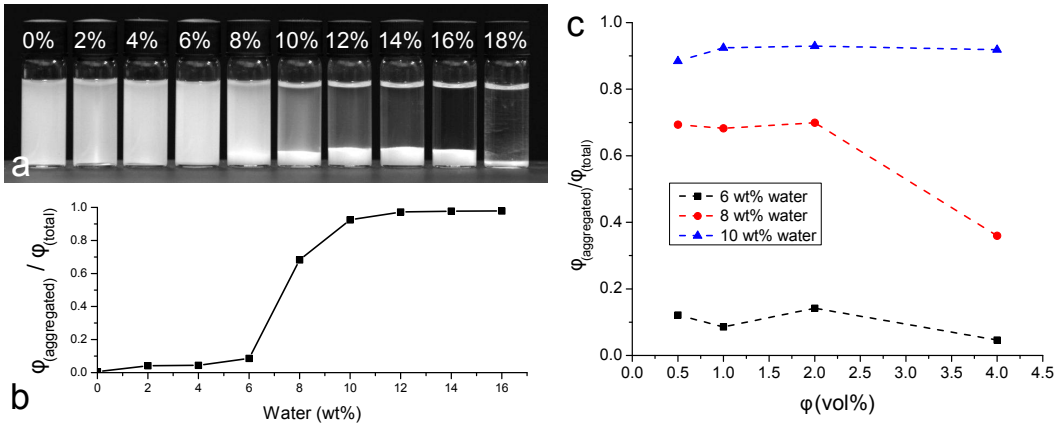

Figure 7.4 *(a) The same samples as shown in Figure 7.3a, but after vigorously shaking the stable suspensions. (b) Estimates of the fraction of aggregated particles by measuring the concentration in the supernatants of the samples shown in (a). (c) Estimates of the fraction of aggregated particles plotted as a function of particle concentration for intermediate water concentrations.*

7.3b). Simply shaking the vials re-disperses the particles to again obtain a stable suspension. As the water concentration is increased, a more solid-like 'cake' is formed, which does not flow under gravity. In this case, particles cannot be re-dispersed properly by shaking, and aggregates remain as evidenced by rapid sedimentation into voluminous sediments. Curiously, this indicates that within the concentrated layer, the particles have aggregated, as opposed to remaining well-stabilized against aggregation due to their charged surfaces.

Another surprising result is obtained when the stable suspensions shown in

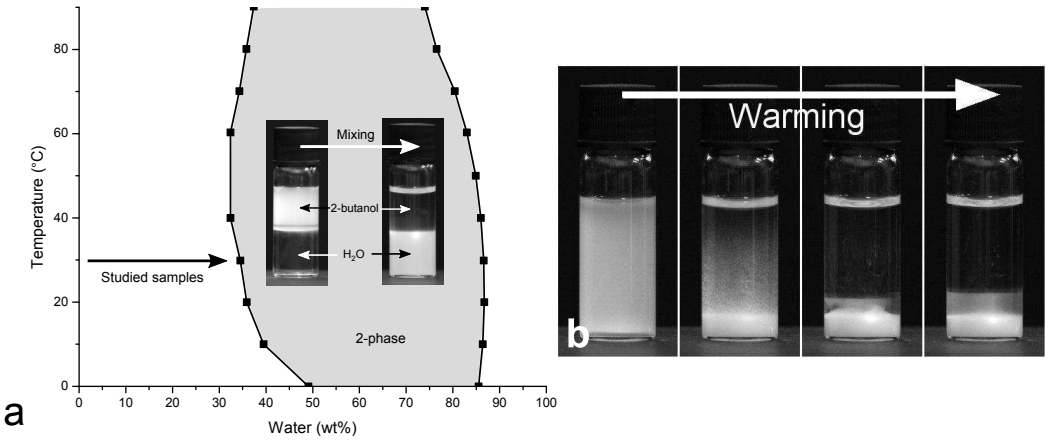

Figure 7.5 *(a) Phase diagram of 2-butanol/water [146] with an inset demonstrating partitioning of particles into the water-rich phase. (b) Sample of a 50/50 (by weight) 2-butanol/water mixture containing silica particles (1 vol.%) warming up to room temperature after being cooled in ice-water: 1st image was taken approximately 5 minutes after removal from ice-water, and frames 2, 3 and 4 were taken, respectively, 5, 10 and 20 minutes after the 1st image.*

Figure 7.3a are vigorously shaken, instead of being left to sediment. There is no effect on colloidal stability for suspensions at low water concentration (Figure 7.4a), as can be expected with the particles being charge-stabilized. However, at higher concentration of the CPC, the particles in the initially stable dispersions (Figure 7.3a) aggregate and quickly settle into voluminous sediments (Figure 7.4a). The supernatants above sediments clearly stay turbid for immediate concentrations (8, 10 wt%). Plotting a fraction of aggregated particles as a function of the CPC concentration indicates this by a relatively sharp increase between 6 and 10 wt% water (Figure 7.4b).

Thus, it appears that for intermediate CPC concentration only a fraction of particles has aggregated. Now the particle concentration was varied for this range of water concentrations. The fraction of aggregated particles appears to be independent of the particle concentration, as demonstrated in Figure 7.4c. Only at 8 wt% water the fraction of aggregated particles is observed to suddenly drop again for the highest particle concentration.

2-Butanol & water

Mixtures of 2-butanol & water are also partially miscible at room temperature (Figure 7.5a). Silica particles present in such mixtures are located in the water-

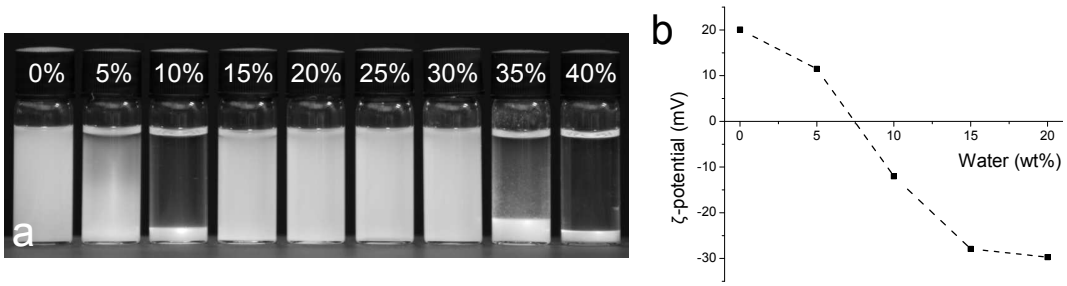

Figure 7.6 *(a) Vials containing silica particles (1 vol.%) dispersed into 2-butanol/water mixtures at various liquid compositions using sonication, and (b) a plot of ζ-potentials at various water concentrations.*

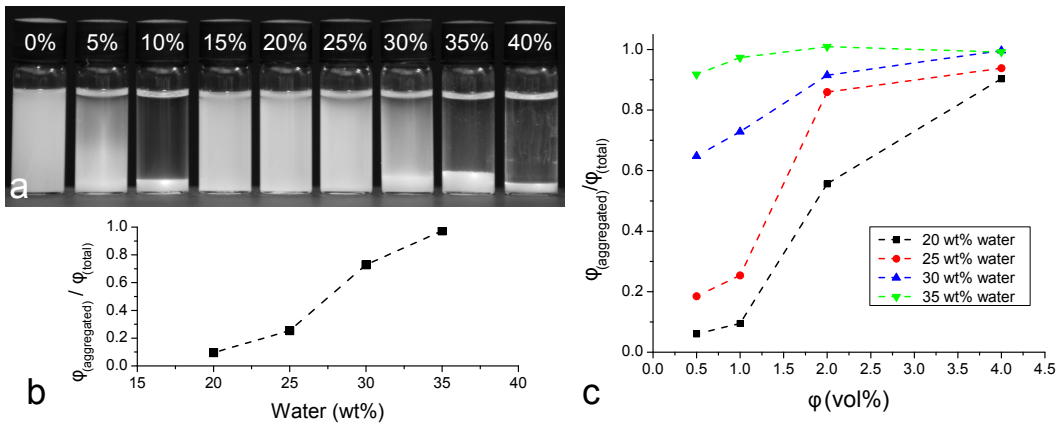

Figure 7.7 *(a) The same samples as shown in Figure 7.6, but now the stable suspensions were shaken vigorously using a vortex mixer, and (b) the fraction of aggregated particles for the relevant samples plotted as a function of water concentration. (c) Shows the fraction of aggregated particles plotted against the total particle volume fraction for several water concentrations.*

rich phase after liquid-liquid phase separation upon heating or mixing, in an analogous way to the propanal/water system (inset of Figure 7.5a and Figure 7.5b). Hence in this system water is again the CPC.

In the 2-butanol/water system, approaching the miscibility gap by increasing the CPC concentration, an onset of colloidal aggregation is already observed at relatively low water concentrations (Figure 7.6a). Aggregation vanishes again at higher water concentration. These observations are consistent with ζ-potentials, which show that when increasing the water concentration the colloids go through a point of zero charge (PZC) (Figure 7.6b). In pure 2-butanol the silica particles are positively charged and, since they are of opposite charge in water, adding water eventually changes the sign of the total particle charge.

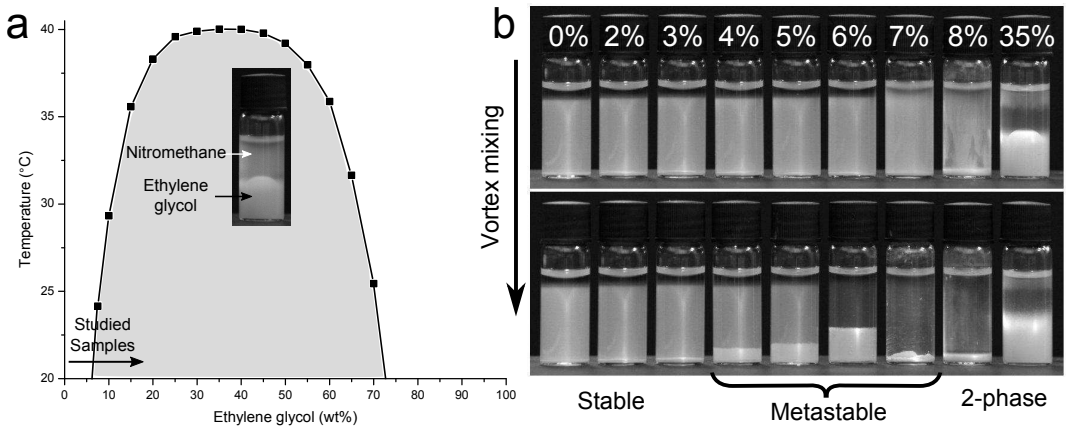

Figure 7.8 *(a) The phase diagram of nitromethane/ethylene glycol [145] with an arrow indicating compositions of the studied samples, and as inset a phase-separated sample where the particles have located themselves in the ethylene glycol-rich phase. (b) Samples at various ethylene glycol concentrations (containing 1 vol.% particles) initially mixed and dispersed by sonication, which were either (top) left undisturbed to sediment for 3 hours, or (bottom) first vigorously shaken and then left undisturbed to sediment for 3 hours.*

Closer to the binary liquid's binodal, aggregation is seen again. The dispersion with a liquid composition where the 2 components only just mix (35 wt% water) is unstable, and the particles aggregate to form a voluminous sediment (Figure 7.6a). At somewhat lower CPC concentration, stable dispersions can be obtained (Figure 7.6a), but shear-induced aggregation is observed (Figure 7.7a,b) after vigorous shaking. In contrast to the propanal/water system, the fraction of aggregated colloids increases with particle concentration (Figure 7.7c).

Nitromethane & ethylene glycol

The non-aqueous liquid mixture included in this study consists of ethylene glycol & nitromethane, which was also used elsewhere in this thesis. FITC-labeled silica particles dispersed in nitromethane completely transfer into the ethylene glycol-rich phase after mixing with an appropriate amount of ethylene glycol (inset of Figure 7.8a). These liquids are also partially miscible at room temperature, but with a fairly low solubility of the CPC, and a low UCST (Figure 7.8a). Ethylene glycol is slightly less dense than nitromethane, hence, in phase-separated samples, some of the colloid-containing phase is rising to the top of the sample, making the top phase appear turbid.

Using sonication, stable suspensions were obtained for ethylene glycol concentra-

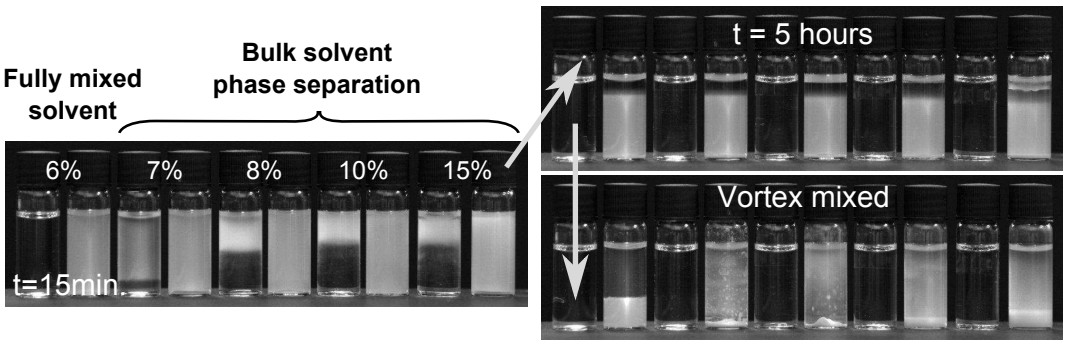

Figure 7.9 *Samples of varying ethylene glycol concentration (sets of two vials: blank on the left and containing 1 vol.% particles on right) dispersed/mixed at approximately 50 °C and then left to cool to room temperature while taking photographs. The image on the left shows vials 15 minutes after having started imaging the hot samples. The images on the right show (top) the vials after 5 hours, (bottom) which were subsequently vortex mixed.*

tions running up to maximum solubility of the CPC at room temperature, while crossing into the miscibility gap results in phase-separated samples (Figure 7.8b, top). As in the propanal/water system, the stable suspensions slowly sediment into compact concentrated layers, which upon adding some CPC appear more solid-like (i.e. do not flow under gravity when tilting the vials). Vigorous shaking of some of these samples results in shear-induced aggregation, as observed in the previously discussed systems (Figure 7.8b, bottom).

At 7 wt% ethylene glycol the situation appears to be different to its neighbours on both sides. No clear supernatant and sharp sedimentation front is observed, 3 hours after dispersal by sonication. After some time the supernatant clears up, and the sedimentation front is visible as in the samples with lower CPC concentration. Once subjected to shear, a compact and very viscous phase is collected at the bottom of the vial, much like what is observed in the phase-separated 8 wt% sample. These observations suggest that a bulk phase-separation takes place in the solvent, possibly due to a slight cooling of the samples after they were transferred into a lab at slightly lower ambient temperature for monitoring them. Initial supernatant turbidity in the first situation might therefore be caused by ethylene glycol-rich droplets. Thus, it appears as if some CPC-rich phase separates out of the bulk solvent, but that not many of the present particles are collected within it. The ethylene glycol-rich droplets then simply float to the the top of the sample.

To test this hypothesis some heated samples at varying ethylene glycol concen-

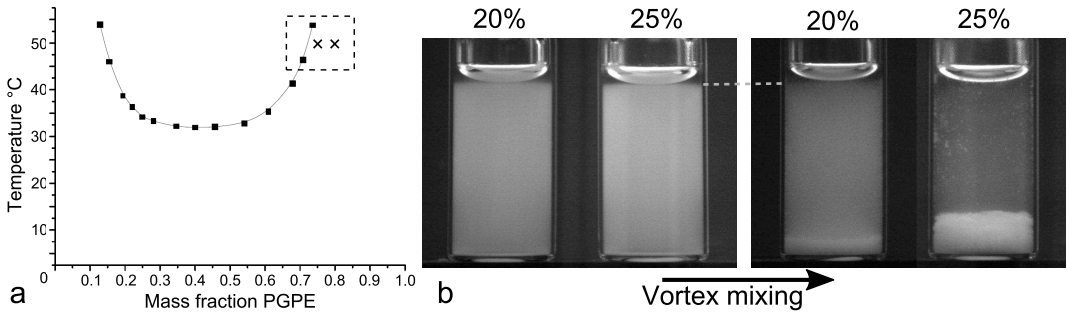

Figure 7.10 *(a) Phase diagram of water/PGPE [147], with the composition and temperature of the prepared samples indicated in it. (b, left) Two samples on the water-poor side of the coexistence curve (wt% water indicated above the images), heated from room temperature to 50 °C in a water bath and left to sediment for 1 hour. (b, right) The heated samples, 1 hour after being vortex mixed.*

tration were monitored as they cooled down to room temperature (Figure 7.9). Blank samples demonstrated that bulk phase-separation has taken place after 15 minutes (Figure 7.9, left), but this leaves colloidal stability unaffected with the particles slowly sedimenting as evidenced by a sharp sedimentation front (Figure 7.9, top right). Some particles, however, do appear to be collected in CPC-rich droplets at the top of the sample. Collecting all the particles in the bulk ethylene glycol-rich phase is achieved by vortex mixing (Figure 7.9, bottom right).

Propylene glycol propyl ether & water

A final system, more similar to those of previous studies mentioned in the introduction (Section 7.1), was studied briefly to check for shear-induced aggregation observed in the results presented before. The liquid mixture consists of propylene glycol propyl ether & water, which have a LCST just above room temperature (Figure 7.10a). This nicely complements the other systems, which were all partially miscible at room temperature.

In the next chapter this system is studied in more detail, adapting an approach similar to that of existing studies (Figure 7.1 arrow B), and it will be demonstrated that water is the CPC. Two samples were prepared with a liquid composition on the water-poor side of the miscibility gap, and heated to 50°C where the liquids are partially miscible (crosses in Figure 7.10a). The dispersions remain stable after being heated, and the colloids slowly sediment (Figure 7.10b, left). Again, subjecting them to shear by vigorous shaking, shear-induced aggregation is observed (Figure 7.10b, right).

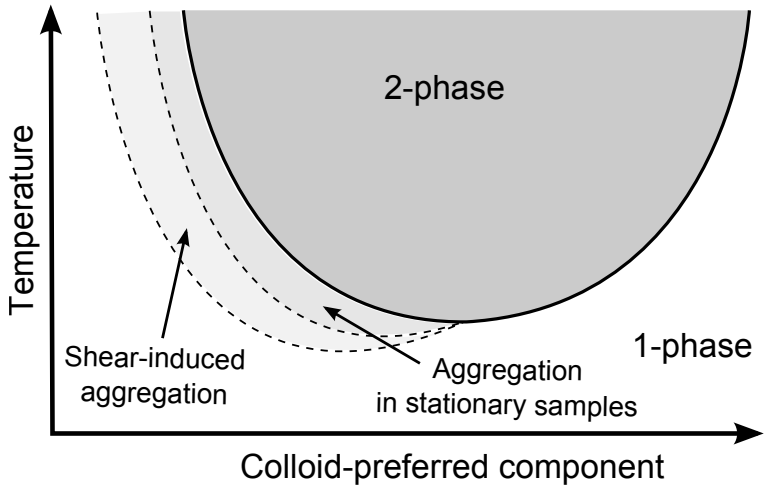

Figure 7.11 *Sketch of the situation as observed by previous studies, with an aggregation region on the CPC-poor side of the binodal, expanded with a sketch of where according to current observations shear-induced aggregation takes place.*

7.4 Measuring CPC-adsorption on colloids

The main finding so far is that shear-induced aggregation is a pronounced feature of the investigated systems. This was possibly not observed in previous studies on similar systems due to the experimental approach, where stationary samples were simply heated (Figure 7.1 arrow B). In these cases, resulting sketches of the situation simply consisted of a narrow region next to the binodal to indicate where aggregation was observed (Figure 7.1 light grey area). The shear-induced aggregation demonstrated above, however, occurs already much further away from the binodal. Thus, with respect to the current systems the sketch of situation should be extended to include a region of shear-induced aggregation (Figure 7.11).

It was shown that, being in the vicinity to the miscibility gap, aggregation can be caused by liquid bridges that form between particles through capillary condensation [50, 51]. This explains the previously reported wetting-induced aggregation on the CPC-poor side of the coexistence curve, away from the critical point [55, 139, 143]. An obvious explanation for the shear-induced aggregation would be that this same mechanism is at play, but that it is induced by supplying energy to the system through mechanical agitation.

An implication of aggregation through capillary condensation is that it removes CPC from the bulk solvent, thereby changing its composition. Here, the use of liquids that are partially miscible at room temperature offers the opportunity to

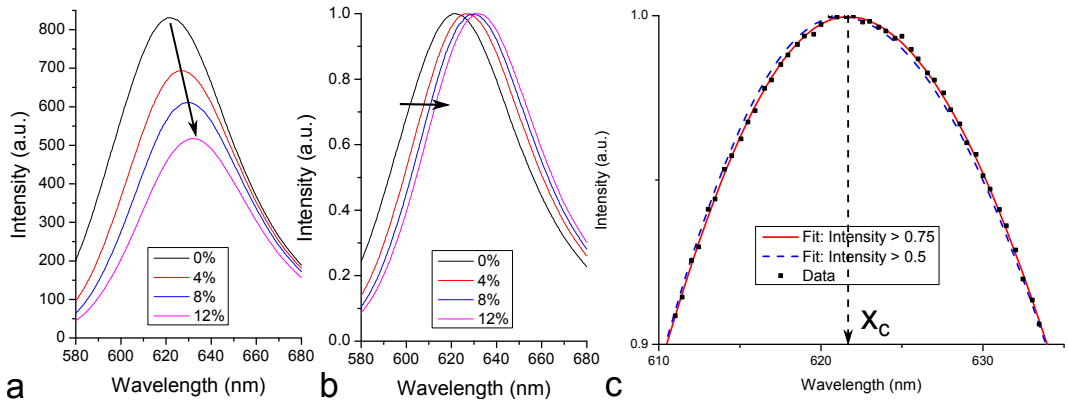

Figure 7.12 *(a) Fluorescence spectra of nile red in propanal/water mixtures at various water concentration (wt%). (b) The spectra in (a) normalized to demonstrate the red-shift for increasingly polar mixtures. (c) Example fits for different intensity cut-offs aimed at finding peak center x_c.*

conveniently study the change in composition of the bulk solvent by analyzing the supernatants of samples. Still this is challenging, considering that it involves detecting only small changes in significant concentrations of CPC.

To attempt measuring changes in composition of the bulk solvent, the fluorescent dye Nile Red was employed as a composition probe. The fluorescence of this dye is known to strongly depend on the solvent, and generally shifts to longer wavelengths in more polar chemical environment (see e.g. [148]). Therefore, the 2 aqueous systems partially miscible at room temperature are most suitable. Measuring fluorescence spectra for varying water concentration shows a red-shift and a decreasing fluorescence intensity for increasing water content, as demonstrated for propanal/water in Figure 7.12a. Intensity was found not so reproducible, and thus less suitable for tracking the liquid composition. The red-shift for propanal/water (Figure 7.12b) and 2-butanol/water are similar in magnitude for concentrations up to the binodal. Clearly, fluorescence is most sensitive to composition changes in propanal/water, since the same shift occurs over a smaller concentration interval. Additionally, judging from the proposed aggregation mechanism, similar amounts of water would be pulled out by aggregation in both systems. Thus, variations in the composition of the bulk solvent are most likely to be detected in the propanal/water system.

Fluorescence spectra of supernatants of sheared propanal/water samples at varying particle− and water concentration have been measured to determine changes in the composition of the bulk solvent. For this, peaks were first normalized (Figure 7.12b) and then intensities below a specified value were cut

off for fitting by an asymmetric Gaussian

$$I(x) = A \exp\left(-\frac{(x-x_c)^2}{2\sigma^2}\right) \begin{cases} \sigma = \sigma_L, A = A_L & \text{if } \lambda < \lambda_c \\ \sigma = \sigma_R, A = A_R & \text{if } \lambda > \lambda_c \end{cases}$$

where fit parameters A, x_c and σ are, respectively, peak height, peak center and peak width (subscripts L and R indicate left and right of x_c, respectively). The quality of the fit depends on the part of the data that is used. An example where the data with $I > 0.5$ and $I > 0.75$ was fitted (Figure 7.12c) shows that the former already gives a reasonable fit, while clearly a better fit is obtained for a larger threshold. In order to carefully determine the peak center position the threshold is set at 0.8 for all data.

The peak centers, x_c, were used as the measure from which information about the composition could be extracted. Spectra were recorded in series of, typically, 5 sequential measurements of a sample (Figure 7.13a). Measurements of supernatants were always preceded and succeeded by measurements of a stock solution of Nile Red in propanal/water into which the particles were dispersed. This provided a guide to the reproducibility of x_c, and established a baseline. Displaying x_c of individual measurements for a particular liquid composition in the sequence in which they were obtained, reveals that often the first measurement in a series is a clear outlier. These were discarded, consistently over all data, and the remaining x_c averaged to get $\bar{x}_c$. Finally, the $\bar{x}_c$ of the samples were shifted to take into account the variability of the baseline, which becomes apparent from the blanks (Figure 7.13b). This was done by assuming that they were shifted with respect to the baseline by the same amount as the average of the 2 sandwiching blanks.

Three liquid compositions were studied in this manner: one at which the dispersion was stable (4 wt% water), one at which part of the colloids aggregate after shearing (8 wt% water), and one at which all particles aggregate after shearing (12 wt% water). Resulting $\bar{x}_c$ plotted as a function of particle concentration for the various liquid compositions demonstrate a blue-shift with increasing particle concentration (Figure 7.14a). This signifies a decrease in the water concentration of the bulk solvent, confirming that water is adsorbed onto the particles.

To convert the $\bar{x}_c$ values into compositions, a calibration curve was constructed, and fitted to a quadratic equation (Figure 7.14b). This allows extraction of the

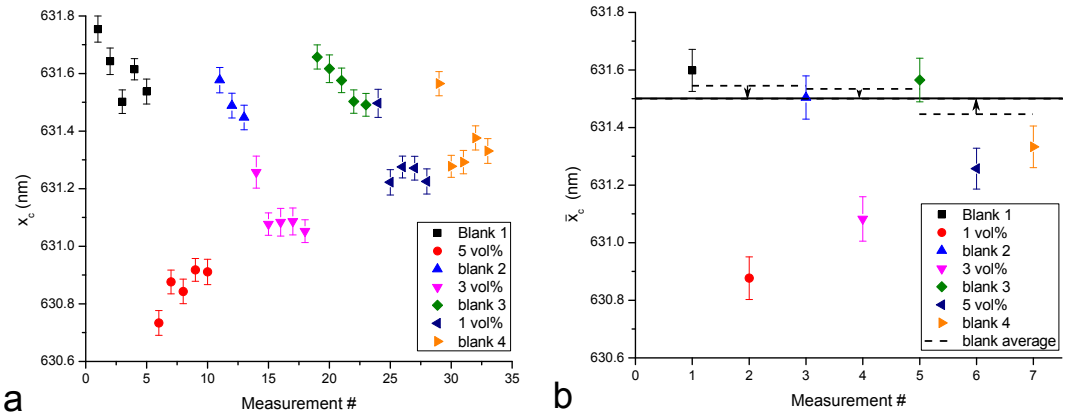

Figure 7.13 *(a) All x_c obtained from a single series of measurements at fixed water concentration (12 wt%). (b) Averaged and adjusted (as indicated by dashed lines and arrows) values of $\bar{x}_c$ from the measurement series in (a).*

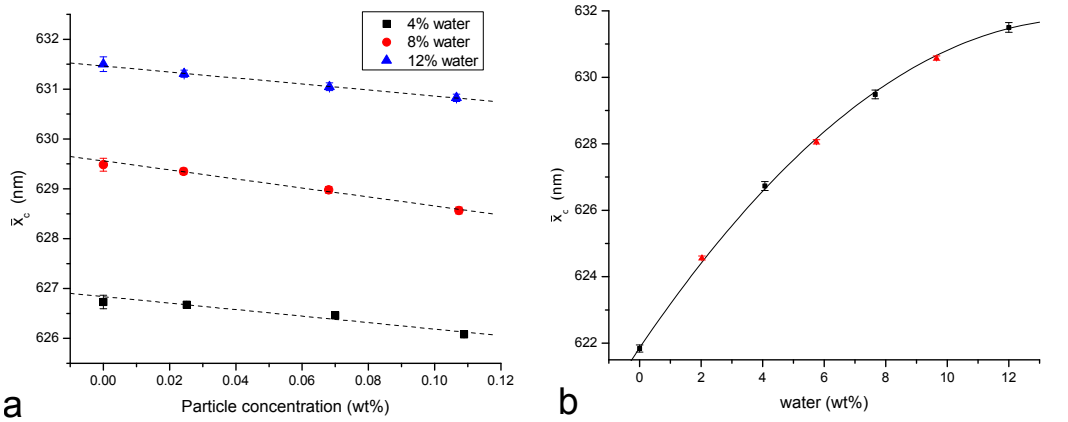

Figure 7.14 *(a) Plots of all $\bar{x}_c$ for various water concentrations, with linear fits shown as dashed lines that serve as a guide to the eye. (b) Calibration curve used to extract water concentration from values plotted in (a). The red triangles are measurements performed at a different time, but were not used for the fit and included only for reference.*

amount of water adsorbed ($[H_2O]_{ads}$) by the particles (Figure 7.15a), and also the mass ratio of adsorbed water to particles can be displayed (Figure 7.15b). Due to the shape of the calibration curve, as the water concentration increases, the error in $\bar{x}_c$ has an increasing impact on the error in the corresponding amount of adsorbed water.

Plotting $[H_2O]_{ads}$ as a function of particle concentration clearly shows an increasing trend for all three liquid compositions (Figure 7.15a). Linear fits to the data obtained at the various liquid compositions with an intersect at 0 wt%, reveals that $[H_2O]_{ads}$ is at least very close to being directly proportional to the

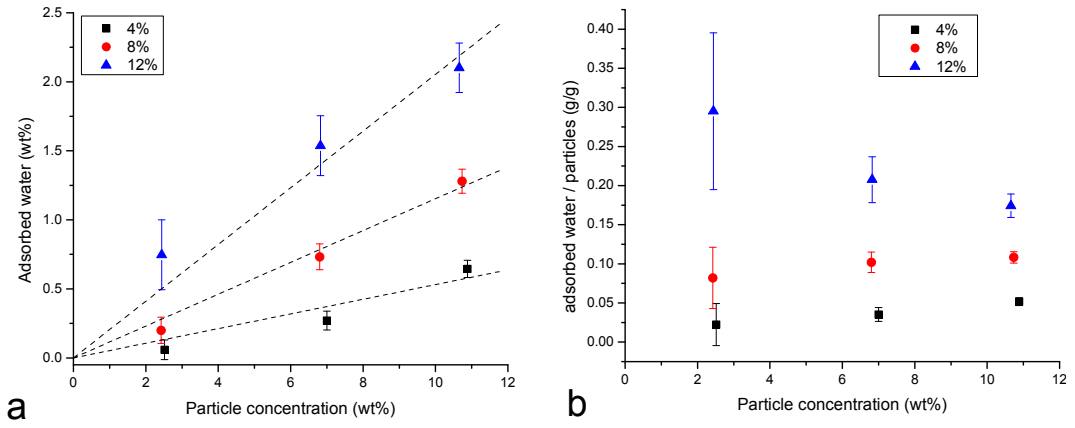

Figure 7.15 *(a) Plots of the amount of adsorbed water against particle concentration for the 3 different water concentrations, where dashed lines are linear fits to the data with the intercept set to 0 wt% adsorbed water, and mainly serve as guide to the eye. (b) Plots of the the ratio of amounts of adsorbed water to particles.*

particle concentration. This agrees with water being adsorbed on the particles. The total amount of adsorbed water increases with increasing water content, and thus also with the amount of aggregation (Figure 7.15a). The same trend can therefore be observed for the amount of water adsorbed by a fixed amount of particles (Figure 7.15b). Additionally, corresponding to $[H_2O]_{ads}$ being close to directly proportional to particle concentration, the amount of water adsorbed by a fixed amount of particles remains roughly constant for increasing particle concentration.

7.5 The mechanism behind aggregation

The measurements presented in the previous section show that colloids indeed adsorb water (the CPC) in the propanal/water system. They therefore appear to support the initial assumption, based on previous reports on similar systems, that the CPC can act as a 'glue' to make particles sticky and cause aggregation. Also some aspects of how the adsorption depends on particle- and CPC concentration were elucidated. Now these results will be discussed in relation to experiments presented in Section 7.3 to try to explain some of the observed effects.

At low concentrations, in the absence of (shear-induced) aggregation, particles are already observed to adsorb CPC (4 wt% water, Figure 7.15b). This confirms that even in the stable suspensions obtained by sonication (Figure 7.3b)

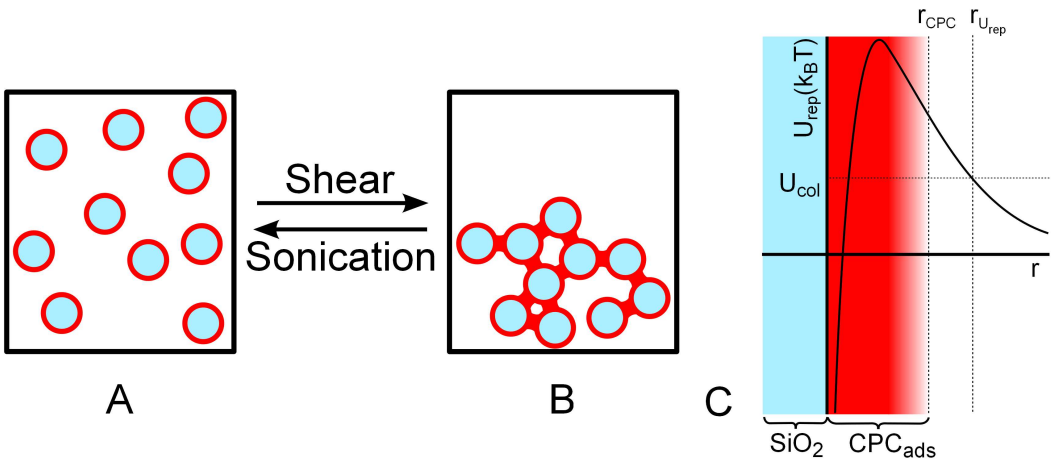

Figure 7.16 *(a) Adsorbed layers of CPC (red rings) are present at the surface of the particles for low CPC concentration approaching the miscibility gap. (b) Upon applying shear liquid bridges are formed between particles, causing instantaneous flocculation of the suspension. (c) Sketch of the situation at the particle surface, showing the adsorbed layer (CPC_{ads}) and a sketch of the pair potential (U_{rep}).*

water is adsorbed onto the particles, although it does not have any effect on the colloidal stability of the dispersion. For these samples, the state of the system can be sketched as in Figure 7.16a. Another observation suggesting the adsorption of *CPC* on particles, far away from the binodal and well before the occurrence of shear-induced aggregation, is the PZC in 2-butanol/water at low water concentrations (Figure 7.6b). Water apparently associates with charged groups on the surface and therefore already manages to reverse the charge at low concentrations.

These adsorbed *CPC*-rich layers would be the precursors for the formation of liquid bridges in between particles, causing them to aggregate. Since measurements were conducted after applying shear, the adsorbed water in the stable suspensions for higher *CPC* concentration was not directly measured. However, the increasingly solid-like sediments of stable suspensions in which particles were allowed to slowly settle to the bottom of the vial (Figure 7.3b), indirectly demonstrate that the influence of adsorbed water increases for increasing *CPC* concentration. It suggests that the thickness of the adsorbed layers increases, causing liquid bridges to form between particles within the dense sediment, sticking them together.

For an increasing fraction of aggregation, occurring at higher water concentration (8 and 12 wt% water, Figure 7.4a,b), the amount of adsorbed *CPC* was observed

to be directly proportional to the particle concentration (Figure 7.15). This is most likely due to thicker adsorption layers on individual particles, but possibly also additional water separates out of the bulk solvent when liquid bridges form. The latter seems a realistic scenario, however whether this occurs cannot clearly be deduced from the presented measurements. In any case, the measurements support the idea of aggregation via liquid bridges, as found previously in stationary samples of similar systems [50, 131], but this is now brought about by shearing the samples. Thus, the act of vigorously shaking a stable dispersion of colloids carrying an adsorbed CPC-rich layer (Figure 7.16a) induces coalescence the adsorbed layers, and instantly flocculates the dispersion (Figure 7.16b).

Apparently, by shearing (at a shear rate $\dot{\gamma}$), the energy of particle collisions, $U_{col}(\dot{\gamma})$, can be increased sufficiently to overcome a barrier that otherwise prevents aggregation. This barrier presumably originates from the electrostatic repulsions between the charged particles. As the CPC concentration increases, the adsorbed layer grows and extends its reach further into the bulk solvent. Furthermore, it is also quite possible that the adsorbed layer reduces the range of the electrostatic repulsions. Overall, there is a balance between the reach of the adsorbed layer (r_{CPC}) and the effective range of the electrostatic repulsion (r_{rep}) (Figure 7.16c). There is an energy barrier $U_{rep}(r_{CPC})$ for the adsorbed layers to meet, and thus a liquid bridge to form, set by the energy of the interparticle repulsion at r_{CPC}. The aggregation rate, analog to the rate at which liquid bridges form, can then roughly be described as

$$k = N(\phi, \dot{\gamma}) \exp\left(\frac{-U_{rep}(r_{CPC})}{U_{col}(\dot{\gamma})}\right)$$

where $N(\phi, \dot{\gamma})$ is the frequency of attempt to aggregate, which will probably depend on the shear rate $\dot{\gamma}$ and the particle concentration ϕ. Thus, once the adsorbed layer reaches far enough into the bulk solvent, the barrier $U_{rep}(r_{CPC})$ decreases and becomes insufficient to prevent liquid bridges from forming. The situation is sketched in Figure 7.16c. Quantitatively, this will depend strongly on the surface chemistry and the properties of the liquid mixture.

When increasing the CPC concentration, there is an onset of shear-induced aggregation with a clear regime of partial aggregation (Figures 7.4b and 7.7b). This would then be related to a higher barrier, resulting in fewer successful aggregation attempts. For propanal/water the fraction of aggregated colloids appears independent of particle concentration (Figure 7.4c), while in 2-

butanol/water samples it increases with increasing particle concentration (Figure 7.7c). The difference in the dependence on ϕ could well be related to the proximity to the binodal where aggregation takes place. For propanal/water aggregation happens much closer to the miscibility gap, possibly related to better charge-stabilized particles in this system, as is suggested by the ζ-potential measurements (Figures 7.3c and 7.6b). Closer to the binodal the particle concentration will influence less the amount of aggregation, since plenty of CPC is present.

After aggregation particle surfaces will, through the liquid bridges, still repel each other via electrostatic interactions, since they form charge-stabilized suspensions in both individual liquids. However, the liquid bridges form quite strong bonds between particles that are difficult to break. In order to restore the suspension to its stable form (Figure 7.16a) this would have to be achieved. This possibly also involves mixing some CPC back into the bulk solvent. Sonication appears to achieve this. The high frequency pressure waves involved in this method of agitating samples allows breaking of the bridges and intimate mixing of the components to go back to the initial situation of well-dispersed particles, carrying an adsorbed CPC-rich layer (Figure 7.16a,b).

Finally, briefly revisiting the nitromethane/ethylene glycol dispersions studied in Section 7.3, it is unclear why particles, likely with adsorbed ethylene glycol layers, are not included in the bulk ethylene glycol-rich phase that separates out from the bulk solvent. Possibly an extremely low interfacial tension is involved. It does stress the sensitivity of the aggregation through the formation of liquid bridges to shear: actual phase-separation is not enough to make the particles aggregate, but shear is (Figure 7.9).

7.6 Summary and outlook

A study has been presented of colloidal suspensions in partially miscible binary liquid mixtures, where the colloids locate themselves in one of the phases when the liquids are phase-separated. It distinguishes itself from other studies that consider this type of system by the choice of control parameter. Instead of varying the temperature to approach the miscibility gap, here the composition is varied to the same effect, which is facilitated by the use of mixtures that are partially miscible at room temperature. Additionally, several liquid mixtures were investigated, all different from the very limited number of systems that were studied previously.

They display a variety of characteristics, with aqueous and non-aqueous mixtures, as well as partial and full miscibility at room temperature.

The various systems were studied with an eye to colloidal stability. In this, a variety of surprising effects were observed, most significantly the shear-induced aggregation. This phenomenon extends the previously reported general picture of the aggregation behaviour in this type of system (Figure 7.11). The effect itself is quite dramatic, with an initially stable suspensions being almost instantly flocculated upon shaking (e.g. before: Figure 7.3a, after: Figure 7.4a). Several systems demonstrate this property, confirming that there is at least some generic physics concerning the shear-induced aggregation.

An explanation, inspired by previous studies, was found in the formation of liquid bridges formed between particles upon shearing. This was confirmed by combining measurements demonstrating the adsorption of CPC on the aggregated particles with the macroscopic observations of the suspensions. The particles, suspended in the liquid mixtures by sonication, carry adsorbed CPC-rich layers which in stationary samples are prevented from interacting via electrostatic repulsions. Shearing can increase the particle collision energy to partly overcome this barrier, allowing adsorbed layers to approach sufficiently for liquid bridges to form. This can only happen after a critical thickness of the adsorbed layer is reached by adding sufficient CPC.

While the basics are understood, details of the mechanism remain unexplained. It is unclear if additional water separates out when liquid bridges form, or if it does merely involve the coalescence of the already present CPC-rich layers. Judging from measurements the former is a scenario that cannot be ruled out. Additional measurements of supernatants of samples where particles are left to sediment under gravity might offer clarity. Though, still liquid bridges form in sediments, and this might affect measurements.

Finally, using microscopy techniques some direct visualization of the aggregation might be achieved, which would possibly offer extra insight. Using rheo-imaging [149] one would be able to apply shear in a controlled way, while observing the colloidal particles directly. Otherwise, a microscope might be used to visualize aggregate structures, and possibly to observe the particles as they form a sediment onto a glass surface (possibly also possessing a CPC-rich adsorbed layer).

To conclude, this study has uncovered a new phenomenon in this type of system. While understood on a qualitative level, a few details are left to be investigated.

Acknowledgments

The colloids used in this project were synthesized by Andy Schofield.

Chapter 8

Assembling colloidal rods by a liquid-liquid phase separation induced confinement

In this chapter a new possibility for assembling colloidal rods, using a phase-separating binary liquid mixture, is explored. Instead of trapping the particles at the interface, they are trapped inside a small volume of the minority phase which separates out of the suspending liquid. Confining the rods in this way is shown to lead to wetted particle networks or liquid crystalline ordering of the rods, depending on the volume ratio of rods to confining liquid.

8.1 Introduction

Possibly the simplest imaginable departure from the typically (near-) spherical shape of a colloidal particle is a rod-like shape. Suspensions of rod-like particles have for many years been the subject of extensive study, as will be evident from the references below. Two important structural features are the potential for liquid crystalline ordering [8, 27, 68] and the lowering of their percolation threshold with increasing particle aspect ratio [71]. This highlights how the simple shape-change of constituent building blocks results in materials with very different properties.

Networks of rods can provide conductive pathways [150, 151] or significantly

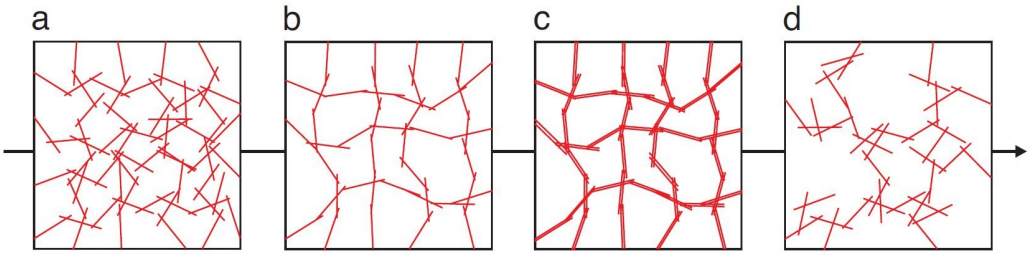

Figure 8.1 *(a) - (d) Network structures resulting from varying attractive interactions. Respectively, homogeneous network, locally anisotropic homogeneous network, network consisting of bundles, and a heterogeneous network of fractal clusters. Taken from [70].*

contribute towards a solid-like rheological response of materials [9]. The low percolation threshold means that only a small quantity of particles is required, reducing cost and density. Naturally, network properties depend on the building blocks (aspect ratio, material) and their particular interparticle interactions [9]. The latter strongly influence the resulting structure (Figure 8.1), which also underpins the network properties [70, 152]. Equilibrium homogeneous networks form through weak attractions between rods (Figure 8.1a). Increasing attractive interactions can result in locally anisotropic structures (Figure 8.1b), while for more anisotropic attractions a network consisting of bundles forms (Figure 8.1c). Heterogeneous networks of fractal clusters form when strong attractive interactions are involved (Figure 8.1d). Furthermore, in the case of strong attractive interactions, experiments have demonstrated the importance of the particle aspect ratio. Here, the diffusion-limited aggregation of rods gives decreasing fractal dimensions for increasing aspect ratio [153]. As a result, gelation occurs at lower particle concentration for increasing aspect ratio, and gels with very low particle density can be formed [154, 155].

An important application of percolating networks of rods is found in polymeric materials, where 'filler' particles are often added to enhance some properties like conductivity or mechanical strength. A more specific example is their addition to binary polymer blends. These usually are immiscible and undergo phase separation, so the question arises: what is the influence of the filler particles on domain-structure evolution in this process? Trapping of the particles into one preferred phase is a relevant scenario [156, 157], but is mainly investigated for spherical particles. In these studies, close to filler particles, the interplay between wetting and phase separation is found to create composition waves [157–159]. Simulations even suggested that during phase separation the preferential

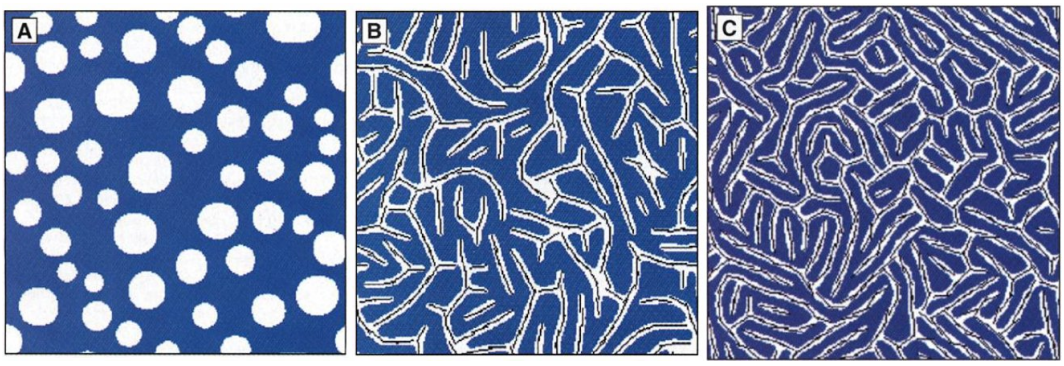

Figure 8.2 *Simulations in 2D of a binary liquid mixture (a) undergoing phase separation, to which (b) rods were added to result in a percolating network, and (c) increasing the particle concentration leads to a more lamellar structures. Taken from [17].*

adsorption induces an attractive dynamic depletion interaction [159, 160]. On a larger length scale, the filler particles typically alter the structural evolution [156, 159, 161] and kinetics of the domain coarsening, which is found to slow down [156, 162, 163]. Consequently, filler particles can be seen as an opportunity to control structuring in these materials.

Switching from spheres to rods again, introduces the coupling between the liquid-liquid phase separation and the possibility of orientational ordering of the rods. Simulations in 2D of rods being trapped into the minority phase of a phase-separating asymmetric binary liquid mixture, showed the formation of percolating networks and lamellar morphologies (Figure 8.2) [17]. In another 2D simulation study, taking mixtures of symmetric composition, droplet and bicontinuous morphologies containing aligned rods were observed [164]. For phase separation via spinodal decomposition of the liquid mixture, simulations in 3D demonstrated a microphase separation if the rod-concentration in the confining phase was sufficient for an isotropic-to-nematic transition to occur [165]. Experiments showed that in this latter case much lower concentrations can suffice if attractive interactions are present between the particles. Short nanorods kinetically arrested the phase separation of a polymer blend as they formed a percolating network within one of the phases [166].

The same scenario can also occur in mixtures of molecular liquids rather than macromolecules [55, 139, 167]. This is entering a situation where, initially, the particles are no longer embedded in a highly viscous macromolecular liquid, and rely on charge-stabilization to remain dispersed. Investigating these systems is mainly motivated by temperature dependent attractive interparticle interactions

in the one-phase regime, close to the coexistence curve of the liquids [131]. Far from the critical composition adsorption of the preferred component to the particle surface eventually leads to the formation of liquid bridges to induce aggregation [51]. Nearer to the critical composition, critical fluctuations in the local composition of the liquid mixture are involved [51]. As far as known, only a single report explicitly studies the trapping of colloids into a preferred phase after phase separation in this type of liquid mixtures [167]. The specific phase that is preferred by the colloids is found to depend on surface chemistry, which in this case is parametrized as the surface charge. By quenching the temperature deeper into the miscibility gap, a wetting transition takes place at a certain temperature, and particles are trapped at the interface. This transition from complete to partial wetting of the colloids' surfaces is analog to that of flat surfaces [168].

The study presented in this chapter aims at using the interplay between phase separation in a molecular liquid mixture and rods trapped inside one of the resulting phases, to assemble particle/liquid composite morphologies. In most cases the end result of this scenario is simply a macroscopic phase separation of the system with one of the liquid phases containing all the colloids. However, the current study takes inspiration from simulation results which suggest that it may be possible for the interaction between particles and the dynamic processes in the suspending liquid to lead to structural arrest. This took an asymmetric liquid mixture and sufficient particles that were trapped inside the minority phase upon phase separation. The formation of percolating networks of spheres [159] and rods [17] was demonstrated, as the presence of the particles prevents further coarsening of the liquid domains. If, ultimately, no structural arrest occurs, the confinement might drive the liquid crystalline ordering of the particles inside the domains.

Below, first the experimental methods are detailed. The results section follows, and describes for various temperature quenches observations of a water/PGPE mixture of fixed composition, containing colloidal rods. This is then discussed in the light of the aim of the study, and related experimental and simulation reports. Finally, the work is summarized and future directions suggested.

8.2 Experimental section

Materials

Chemicals: Ethanol (absolute, from VWR), ammonium hydroxide solution (35%, reagent grade, from VWR), tetraethyl orthosilicate (TEOS, reagent grade 98%, from Sigma Aldrich), propylene glycol propyl ether (PGPE, 1-propoxy-2-propanol, 99%, from Sigma Aldrich), hexane (≥97%, from Sigma Aldrich), and dichlorodimethylsilane (DCDMS, ≥99.5% from Sigma Aldrich). Water was obtained from a Milli-Q system.

Colloidal Rods: Hollow, fluorescent rods were prepared as described in Chapters 3 and 4. A full batch (see Chapter 3 for starting amounts) was coated with a thin layer of unlabeled silica. For this, first the particles were dispersed in 130 g ethanol, to which 11 g ammonium hydroxide solution (35%) was added, followed by 2 additions (dropwise and under stirring, with a 1 hour interval) of 0.6 mL TEOS/ethanol (1:1 v/v). The mixture was left under stirring overnight, and subsequently the product was washed several times with water (basic pH from residual ammonia) to render the particles well-charged. Finally a stock suspension in ethanol was prepared. The dimensions of the resulting particles were determined from TEM images: L = 3.54 μm (σ = 15%), D = 0.37 μm (σ = 13%), aspect ratio = 9.7 (σ = 16%).

Sample preparation

Portions of the stock suspension were transferred into weighed vials, and most of the solvent was removed with a pipette after centrifugation. Particles were dried in an oven (80 °C Gallenkamp), first 60 minutes without vacuum, then 30 minutes with vacuum. Vials were weighed after drying to determine the amount of particles. The rods were then dispersed in a pre-made mixture of 30 wt% (or 35 wt%, where stated so) water in propylene glycol propyl ether at a desired concentration. The effect of the hollowness of the particles was taken into account by estimating the volume of the cavity from the mass ratio silica/akaganéite (see experimental section Chapter 5), and assuming that these cavities fill up completely with the solvent. Where needed Nile Red dye was first dissolved in PGPE before making up the liquid mixtures.

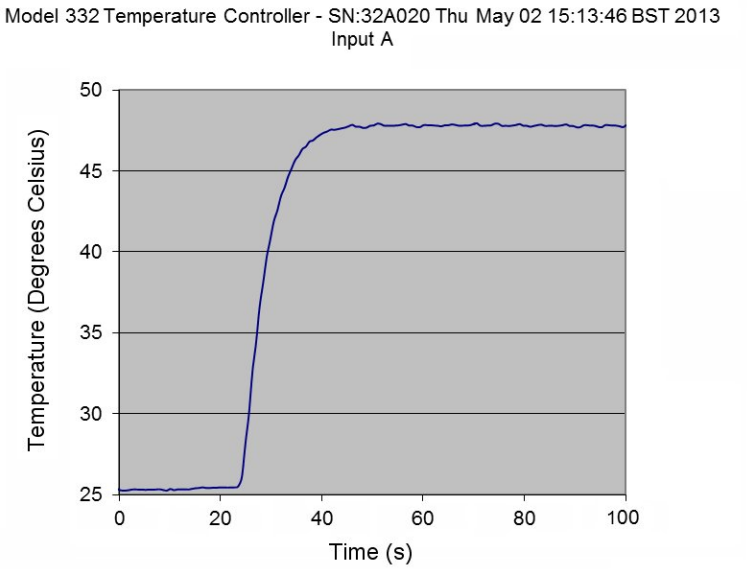

Figure 8.3 *Temperature of a sample inside a cuvette as a function of time, before, and after the cuvette being immersed in a pre-heated water bath.*

The samples were then transferred into cuvettes (1 mm path length from Starna Scientific) tightly sealed with Teflon stoppers. The inner glass surfaces of the cuvettes had been rendered hydrophobic by exposing them for 30 minutes to a 50/50 (v/v) DCDMS / hexane mixture. To ensure removal of DCDMS/hexane cuvettes were washed first 10× with hexane, followed by drying in an oven (50 °C), and then followed by more washing with, first, water and finally ethanol to be dried again and used to study samples.

Macroscopic dispersion behaviour

Samples contained in cuvettes were subjected to quick (rate = $\sim$ 1°C/s) temperature quenches by quickly and fully immersing them into a water bath at a set temperature. The temperature of the water bath was controlled by a IKA ETS-D5 temperature controller connected to a IKA RCT-basic hotplate, and kept homogeneous by constant stirring with a magnetic stirrer bar. Accurately measuring the temperature of the bath was done with a calibrated thermocouple connected to a Lakeshore 332, which was hooked up to a computer for recording the temperature. A typical temperature quench of a sample contained inside a cuvette was recorded using this setup (Figure 8.3). Following the macroscopic appearance of the sample in the water bath was done using a DSLR camera (Canon EOS 40D with a Tamron 70-300 mm Tele-Macro lens) in combination

with a light bulb offering proper illumination. The camera was attached to a computer to allow it to be controlled using software (Canon EOS utility), which enabled time-lapse photography.

Microscopy

Samples were also studied using a Zeiss LSM 700 confocal microscope. Here, to achieve temperature control an Instec TSA02i thermal stage in combination with an Instec mK1000 temperature controller were used. After a temperature quench in the water bath, the cuvettes were inserted in a tightly fitting aluminium sample holder, which was pre-heated inside the Instec thermal stage to the same temperature as the water bath. The calibrated thermocouple used to record the temperature in the water bath confirmed that the temperature in the thermal stage was not significantly different (typically slightly higher, at most 0.1 °C). Changing the temperature with the temperature controller, however, there was a significant lag in the temperature change of the sample. Therefore, when doing this, the temperature in the thermal stage was allowed to equilibrate.

With the sample being buried inside this device, the setup allowed imaging only with a long working distance (20×) objective. Due to the fixed position of sample holder's tiny imaging hole, all confocal microscopy imaging was done at roughly the same location in the sample: in the center, ∼1 cm from the bottom when the cuvette is positioned as shown in the photographs throughout this Chapter. Since an inverted microscope was used, the sample was put down flat for imaging.

A Nikon Eclipse E800 microscope with a 10× objective and QImaging Micropublisher 3.3 camera were used for recording birefringence. On this microscope a Linkam temperature stage was used for heating.

8.3 Results

As outlined at the end of the introduction, the studied samples consist of a binary liquid mixture of asymmetric composition, containing colloidal rods that become trapped in the minority phase upon phase-separation. Silica colloids in a mixture of water / propylene glycol propyl ether (PGPE) was found to be a suitable model system. This relevant liquid pair has a LCST just above room temperature

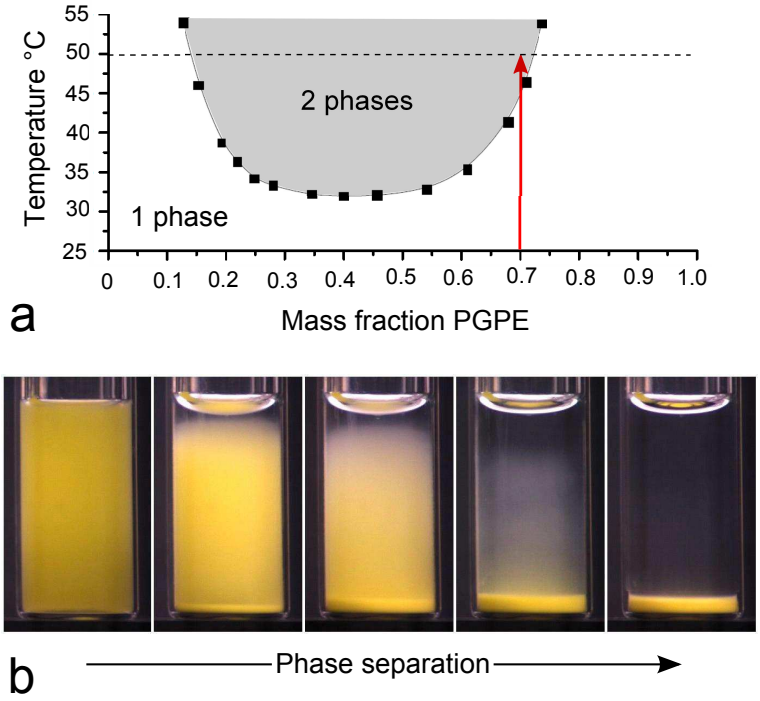

Figure 8.4 *(a) Phase diagram of water and propylene glycol propyl ether (PGPE) [147] with a red arrow to indicate a temperature quench. (b) Time series of photographs, after immersing a vial containing a suspension of spherical silica colloids (1 vol%) in a mixture of 30 wt% water in PGPE at room temperature, in a water bath equilibrated at 50 °C. Temperature quench the sample undergoes in (b) corresponds to the red arrow in (a). Panels in (b) are, respectively, at times 0, 10, 20, 40, and 70 minutes after immersion in the water bath.*

(Figure 8.4a), conveniently allowing a liquid-liquid phase separation to be induced by only mild heating. Silica particles strongly prefer the water-rich phase, as was already noted in the previous chapter. Liquid-liquid phase separation results in water droplets with particles trapped inside, which sediment, coalesce, and form a colloid-rich phase at the bottom of the container (Figure 8.4b).

Small volumes of the minority phase would be advantageous for achieving structural arrest by overcrowding the minority phase using a modest quantity of colloidal rods. Therefore, the composition was fixed at 30 wt% water in PGPE, where small volumes of water-rich phase can be formed by shallow temperature quenches across the binodal. From the coexistence curve, by using the lever rule, the dependence of the minority phase volume on temperature can be estimated for this composition (Figure 8.5).

At this fixed liquid composition, the temperature-dependent behaviour at varying concentration of colloidal rods was investigated. To approach or cross the

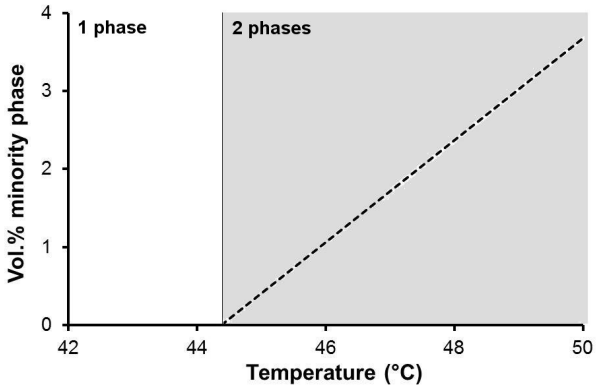

Figure 8.5 *Estimated volume of the water-rich phase of a 30 wt% water in PGPE mixture, as a function of temperature (dashed line). It is a linear fit of values obtained from the coexistence curve (Figure 8.4a) using the lever rule.*

coexistence curve, the temperature was quenched from 25 °C to various end-points. Observations of

1. quenches approaching the coexistence curve (42 and 44 °C, see Figure 8.5), and
2. shallow quenches across the coexistence curve (46 and 48 °C, see Figure 8.5)

are presented below. At the end of this section, briefly, deeper quenches for higher rod concentrations are demonstrated.

Approaching the binodal

That the liquids fully mix at room temperature is convenient for preparing stable suspensions of the desired composition that serve as a starting point. Approaching the binodal by heating samples to 42 °C suspensions are still found to be stable. Independent of particle concentration, a straight sedimentation front is observed as the particles are slowly settling under gravity (Figure 8.6). Tilting the samples demonstrates they are is still flowing freely under gravity, indicating that the particles have remained well-dispersed (Figure 8.6).

At a slightly higher temperature of 44 °C, closer to, but not yet crossing the coexistence curve, aggregation is observed. At a low particle concentration (0.1 vol.%), rods in the initially stable, homogeneous suspension (Figure 8.7a, left

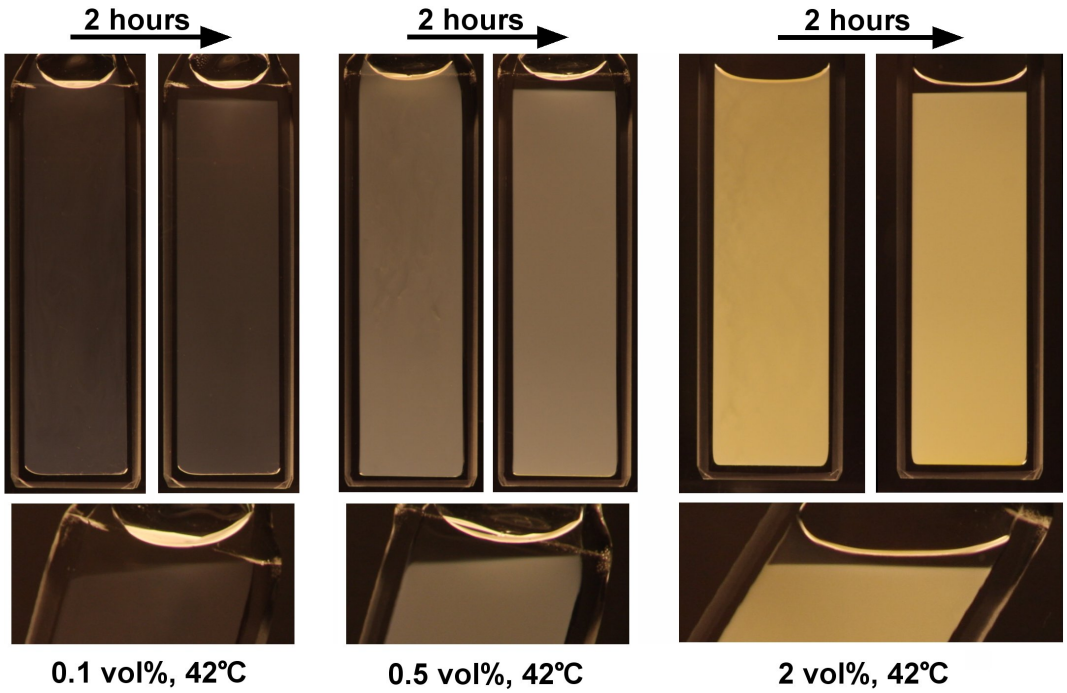

Figure 8.6 *Cuvettes immersed in a water bath at 42 °C, containing stable suspensions of various concentrations of colloidal silica rods in a liquid mixture of 30 wt% water in PGPE. Each sample is shown (left) directly after immersion, (right) 2 hours after immersion, and (bottom) tilted, 2 hours after immersion.*

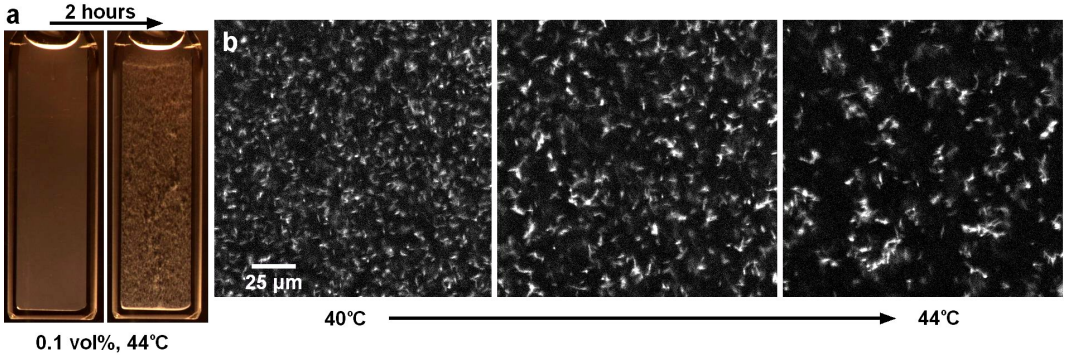

Figure 8.7 *(a) Cuvette immersed in a water bath at 44 °C, containing a suspension of colloidal silica rods (0.1 vol.%) in a liquid mixture of 30 wt% water in PGPE, immediately (left), and 2 hours (right) after immersion. (b) Time series of a sample of the same composition as in (a), while heating it from 40 °C to 44 °C.*

panel) aggregate into big lumps, most of which get stuck by the presence of the glass cuvette walls (Figure 8.7a, right panel). Monitoring the sample with CLSM, stably suspended particles are observed at 40 °C, and the formation of aggregates can be followed when heating to 44 °C (Figure 8.7b).

Increasing the concentration of rods, suspensions remain more homogeneous in

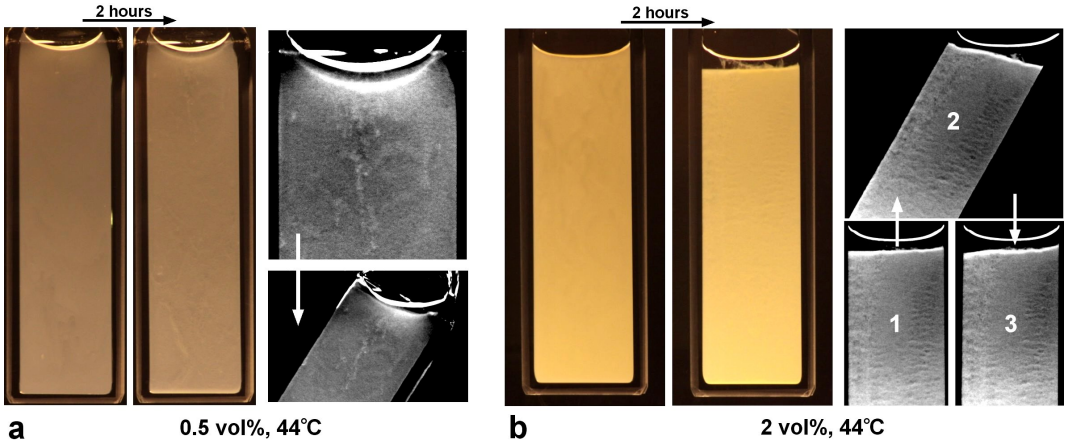

Figure 8.8 *Cuvettes immersed in a water bath at 44 °C, containing suspensions of (a) 0.5 and (b) 2 vol.% colloidal silica rods in a liquid mixture of 30 wt% water in PGPE. Both samples are shown immediately (left panel), and 2 hours (middle panel) after immersion. The panels on the right in black and white, for each sample, show the effect of tilting.*

appearance. At 0.5 vol.%, after 2 hours, no dramatic change is observed in contrast to the lowest particle concentration. A stationary structure appears to have formed, with its edge close to, and following the shape of the liquid-air interface (Figure 8.8a, middle panel). This is in sharp contrast to the straight, slowly lowering, sedimentation front observed at 42 °C. Enhancing the contrast of the image demonstrates that the top edge is slightly more dense, and clearly shows heterogeneities in the particle concentration (Figure 8.8a, top image of the right panel). Tilting the sample confirms the structure being stationary and, only on the side where the interface pushes down onto it, is it seen to deform (Figure 8.8a, bottom image of the right panel).

Something similar is observed at 2 vol.% of rods. Here, however, the structure slowly collapses with a fairly straight edge slowly moving downwards (Figure 8.8b, middle panel). Some bigger clumps on top of this edge give away that the particles have indeed aggregated. Enhancing the contrast demonstrates heterogeneities in particle concentration (Figure 8.8b, right panel), also corresponding to a structure having formed by aggregating rods. Tilting the sample, similar to the lower concentration, demonstrates that the structure is stationary (Figure 8.8b, right panel # 1 to # 2). It does deform permanently where the interface has pushed onto it (Figure 8.8b, right panel # 2 to # 3).

With CLSM the structures formed by the aggregating particles can be visualized in some more detail. Spiky-looking, fractal aggregates have sunk to the bottom

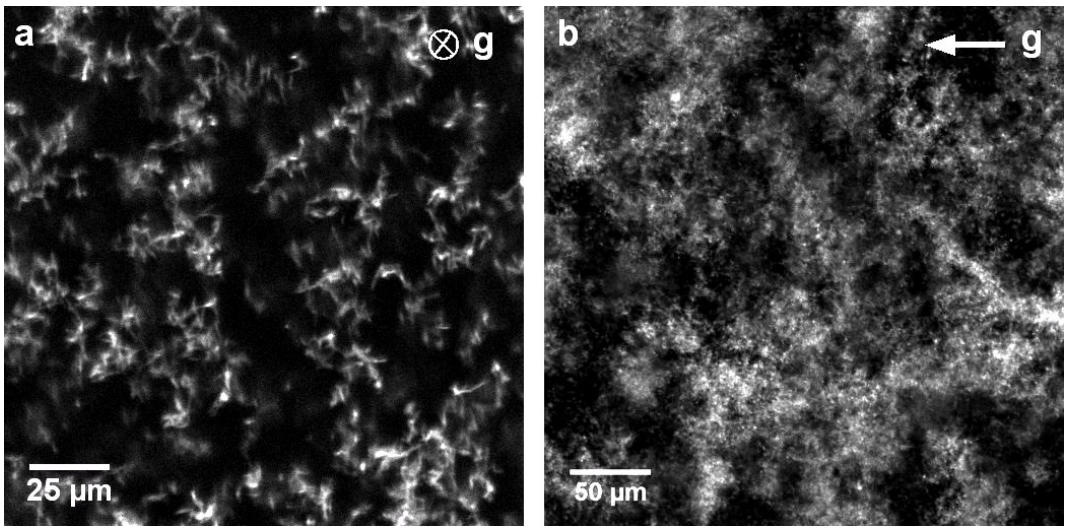

Figure 8.9 *CLSM images of (a) aggregates formed in the quench shown in Figure 8.7b, and (b) the network formed by particle aggregation shown in Figure 8.8a.*

in the sample with 0.1 vol.% rods (Figure 8.9a). In the sample containing rods at 2 vol.%, aggregation has lead to heterogeneous, slightly fluffy-looking particle networks (Figure 8.9b) built up from fractal aggregates.

Temperature quenches into the miscibility gap

A sudden and much more dramatic change in the state of the sample can be observed when the coexistence curve is crossed by a rapid temperature quench into the miscibility gap. Doing this only just, by taking a final temperature of 46 °C, the resulting liquid-liquid phase separation can be followed with CLSM. This very shallow quench leads to only a very small volume (∼1 vol.% of the total liquid) of minority phase to form, and the nucleation and growth (coalescence will be involved as well) of tiny droplets can be observed (middle and right columns of Figure 8.10). Here, the liquid contains a fluorescent dye as label, which preferentially sits in the PGPE-rich phase, leaving the water-rich droplets dark (middle column of Figure 8.10b). Overall, the picture becomes darker due to the formation of rod-filled droplets, as these larger objects scatter more light, thus to a larger extent preventing it from reaching the PMT's (Figure 8.10b,c). Rods present in the sample (at 0.1 vol.%) are captured in the droplets, and the initially finely dispersed particles are ultimately observed as bigger blobs (Figure 8.9a).

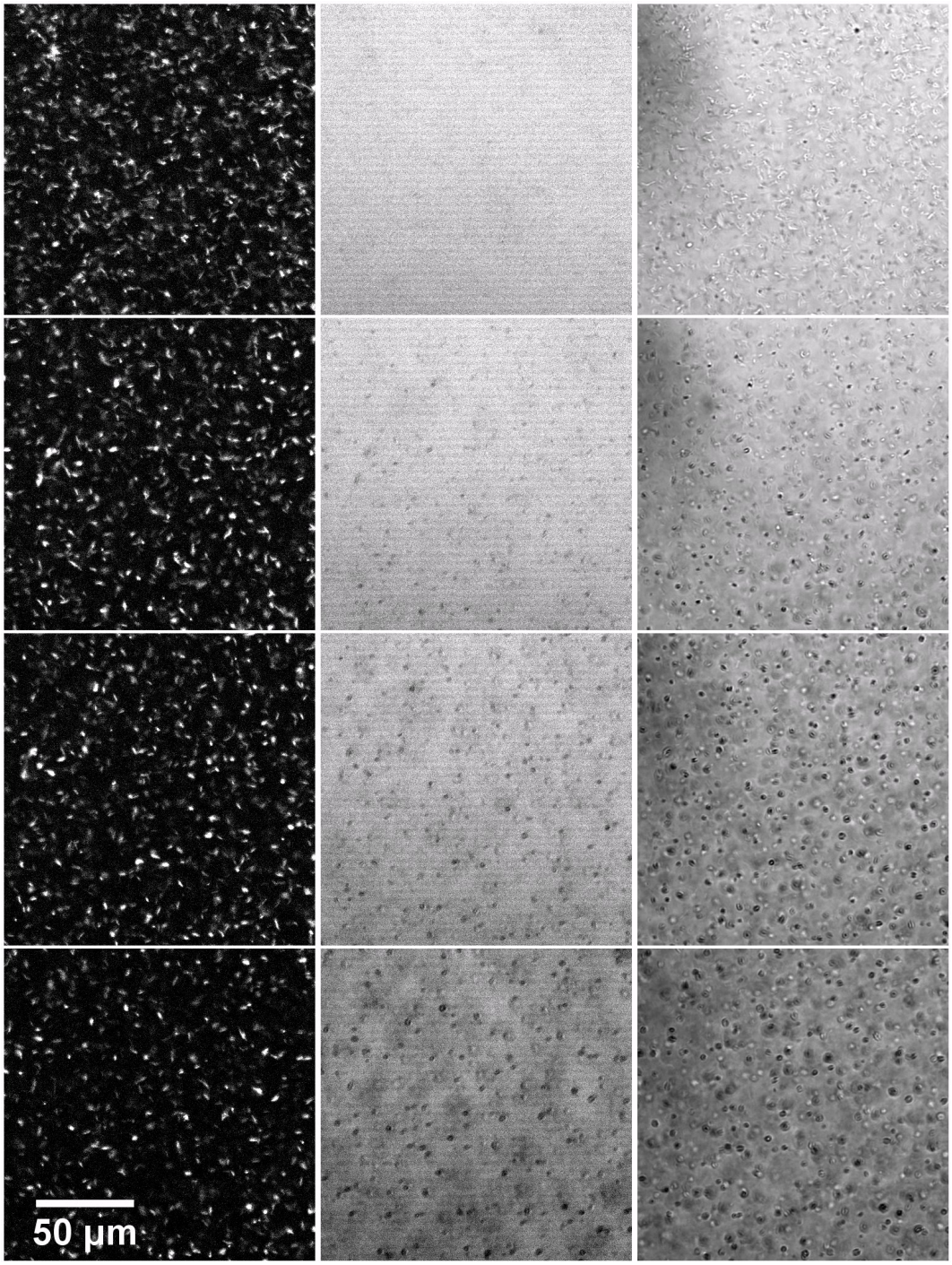

Figure 8.10 *CLSM time series of a sample (0.1 vol.% rods) quenched to 46 °C images. The columns are (left) FITC-particle signal, (middle) Nile Red label in the PGPE-rich majority phase, and (right) transmitted laser light.*

Since the PGPE-rich phase is the least dense, the rod-filled droplets sediment and end up collecting on the bottom glass surface of the container. They open up on the hydrophobic glass, since it is partially wetted by water-rich droplets

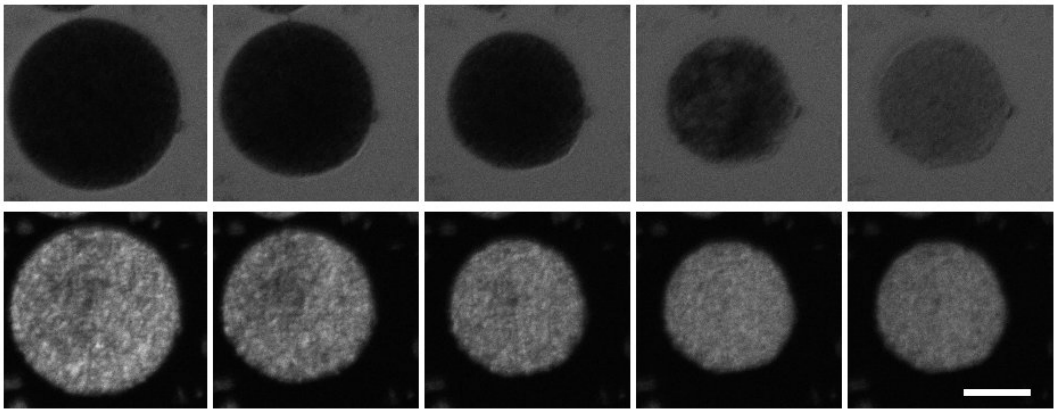

Figure 8.11 *CLSM time series of droplet filled with rods, stuck on the bottom (hydrophobic) glass surface, formed by a quench to 46 °C (Figure 8.10) being cooled to 44 °C. Rows are (bottom) FITC-particle signal, and (top) Nile Red label in the PGPE-rich majority phase. (Scale bar = 15 μm)*

(Figure 8.11, far left column). Allowing the sample to cool back to 44 °C, where the liquids re-mix, the droplets are first observed to shrink (Figure 8.11, top row, panels 1 - 4). Ultimately, the re-mixing of the liquids is evidenced by the gradual disappearance of the dark, water-rich regions (Figure 8.10, top row, panels 4 to 5). The decreasing volume of the droplet forces the particles into a small clump, which is left behind (Figure 8.11, bottom row, left to right).

Macroscopically, this leads to the formation of large, rod-filled droplets that collect at the bottom of the cuvette, with some small droplets getting stuck on the glass walls (Figure 8.12a). Qualitatively the same is observed when increasing the rod concentration to 0.5 vol.% (Figure 8.12b). The final state is dramatically different when the rod concentration, at 2 vol.%, exceeds the volume fraction of the minority phase. In contrast to the formation of large, rod-filled droplets, this sample's appearance remains almost unchanged upon liquid-liquid phase separation (Figure 8.12c). A closer look near the interface reveals that rods and minority phase have, most likely, formed a stationary structure. Where the liquid-air interface curves up, the edge of the structure is visible, with only a very small volume of clear PGPE-rich phase on top. Tilting the sample demonstrates that the structure deforms under influence of the moving liquid-air interface. A fracture appears, and after orienting the sample back to its original position, some permanent structural damage seems to have been inflicted (Figure 8.12d).

The structure formed by the particles in the sample at 2 vol.% rods (Figure 8.12c,d), can be studied in some detail with CLSM. It demonstrates that a fine,

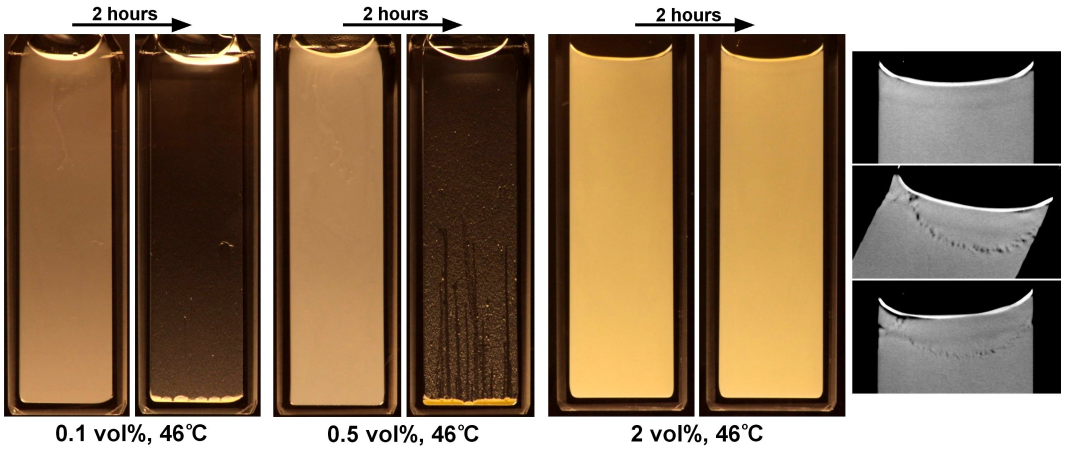

Figure 8.12 *Cuvettes containing rods at (a) 0.1 vol.%, (b) 0.5 vol.%, and (c) 2 vol.% in a liquid mixture of 30 wt% water in PGPE, immersed in a water bath at 46 °C. For each of these, the cuvette is shown (left pannel) directly, and (right pannel) 2 hours after immersion. (d) The same sample as in (c), after 2 hours, zoomed in on the interface with enhanced contrast, (top) before, (middle) during, and (bottom) after tilting it.*

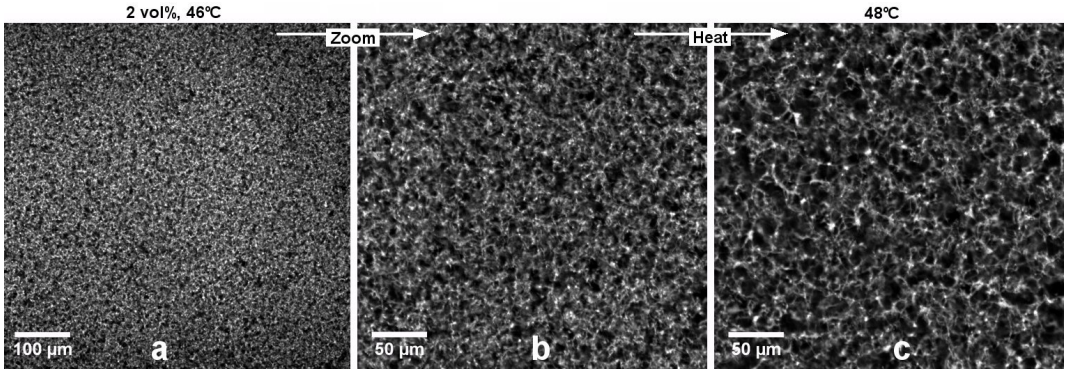

Figure 8.13 *CLSM images of (a & b) the sample shown in Figure 8.12c,d at 2 different magnifications. (c) Resulting structure after heating the sample to 48 °C.*

homogeneous network of rods has formed (Figure 8.13a,b). With gravity coming out of the plane of view, heating the sample further to 48 °C, more minority phase separates out. This results in a more open, heterogeneous structure (Figure 8.13b,c). Some larger bright blobs appear, as well as some very thin stringy/thread-like connections.

Repeating this quench from 46 °C to 48 °C in a water bath demonstrates the effect of gravity being oriented along the length of the cuvette. The initially nearly completely space-filling structure, is seen to shrink as a whole (Figure 8.14a). A direct, quick quench to 48 °C results in a more heterogeneous looking sample

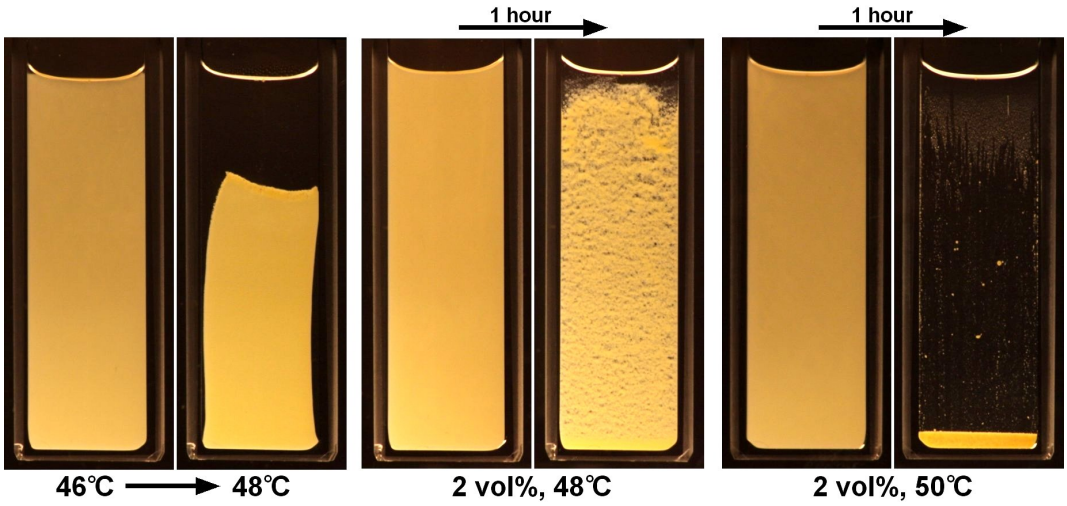

Figure 8.14 *(a) Sample of 2 vol.% rods, (left panel) first immersed in a water bath at 46 °C, and subsequently (right panel) slowly heated the water bath to 48 °C. (b) Sample of 2 vol.% rods immersed in a water bath at 48 °C, (left panel) immediately, and (right panel) hour after immersion. (c) Sample of 2 vol.% rods immersed in a water bath at 50 °C, (left panel) immediately, and (right panel) hour after immersion.*

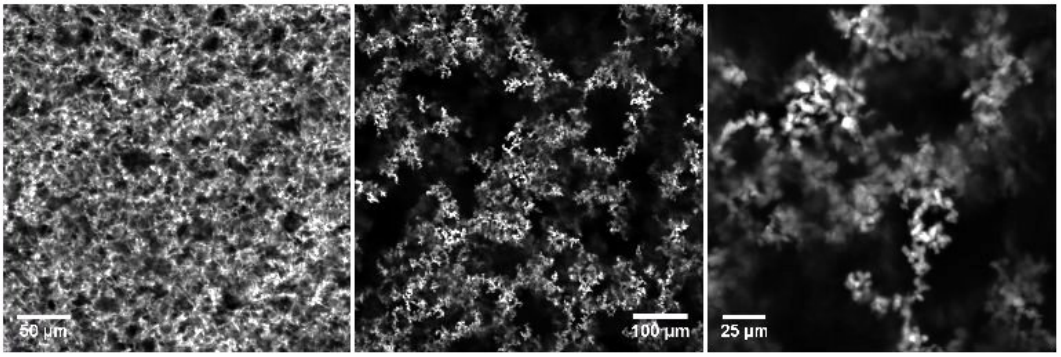

Figure 8.15 *CLSM images of samples at 48 °C, shown in (a) Figure 8.14a and (b & c) Figure 8.14b.*

(Figure 8.14b). Still, the rods appear to form a stable, stationary structure. Complete, macroscopic phase separation occurs for a quench to 50 °C, where rod-filled droplets form and are collected into a small, dense region at the bottom of the cuvette (Figure 8.14c).

The structuring of the particles after the water-bath quenches to 48 °C can be compared to those in Figure 8.13. Corresponding to the observed shrinkage, doing the 46 °C to 48 °C quench in a water bath results a more dense structure (Figure 8.15a, as compared to Figure 8.13c). For the direct quench a very heterogeneous, more fractal-like structure was formed (Figure 8.15b,c).

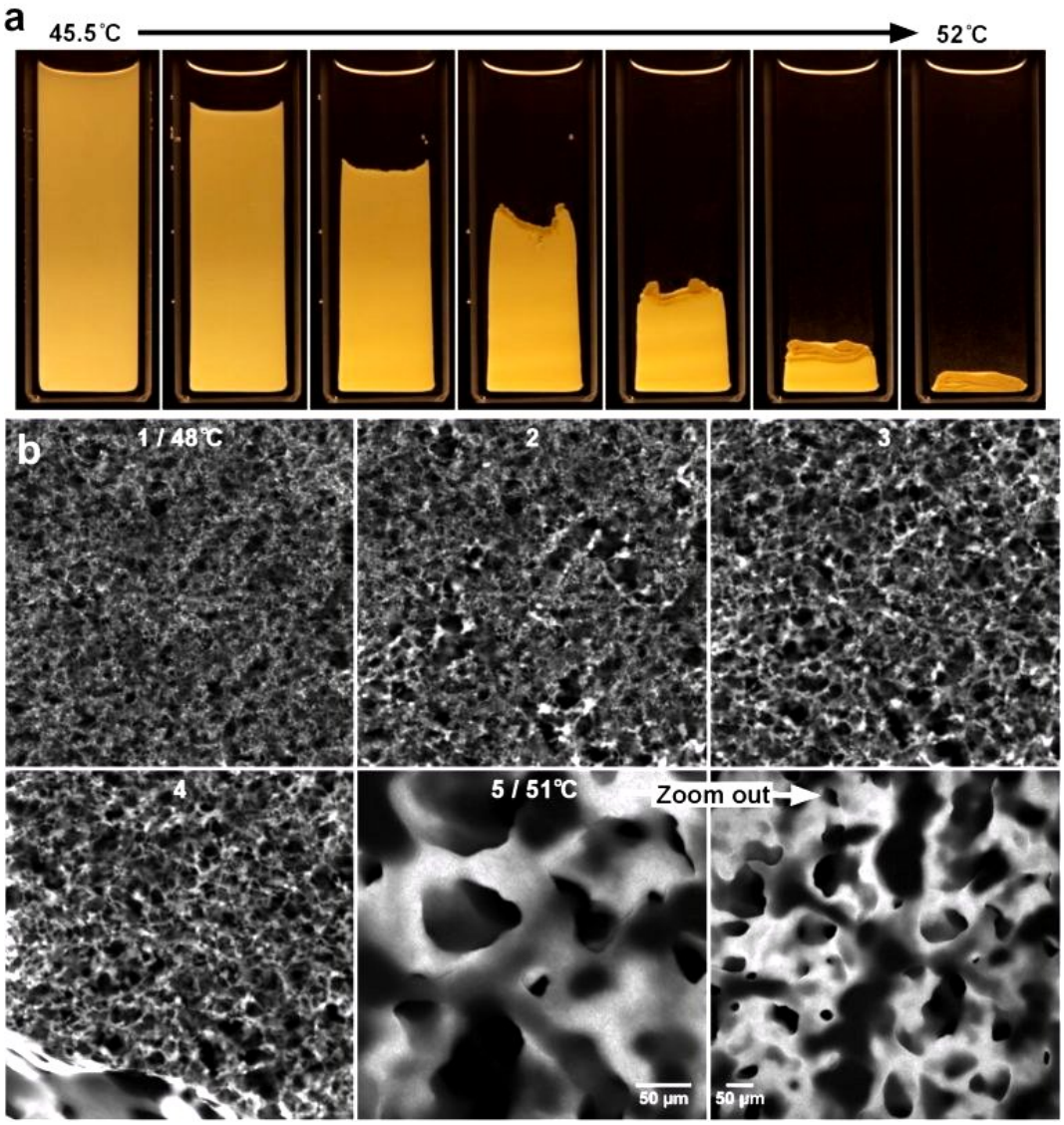

Figure 8.16 *(a) A sample (2 vol.% rods) quenched to 45.5 °C and then slowly heated to 52 °C (for the water-rich phase it is estimated that here ϕ_{final} = 30 vol.% rods). (b) CLSM time series showing (panel 1) the structure at 48 °C of the sample in Figure 8.15, which is subsequently heated (panels 2 - 5) to 51 °C. The bottom right panel is a lower magnification of the structure in panel # 5.*

In a water bath, slowly continuing heating after an initial, quick quench into the miscibility gap, shows the particle network shrinking into a compact, dense region as more minority phase separates out (Figure 8.16a). Assuming that all the water-rich phase is present in this dense region at the bottom of the cuvette, the volume fraction of rods here can be estimated at just over 0.3 (for 52 °C). Similarly, the structure formed by a water-bath quench from 46 °C to 48 °C (Figures 8.14a and 8.15a) was slowly heated to 51 °C, while imaging it with CLSM (Figure 8.16b). First the structure becomes more open and coarse (reminiscent

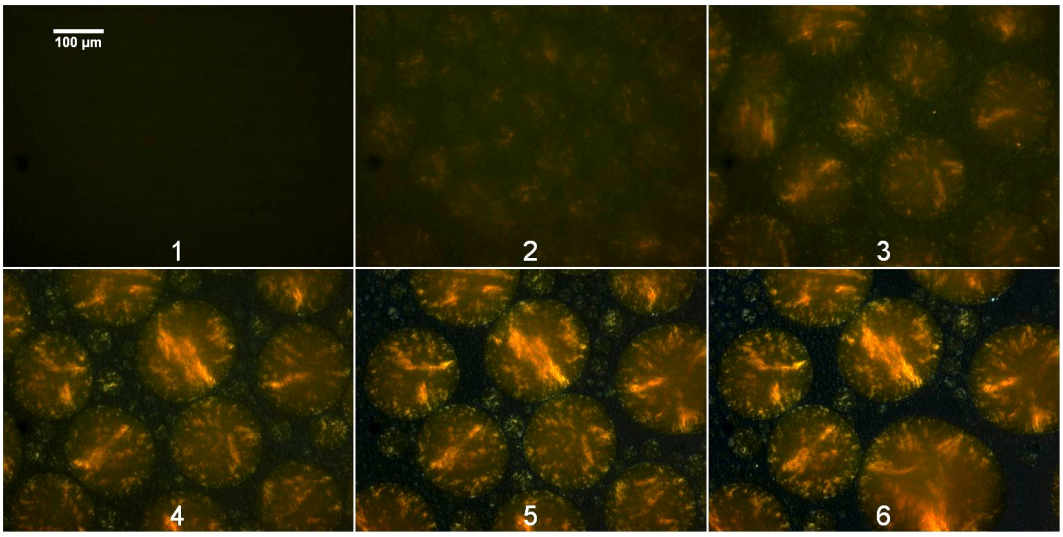

Figure 8.17 *A sample (2 vol.% rods) quenched to 50 °C. Panels demonstrate sample evolution, viewed between crossed polarizers, over the course of approximately 10 minutes.*

of Figures 8.13b,c). Then, a sudden catastrophic event occurs, where it looks like a front moves through the structure, sweeping up all the particles into larger domains. This results in a bicontinuous-like, dense, rod-filled structure, which coarsens only very slowly due to a high viscosity.

Deeper quenches: Ordering of rods

As demonstrated by some of the previously presented experiments, it is easy to trap colloidal rods in the minority phase, and so confine the particles to a small volume. Droplets of minority phase containing rods attached to hydrophobic glass surfaces have been found, owing to partial wetting. Otherwise, all droplets are allowed to coalesce, collecting nearly all rods into a single domain of minority phase. Of the lowest density is the PGPE-rich majority phase, and minority phase filled with rods therefore always sediments to the lower surface of the container.

With the cuvettes placed horizontally on a microscope, after a deep enough temperature quench, a large number of rod-filled droplets (like that in Figure 8.11) are distributed over the bottom glass surface. This is the case for a liquid mixture containing a relatively high concentration of rods (2 vol%), quenched to 50 °C, where birefringent droplets are observed (Figure 8.17).

A further quench to 53 °C results in the nucleation of 'empty' droplets in the liquid above the existing rod-filled droplets. Some of these end up on the glass

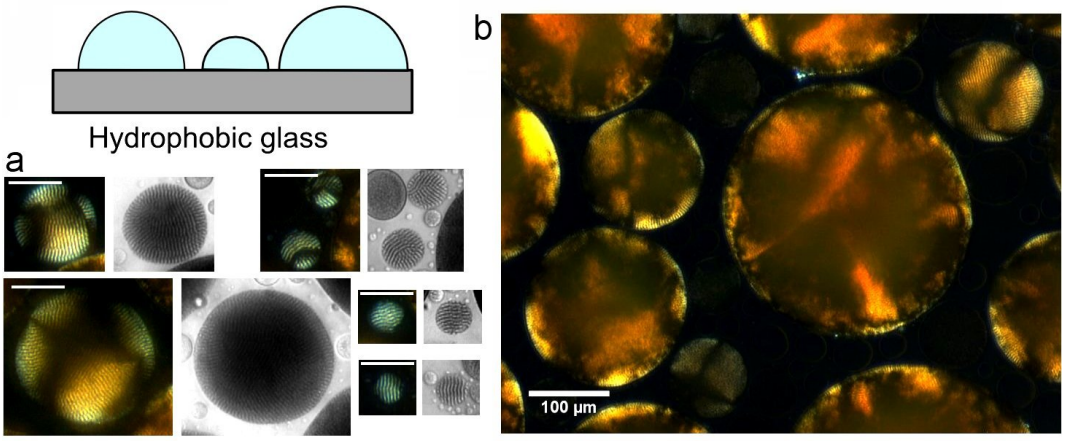

Figure 8.18 *A sample (2 vol.% rods), first quenched to 50 °C, subsequently heated to 53 °C, and then left to equilibrate for 2 hours. (b) Pairs of images of small droplets, (left) with, and (right) without crossed polarizers (scale bars are 50 µm). (b) Image of some larger droplets through crossed polarizers.*

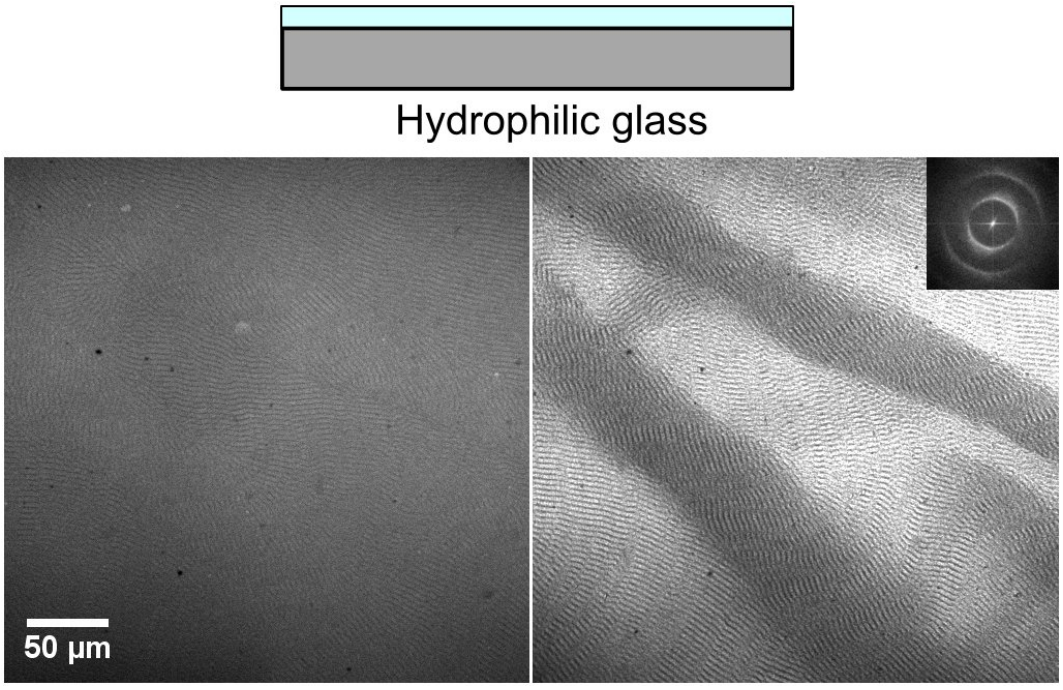

Figure 8.19 *A sample of 2 vol.% rods in a mixture of 35 wt% water in PGPE, contained in a cuvette with hydrophilic glass walls, quenched to 48 °C. (left panel) CLSM image of the particles confined to a thin layer of minority phase, and the corresponding bright field image (right panel). The inset is a FFT of the bright field image.*

surface, while others coalesce with rod-filled droplets. Empty droplets in the spaces between rod-filled droplets can be seen in some panels of Figure 8.18a, and they appear as faint rings in Figure 8.18b. After leaving the sample to

equilibrate for some time, striped patterns are visible inside droplets, especially in smaller droplets, and near the 3-phase contact line (Figure 8.18a).

Taking a hydrophilic glass surface, which is completely wetted by the minority phase, onto which the droplets settle, results in a thin film of minority phase. In these films, over time also a striped pattern is observed (Figure 8.19). From a FFT (inset of Figure 8.19) a typical length scale of 3.3 μm can be determined.

8.4 Discussion

Experiments presented above demonstrate the temperature dependent behaviour of the investigated system, as well as how the sample's final morphology can change with the concentration of rods. The starting point being a stable suspension in a liquid mixture of fixed composition, samples were heated to approach, and ultimately enter the miscibility gap. It was possible to get within a few degrees of the coexistence curve without observing any change in the stable, charge-stabilized suspensions (Figure 8.6).

Slightly closer to the binodal curve the rods aggregate (Figure 8.7), indicating that flocculation occurs in a narrow temperature interval, bordering the coexistence curve. This corresponds to the previously observed wetting-induced aggregation [55], and is inherent to the type of system studied here. Since the chosen composition here is far from the critical point, in the absence of critical fluctuations, wetting layers are formed which eventually coalesce to form liquid bridges between particles, leading to aggregation [51].

The quite rapid aggregation of rods into open, fractal-like clusters (Figures 8.7 and 8.9), suggests that it proceeds through diffusion-limited cluster aggregation (DLCA). This is not surprising considering that the liquid bridges will result in strong, short-range, attractive interactions between rods. Fractal aggregates and DLCA were also found in a study looking into aggregation through critical Casimir forces [135]. Elsewhere, at liquid compositions further from the critical one, kinetics also indicated that DLCA was involved [169]. Here, a notable difference is that the formed clusters were compact, instead of open and fractal. Within clusters the particles were still separated significantly, indicating that their charged surfaces remain mutually repulsive. Additionally, being embedded in close to index matching 2,6-lutidine, strongly reduced the contribution of van der

Waals forces to the interaction potential. Similarly, in another system compact clusters were observed, in which the highly charged constituent particles exhibited crystalline order [139].

The rigid and fractal-like nature of the aggregates in the system studied here, suggests that the particles fall into the primary minimum of the interaction potential. If, through the liquid that binds the particles, there was an effective repulsive force between their surfaces, one would expect them to be able to reorient themselves. This scenario would even favor alignment as it would maximize the contact area between particles, and minimizes interfacial area of the wetting layers. This would result in ordered aggregates, reminiscent of those observed in the experiments mentioned above [139, 169]. Another observation that indicates aggregation into the primary minimum, is that after re-mixing the liquids the particles did not spontaneously re-disperse. To achieve re-dispersion sonication was required. A possible factor in this behaviour is that any (trace) ionic species are likely to collect in the water-rich wetting layers. This would screen the interactions between the particles' surface charge through the liquid bridge.

Gels form at higher particle concentration, where the rods form heterogeneous networks of fractal clusters. This is similar to the effect of adding salt for the gelation of charge-stabilized rod suspensions [154, 155].

When quenching into the miscibility gap at low colloid concentration, phase-separation is not much affected, as can be expected (Figures 8.10 and 8.12). At higher rod concentration, what appears to be a microphase separation occurs, resulting in the formation of a practically space-filling homogeneous network of rods (Figures 8.12 and 8.13), which must be encapsulated by the minority liquid phase. Such a 'wetted' network has been suggested to form in this scenario, by simulations, neglecting any pre-transitional aggregation effects and using hard particles [17, 159].

The wetting layer covering the network is emphasized by separating out more minority phase (Figure 8.13). As this happens, newly nucleated water-rich droplets are included in the network, resulting in the observed coarsening of the network. The amount of liquid covering the network, and the interfacial tension increase. Therefore, the minority phase imparts an increasing stress on the particle structure, while the rods are given more space to move around, and local rearrangements start to occur. This will happen more frequently close

to larger cavities in the network where larger volumes of water can separate out and merge with the network in one spot. This causes the structure to become more heterogeneous. In some places rods get pulled together into bigger blobs, and in other places connections are being stretched leading to thin thread-like connections (Figure 8.13). Continuing to heat weakens the structure as it becomes more flexible by the increased minority phase volume, and the increasing interfacial tension increases the driving force for the minority phase to coarsen. When the structure suddenly cannot cope with the volume of the minority phase anymore, a fast chain reaction of coarsening events can be set in motion. The whole structure coalesces into larger domains (Figure 8.16b), at a point where the volume fraction of rods in the minority phase is estimated at $\sim$0.35 (for a temperature of $\sim$51 °C). For rods of the current aspect ratio, this value is similar to where the isotropic-nematic transition is expected to happen for hard rods [27] (Figure 2.5b). Additionally, it is close to sediment densities found experimentally ($\sim$0.3, charge-stabilized particles [170]), as well as random packing densities from simulations ($\sim$0.4, hard spherocylinders [72]) for rods of similar aspect ratio. It might thus be possible here to consider particles within the wetted network behaving as hard rods, where, as is not surprising, their ability to support the network strongly depends on their volume fraction in the minority phase.

The structural changes also mean that the network can no longer support as much weight, which results in the shrinkage of the structure when the sample is heated in an upright configuration (Figure 8.14a). The weight of the network increases, and as locally the network contracts, it creates weak-spots such as the thready connections that do not offer much support. With the weight pushing in from the top causing further rearrangements, the structure becomes more dense, but remains quite homogeneous (Figure 8.15a). Ultimately, complete shrinkage (Figure 8.16a) is caused by including increasingly more water into the network, and the final state equals that of macroscopic phase separation taking place for lower rod concentration. This contrasts the sudden collapse observed on the microscope, possibly due to a quicker raise in temperature, or the absence of the more gradual collapse guided by gravity. On another, less controlled, occasion a more dramatic collapse was observed in an upright sample (not shown), with large dense chunks crashing downward through the network. Most likely this has to do with the rate at which additional minority phase separates out.

When slightly more minority phase is allowed to quickly nucleate, the final morphology of the sample seems intermediate between the ‘wetted’ network and

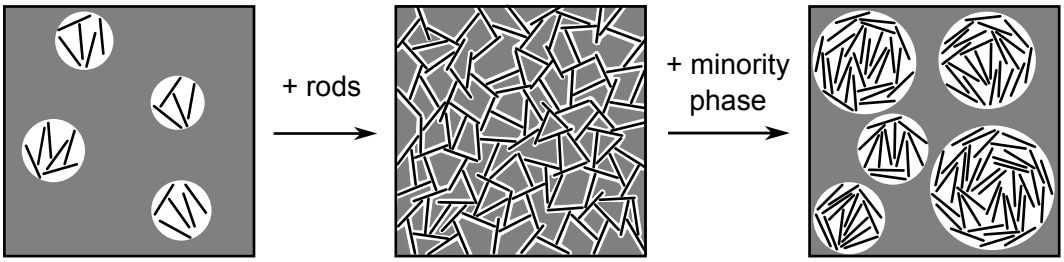

Figure 8.20 *Schematic drawing of the behaviour of the system.*

the rod-filled droplets. A heterogeneous fractal-like structure is found, which appears to have formed out of individual blobs of densely packed rods in small minority phase droplets (Figures 8.14b and 8.15b,c). Comparing this to a sample heated to 48 °C after an initial quench to 46 °C, demonstrates that quench rate, or temperature trajectory, is clearly of importance for determining the final morphology (Figures 8.14a and 8.15a). Another scenario would involve first the aggregation of particles prior to phase separation (Figure 8.9b), en route into the miscibility gap. This way, a homogeneous network like that from a direct quench (Figure 8.13a,b) can never be obtained.

It is possible that these structures could receive support from the glass walls of the container, since it is clearly partially wetted by the minority phase. This is a result from making it hydrophobic to prevent the formation of a water-rich wetting layer on the glass.

The situation goes full circle when allowing even more minority phase to nucleate. The behaviour now reverts back to that initially seen for lower particle concentration, with droplets being formed again (Figure 8.14c). These droplets contain a high concentration of rods and partially wet the hydrophobic glass, where birefringence indicates that rods exhibit orientational ordering (Figure 8.17). Within the droplets the rods will sediment to form a dense layer on the glass surface, where they eventually exhibit smectic ordering. The striped pattern represents the layering, and has a periodicity corresponding to the length of the rods. The minority phase completely wets a hydrophilic surface, resulting in a thin film in which a 2D smectics can form, no longer confined to spherical droplets. This offers some control over the geometry in which the smectics are forced to form.

The general outcome of a phase separation in the liquid mixture, deduced from the whole range of observations, can now be summarized by a schematic drawing (Figure 8.20).

The broader picture

In the study presented here, only a single system was investigated to explore the proposed scenario. Results demonstrate the importance of the volume ratio of rods to minority phase (as shown in Figure 8.20), but also the quench rate. While clearly the volume ratio of rods to minority phase is crucial, and should not be too small, the total amount of rods will determine if really a space-spanning percolating network can be formed. The advantage of using rods instead of spheres is their lower percolation threshold and large surface-to-volume ratio. The latter means that the thickness of a wetting layer increases less rapidly. In the current study, the volume of minority phase was only estimated, and also the type of rods used in this case makes knowing their concentration tricky. Overall, this study offers only a qualitative view of the situation.

Additionally, it is important to consider the relation between the basic scenario and the nature of these systems. The simulations from which inspiration was drawn here, appear to paint a too simplistic picture. In fact the favorable interaction between the particles and minority phase locally affects the composition of the system, already long before the coexistence curve is reached. This is evident from pre-transitional aggregation phenomena (chapter 8 and [51, 55]). Formation of wetting layers and liquid bridges happen well before phase separation of the bulk mixture. They still affect the bulk liquid composition and therefore the temperature at which the liquids phase separate. Judging from this, a dependence on the particle concentration can be expected.

One could consider the formation of wetting layers and liquid bridges to be phase separation. The effect of aggregation due to liquid bridges can be considered to mark the occurrence of a local first order phase transition at least between particle surfaces. In contrast, the current study set out to investigate the interplay between the particles and a global first order phase transition in the bulk liquid mixture. Comparing Figures 8.9 and 8.13 clearly demonstrates the difference of the structures particles form in these 2 distinct cases.

Comparing different studies, including this one, the behaviour of this type of system clearly depends strongly on its physical chemical properties. Both the constituent particles (interparticle interactions) and liquids (interfacial tension), as well as their combination (wetting characteristics) are crucial.

In particular, colloidal stabilization seems to be important for the behaviour.

Apart from the general characteristic that colloids are stable when the liquids are fully mixed, colloidal interactions through the minority phase seem to vary. Here particles appear to fall into the primary minimum of the interaction potential, when brought together by the minority phase, in contrast to other reports [139, 169]. Effective attractive interactions when confined to the minority phase might well be essential to stabilize the network. This would be somewhat similar to observations of nanorods in a phase-separating polymer blend [166].

Physical properties of the used liquids are important as well, for structure formation. They affect the interaction potential of the charge stabilized colloids through their permittivities, while particle translation will be affected by their (relative) viscosities and densities. In the studied system, the minority phase is the most dense liquid component, so gravity increasingly affects the structure upon increasing volume of the minority phase. Finally, there is the interfacial tension that drives the coalescence and coarsening of formed liquid domains. There will obviously be differences between liquid pairs, but the interfacial tension can be expected to be relatively low due to the proximity to the binodal.

It must also be realized that the behaviour of particles upon phase separation is not always as straightforward as assumed in the investigated scenario. As mentioned in the introduction, deeper quenches can lead to the attachment of particles to the interface after a wetting transition. Where this wetting transition occurs could be interpreted as a 'degree' of the colloids' preference for the minority phase. For instance, for water/2,6-lutidine this transition has been observed at temperatures not too far from the phase separation temperature. In preliminary experiments it was observed that silica particles in water/2,6-lutidine upon a rapid quench would partition over the 2 phases, instead of exclusively into the 'preferred' 2,6-lutidine-rich phase. Only after some shaking particles would locate themselves into the latter phase. A similar observation was done in the nitromethane/ethylene glycol mixtures (see Chapter 7). The only partial uptake in the 'preferred' phase upon a rapid quench might be related to a wetting transition upon a deeper quench into the miscibility gap. Namely, this would would indicate that the preference of the colloids for the minority phase is not very strong. Alternatively it could be related to the actual physical process of trapping the particles inside the minority phase.

8.5 Conclusions and outlook

A scenario, of rods being trapped inside the minority phase of a phase-separating binary liquid mixture, was explored with experiments. Other experimental studies on similar systems mainly look into a temperature dependent, wetting-induced attractive interaction prior to phase separation. In contrast, here the focus was on using the brute force of a liquid-liquid phase separation to trap rods into a small volume to guide their assembly. This was inspired by 'wetted' networks that were predicted to form by simulations, when, by a solvent phase separation, a large amount of colloids are confined to a small volume of minority phase.

The investigated system showed the same pre-transitional, wetting induced aggregation studied in other reports, which is inherent to this type of system. At higher colloid concentration heterogeneous networks of rods were formed as a result of this.

Crossing into the miscibility gap of the liquid mixture, the final state depended on the volume ratio of rods-to-minority phase. At low particle concentration this ratio is low, leading to bulk phase separation with the rods confined the minority phase. For sufficient rods, at a high rod-to-minority phase ratio, homogeneous 'wetted' percolating networks were observed, that span the entire sample volume. These have a distinctly different structure from the heterogeneous networks formed by pre-transitional aggregation, and coarsen as more minority phase is included by a further phase separation.

The formation of these 'wetted' networks can be approached in 2 ways. It can be regarded as the structural arrest of the rods by a phase separation, or a microphase separation caused by the coarsening of liquid domains being arrested by the rods. All in all, the route leads to the formation of a metastable structure, trapped out of equilibrium. It can be seen as an intermediate regime between pre-transitional aggregation and a bulk phase separation.

The final state reverts back to a bulk phase separation when nucleating more minority phase, but this now contains a very high concentration of rods. The resulting smectic ordering of the rods could be controlled to be contained in spherical droplets and in thin flat layers of minority phase.

Considering the situation in a more general sense, and comparing observations in

different systems, it became clear that a lot depends on the physical interactions between constituents. Changing the system on this level would be would be interesting.

One thing would be to get particles to repel each other through the minority phase, as was achieved in a similar system using highly charged particles. This led to ordered aggregates, and might do for rods as well, possibly with an interesting scenario of orientationally ordered aggregates. A possibility is to functionalize the particle surface with other charged groups (APTES or TPM/3-Sulfopropyl methacrylate). Alternatively, an ion exchange resin could be used to attempt removing any ionic impurities from the system. This case could also shed light on the effect of aggregation into the primary minimum of the interaction potential on the stability of 'wetted' networks.

Changing the liquid pair to one that is partially miscible at room temperature would be another option. Quenches to room temperature can then be employed for structure formation, with the minority phase volume adjusted through the liquid composition.

A final suggestion can be made considering that the case of complete wetting by the minority phase was studied here. It was shown that small amounts of liquid added to a suspension can significantly alter suspension rheology, if the added liquid is immiscible with the main solvent and the particles are partially wetted by both liquids [171]. This is due to capillary bridges binding particles together in a manner similar to here. Therefore, one could try if a similar scenario can be achieved with partially miscible liquids by 'adding' the required small amount of immiscible liquid that partially wets the colloids through a phase separation. Temperature would then be a convenient control parameter.

In any case, results presented here demonstrate that 'wetted' networks can indeed be realized. Additionally, besides disordered structures, the phase separation can also drive the formation and deposition of ordered assemblies of rods.

Chapter 9

Conclusions & outlook

Various scenarios involving colloidal rods or spheres in binary mixtures of partially miscible liquids were studied experimentally. First, however, a way to prepare the necessary colloidal rods was found.

Colloidal rods

A method was developed for synthesizing large quantities of versatile colloidal rods, required for proposed experiments. They are micrometer-sized core-shell type particles consisting of akaganéite (iron oxide, β-FeOOH) needle-like core particles onto which a silica shell is deposited. Synthesis of the akagenéite particles was optimized for their use as cores. Properties of the final rods can be tuned at different levels. Their aspect ratio is simply adjusted by changing the thickness of the silica shell, and hollow rods are obtained by removing the akaganéite cores. Transforming akaganéite of the cores into a different iron oxide polymorph gives the rods a significant magnetic dipole moment through which they can aggregate or align in a magnetic field. Finally, the surface chemistry of the silica shells can be adjusted to change the wetting of the rods.

The demonstrated versatility of the rods offers potential for their applicability in a wide variety of experiments. Also of importance here is their easy preparation, and the rods being of dimensions that allow single particles to be resolved with optical microscopy. Possessing silica surfaces makes them ideal for studying rods in liquid mixtures. Therefore they could be used to study rods at interfaces, which is an emerging area of research. Currently flat air-water interfaces on

which these rods are trapped are investigated using a Langmuir trough[1]. In the future, using magnetic rods, particle-stabilized interfaces or other structures can be made responsive to magnetic fields. More detailed characterization (XRD, magnetometer) of the presented magnetic rods would therefore be required.

Partial wetting of colloids

Two routes to assembling colloids that are trapped at the interface of the partially miscible liquids were investigated.

Rod-stabilized bijels. Bijels, where colloidal particles are trapped on percolating liquid-liquid interfaces, were formed with rod-like particles. These were compared with bijels prepared using spherical particles with a nearly identical volume per particle to be able to observe the effect of only the particle shape. No significantly different structuring of the particle-stabilized liquid domains was found. The only clear difference was that for rods the domain size decreased at a faster rate with increasing particle concentration, since the particles occupy a larger area of the interface. By fluorescently labeling only the inner part of the silica shells the packing of rods at the interface could be resolved. This way side-side stacks and rods that partially detach from the interface were revealed to be characteristic features.

Future work on rod-stabilized bijels can take various directions. It is likely that mechanical properties may be more significantly affected by using rod-like particles instead of spherical particles. Investigating this would therefore be a sensible addition to the presented structural study. In case any small structural changes are to be characterized, the experimental system should be adapted slightly. Using hollow fluorescent rods and preventing wetting layers to form near the glass through which the structures are observed will improve data. Another aspect that, by some of the presented results, is suggested to be worth looking into, are the phase separation kinetics.

Cellular networks. The other route used particle-stabilized droplets to yield cellular networks of colloidal particles in a single fluid phase. These were formed by the evaporation of liquid, mainly from the continuous phase, squeezing the droplets together and eventually fully mixing the liquid components. The stability of the particle networks left behind in this way, depended on the surface

[1]PhD student Tao Li is working on this.

chemistry, being stable for more hydrophobic particles, suggesting that sufficient interparticle attractions are crucial. Using confocal microscopy formation was observed in detail, demonstrating mixing of the liquids and how coalescence events affect the structure. Fortification of these networks was achieved by covalently linking particles together after network formation.

While they can still be investigated further fundamentally, also subsequent processing and modification of these cellular networks is interesting. One of the main curiosities would be if the method can easily be extended to different materials, both in terms of liquids and particles, and larger volumes. Different starting materials might pose new challenges with respect to fortifying the networks for further processing. Related to this, also the mechanical properties could be investigated.

Complete wetting of colloids

In another scenario the colloids are suspended in a very asymmetric binary liquid of which the minority component strongly prefers the particle surface. Thus, if here the liquid mixture is phase-separated, the colloids locate themselves into the minority phase.

Shear-induced aggregation. It is found that if the minority component of a binary liquid strongly prefers the colloid surface, outside the binodal line shear-induced aggregation can occur. This is in addition to wetting-induced aggregation observed in stationary samples, but happens in a wider range of temperatures and compositions further away from the coexistence curve. Various systems showed this aggregation behaviour. The underlying cause is the coalescence of adsorbed (wetting) layers of the minority component, present at the particle surfaces. This was demonstrated by an increase of the amount of minority component removed from the bulk of the suspending solvent, as the particle concentration was higher.

A few small things would be nice additions to this. One could study the structure of the formed aggregates, and also the direct observation of the liquid bridges would be a nice additional proof. The partial aggregation observed for certain compositions remains to be clarified in detail as well.

Percolating networks of rods. The formation of percolating networks of rods was found possible when, upon phase separation of an asymmetric liquid

mixture, rods at a sufficiently high concentration are trapped in a very small volume of minority phase. Here, prior to phase separation, first wetting-induced aggregation takes place. At a shallow temperature-quench across the binodal line, and at high enough particle concentration, a space-filling network of rods covered by the minority phase is formed. If the particle concentration is too low rod-filled droplets result. Separating out more minority phase made the networks weaker and eventually they contract into a small volume. At high rod concentration and for a rapid, but slightly deeper quench, droplets of a dense suspension are formed. Depending on how these droplets wet the glass onto which they sediment, they either remain as distinct droplets partially wetting the glass, or spread out to completely wet the glass. In both cases smectic ordering of the rods is eventually observed.

Plenty remains to be explored in this system. Different quench trajectories can be taken, and finding more precise conditions for percolating networks will be valuable. It would also be interesting to make the system more reversible by introducing stronger repulsions between particles, through the minority phase that connects them. For this purpose more-charged or sterically stabilized particles could be used.

Bibliography

[1] N. Hijnen and P. S. Clegg. Simple synthesis of versatile akaganéite-silica core-shell rods. *Chemistry of Materials*, 24:3449–3457, 2012.

[2] D. H. Everett. *Basic principles of colloid science*. The Royal Society of Chemistry, 1988.

[3] S. C. Glotzer and M. J. Solomon. Anisotropy of building blocks and their assembly into complex structures. *Nature Materials*, 6(8):557–562, 2007.

[4] A. Yethiraj. Tunable colloids: control of colloidal phase transitions with tunable interactions. *Soft Matter*, 3(9):1099–1115, 2007.

[5] M. J. Solomon. Directions for targeted self-assembly of anisotropic colloids from statistical thermodynamics. *Current Opinion in Colloid & Interface Science*, 16(2):158–167, 2011.

[6] S. Sacanna and D. J. Pine. Shape-anisotropic colloids: Building blocks for complex assemblies. *Current Opinion in Colloid & Interface Science*, 16(2):96–105, 2011.

[7] S. Sacanna, D. J. Pine, and G.-R. Yi. Engineering shape: the novel geometries of colloidal self-assembly. *Soft Matter*, 9:8096–8106, 2013.

[8] L. Onsager. The effects of shape on the interaction of colloidal particles. *Annals of the New York Academy of Sciences*, 51:627–659, 1949.

[9] M. J. Solomon and P. T. Spicer. Microstructural regimes of colloidal rod suspensions, gels, and glasses. *Soft Matter*, 6(7):1391–1400, 2010.

[10] L. Botto, E. P. Lewandowski, M. Cavallaro, and K. J. Stebe. Capillary interactions between anisotropic particles. *Soft Matter*, 8(39):9957–9971, 2012.

[11] B. Madivala, S. Vandebril, J. Fransaer, and J. Vermant. Exploiting particle shape in solid stabilized emulsions. *Soft Matter*, 5(8):1717–1727, 2009.

[12] J. C. Loudet, A. Alsayed, J. Zhang, and A. Yodh. Capillary Interactions Between Anisotropic Colloidal Particles. *Physical Review Letters*, 94(1):018301, 2005.

[13] E. P. Lewandowski, J. A. Bernate, A. Tseng, P. C. Searson, and K. J. Stebe. Oriented assembly of anisotropic particles by capillary interactions. *Soft Matter*, 5(4):886–890, 2009.

[14] B. Madivala, J. Fransaer, and J. Vermant. Self-assembly and rheology of ellipsoidal particles at interfaces. *Langmuir*, 25(5):2718–2728, 2009.

[15] M. Grzelczak, J. Vermant, E. M. Furst, and L. M. Liz-Marzán. Directed self-assembly of nanoparticles. *ACS Nano*, 4(7):3591–3605, 2010.

[16] M. E. Cates and P. S. Clegg. Bijels: a new class of soft materials. *Soft Matter*, 4(11):2132–2138, 2008.

[17] G. Peng, F. Qiu, V. V. Ginzburg, D. Jasnow, and A. C. Balazs. Forming supramolecular networks from nanoscale rods in binary, phase-separating mixtures. *Science*, 288:1802–1804, 2000.

[18] E. M. Herzig, K. A. White, A. B. Schofield, W. C. K. Poon, and P. S. Clegg. Bicontinuous emulsions stabilized solely by colloidal particles. *Nature Materials*, 6(12):966–971, 2007.

[19] D. Fermin and J. Riley. Charge in colloidal systems. In T. Cosgrove, editor, *Colloid Science: Principles, methods and applications*, pages 23–43. John Wiley & Sons Ltd, 2nd edition, 2010.

[20] J. Eastman. Stability of charge-stabilized colloids. In T. Cosgrove, editor, *Colloid Science: Principles, methods and applications*, pages 45–59. John Wiley & Sons Ltd, 2nd edition, 2010.

[21] A. van Blaaderen. DLVO Theory & Measurement of Interaction Forces. In *Lecture notes "Soft Condensed Matter & Advanced Colloid Science"*, pages 221–261. 2007.

[22] M. Minor and H. P. van Leeuwen. Dynamics and Kinetics. In J. Lyklema, editor, *Fundamentals of Colloid and Interface Science, Vol. IV*, pages 4.1–4.53. Elsevier, 2005.

[23] R. A. L. Jones. *Soft Condensed Matter*. Oxford University Press, 2002.

[24] P. N. Pusey and W. van Megen. Phase behaviour of concentrated suspensions of nearly hard colloidal spheres. *Nature*, 320:340–342, 1986.

[25] S. M. Ilett, A. Orrock, W. C. K. Poon, and P. N. Pusey. Phase behavior of a model colloid-polymer mixture. *Physical Review E*, 51(2):1344–1353, 1995.

[26] E. Zaccarelli. Colloidal gels: equilibrium and non-equilibrium routes. *Journal of Physics: Condensed Matter*, 19(32):323101, 2007.

[27] P. Bolhuis and D. Frenkel. Tracing the phase boundaries of hard spherocylinders. *Journal of Chemical Physics*, 106(2):666–687, 1997.

[28] V. R. Dugyala, S. V. Daware, and M. G. Basavaraj. Shape anisotropic colloids: synthesis, packing behavior, evaporation driven assembly, and their application in emulsion stabilization. *Soft Matter*, 9:6711–6725, 2013.

[29] D. B. Murphy. *Fundamentals of light microscopy and electronic imaging*. John Wiley & Sons Ltd, 2001.

[30] P. G. Debenedetti. *Metastable Liquids: Concepts and Principles*. Princeton University Press, 1996.

[31] P. Atkins and J. de Paula. *Atkins' Physical Chemistry*. Oxford University Press, 7th edition, 2002.

[32] H. N. W. Lekkerkerker and S. M. Oversteegen. *Lecture notes "Physical Chemistry 3: Interfaces"*. Utrecht University, 2004.

[33] J. Zhu, L. Q. Chen, J. Shen, and V. Tikare. Coarsening kinetics from a variable-mobility Cahn-Hilliard equation: application of a semi-implicit Fourier spectral method. *Physical Review E*, 60(4):3564–3572, 1999.

[34] P. M. Chaikin and T. C. Lubensky. *Principles of Condensed Matter Physics*. Cambridge University Press, 1st edition, 1995.

[35] C. M. F. Jantzen and H. Herman. Volume 6-v. In A. M. Alper, editor, *Phase Diagrams, Materials Science and Technology*, pages 127–184. Academic Press, 1978.

[36] H.-J. Butt, K. Graf, and M. Kappl. *Physics and Chemistry of Interfaces*. John Wiley & Sons Ltd, 2003.

[37] B. P. Binks and T. S. Horozov. Colloidal particles at liquid interfaces: An introduction. In B. P. Binks and T. S. Horozov, editors, *Colloidal Particles at Liquid Interfaces*, pages 1–74. Cambridge University Press, 2006.

[38] J. W. Cahn. Critical point wetting. *The Journal of Chemical Physics*, 66(8):3667–3672, 1977.

[39] D. Bonn and D. Ross. Wetting transitions. *Reports on Progress in Physics*, 64(9):1085–1163, 2001.

[40] R. Aveyard, B. P. Binks, and J. H. Clint. Emulsions stabilised solely by colloidal particles. *Advances in Colloid and Interface Science*, 100-102:503–546, 2003.

[41] R. McGorty, J. Fung, D. Kaz, and V. N. Manoharan. Colloidal self-assembly at an interface. *Materials Today*, 13(6):34–42, 2010.

[42] H. Lehle, E. Noruzifar, and M. Oettel. Ellipsoidal particles at fluid interfaces. *The European Physical Journal E*, 26:151–160, 2008.

[43] J. C. Loudet, A. Yodh, and B. Pouligny. Wetting and Contact Lines of Micrometer-Sized Ellipsoids. *Physical Review Letters*, 97(1):018304, 2006.

[44] E. P. Lewandowski, J. A. Bernate, P. C. Searson, and K. J. Stebe. Rotation and alignment of anisotropic particles on nonplanar interfaces. *Langmuir*, 24(17):9302–9307, 2008.

[45] E. P. Lewandowski, M. Cavallaro, L. Botto, J. C. Bernate, V. Garbin, and K. J. Stebe. Orientation and self-assembly of cylindrical particles by anisotropic capillary interactions. *Langmuir*, 26(19):15142–15154, 2010.

[46] E. P. Lewandowski, P. C. Searson, and K. J. Stebe. Orientation of a nanocylinder at a fluid interface. *The Journal of Physical Chemistry B*, 110(9):4283–4290, 2006.

[47] S. W. Pickering. CXCVI.−Emulsions. *Journal of the Chemical Society, Transactions*, 91:2001–2021, 1907.

[48] W. Ramsden. Separation of Solids in the Surface-Layers of Solutions and 'Suspensions' (Observations on Surface-Membranes, Bubbles, Emulsions, and Mechanical Coagulation). – Preliminary Account. *Proceedings of the Royal Society of London*, 72:156–164, 1903.

[49] B. P. Binks. Particles as surfactantssimilarities and differences. *Current Opinion in Colloid & Interface Science*, 7:21–41, 2002.

[50] A. Gambassi, A. Maciolek, C. Hertlein, U. Nellen, L. Helden, C. Bechinger, and S. Dietrich. Critical Casimir effect in classical binary liquid mixtures. *Physical Review E*, 80(6):061143, 2009.

[51] C. Hertlein, L. Helden, A. Gambassi, S. Dietrich, and C. Bechinger. Direct measurement of critical Casimir forces. *Nature*, 451(7175):172–175, 2008.

[52] H. T. Dobbs, G. A. Darbellay, and J. M. Yeomans. Capillary condensation between spheres. *Europhysics Letters*, 18(5):439–444, 1992.

[53] H. T. Dobbs and J. M. Yeomans. Capillary condensation and prewetting between spheres. *Journal of Physics: Condensed Matter*, 4:10133–10138, 1992.

[54] J. M. Petit, B. M. Law, and D. Beysens. Adsorption-induced aggregation of colloidal particles in binary mixtures: Modeling the pair free energy. *Journal of Colloid and Interface Science*, 449(202):441–449, 1998.

[55] D. Beysens and D. Esteve. Adsorption phenomena at the surface of silica spheres in a binary liquid mixture. *Physical Review Letters*, 54(19):2123–2126, 1985.

[56] W. Stöber, A. Fink, and E. Bohn. Controlled growth of monodisperse silica spheres in the micron size range. *Journal of Colloid and Interface Science*, 26:62–69, 1968.

[57] A. P. Philipse. Particulate Colloids: Aspects of preparation and characterization. In J. Lyklema, editor, *Fundamentals of Colloid and Interface Science, Vol. IV*, pages 2.1–2.71. Elsevier, 2005.

[58] A. van Blaaderen and A. Vrij. Synthesis and characterization of colloidal dispersions of fluorescent, monodisperse silica spheres. *Langmuir*, 81(2):2921–2931, 1992.

[59] N. A. M. Verhaegh and A. Blaaderen. Dispersions of rhodamine-labeled silica spheres: synthesis, characterization, and fluorescence confocal scanning laser microscopy. *Langmuir*, 96(9):1427–1438, 1994.

[60] T. I. Suratwala, M. L. Hanna, and E. L. Miller. Surface chemistry and trimethylsilyl functionalization of Stöber silica sols. *Journal of Non-Crystalline Solids*, 316:349–363, 2003.

[61] G. B. Alexander, W. M. Heston, and R. K. Iler. The solubility of amorphous silica in water. *The Journal of Physical Chemistry*, 58(6):453–455, 1954.

[62] L. T. Zhuravlev. The surface chemistry of amorphous silica. Zhuravlev model. *Colloids and Surfaces A*, 173(1-3):1–38, 2000.

[63] P. S. Clegg, E. M. Herzig, A. B. Schofield, S. U. Egelhaaf, T. S. Horozov, B. P. Binks, M. E. Cates, and W. C. K. Poon. Emulsification of partially miscible liquids using colloidal particles: nonspherical and extended domain structures. *Langmuir*, 23(11):5984–5994, 2007.

[64] J. W. Tavacoli, J. H. J. Thijssen, A. B. Schofield, and P. S. Clegg. Novel, Robust, and Versatile Bijels of Nitromethane, Ethanediol, and Colloidal Silica: Capsules, Sub-Ten-Micrometer Domains, and Mechanical Properties. *Advanced Functional Materials*, 21(11):2020–2027, 2011.

[65] Z. Dogic and S. Fraden. Ordered phases of filamentous viruses. *Current Opinion in Colloid & Interface Science*, 11(1):47–55, 2006.

[66] Z. X. Zhang and J. S. van Duijneveldt. Isotropic-nematic phase transition of nonaqueous suspensions of natural clay rods. *The Journal of Chemical Physics*, 124(15):154910, 2006.

[67] P. A. Buining, A. P. Philipse, and H. N. W. Lekkerkerker. Phase Behavior of Aqueous Dispersions of Colloidal Boehmite Rods. *Langmuir*, 10(7):2106–2114, 1994.

[68] G. J. Vroege and H. N. W. Lekkerkerker. Phase transitions in lyotropic colloidal and polymer liquid crystals. *Reports on Progress in Physics*, 55:1241–1309, 1992.

[69] A. Hirai, O. Inui, F. Horii, and M. Tsuji. Phase separation behavior in aqueous suspensions of bacterial cellulose nanocrystals prepared by sulfuric acid treatment. *Langmuir*, 25(1):497–502, 2009.

[70] A. V. Kyrylyuk and P. van der Schoot. Continuum percolation of carbon nanotubes in polymeric and colloidal media. *Proceedings of the National Academy of Sciences*, 105(24):2923–2927, 2008.

[71] A. P. Philipse. The Random Contact Equation and Its Implications for (Colloidal) Rods in Packings, Suspensions, and Anisotropic Powders. *Langmuir*, 12(24):5971–5971, 1996.

[72] S. Williams and A. P. Philipse. Random packings of spheres and spherocylinders simulated by mechanical contraction. *Physical Review E*, 67(5):051301, 2003.

[73] M. G. Basavaraj, G. G. Fuller, J. Fransaer, and J. Vermant. Packing, flipping, and buckling transitions in compressed monolayers of ellipsoidal latex particles. *Langmuir*, 22(15):6605–6612, jul 2006.

[74] K. Stratford, R. Adhikari, I. Pagonabarraga, J.-C. Desplat, and M. E. Cates. Colloidal jamming at interfaces: a route to fluid-bicontinuous gels. *Science*, 309:2198–2201, 2005.

[75] S. Sacanna, L. Rossi, B. W. M. Kuipers, and A. P. Philipse. Fluorescent monodisperse silica ellipsoids for optical rotational diffusion studies. *Langmuir*, 22(4):1822–1827, 2006.

[76] M. P. B. van Bruggen. Preparation and Properties of Colloidal Core - Shell Rods with Adjustable Aspect Ratios. *Langmuir*, 14:2245–2255, 1998.

[77] H. Zhang, T. J. Bandosz, and D. L. Akins. Template-free synthesis of silica ellipsoids. *Chemical Communications*, 47(27):7791–7793, 2011.

[78] S. Shen, T. Gu, D. Mao, X. Xiao, P. Yuan, M. Yu, L. Xia, Q. Ji, L. Meng, W. Song, C. Yu, and G. Lu. Synthesis of Nonspherical Mesoporous Silica Ellipsoids with Tunable Aspect Ratios for Magnetic Assisted Assembly and Gene Delivery. *Chemistry of Materials*, 24(1):230–235, 2012.

[79] A. Kuijk, A. van Blaaderen, and A. Imhof. Synthesis of monodisperse, rodlike silica colloids with tunable aspect ratio. *Journal of the American Chemical Society*, 133(8):2346–2349, 2011.

[80] E. Matijevic and P. Scheiner. Ferric Hydrous Oxide Sols III. Preparation of Uniform Particles by Hydrolysis of Fe(III)-Chloride, -Nitrate, and -Perchlorate Solutions. *Journal of Colloid and Interface Science*, 63(3):509–524, 1978.

[81] H. Maeda and Y. Maeda. Liquid Crystal Formation in Suspensions of Hard Rodlike Colloidal Particles: Direct Observation of Particle Arrangement and Self-Ordering Behavior. *Physical Review Letters*, 90(1):018303, 2003.

[82] H. Maeda and Y. Maeda. Atomic Force Microscopy Studies for Investigating the Smectic Structures of Colloidal Crystals of β-FeOOH. *Langmuir*, 12(6):1446–1452, 1996.

[83] X.-L. Fang, Y. Li, C. Chen, Q. Kuang, X.-Z. Gao, Z.-X. Xie, S.-Y. Xie, R.-B. Huang, and L.-S. Zheng. pH-induced simultaneous synthesis and self-assembly of 3D layered beta-FeOOH nanorods. *Langmuir*, 26(4):2745–2750, 2010.

[84] J. K. Bailey, C. J. Brinker, and M. L. Mecartney. Growth mechanisms of iron oxide particles of differing morphologies from the forced hydrolysis of ferric chloride solutions. *Journal of Colloid and Interface Science*, 157:1–13, 1993.

[85] M. Blesa and E. Matijevic. Phase transformations of iron oxides, oxyhydroxides, and hydrous oxides in aqueous media. *Advances in Colloid and Interface Science*, 29:173–221, 1989.

[86] J. Yue, X. Jiang, and A. Yu. Experimental and theoretical study on the β-FeOOH nanorods: growth and conversion. *Journal of Nanoparticle Research*, 13(9):3961–3974, 2011.

[87] N. K. Chaudhari and J.-S. Yu. Size Control Synthesis of Uniform β-FeOOH to High Coercive Field Porous Magnetic α-Fe_2O_3 Nanorods. *The Journal of Physical Chemistry C*, 112:19957–19962, 2008.

[88] S. Musić, S. Krehula, and S. Popović. Effect of HCl additions on forced hydrolysis of $FeCl_3$ solutions. *Materials Letters*, 58(21):2640–2645, 2004.

[89] Z. Pu, M. Cao, J. Yang, K. Huang, and C. Hu. Controlled synthesis and growth mechanism of hematite nanorhombohedra, nanorods and nanocubes. *Nanotechnology*, 17(3):799–804, 2006.

[90] C. Graf, D. L. J. Vossen, A. Imhof, and A. van Blaaderen. A General Method To Coat Colloidal Particles with Silica. *Langmuir*, 19(17):6693–6700, 2003.

[91] W. Rasband. Imagej 1.46r. http://imagej.nih.gov/ij/, 2013.

[92] C. C. Ho, A. Keller, J. A. Odell, and R. H. Ottewill. Preparation of monodisperse ellipsoidal polystyrene particles. *Colloid and Polymer Science*, 271:469–479, 1993.

[93] E. Matijevic and Y. Kitazawa. Heterocoagulation VII. Interactions of rod-like β-FeOOH with spherical latex particles. *Colloid & Polymer Science*, 261:527–534, 1983.

[94] M. Schudel, S. H. Behrens, H. Holthoff, R. Kretzschmar, and M. Borkovec. Absolute Aggregation Rate Constants of Hematite Particles in Aqueous Suspensions: A Comparison of Two Different Surface Morphologies. *Journal of Colloid and Interface Science*, 196(2):241–253, 1997.

[95] B. C. Blakey and D. F. James. The viscous behaviour and structure of aqueous suspensions of goethite. *Colloids and Surfaces A*, 231:19–30, 2003.

[96] D. M. E. Thies-Weesie, A.P. Philipse, and G. J. M. Kluijtmans. Preparation of sterically stabilized silica-hematite ellipsoids: Sedimentation, permeation, and packing properties of prolate colloids. *Journal of Colloid and Interface Science*, 174:211–223, 1995.

[97] Y. Song, B. H. Bac, Y.-B. Lee, M. H. Kim, and I. M. Kang. Highly ordered Ge-incorporated akaganeite (β-FeOOH): a tunnel-type nanorod. *CrystEngComm*, 13(1):287–292, 2011.

[98] A. Urtizberea, F. Luis, A. Millán, E. Natividad, F. Palacio, E. Kampert, and U. Zeitler. Thermoinduced magnetic moment in akaganéite nanoparticles. *Physical Review B*, 83:214426, 2011.

[99] I. Milosevic, H. Jouni, C. David, F. Warmont, D. Bonnin, and L. Motte. Facile Microwave Process in Water for the Fabrication of Magnetic Nanorods. *The Journal of Physical Chemistry C*, 115(39):18999–19004, oct 2011.

[100] M. Reufer, H. Dietsch, U. Gasser, B. Grobety, A. M. Hirt, V. K. Malik, and P. Schurtenberger. Magnetic properties of silica coated spindle-type hematite particles. *Journal of Physics: Condensed Matter*, 23(6):065102, 2011.

[101] Y. Piao, J. Kim, H. B. Na, D. Kim, J. S. Baek, M. K. Ko, J. H. Lee, M. Shokouhimehr, and T. Hyeon. Wrap-bake-peel process for nanostructural transformation from beta-FeOOH nanorods to biocompatible iron oxide nanocapsules. *Nature Materials*, 7(3):242–247, 2008.

[102] M. Ohmori and E. Matijevic. Preparation and Properties of Uniform Coated Inorganic Colloidal Particles 8. Silica on Iron. *Journal of Colloid and Interface Science*, 160:288–292, 1993.

[103] V. Städele, U. Gasser, and H. Dietsch. Ellipsoidal hybrid magnetic microgel particles with thermally tunable aspect ratios. *Soft Matter*, 8:4427–4431, 2012.

[104] M. Reufer, V.A. Martinez, P. Schurtenberger, and W. C. K. Poon. Differential dynamic microscopy for anisotropic colloidal dynamics. *Langmuir*, 28(10):4618–4624, 2012.

[105] M. Reufer, H. Dietsch, U. Gasser, A. Hirt, A. Menzel, and P. Schurtenberger. Morphology and orientational behavior of silica-coated spindle-type hematite particles in a magnetic field probed by small-angle X-ray scattering. *The Journal of Physical Chemistry B*, 114(14):4763–4769, 2010.

[106] B. J. Lemaire, P. Davidson, J. Ferré, J. P. Jamet, D. Petermann, P. Panine, I. Dozov, and J. P. Jolivet. Physical properties of aqueous suspensions of goethite (alpha-FeOOH) nanorods. Part I: In the isotropic phase. *The European physical journal. E, Soft matter*, 13(3):291–308, 2004.

[107] D. M. E. Thies-weesie, J. P. de Hoog, M. H. H. Mendiola, A. V. Petukhov, and G. J. Vroege. Synthesis of Goethite as a Model Colloid for Mineral Liquid Crystals. *Chemistry of Materials*, 19:5538–5546, 2007.

[108] H. Maeda and Y. Maeda. Spectroscopic Ellipsometry Study on Refractive Index Spectra of Colloidal β-FeOOH Nanorods with Their Self-Assembled Thin Films. *Langmuir*, 27:2895–2903, 2011.

[109] T. Chappuis, I. Bobowska, S. Hengsberger, E. Vanoli, and H. Dietsch. Influence of the hydrogen reduction time and temperature on the morphology evolution and hematite/magnetite conversion of spindle-type hematite nanoparticles. *Chimia*, 65(12):979–981, 2011.

[110] E. Sanz, K. A. White, P. S. Clegg, and M. E. Cates. Colloidal Gels Assembled via a Temporary Interfacial Scaffold. *Physical Review Letters*, 103(25):255502, 2009.

[111] M. N. Lee, J. H. J. Thijssen, J. A. Witt, P. S. Clegg, and A. Mohraz. Making a Robust Interfacial Scaffold: Bijel Rheology and its Link to Processability. *Advanced Functional Materials*, 23(4):417–423, 2013.

[112] M. N. Lee and A. Mohraz. Bicontinuous macroporous materials from bijel templates. *Advanced Materialss*, 22(43):4836–4841, nov 2010.

[113] M. N. Lee and A. Mohraz. Hierarchically porous silver monoliths from colloidal bicontinuous interfacially jammed emulsion gels. *Journal of the American Chemical Society*, 133:6945–6947, 2011.

[114] F. Günther, F. Janoschek, S. Frijters, and J. Harting. Lattice Boltzmann simulations of anisotropic particles at liquid interfaces. *Computers & Fluids*, 80:184–189, 2013.

[115] T.-L. Cheng and Y. U. Wang. Shape-anisotropic particles at curved fluid interfaces and role of Laplace pressure: a computational study. *Journal of Colloid and Interface Science*, 402:267–78, 2013.

[116] K. A. White, A. B. Schofield, B. P. Binks, and P. S. Clegg. Influence of particle composition and thermal cycling on bijel formation. *Journal of Physics: Condensed Matter*, 20(49):494223, 2008.

[117] K. A. White, A. B. Schofield, P. Wormald, J. W. Tavacoli, B. P. Binks, and P. S. Clegg. Inversion of particle-stabilized emulsions of partially miscible liquids by mild drying of modified silica particles. *Journal of Colloid and Interface Science*, 359(1):126–135, 2011.

[118] W. Zhou, J. Cao, W. Liu, and S. Stoyanov. How rigid rods self-assemble at curved surfaces. *Angewandte Chemie (International edition)*, 48(2):378–381, 2009.

[119] E. M. Herzig. *Bijel: a novel composite material from colloids on liquid-liquid interfaces*. PhD thesis, University of Edinburgh, 2008.

[120] D. Gazeau, A. M. Bellocq, D. Roux, and T. Zemb. Experimental evidence for random surface structures in dilute surfactant solutions. *Europhysics Letters*, 9(5):447–452, 1989.

[121] D. Roux, C. Coulon, and M. E. Cates. Sponge phases in surfactant solutions. *The Journal of Physical Chemistry*, 4187(8):4174–4187, 1992.

[122] H. Tanaka and T. Araki. Surface effects on spinodal decomposition of incompressible binary fluid mixtures. *Europhysics Letters*, 51(2):154–160, 2000.

[123] L. J. Gibson and M. F. Ashby. *Cellular solids: Structure and properties*. Cambridge University Press, 2nd edition, 1999.

[124] S. P. Meeker, W. C. K. Poon, J. Crain, and E. M. Terentjev. Colloid-liquid-crystal composites: An unusual soft solid. *Physical Review E*, 61(6):R6083, 2000.

[125] C. A. L. Colard, R. A. Cave, N. Grossiord, J. A. Covington, and S. A. F. Bon. Conducting Nanocomposite Polymer Foams from Ice-Crystal-Templated Assembly of Mixtures of Colloids. *Advanced Materials*, 21(28):2894–2898, 2009.

[126] M. Destribats, B. Faure, and M. Birot. Tailored Silica Macrocellular Foams: Combining Limited Coalescence-Based Pickering Emulsion and Sol-Gel Process. *Advanced Functional Materials*, pages 2642–2654, 2012.

[127] I. Akartuna, A. R. Studart, E. Tervoort, and L. J. Gauckler. Macroporous Ceramics from Particle-stabilized Emulsions. *Advanced Materials*, 20(24):4714–4718, 2008.

[128] I. Aranberri, B. P. Binks, J. H. Clint, and P. D. I. Fletcher. Synthesis of macroporous silica from solid-stabilised emulsion templates. *Journal of Porous Materials*, 16(4):429–437, 2008.

[129] S. Barg, B. P. Binks, H. Wang, D. Koch, and G. Grathwohl. Cellular ceramics from emulsified suspensions of mixed particles. *Journal of Porous Materials*, 19(5):859–867, 2011.

[130] J. H. J. Thijssen and P. S. Clegg. Demixing, remixing and cellular networks in binary liquids containing colloidal particles. *Soft Matter*, 6(6):1182–1190, 2010.

[131] D. Beysens and T. Narayanan. Wetting-induced aggregation of colloids. *Journal of Statistical Physics*, 95(5/6):997–1008, 1999.

[132] V. Gurfein, D. Beysens, and F. Perrot. Stability of colloids and wetting phenomena. *Physical Review A*, 40(5):2543–2546, 1989.

[133] C. Gögelein and M. Brinkmann. Controlling the Formation of Capillary Bridges in Binary Liquid Mixtures. *Langmuir*, 26(22):17184–17189, 2010.

[134] Y. Jayalakshmi and E. W. Kaler. Phase behavior of colloids in binary liquid mixtures. *Physical Review Letters*, 78(7):1379–1382, 1997.

[135] D. Bonn, J. Otwinowski, S. Sacanna, H. Guo, G. Wegdam, and P. Schall. Direct observation of colloidal aggregation by critical Casimir forces. *Physical Review Letters*, 103(15):156101, 2009.

[136] D. Pontoni, T. Narayanan, J.-M. Petit, G. Grubel, and D. Beysens. Microstructure and dynamics near an attractive colloidal glass transition. *Physical Review Letters*, 90(18):188301, 2003.

[137] H. Guo, T. Narayanan, M. Sztuchi, P. Schall, and G. H. Wegdam. Reversible phase transition of colloids in a binary liquid solvent. *Physical Review Letters*, 100(18):188303, 2008.

[138] F. Soyka, O. Zvyagolskaya, C. Hertlein, L. Helden, and C. Bechinger. Critical Casimir Forces in Colloidal Suspensions on Chemically Patterned Surfaces. *Physical Review Letters*, 101(20):208301, 2008.

[139] R. D. Koehler and E. W. Kaler. Colloidal phase transitions in aqueous nonionic surfactant solutions. *Langmuir*, 13(9):2463–2470, 1997.

[140] B.M. Law, J.-M. Petit, and D. Beysens. Adsorption-induced reversible colloidal aggregation. *Physical Review E*, 57(5):5782–5794, 1998.

[141] B. Vincent, Z. Király, S. Emmett, and A. Beaver. The stability of silica dispersions in ethanol/cyclohexane mixtures. *Colloids and Surfaces*, 49:121–132, 1990.

[142] S. R. Kline and E. W. Kaler. Colloidal interactions in water/2-butoxyethanol solvents. *Langmuir*, 10(2):412–417, 1994.

[143] P. D. Gallagher, M. L. Kurnaz, and J. V. Maher. Aggregation in polystyrene-sphere suspensions in near-critical binary liquid mixtures. *Physical Review A*, 46(12):7750–7755, 1992.

[144] B. Rathke, H. Grüll, and D. Woermann. Stability of dilute colloidal silica suspensions in the vicinity of the binodal curve of the system 2-butoxyethanol/water. *Journal of Colloid and Interface Science*, 192:334–337, 1997.

[145] J.M. Sørenson and W. Arlt. *Liquid-Liquid Equilibrium Data Collection*. Dechema, 1979.

[146] R. Stephenson and J. Stuart. Mutual binary solubilities: water-alcohols and water-esters. *Journal of Chemical and Engineering Data*, 31:56–70, 1986.

[147] P. Bauduin, L. Wattebled, S. Schrödle, D. Touraud, and W. Kunz. Temperature dependence of industrial propylene glycol alkyl ether/water mixtures. *Journal of Molecular Liquids*, 115(1):23–28, 2004.

[148] P. Greenspan, E. P. Mayer, and S. D. Fowler. Nile red: a selective fluorescent stain for intracellular lipid droplets. *The Journal of Cell Biology*, 100(3):965–73, 1985.

[149] R. Besseling, L. Isa, E. R. Weeks, and W. C. K. Poon. Quantitative imaging of colloidal flows. *Advances in Colloid and Interface Science*, 146(1-2):1–17, 2009.

[150] N. Grossiord, J. Loos, O. Regev, and C. E. Koning. Toolbox for Dispersing Carbon Nanotubes into Polymers To Get Conductive Nanocomposites. *Chemistry of Materials*, 18(5):1089–1099, 2006.

[151] G. A. Buxton and A. C. Balazs. Predicting the mechanical and electrical properties of nanocomposites formed from polymer blends and nanorods. *Molecular Simulation*, 30(4):249–257, 2004.

[152] A. P. Philipse and A. M. Wierenga. On the density and structure formation in gels and clusters of colloidal rods and fibers. *Langmuir*, 14(1):49–54, 1998.

[153] A. Mohraz, D. Moler, R. Ziff, and M. J. Solomon. Effect of Monomer Geometry on the Fractal Structure of Colloidal Rod Aggregates. *Physical Review Letters*, 92(15):155503, 2004.

[154] A. Mohraz and M. J. Solomon. Gelation and internal dynamics of colloidal rod aggregates. *Journal of Colloid and Interface Science*, 300(1):155–162, 2006.

[155] A. Wierenga, A. P. Philipse, H. N. W. Lekkerkerker, and D. V. Boger. Aqueous dispersions of colloidal boehmite: Structure, dynamics, and yield stress of rod gels. *Langmuir*, 14(1):55–65, 1998.

[156] H. Tanaka, A. J. Lovinger, and D. D. Davis. Pattern evolution caused by dynamic coupling between wetting and phase separation in binary liquid mixture containing glass particles. *Physical Review Letters*, 72(16):2581, 1994.

[157] A. Karim, J. F. Douglas, G. Nisato, D.-W. Liu, and E. J. Amis. Transient Target Patterns in Phase Separating Filled Polymer Blends. *Macromolecules*, 32(18):5917–5924, 1999.

[158] B. P. Lee, J. F. Douglas, and S. C. Glotzer. Filler-induced composition waves in phase-separating polymer blends. *Physical Review E*, 60(5):5812–5822, 1999.

[159] T. Araki and H. Tanaka. Wetting-induced depletion interaction between particles in a phase-separating liquid mixture. *Physical Review E*, 73(6):061506, 2006.

[160] T. Araki and H. Tanaka. Dynamic depletion attraction between colloids suspended in a phase-separating binary liquid mixture. *Journal of Physics: Condensed Matter*, 20(7):072101, 2008.

[161] A. C. Balazs. Interactions of nanoscopic particles with phase-separating polymeric mixtures. *Current Opinion in Colloid & Interface Science*, 4:443–448, 2000.

[162] M. Laradji and G. MacNevin. Phase separation dynamics in binary fluids containing quenched or mobile filler particles. *The Journal of Chemical Physics*, 119(4):2275–2283, 2003.

[163] M. Laradji. A Langevin dynamics study of mobile filler particles in phase-separating binary systems. *The Journal of Chemical Physics*, 120(19):9330–9334, 2004.

[164] K. Chen and Y. Ma. Self-assembling morphology induced by nanoscale rods in a phase-separating mixture. *Physical Review E*, 65(4):041501, 2002.

[165] M. J. A. Hore and M. Laradji. Prospects of nanorods as an emulsifying agent of immiscible blends. *The Journal of Chemical Physics*, 128(5):054901, 2008.

[166] L. Li, C. Miesch, P. K. Sudeep, A. C. Balazs, T. Emrick, T. P. Russell, and R. C. Hayward. Kinetically trapped co-continuous polymer morphologies through intraphase gelation of nanoparticles. *Nano Letters*, 11:1997–2003, 2011.

[167] P. D. Gallagher and J. V. Maher. Partitioning of polystyrene latex spheres in immiscible critical liquid mixtures. *Physical Review A*, 46(4):2012–2021, 1992.

[168] D. W. Pohl and W. I. Goldburg. Wetting transition in lutidine-water mixtures. *Physical Review Letters*, 48(16):1111–1114, 1982.

[169] M. L. Broide, Y. Garrabos, and D. Beysens. Nonfractal colloidal aggregation. *Physical Review E*, 47(5):3768–3771, 1993.

[170] A. P. Philipse, A. M. Nechifor, and C. Patmamanoharan. Isotropic and birefringent dispersions of surface modified silica rods with a boehmite-needle core. *Langmuir*, 10(12):4451–4458, 1994.

[171] E. Koos and N. Willenbacher. Capillary forces in suspension rheology. *Science*, 331:897–900, 2011.